

SANDIA REPORT

SAND92-0700/2 • UC-721

Unlimited Release

Printed December 1992

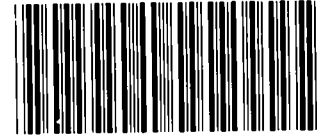
MICROFICHE

Preliminary Performance Assessment for the Waste Isolation Pilot Plant, December 1992

Volume 2: Technical Basis

WIPP Performance Assessment Department

Prepared by
Sandia National Laboratories
Albuquerque, New Mexico 87185 and Livermore, California 94550
for the United States Department of Energy
under Contract DE-AC04-76DP00789



* 8564424*

**SANDIA NATIONAL
LABORATORIES
TECHNICAL LIBRARY**

Issued by Sandia National Laboratories, operated for the United States Department of Energy by Sandia Corporation.

NOTICE: This report was prepared as an account of work sponsored by an agency of the United States Government. Neither the United States Government nor any agency thereof, nor any of their employees, nor any of their contractors, subcontractors, or their employees, makes any warranty, express or implied, or assumes any legal liability or responsibility for the accuracy, completeness, or usefulness of any information, apparatus, product, or process disclosed, or represents that its use would not infringe privately owned rights. Reference herein to any specific commercial product, process, or service by trade name, trademark, manufacturer, or otherwise, does not necessarily constitute or imply its endorsement, recommendation, or favoring by the United States Government, any agency thereof or any of their contractors or subcontractors. The views and opinions expressed herein do not necessarily state or reflect those of the United States Government, any agency thereof or any of their contractors.

Printed in the United States of America. This report has been reproduced directly from the best available copy.

Available to DOE and DOE contractors from
Office of Scientific and Technical Information
PO Box 62
Oak Ridge, TN 37831

Prices available from (615) 576-8401, FTS 626-8401

Available to the public from
National Technical Information Service
US Department of Commerce
5285 Port Royal Rd
Springfield, VA 22161

NTIS price codes
Printed copy: A12
Microfiche copy: A01

Preliminary Performance Assessment for the Waste Isolation Pilot Plant, December 1992

Volume 2: Technical Basis

WIPP Performance Assessment Department
Sandia National Laboratories
Albuquerque, New Mexico 87185

ABSTRACT

Before disposing of transuranic radioactive waste in the Waste Isolation Pilot Plant (WIPP), the United States Department of Energy (DOE) must evaluate compliance with applicable long-term regulations of the United States Environmental Protection Agency (EPA). Sandia National Laboratories is conducting iterative performance assessments (PAs) of the WIPP for the DOE to provide interim guidance while preparing for a final compliance evaluation. This volume contains the technical basis for the 1992 PA. Specifically, it describes the conceptual basis for consequence modeling and the PA methodology, including the selection of scenarios for analysis, the determination of scenario probabilities, and the estimation of scenario consequences using a Monte Carlo technique and a linked system of computational models.

Additional information about the 1992 PA is provided in other volumes. Volume 1 contains an overview of WIPP PA and results of a preliminary comparison with the long-term requirements of the EPA's *Environmental Protection Standards for Management and Disposal of Spent Nuclear Fuel, High-Level and Transuranic Radioactive Wastes* (40 CFR 191, Subpart B). Volume 3 contains the reference data base and values for input parameters used in consequence and probability modeling. Volume 4 contains uncertainty and sensitivity analyses related to the preliminary comparison with 40 CFR 191B. Volume 5 contains uncertainty and sensitivity analyses of gas and brine migration for undisturbed performance. Finally, guidance derived from the entire 1992 PA is presented in Volume 6.

This volume of the report should be referenced as:

WIPP PA (Performance Assessment) Department. 1992. *Preliminary Performance Assessment for the Waste Isolation Pilot Plant, December 1992 — Volume 2: Technical Basis*. SAND92-0700/2. Albuquerque, NM: Sandia National Laboratories.

ACKNOWLEDGMENTS

The Waste Isolation Pilot Plant (WIPP) Performance Assessment (PA) Department is comprised of both Sandia National Laboratories (SNL) and contractor employees working as a team to produce preliminary comparison with Environmental Protection Agency (EPA) regulations, assessments of overall long-term safety of the repository, and interim technical guidance to the program. The on-site team, affiliations, and contributions to the 1992 performance assessment are listed in alphabetical order:

Performance Assessment Department

Name	Affil.*	Primary Author of Major Code	Area of Responsibility
R. Anderson	SNL		Department Manager
B. Baker	TEC		SEC02D, Hydrology, Office Manager
J. Bean	UNM		BRAGFLO, 2-Phase Flow
J. Berglund	UNM	CUTTINGS	Task Ldr., Cuttings/Cavings/Spallings, Engr. Mech.
S. Bertram-Howery	SNL		PA Liaison with DOE, Criteria Document, Test Phase Plan
W. Beyeler	SAI	PANEL, GARFIELD	Geostatistics, Analytical Models, CAMCON Systems Codes
K. Brinster	SAI		Geohydrology, Conceptual Models
R. Blaine	ECO		SEC02D, SEC0TP, & CAMCON Systems Codes
T. Blaine	GC		Drilling Technology, Exposure Pathways Data
K. Byle	UNM		Software and Analysis QA
J. Chapman	TRI		Documentation V.3
D. Duncan	MAC		Data QA
K. Economy	ECO		SEC02D, SEC0TP, Hydrology & Transport
D. Gallegos	SNL		Task Ldr., Hydrology, Geostatistics, NEA, PSAG
D. Galson	GS		NEA Working Groups, PSAG, PAAG, Human Intrusion
J. Garner	API	PANEL	Source Term, Sens. Anal.
A. Gilkey	UNM		CAMCON Systems Codes
L. Gomez	SNL		Task Ldr., Safety Assessments
M. Gruebel	TRI		EPA Regulations, Documentation V.1, Editor V.1
R. Guzowski	SAI		Geology, Scenario Construction
J. Helton	ASU	CCDFPERM	Task Ldr., Uncert./Sens. Anal., Probability Models, Editor V.4
S. Hora	UHH		Expert Elicitation, Probability Models
H. Iuzzolino	GC	CCDFCALC, CCDFPERM	LHS, CAMCON System Codes, Probability Models
R. Klett	SNL		EPA Regulations
P. Knupp	ECO	SEC0TP	Comp. Fluid Dyn.
M. LaVenue	INT	GRASP-INV	Hydrology/Geostatistics
C. Leigh	SNL	GENII-S	Exposure Pathways
M. Marietta	SNL		Dep. Dept. Manager, Tech. Coord.
G. de Marsily	UP		Geostatistics Expert Group Chair
R. McCurley	UNM		CAMCON System Codes
B. Napier	PNL	GENII	Safety Assessments
A. Peterson	SNL		Task Ldr., Inventory

Acknowledgments

B. RamaRao	INT	GRASP-INV	Geostatistics
J. Rath	UNM		CAMCON System Codes
R. Rechar	SNL		Task Ldr., CAMCON, QA
P. Roache	ECO	SECO	Task Ldr., Comp. Fluid Dyn.
D. Rudeen	UNM		STAFF2D, SECOTP, Transport
J. Ruge	ECO		Multigrid Methods/BRAGFLO
T. Russell	ECO		Upscaling
K. Salari	ECO	SECOTP	Transport, Computational Fluid Dynamics
J. Sandha	SAI		INGRES, PA Data Base
J. Schreiber	SAI		BRAGFLO, 2-Phase Flow
D. Scott	TRI		Documentation V.2
P. Swift	TRI		Task Ldr., Geology, Climate Var., Documenta- tion V.1 & 2, Editor V.1, 2, 4, & 5
M. Tierney	SNL		Task Ldr., CDF Constr., Probability Models, Ref. Data, Editor V.2 & 3
K. Trauth	SNL		Task Ldr., Expert Panels
P. Vaughn	API	BRAGFLO	Task Ldr., 2-Phase Flow & Waste Panel Chemistry, Editor V.4 & 5
T. Zimmerman	GRA		Geostatistics Test Problem

The foundation of the annual WIPP performance assessment is the underlying data set and understanding of the important processes in the engineered and natural barrier systems. Other SNL Departments are the primary source of these data and understanding. Assistance with the waste inventory comes from Westinghouse Electric Corporation and its contractors. We gratefully acknowledge the support of our departmental and project colleagues. Some individuals have worked closely with the performance assessment team, and we wish to acknowledge their contributions individually:

H. Batchelder	WEC	CH & RH Inventories
R. Beauheim	SNL	Natural Barrier System, Hydrologic Parameters
D. Borns	SNL	Geology, Geophysics
B. Butcher	SNL	Engineered Barrier System, Unmodified Waste-Form Parameters, Disposal Room Systems Parameters
L. Brush	SNL	Engineered Barrier System, Source Term (Solubility) and Gas Generation Parameters
L. Clements	ReS	Computer System Support
T. Corbet	SNL	Natural Barrier System, Geologic & Hydrologic Parameters, Conceptual Models
P. Davies	SNL	Natural Barrier System, Hydrologic & Transport Parameters, & 2-Phase Flow Mechanistic Modeling
P. Drez	DE	CH & RH Inventories
R. Finley	SNL	Repository Isolation Systems Parameters
F. Gelbard	SNL	Natural Barrier System, Retardation
E. Gorham	SNL	Natural Barrier System, Fluid Flow & Transport Parameters
R. Holt	CON	Geology
S. Howarth	SNL	Natural Barrier System, Hydrologic Parameters
R. Kehrman	WEC	Ch & RH Waste Characterization
K. Lickliter	BEC	EPA Regulations
R. Lincoln	SNL	Room Modeling
F. Mendenhall	SNL	Engineered Barrier System, Unmodified Waste Form Parameters, Waste Panel Closure (Expansion)
D. Munson	SNL	Reference Stratigraphy, Constitutive Models, Physical & Mechanical Parameters
C. Novak	SNL	Natural Barrier Systems, Chemistry
E. Nowak	SNL	Room Modeling, Source Term
J. Orona	ReS	Computer System Support
A. Stevens	SNL	DOE Liaison
J. Tillerson	SNL	Repository Isolation Systems Parameters

W. Wawersik SNL Fracturing
 S. Webb SNL 2-Phase Flow Sensitivity Analysis & Benchmarking

*** Affiliation**

API = Applied Physics Incorporated	ReS = ReSpec
ASU = Arizona State University	SAI = Scientific Applications International Corporation
BEC = Benchmark Environmental Corp.	SNL = Sandia National Laboratories
CON = Consultant	TEC = Technadyne Engineering Consultants
DE = Drez Environmental	TRI = Tech Reps, Inc.
ECO = Ecodynamics Research Associates	UHH = University of Hawaii at Hilo
GC = Geo-Centers Incorporated	UNM = University of New Mexico/New Mexico Engineering Research Institute
GRA = GRAM, Inc.	UP = University of Paris
GS = Galson Sciences	WEC = Westinghouse Electric Corporation
INT = Intera	
MAC = MACTEC	
PNL = Pacific Northwest Laboratory	

Peer Review

Internal/Sandia

L. Gomez
 D. Schafer

Management/Sandia

W. Weart

PA Peer Review Panel

R. Heath, Chair
 R. Budnitz
 T. Cotton
 J. Mann
 T. Pigford
 F. Schwartz

University of Washington
 Future Resources Associates, Inc.
 JK Research Associates, Inc.
 University of Illinois
 University of California, Berkeley
 Ohio State University

Department of Energy

R. Becker

Expert Panels

Futures

M. Baram
 W. Bell
 G. Benford
 D. Chapman
 B. Cohen
 V. Ferkiss
 T. Glickman
 T. Gordon
 C. Kirkwood
 H. Otway

Boston University
 Yale University
 University of California, Irvine
 The World Bank, Cornell University
 University of Pittsburgh
 Georgetown University
 Resources for the Future
 Futures Group
 Arizona State University
 Joint Research Center (Ispra), Los Alamos National
 Laboratory

Acknowledgments

M. Pasqualetti
D. Reicher
N. Rosenberg
M. Singer
T. Taylor
M. Vinovskis

Arizona State University
Natural Resources Defense Council
Resources for the Future
The Potomac Organization
Consultant
University of Michigan

Markers

D. Ast
V. Baker
M. Brill

F. Drake
B. Finney
D. Givens
W. Goodenough
M. Kaplan
J. Lomborg
L. Narens
F. Newmeyer
W. Sullivan
W. Williams

Cornell University
University of Arizona
Buffalo Organization for Social and Technological
Innovation
University of California at Santa Cruz
University of Hawaii at Manoa
American Anthropological Association
University of Pennsylvania
Eastern Research Group
Consultant
University of California at Irvine
University of Washington
University of Washington
Case Western Reserve University

Source Term

C. Bruton
I-Ming Chou
D. Hobart
F. Millero

Lawrence Livermore National Laboratory
U.S. Geological Survey
Los Alamos National Laboratory
University of Miami

Retardation

R. Dosch
C. Novak
M. Siegel

Sandia National Laboratories
Sandia National Laboratories
Sandia National Laboratories

Geostatistics Expert Group

G. de Marsily, Chair
R. Bras
J. Carrera
G. Dagan
A. Galli
S. Gorlick
P. Grindrod
A. Gutjahr
D. McLaughlin
S. Neuman
C. Ravenne
Y. Rubin

U. of Paris
Massachusetts Inst. of Tech.
U. Polit cnica de Catalu a
Tel Aviv U.
Ecole des Mines de Paris
Stanford U.
Intera Sciences
New Mexico Tech
Massachusetts Inst. of Tech.
U. of Arizona
Institut Fran ais du P trole
U. of California, Berkeley

Report Preparation (TRI)

Volume 1: M. Minahan (text); D. Marchand (illustrations)
Volume 2: M. Minahan (text); D. Marchand (illustrations)
Volume 3: J. Chapman (text); D. Marchand (illustrations)

D. Rivard and the Word Processing Department
R. Rohac, R. Andree, and the Illustration and Computer Graphics Departments
S. Tullar and the Production Department

CONTENTS

1. Introduction.....	1-1
1.1 Purpose of Volume 2.....	1-1
1.2 Organization of Volume 2.....	1-1
1.3 Code Linkage and Data Flow.....	1-3
1.3.1 Data Bases.....	1-4
1.3.2 Program Linkage and Model Applications.....	1-4
2. Conceptual Basis for Consequence Modeling.....	2-1
2.1 Introduction.....	2-1
2.1.1 Conceptual Models.....	2-1
2.1.2 Chapter Organization.....	2-2
2.2 Natural Barrier System.....	2-2
2.2.1 Regional Geology.....	2-2
2.2.2 Stratigraphy.....	2-10
2.2.2.1 Bell Canyon Formation.....	2-10
2.2.2.2 Capitan Limestone.....	2-10
2.2.2.3 Castile Formation.....	2-11
2.2.2.4 Salado Formation.....	2-11
2.2.2.5 Rustler-Salado Contact Zone.....	2-12
2.2.2.6 Rustler Formation.....	2-12
The Unnamed Lower Member.....	2-14
Culebra Dolomite Member.....	2-16
Tamarisk Member.....	2-23
Magenta Dolomite Member.....	2-23
Forty-niner Member.....	2-24
2.2.2.7 Supra-Rustler Rocks.....	2-24
2.2.3 Hydrology.....	2-26
2.2.3.1 Present Climate.....	2-26
2.2.3.2 Paleoclimates and Climatic Variability.....	2-26
2.2.3.3 Surface Water.....	2-29
2.2.3.4 The Water Table.....	2-29
2.2.3.5 Regional Water Balance.....	2-29
2.2.3.6 Groundwater Flow Above the Salado Formation.....	2-30
Potentiometric Surfaces.....	2-30
Groundwater Geochemistry.....	2-34
Recharge and Discharge.....	2-36
2.2.4 Radionuclide Transport in the Culebra Dolomite.....	2-38
2.2.4.1 Expert Judgment Elicitation for K_d s.....	2-39
2.2.4.2 Planned and Ongoing Experimental Work Related to Radionuclide Transport in the Culebra.....	2-40
2.3 Engineered Barrier System.....	2-41
2.3.1 The Salado Formation at the Repository Horizon.....	2-41
2.3.2 Repository and Seal Design.....	2-45
2.3.2.1 Waste Characterization.....	2-45
2.3.2.2 Seals.....	2-48
2.3.2.3 Backfill.....	2-48
2.3.2.4 Engineered Alternatives.....	2-50
2.3.3 Radionuclide Inventory.....	2-50
2.3.4 Radionuclide Solubility and the Source Term for Transport Calculations.....	2-52
2.3.4.1 Expert Judgment Elicitation.....	2-52
2.3.4.2 Experimental Work.....	2-55
2.3.5 Creep Closure, Fluid Flow, and Room/Waste Interactions.....	2-55

Contents

- 3. Performance Assessment Methodology 3-1
 - 3.1 Conceptualization of Risk for the WIPP Performance Assessment 3-1
 - 3.1.1 Calculation of Risk 3-2
 - 3.1.2 Characterization of Uncertainty in Risk 3-4
 - 3.1.3 Risk and the EPA Limits..... 3-8
 - 3.2 Selection of Scenarios 3-9
 - 3.2.1 Conceptual Basis for Scenario Development..... 3-9
 - 3.2.2 WIPP Performance-Assessment Approach to Scenario Development 3-13
 - 3.3 Determination of Scenario Probabilities 3-15
 - 3.4 Calculation of Scenario Consequences 3-16
 - 3.5 Monte Carlo Analysis Techniques..... 3-16
 - 3.5.1 Selection of Variables and Their Ranges and Distributions 3-19
 - 3.5.2 Generation of the Sample..... 3-21
 - 3.5.3 Propagation of the Sample through the Analysis..... 3-21
 - 3.5.4 Uncertainty Analysis..... 3-22
 - 3.5.5 Sensitivity Analysis 3-22

- 4. Scenario Construction 4-1
 - 4.1 Evaluation of Events and Processes 4-1
 - 4.1.1 Identifying Events and Processes 4-1
 - 4.1.2 Classifying Events and Processes 4-3
 - 4.1.3 Screening Events and Processes..... 4-3
 - 4.1.4 Summary of Screened Events and Processes..... 4-4
 - 4.2 Summary Scenarios 4-7
 - 4.2.1 Development of Summary Scenarios..... 4-7
 - 4.2.2 Screening of Summary Scenarios 4-9
 - 4.2.3 Retained Summary Scenarios..... 4-10
 - 4.2.3.1 Undisturbed Summary Scenario (S_B) 4-10
 - Guidance from 40 CFR 191 4-10
 - Base-Case Description..... 4-11
 - 4.2.3.2 Human-Intrusion Summary Scenarios..... 4-13
 - Guidance from 40 CFR 191 4-13
 - Intrusion Borehole through a Room or Drift into Pressurized
Brine in the Castile Formation (Summary Scenario E1) 4-13
 - Intrusion Borehole into a Room or Drift (Summary Scenario E2)..... 4-15
 - Intrusion Borehole through a Room or Drift into Pressurized
Brine in the Castile Formation and Another Intrusion Borehole
into the Same Panel (Summary Scenario E1E2) 4-15
 - 4.2.4 Computational Approximations of Scenarios E1, E2, and E1E2..... 4-18

- 5. Drilling Intrusion Probabilities 5-1
 - 5.1 Introduction 5-1
 - 5.2 Probability Computations..... 5-2
 - 5.3 Lambda Function Generation 5-5
 - 5.3.1 The Expert Judgment Process 5-5
 - 5.3.2 Algorithm for Generating Lambda Functions..... 5-7
 - 5.3.3 Use of the Lambda Functions 5-8

- 6. Data and CDFs..... 6-1
 - 6.1 Conventions 6-1
 - 6.1.1 Probability Distribution Functions..... 6-1
 - 6.1.2 Empirical Distribution Functions 6-2
 - 6.1.3 Range 6-2
 - 6.1.4 Mean and Sample Mean..... 6-2
 - 6.1.5 Median and Sample Median..... 6-2
 - 6.1.6 Variance and Coefficient of Variation 6-2

6.1.7	Categories of Distributions	6-3
6.1.7.1	Continuous Distributions.....	6-3
6.1.7.2	Discrete Distributions.....	6-4
6.1.7.3	Constructed Distributions (Data).....	6-4
6.1.7.4	Constructed Distributions (Subjective).....	6-4
6.1.7.5	Miscellaneous Categories.....	6-4
6.2	Selection of Parameter Distributions	6-5
6.2.1	Requests for Data from Sandia Investigators and Analysts	6-5
6.2.2	Construction of Distributions.....	6-6
6.2.3	Some Limitations on Distributions	6-6
7.	Consequence Modeling	7-1
7.1	Radioactive Decay.....	7-1
7.2	Multiphase Flow Through Porous Media	7-1
7.2.1	Features and Capabilities of BRAGFLO	7-2
7.2.2	Interaction of Important Repository Processes.....	7-3
7.2.3	General Assumptions Used in 1992 PA Two-Phase Flow Modeling.....	7-3
7.3	Waste-Filled Room Deformation	7-5
7.4	Waste Mobilization.....	7-7
7.4.1	Assumptions.....	7-7
7.4.2	Simplified Mathematical Model	7-9
7.5	Groundwater Transmissivity Fields	7-10
7.5.1	Unconditional Simulation.....	7-10
7.5.2	Conditional Simulation.....	7-11
7.5.3	Automated Calibration	7-11
7.6	Groundwater Flow and Transport	7-13
7.6.1	Groundwater Flow in the Culebra.....	7-15
7.6.1.1	Boundary Conditions.....	7-16
7.6.1.2	Effects of Climate Change.....	7-16
7.6.2	Solute Transport in Culebra	7-18
7.6.2.1	Modeling Hydrodynamic Dispersion.....	7-18
7.6.2.2	Modeling Chemical Sorption in Fracture Flows	7-21
7.7	Direct Removal of Waste	7-23
7.7.1	Cuttings.....	7-25
7.7.2	Cavings.....	7-25
7.7.2.1	Laminar Flow.....	7-25
7.7.2.2	Turbulent Flow.....	7-26
7.7.3	Spallings.....	7-27
8.	References.....	8-1
Appendix A:	BRAGFLO and PANEL	A-1
Appendix B:	SANCHO.....	B-1
Appendix C:	SECO Flow and Transport Model.....	C-1
Appendix D:	Culebra Transmissivity Field Simulations	D-1

Figures

1-1	1992 Organization of Programs in CAMCON	1-5
2-1	Generalized geology of the Delaware Basin, showing the location of the Capitan Reef and the erosional limits of the basinal formations	2-4
2-2	Geologic time scale	2-5
2-3	Stratigraphy of the Delaware Basin	2-6
2-4	Schematic east-west cross section through the northern Delaware Basin	2-7

Contents

2-5	Schematic north-south cross section through the northern Delaware Basin.....	2-8
2-6	Map of the WIPP vicinity showing the land-withdrawal area (labeled “WIPP Boundary”), the study area of Brinster, and the location of observation wells.....	2-9
2-7	East-west cross section showing stratigraphy of the Rustler Formation and the Dewey Lake Red Beds	2-13
2-8	Rustler Formation halite around the WIPP.....	2-15
2-9	Log hydraulic conductivities of the Culebra Dolomite Member of the Rustler Formation... ..	2-17
2-10	Sources of geologic information about the Culebra Dolomite	2-18
2-11	Isopach overburden for the Culebra Dolomite Member.....	2-20
2-12	Interpreted extent of Salado dissolution.....	2-21
2-13	Percentage of natural fractures in the Culebra Dolomite Member filled with gypsum.....	2-22
2-14	Log hydraulic conductivities of the Magenta Dolomite Member of the Rustler Formation..	2-25
2-15	Estimated mean annual precipitation at the WIPP during the Late Pleistocene and Holocene.....	2-28
2-16	Adjusted potentiometric surface of the Rustler-Salado contact zone in the WIPP vicinity....	2-31
2-17	Adjusted potentiometric surface of the Culebra Dolomite Member of the Rustler Formation in the WIPP vicinity.....	2-32
2-18	Adjusted potentiometric surface of the Magenta Dolomite Member of the Rustler Formation in the WIPP vicinity.....	2-33
2-19	Hydrochemical facies in the Culebra Dolomite Member of the Rustler Formation.....	2-35
2-20a	Reference local stratigraphy near repository	2-43
2-20b	Stratigraphy at the repository horizon.....	2-44
2-21	Plan view of waste-disposal horizon showing shaft, drift, and panel seal locations	2-46
2-22	Representative shaft and plug seals	2-49
3-1	Estimated CCDF for consequence result CS	3-3
3-2	Example distribution of CCDFs obtained by sampling imprecisely known variables.....	3-6
3-3	Example summary curves derived from an estimated distribution of CCDFs	3-7
3-4	Decomposition of the sample space S into high-level subsets	3-10
3-5	Construction of a CCDF for comparison with the EPA release limits	3-12
3-6	Models used in 1992 WIPP performance assessment	3-17
3-7	Distribution function for an imprecisely known analysis variable	3-20
3-8	Example of box plots.....	3-23
4-1	Potential scenarios for the WIPP disposal system.....	4-8
4-2	Conceptual model used in simulating undisturbed performance.....	4-12
4-3	Conceptual model for scenario E1.....	4-14
4-4	Conceptual model for scenario E2.....	4-16
4-5	Conceptual model for scenario E1E2.....	4-17
5-1	A realization of effective drilling intensity $\lambda(t)$ and its associated integrated effective drilling intensity as functions of time.....	5-9
7-1	Interaction of some important repository processes	7-4
7-2	Surface giving porosity of waste-filled disposal room as a function of total volume of gas produced and time after sealing.....	7-6
7-3	Idealized collapsed WIPP panel in a PANEL model	7-8
7-4	Conceptual hydrologic model of the Culebra Dolomite Member.....	7-14
7-5	Example of regional and local grids used for disturbed fluid flow and transport calculations.....	7-17
7-6	Rotary drilling.....	7-24

Tables

2-1	Properties of the Rustler Formation Units and Rustler-Salado Contact Zone.....	2-14
3-1	Summary of Computer Models Used in the 1992 WIPP Performance Assessment	3-18
4-1	Potentially Disruptive Events and Processes.....	4-2
4-2	Summary of Screened Events and Processes.....	4-5

1. INTRODUCTION

The Waste Isolation Pilot Plant (WIPP) is planned as a research and development facility to demonstrate the safe disposal of transuranic (TRU) wastes generated by defense programs of the United States Department of Energy (DOE). Before disposing of waste in the WIPP, the DOE must evaluate compliance with applicable long-term regulations of the United States Environmental Protection Agency (EPA), including 40 CFR 191 Subpart B (*Environmental Radiation Protection Standards for Management and Disposal of Spent Nuclear Fuel, High-Level and Transuranic Radioactive Wastes*) [U.S. EPA, 1985]) and 40 CFR 268.6 (U.S. EPA, 1986), which is the portion of the *Land Disposal Restrictions of the Hazardous and Solid Waste Amendments to the Resource Conservation and Recovery Act (RCRA)* that states the conditions for disposal of specified hazardous wastes. Performance assessments (PAs) will form the basis for evaluating compliance with all applicable long-term regulations of the EPA. The WIPP Performance Assessment (PA) Department of Sandia National Laboratories (SNL) is performing annual iterative preliminary PAs to provide guidance to the Project while preparing for final compliance evaluation. The 1991 preliminary performance assessment for comparison with 40 CFR 191B was documented in 4 volumes (WIPP PA Division, 1991 a, b, c; Helton et al., 1992).

1.1 Purpose of Volume 2

This volume describes the technical basis for the 1992 WIPP preliminary PA: conceptual model development, probability modeling, and consequence modeling of the WIPP disposal system for evaluating compliance with the quantitative requirements of applicable long-term regulations. Volume 1 deals primarily with the regulations in Subpart B of 40 CFR Part 191 and their application to the WIPP, but also summarizes aspects of this volume and explains the 1992 status of the WIPP PA. Volume 3 compiles model parameters, constructs cumulative distribution functions (cdfs) and discusses their derivation from the pertinent data of disposal system characterization. Uncertainty and sensitivity analysis results related to 40 CFR 191B are discussed in Volume 4. Uncertainty and sensitivity analysis results of gas and brine migration for undisturbed performance are discussed in Volume 5. Finally, guidance derived from the entire 1992 PA is presented in Volume 6.

1.2 Organization of Volume 2

Volume 2 consists of seven chapters and four appendices. This chapter (Chapter 1) describes the organization of Volume 2. The remaining six chapters are organized following the PA methodology described in Volume 1.

- Chapter 2 (Conceptual Basis for Consequence Modeling) describes the conceptual basis for consequence modeling. This chapter is a detailed expansion of the brief discussion in Chapter 2 of Volume 1, and provides a bibliographic mapping into the published literature of the site characterization and engineered design programs.
- Chapter 3 (Performance Assessment Methodology) describes the conceptual model for risk that forms the framework (scenarios, frequency or probability of scenarios, and consequences of scenarios) for the WIPP

- 1 PA, presents an outline of the Monte Carlo technique that is used for uncertainty and sensitivity analyses,
2 and discusses the construction of complementary cumulative distribution functions (CCDFs). This chapter
3 is a detailed expansion of Chapter 4 of Volume 1, and is generally unchanged from the 1991 PA.
- 4 • Chapter 4 (Scenario Construction) examines the first element (scenarios) of the conceptual model for risk.
5 This chapter discusses the application of the methodology for scenario construction—identifying, screening,
6 and classifying events and processes; developing scenarios using a logic diagram; and screening of scenarios
7 —for the WIPP. Retained scenarios that are analyzed in the 1992 PA are described. This material is
8 generally unchanged from the 1991 PA and therefore references previous documents extensively. Scenarios
9 included in the Monte Carlo analysis in 1991 are included again in 1992.
 - 10 • Chapter 5 (Drilling Intrusion Probabilities) examines the second element (probabilities or frequencies of
11 scenarios) of the conceptual model for risk. The probability model that is used for the 1992 analysis was
12 presented in the 1991 documentation, so this chapter is a much briefer description that references previous
13 documentation. The significant difference in the application of this model is that time-varying drilling
14 intensities were used in 1992, whereas in 1991 only constant, but imprecisely known, drilling intensities
15 were used. A brief discussion of how these new drilling intensity functions were derived from expert panel
16 output that references material in Volume 3 is included.
 - 17 • Chapter 6 (Data and cdfs) begins the description of the different steps of the Monte Carlo technique:
18 selection of imprecisely known parameters, construction of ranges and distributions for these parameters,
19 generation of the sample, propagation of uncertainty through the system model, uncertainty analysis, and
20 sensitivity analysis. This chapter briefly describes the first steps: selection of imprecisely known
21 parameters and construction of their ranges and distributions. The entire data base, especially model
22 parameters, is the subject of Volume 3.
 - 23 • Chapter 7 (Consequence Modeling) describes the modeling system that is used to calculate consequences of
24 scenarios. The Latin hypercube sampling technique that is used to generate the sample for Monte Carlo
25 analysis is described elsewhere (Helton et al., 1991) and is not repeated. This chapter focuses on the 1992
26 modeling system through which uncertainty is propagated for the uncertainty and sensitivity analysis. Each
27 major module of this system is described in terms of governing equations and modeling assumptions.
28 More detailed code descriptions are contained in the four appendices as follows:
- 29 Appendix A. A repository and shaft seal module is used that simulates two-phase (gas and brine) flow
30 through the repository, shaft seals, and surrounding environs (BRAGFLO) with an equilibrium-
31 mixing cell for calculating radionuclide concentrations in the brine phase (PANEL). These
32 codes were used in the 1991 PA.
- 33 Appendix B. A module (SANCHO) for simulating quasistatic, large-deformation, inelastic response of the
34 halite is used to provide waste porosity as a function of time. These calculations incorporate
35 the effect of creep closure and of halite response to waste-generated gas into the PA; they are
36 performed outside the Monte Carlo analysis. Only the waste porosity functions are used during

1 consequence calculations. This is the first year that the effects of halite creep have been
2 included in PA calculations.

3 Appendix C. Groundwater flow and transport models (SECO-2DH and SECO-TP) are used to calculate
4 subsurface transport through the Culebra Dolomite Member of the Rustler Formation to the
5 land-withdrawal boundary. First, the groundwater flow is calculated for a single-porosity,
6 matrix-only, porous medium (dolomite). The flow calculation is performed first on a regional
7 scale and second on a local scale with boundary conditions derived from the regional-scale
8 distribution. Climate variability enters through time-varying boundary conditions that are
9 based on a simple precipitation/recharge conceptualization. Spatial variability enters by
10 drawing one field from a set of multiple, plausible transmissivity fields that are generated
11 outside the Monte Carlo analysis (GRASP-INV). SECO-2DH was used in the 1991 PA.

12 Second, the flow field is used for a radionuclide-transport simulation. The transport simulator
13 SECO-TP was used for the first time in 1992. It models single- or dual-porosity transport
14 through an idealized, fractured medium. Retardation in pore volume of the dolomite matrix
15 and/or the fracture-lining clay can be included simultaneously or separately. SECO-TP is a
16 further improvement over previous capability in that it is more accurate and numerically
17 efficient, allowing higher-resolution, higher-accuracy simulations in the same time.

18 Appendix D. A module (GRASP-INV) for generating multiple, plausible transmissivity fields to be used by
19 SECO-2DH is used for the first time in 1992. This module is an improvement over previous
20 capability in that it produces transmissivity fields that reproduce the measured values of
21 transmissivity at well locations and that are calibrated, i.e., flow calculations with these fields
22 reproduce (to within a pre-selected criterion) steady-state and transient pressure data at the well
23 locations. Therefore, each field is a plausible realization of the true but unknown transmissivity
24 field. One entire field is drawn and used for a single consequence calculation during the Monte
25 Carlo analysis.

26 **1.3 Code Linkage and Data Flow**

27 The complexity of the compliance-assessment modeling system for the WIPP requires that calculations be
28 controlled by an executive program (Rechard, 1989; Rechard et al., 1989; Rechard, 1992). CAMCON
29 (Compliance Assessment Methodology CONTroller) controls code linkage and data flow during lengthy and
30 iterative consequence analyses, minimizes analyst intervention during data transfer, and automatically handles
31 quality assurance during the calculations. CAMCON currently consists of about 75 codes and FORTRAN object
32 libraries; it includes approximately 293,000 lines of FORTRAN software written specifically for the WIPP
33 Project and another 175,000 lines of software adapted from other applications.

34 The controller allows easy examination of intermediate diagnostics and final results. Computer modules
35 within the executive program can be easily replaced for model comparisons. CAMCON modularizes tasks so
36 computer programs for a particular module are interchangeable. CAMCON is fully described in Rechard (1992).

1 **1.3.1 Data Bases**

2 Three data bases, primary, secondary, and computational, are included in CAMCON. The primary data base
3 contains measured field and laboratory data gathered during the disposal-system and regional characterization.
4 Because the analysis can be no better than these data, the data base should contain all necessary data for the
5 compliance assessment and repository design, have as little subjective interpretation as possible, and be quality
6 assured. Data base structure must be flexible to accommodate different organizations and unforeseen types of data.
7 Practical experience suggests that a relational data base is best.

8 The secondary data base contains interpreted data, usually interpolated onto a regular grid, and incorporates
9 information that comprises the conceptual model of the disposal system. Levels of interpretation can vary from
10 objective interpolation of data combined with subjective judgments to totally subjective extrapolations of data; all
11 interpretations are well documented to ensure the secondary data is reproducible by others. Data from literature or
12 professional judgment are used to fill knowledge gaps to complete the conceptual model. The secondary data base
13 must be accessible to both the analyst and the executive package controlling the system.

14 The computational data base is CAMDAT (Compliance Assessment Methodology DATA). CAMDAT uses a
15 neutral-file format so that a series of computer programs can be linked by a "zig-zag" connection rather than the
16 usual serial connection. The file format chosen for CAMDAT was based on GENESIS (Taylor et al., 1987) and
17 EXODUS and their associated data manipulation and plotting programs (Gilkey, 1986a,b, 1988; Gilkey and
18 Flanagan, 1987). CAMDAT is fully described in Rechar (1992).

19 **1.3.2 Program Linkage and Model Applications**

20 Program linkage and data flow through CAMDAT are controlled by CAMCON. Computer programs that
21 make up the CAMCON system are major program modules, support program modules, and translators. Major
22 program modules refer to programs that represent major tasks of the consequence modeling. Support program
23 modules refer to programs such as interpolators that are necessary to facilitate use of major program modules.
24 Translator program modules refer to programs that translate data either into or out of the computational data base.
25 Figure 1-1 shows how programs are used in the 1992 PA to evaluate human-intrusion scenarios. BRAGFLO,
26 GRASP-INV, SECO-TP, and CUTTINGS were run outside of CAMCON, with manual data transfer. GENII-S
27 was not used because a safety assessment was not included in the 1992 PA. All other codes were used within
28 CAMCON as shown (Figure 1-1).

2. CONCEPTUAL BASIS FOR CONSEQUENCE MODELING

2.1 Introduction

2.1.1 Conceptual Models

This chapter describes the conceptual basis for modeling the performance of the WIPP repository, the waste it contains, and the surrounding geology and hydrology, and summarizes the available knowledge of the site and the physical processes that operate there. This knowledge forms the framework for the preferred conceptual model used in WIPP PA (i.e., the model believed by the WIPP PA Department to be the most realistic representation for the behavior of the disposal system), and for alternative conceptual models. Conceptual model and alternative conceptual models are defined as follows (Gallegos et al., 1992; NEA, 1992):

- Conceptual model: A set of qualitative assumptions used to describe a system or subsystem for a given purpose. At a minimum, these assumptions concern the geometry and dimensionality of the system, initial and boundary conditions, time dependence, and the nature of the relevant physical and chemical processes. The assumptions should be consistent with one another and with existing information within the context of the given purpose.
- Alternative conceptual models: Alternative sets of assumptions that describe the same system for the same purpose, where each set of assumptions is consistent with the existing information.

Each alternative conceptual model identifies the processes that the mathematical models must characterize and provides the context within which the mathematical models must operate.

As an example of the role alternative conceptual models play in performance assessment, Volume 1 of the 1992 WIPP PA documents the use of three alternative conceptual models for the subsurface transport of radionuclides in the Culebra Dolomite Member of the Rustler Formation. (See Section 2.2 for an explanation of the regional geohydrology, Section 4.2 for an explanation of the transport pathway, and Section 7.6 for a discussion of the transport model. See Section 5.1 of Volume 1 of this report for a comparison of disposal-system performance estimated using each of the three conceptual models. See Volume 4 of this report for additional analysis of these and other alternative conceptual models.) In the first conceptual model, transport occurs only in clay-lined fractures in a single-porosity medium, and chemical retardation does not occur. In the second conceptual model, transport occurs in a dual-porosity medium (clay-lined fractures and matrix); radionuclides may diffuse into the pore volume of both the clay linings and the rock matrix. Chemical retardation does not occur. In the third conceptual model, believed by the WIPP PA Department to be the most realistic representation for the behavior of the system, transport occurs in a dual-porosity medium, as in the second conceptual model, except that chemical retardation does occur as a result of sorption of radionuclides in both clay linings and rock matrix.

1 The first of these three alternative conceptual models is not supported by available information (see Section
2 2.2.4), and is included in the analysis as an unrealistic, but known, endpoint of a continuum on which a realistic
3 endpoint is unknown. As such, it provides useful guidance on the largest releases that may be anticipated as a
4 result of groundwater transport in the Culebra. Comparison of all three conceptual models provides insight into
5 the uncertainty in performance estimates resulting from an incomplete understanding of the dual-porosity behavior
6 of the Culebra and the lack of defensible data describing chemical retardation of radionuclides (see Section 2.2.4).

7 Other major aspects of the conceptual model for the WIPP used in the 1992 PA include the following:
8 generation of gas in the waste-emplacements panels by degradation of waste and containers; closure and re-
9 expansion of the panels by salt creep; the release of radionuclides at the ground surface and into the Culebra as a
10 result of borehole intrusion during exploratory drilling; changes in groundwater flow resulting from future climatic
11 changes; and the effect of passive marker systems on intrusion rates.

12 2.1.2 Chapter Organization

13 The WIPP and surrounding environment provide multiple barriers to radionuclide migration. This chapter
14 explains the WIPP PA's present understanding of the conceptual basis of these barriers. The chapter is organized
15 into two major parts:

- 16 • natural barrier system (Section 2.2)—the regional geology and hydrology surrounding the WIPP (Section
17 2.2.1); the stratigraphy below and above the repository (Section 2.2.2); climate, water balance, and
18 groundwater flow in the WIPP vicinity (Section 2.2.3); and radionuclide transport in the Culebra Dolomite
19 (Section 2.2.4)
- 20 • engineered barrier system (Section 2.3)—the repository and seal design (Section 2.3.2); the waste itself
21 (Section 2.3.3); the radionuclide source term (Section 2.3.4); and closure, flow, and room/waste interactions
22 (Section 2.3.5)

23 2.2 Natural Barrier System

24 2.2.1 Regional Geology

25 The geology of the WIPP and the surrounding area has been introduced briefly in Chapter 2 of Volume 1, and
26 is described elsewhere in detail (e.g., Hiss, 1975; Powers et al., 1978a,b; Cheeseman, 1978; Williamson, 1978;
27 Hills, 1984; Ward et al., 1986; Harms and Williamson, 1988; Holt and Powers, 1988, 1990; Beauheim and Holt,
28 1990; Brinster, 1991). The brief review presented here describes regional structural features and introduces the
29 major stratigraphic units. Specific geologic features that affect compliance-assessment modeling are described in
30 subsequent sections of this chapter.

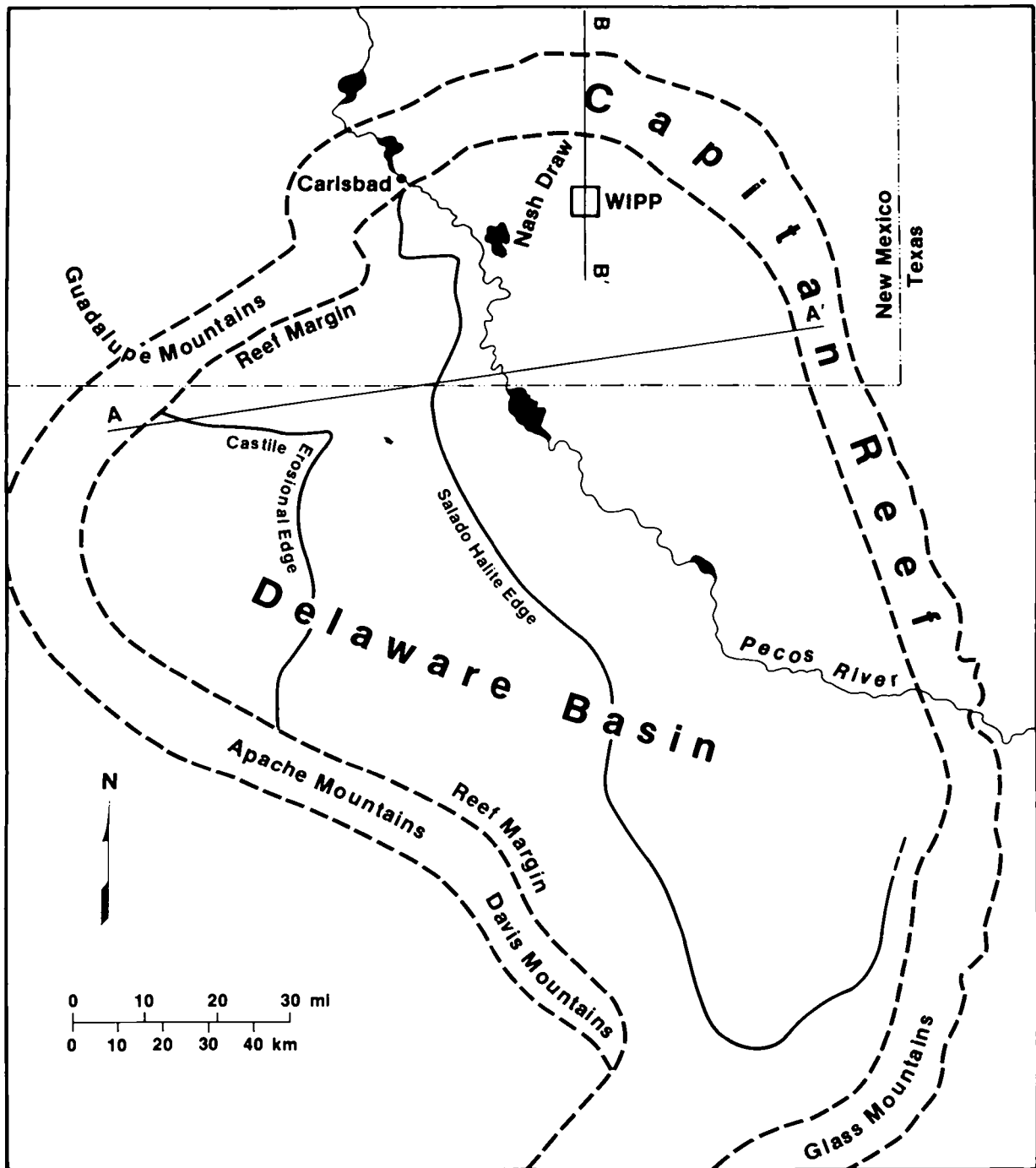
1 The WIPP is located near the northern end of the Delaware Basin, a structural depression that formed during
 2 the Late Pennsylvanian and Permian Periods, approximately 300 to 245 million years ago (Figures 2-1 and 2-2).
 3 Sedimentation within the subsiding basin resulted in the deposition of up to 4,000 m (13,000 ft) of marine strata.
 4 Organic activity at the basin margins produced massive carbonate reefs that separated deep-water facies from the
 5 shallow-water shelf sediments deposited landward.

6 Permian-age rocks of importance to WIPP performance-assessment modeling are those of the Guadalupian and
 7 Ochoan Series, deposited between approximately 265 and 245 million years ago (Figure 2-3). During this time
 8 subsidence in the Delaware Basin was initially rapid, resulting in deposition of deep-water shales, sandstones, and
 9 limestones of the Delaware Mountain Group. Intermittent connection with the open ocean and a decrease in
 10 clastic sediment supply, possibly in response to regional tectonic adjustments, led to the deposition of a thick
 11 evaporite sequence. Anhydrites and halites of the Castile Formation are limited to the structurally deeper portion
 12 of the basin, enclosed within the reef-facies rocks of the Capitan Limestone. Subsidence within the basin slowed
 13 in Late Permian time, and the halites of the Salado Formation, which include the host strata for the WIPP, extend
 14 outward from the basin center over the Capitan Reef and the shallow-water shelf facies. Latest Permian-age
 15 evaporites, carbonates, and clastic rocks of the Rustler Formation and the Dewey Lake Red Beds record the end of
 16 regional subsidence and include the last marine rocks deposited in southeastern New Mexico during the Paleozoic.
 17 The overlying sandstones of the Triassic-age Dockum Group reflect continental deposition and mark the onset of a
 18 period of regional tectonic stability that lasted approximately 240 million years, until late in the Tertiary Period.

19 Permian-age strata of the Delaware Basin now dip gently (generally less than 1°) to the east, and erosion has
 20 exposed progressively older units toward the western edge of the basin (Figures 2-1 and 2-4). This tilting reflects
 21 the Late Pliocene and early Pleistocene (approximately 3.5 million to 1 million years ago) uplift of the Capitan
 22 Reef to form the Guadalupe Mountains more than 60 km (37 miles) west of the WIPP (Figures 2-1, 2-4). Field
 23 evidence suggests that additional uplift may have occurred during the late Pleistocene and Holocene, and some
 24 faults of the Guadalupe Mountains may have been active within the last 1,000 years (Powers et al., 1978a,b).
 25 North and east of the WIPP, the Capitan Reef has not been uplifted and remains in the subsurface (Figure 2-5).

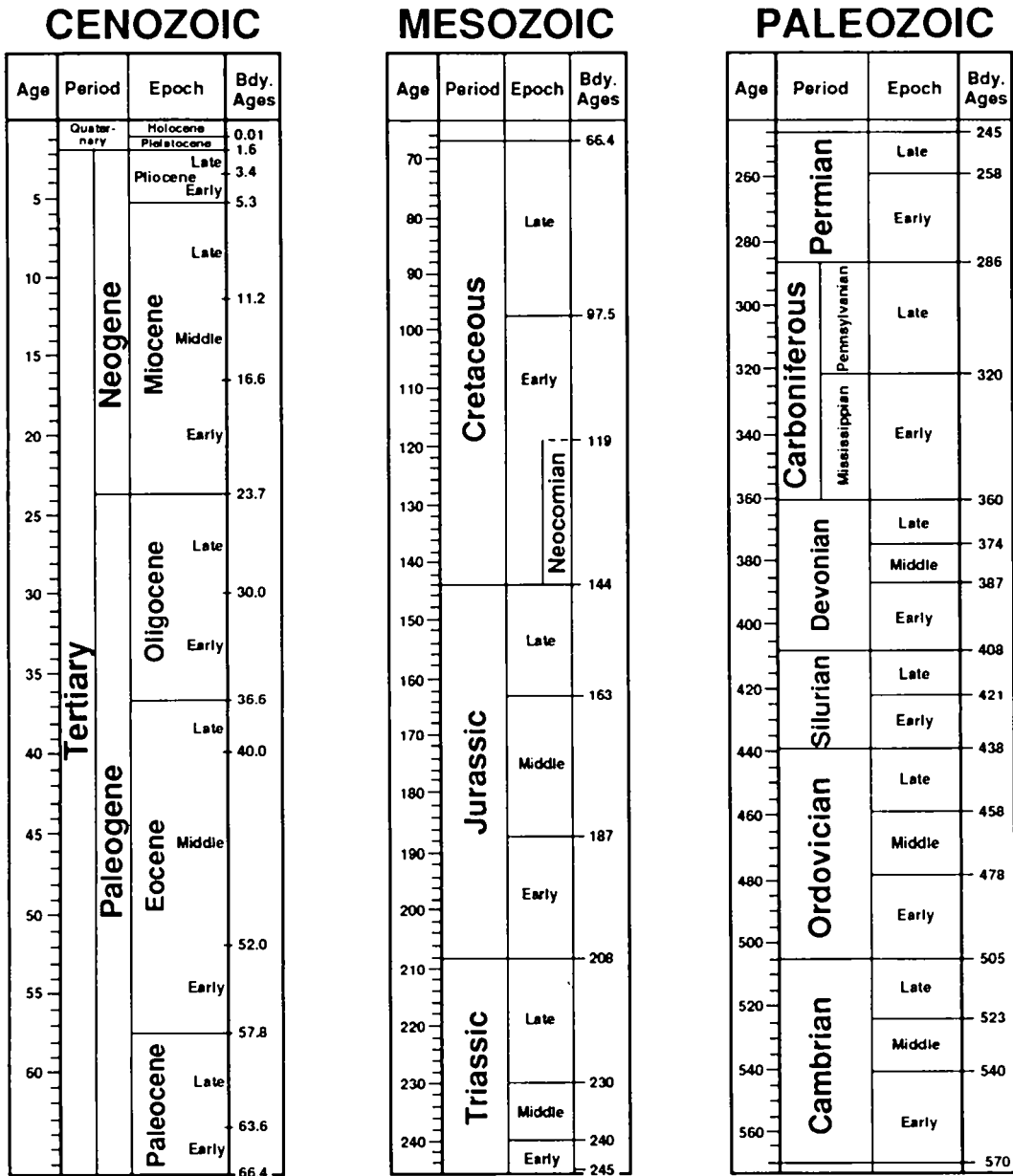
26 The present landscape of the Delaware Basin has been influenced by near-surface dissolution of the evaporites
 27 (Bachman, 1984, 1987). Karst features created by dissolution include sinkholes, subsidence valleys, and breccia
 28 pipes. Most of these features formed during wetter climates of the Pleistocene, although active dissolution is still
 29 occurring wherever evaporites are exposed at the surface. Some dissolution may also be occurring in the
 30 subsurface where circulating groundwater comes in contact with evaporites: for example, modern subsidence in
 31 San Simon Swale east of the WIPP (Figure 2-6) may be related to localized dissolution of the Salado Formation
 32 (Anderson, 1981; Bachman, 1984; Brinster, 1991). Nash Draw, which formed during the Pleistocene by
 33 dissolution and subsidence, is the most prominent karst feature near the WIPP. As discussed again in Section
 34 2.2.2.6 following, evaporites in the Rustler Formation have been affected by dissolution near Nash Draw.

35 The largest karst feature in the Delaware Basin is the Balmorhea-Loving Trough, south of the WIPP along the
 36 axis of the basin (Figure 2-6). Dissolution of evaporites, perhaps along the course of a predecessor of the modern
 37 Pecos River, resulted in subsidence and the deposition of Cenozoic alluvium up to 300 m (984 ft) thick in south-



TRI-6342-237-4

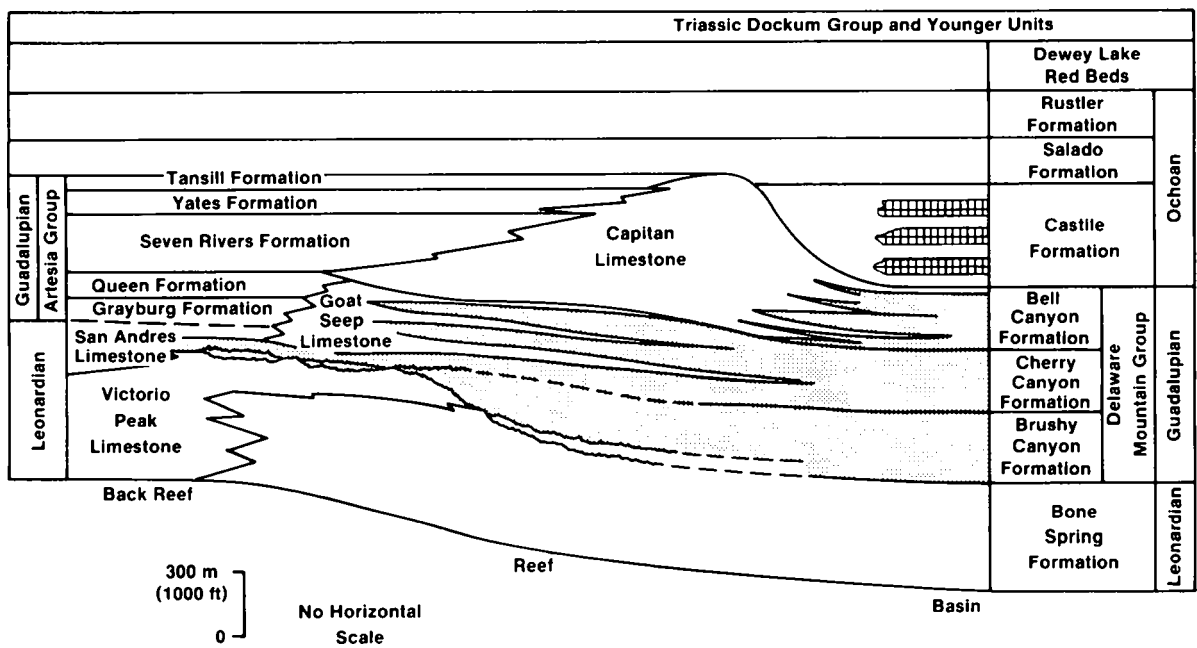
Figure 2-1. Generalized geology of the Delaware Basin, showing the location of the Capitan Reef and the erosional limits of the basinal formations (Lappin, 1988).



All Ages in Millions of Years

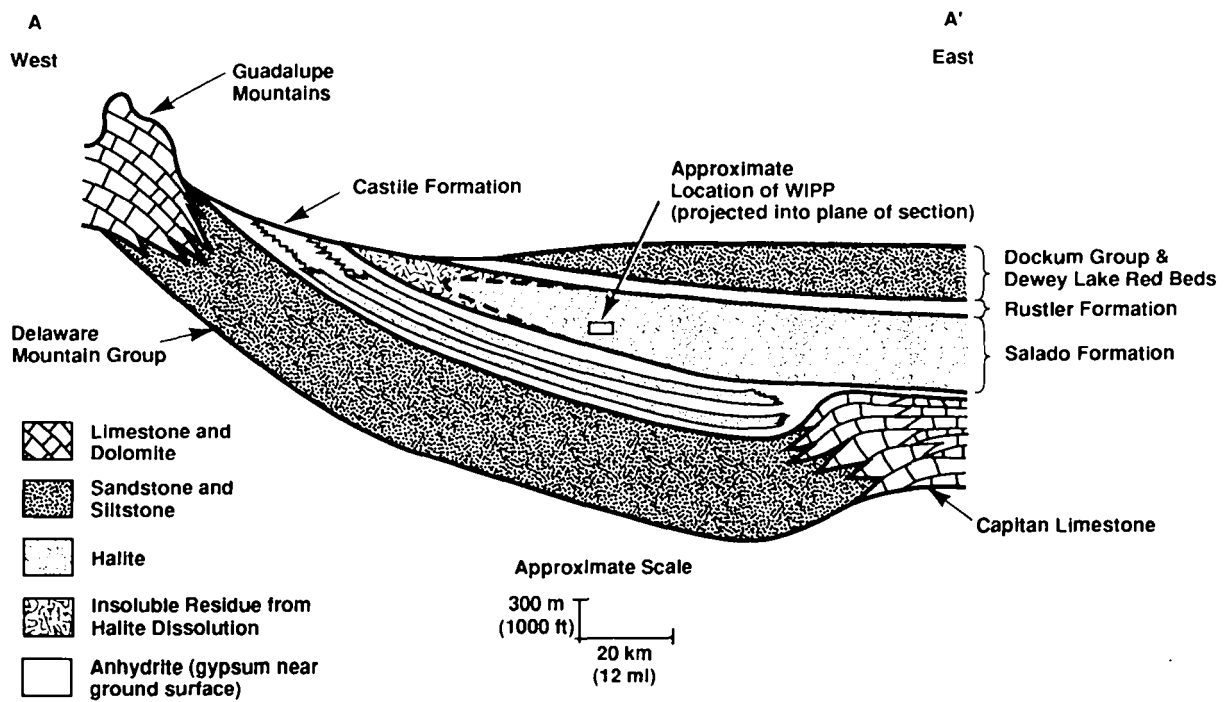
TRI-6342-611-1

Figure 2-2. Geologic time scale (simplified from Geological Society of America, 1984).



TRI-6342-119-1

Figure 2-3. Stratigraphy of the Delaware Basin (modified from Mercer, 1983; Brinster, 1991)



TRI-6342-1076-0

Figure 2-4. Schematic east-west cross section through the northern Delaware Basin (modified from Davies, 1984). Note extreme vertical exaggeration. Approximate location of line of section shown on Figure 2-1.

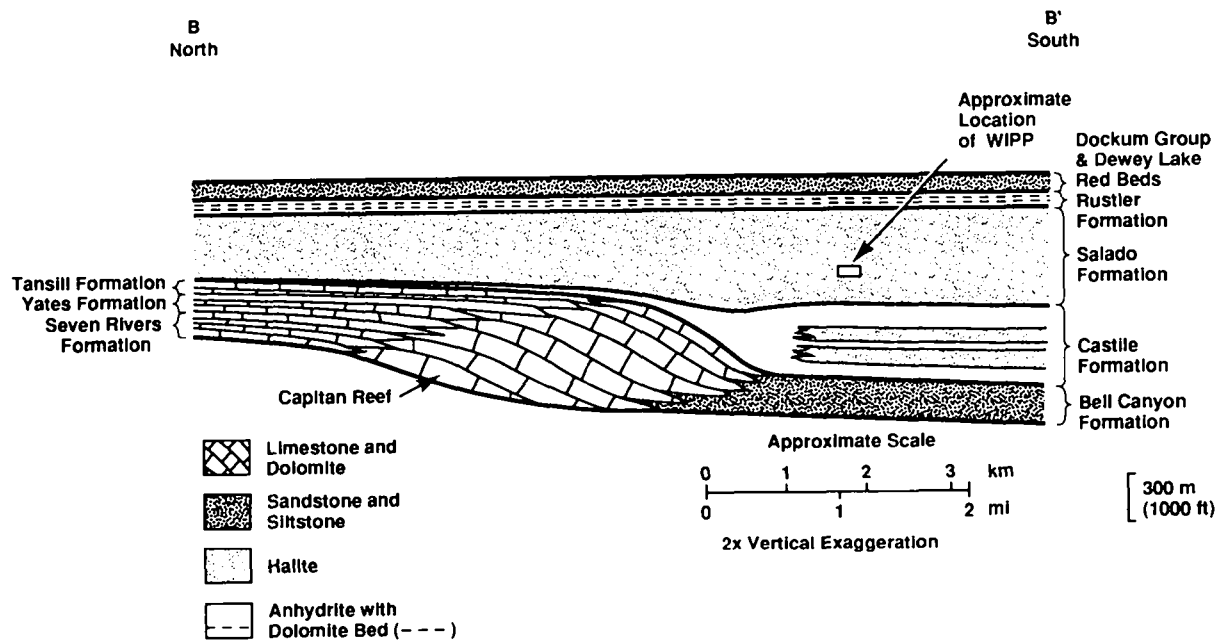
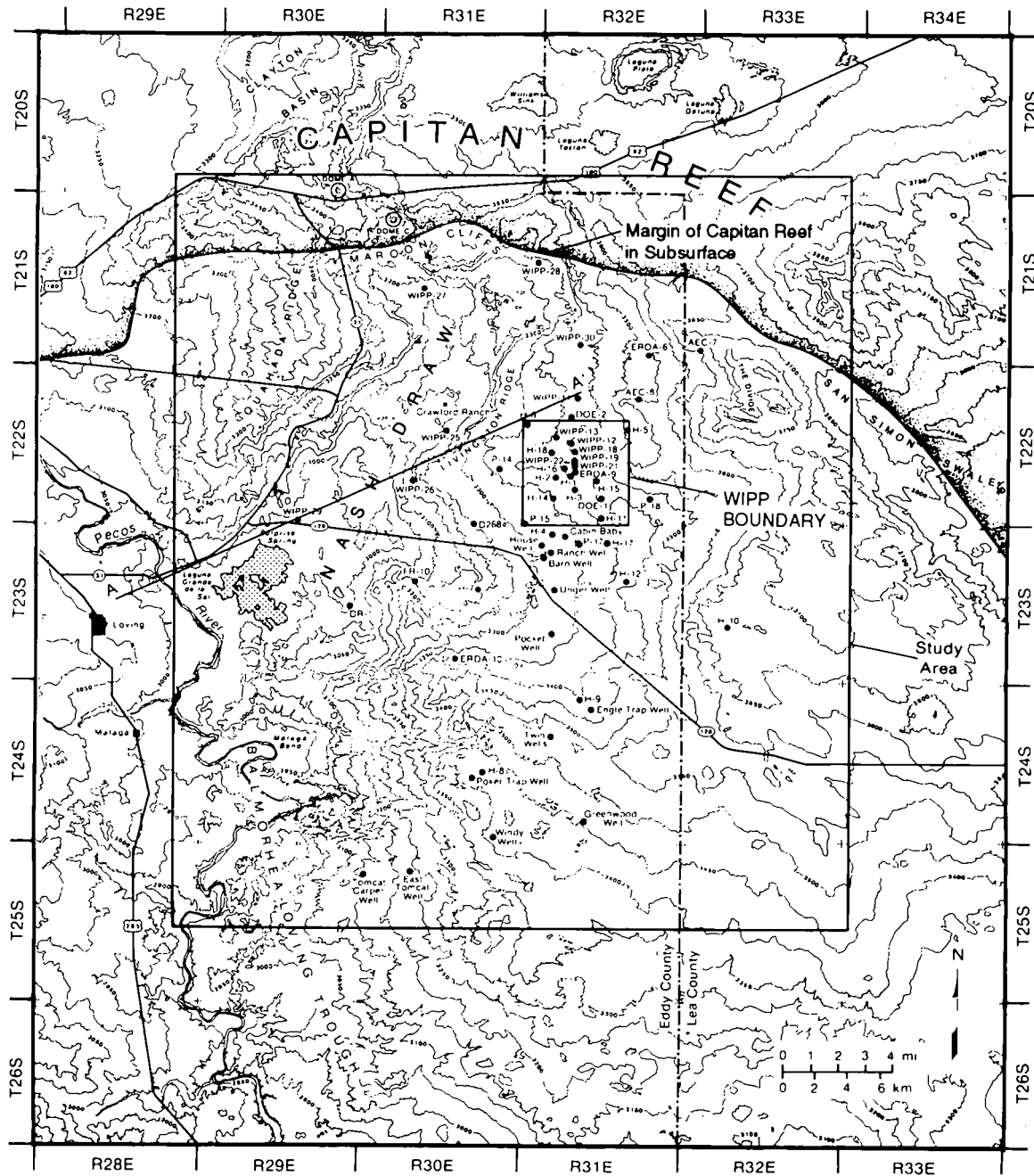


Figure 2-5. Schematic north-south cross section through the Northern Delaware Basin (modified from Davies, 1984). Note extreme vertical exaggeration. Approximate location of line of section shown on Figure 2-1.



TRI-6342-3416-0

Figure 2-6. Map of the WIPP vicinity showing the land-withdrawal area (labeled "WIPP Boundary"), the study area of Brinster (1991), and the location of observation wells (Haug et al., 1987; Brinster, 1991).

1 ern Eddy County, and up to almost 600 m (1970 ft) thick across the state line in Texas (Bachman, 1984, 1987;
2 Brinster, 1991).

3 **2.2.2 Stratigraphy**

4 This review is based primarily on the summary presented by Brinster (1991), and is limited to those units that
5 may have an important role in future performance of the disposal system. Hydrologic data about the units have
6 been summarized by Brinster (1991), and are, in general, not repeated here. Stratigraphic relationships between the
7 units are shown in Figure 2-3. Figure 2-6 shows the region examined in detail by Brinster (1991) and the location
8 of wells that provide basic data.

9 **2.2.2.1 BELL CANYON FORMATION**

10 The Bell Canyon Formation consists of 210 to 260 m (690 to 850 ft) of sandstones and siltstones with minor
11 limestones, dolomites, and conglomerates (Williamson, 1978; Mercer, 1983; Harms and Williamson, 1988).
12 Sandstones within the upper portion of the Bell Canyon Formation occur as long, sinuous channels separated by
13 siltstones, reflecting their deposition by density currents that flowed into the deep basin from the Capitan Reef
14 (Harms and Williamson, 1988). These sandstones have been targets for hydrocarbon exploration elsewhere in the
15 Delaware Basin and are also of interest for the WIPP performance assessment because they are the first aquifers
16 below the evaporite sequence that hosts the repository.

17 Simulations of undisturbed repository performance do not include the Bell Canyon Formation because a thick
18 sequence of evaporites with very low permeability separates the formation from the overlying units. Simulations
19 of human intrusion scenarios do not include a borehole pathway for fluid migration between the Bell Canyon
20 Formation (or deeper units) and the repository. Relatively little is known about the head gradient that would drive
21 flow along this pathway, but data from five wells in the Bell Canyon Formation suggest that flow would be
22 slight, and, in an uncased hole, downward because of brine density effects (Mercer, 1983; Beauheim, 1986; Lappin
23 et al., 1989).

24 **2.2.2.2 CAPITAN LIMESTONE**

25 The Capitan Limestone is not present at the WIPP, but is a time-stratigraphic equivalent of the Bell Canyon
26 Formation to the west, north, and east (Figures 2-1, 2-3). The unit is a massive limestone ranging from 76 to
27 230 m (250 to 750 ft) thick. Dissolution and fracturing have enhanced effective porosity, and the Capitan is a
28 major aquifer in the region, providing the principal water supply for the city of Carlsbad. Upward flow of
29 groundwater from the Capitan aquifer may be a factor in dissolution of overlying halite and the formation of
30 breccia pipes. Existing breccia pipes are limited to the vicinity of the reef, as is the active subsidence in San
31 Simon Swale (Figure 2-6) (Brinster, 1991).

1 2.2.2.3 CASTILE FORMATION

2 The Castile Formation is approximately 470 m (1540 ft) thick at the WIPP and contains anhydrites with
3 intercalated limestones near the base and halite layers in the upper portions. Primary porosity and permeability in
4 the Castile Formation are extremely low. However, approximately 18 wells in the region have encountered brine
5 reservoirs in fractured anhydrite in the Castile Formation (Brinster, 1991). Hydrologic and geochemical data have
6 been interpreted as indicating that these brine occurrences are hydraulically isolated (Lambert and Mercer, 1978;
7 Lappin, 1988). Fluid may have been derived from interstitial entrapment of connate water after deposition
8 (Popielak et al., 1983), dehydration of the original gypsum to anhydrite (Popielak et al., 1983), or intermittent
9 movement of meteoric waters from the Capitan aquifer into the fractured anhydrites between 360,000 and 880,000
10 years ago (Lambert and Carter, 1984). Pressures within these brine reservoirs are greater than those at comparable
11 depths in other relatively permeable units in the region and range from 7 to 17.4 MPa (Lappin et al., 1989).

12 Pressurized brine in the Castile Formation is of concern for performance assessment because occurrences have
13 been found at WIPP-12 within the WIPP land-withdrawal area and at ERDA-6 and other wells in the vicinity. The
14 WIPP-12 reservoir is at a depth of 918 m (3012 ft), about 250 m (820 ft) below the repository horizon, and is
15 estimated to contain 2.7×10^6 m³ (1.7×10^7 barrels) of brine at a pressure of 12.7 MPa (Lappin et al., 1989).
16 This pressure is greater than the nominal freshwater hydrostatic pressure at that depth (9 MPa) and is slightly
17 greater than the nominal hydrostatic pressure for a column of equivalent brine at that depth (11.1 MPa). The brine
18 is saturated, or nearly so, with respect to halite, and has little or no potential to dissolve the overlying salt
19 (Lappin et al., 1989). Brine could, however, reach the repository, overlying strata, and the ground surface through
20 an intrusion borehole.

21 Early geophysical surveys mapped a structurally disturbed zone in the vicinity of the WIPP that may correlate
22 with fracturing or development of secondary porosity within the Castile Formation; this zone could possibly
23 contain pressurized brine (Borns et al., 1983). Later electromagnetic surveys indicated that the brine present at
24 WIPP-12 could underlie part of the waste panels (Earth Technology Corporation, 1988). WIPP-12 data are
25 therefore used to develop a conceptual model of the brine reservoir for analyzing scenarios that include the
26 penetration of pressurized brine. Data describing the Castile Formation brine reservoir are summarized in Volume
27 3, Section 4.3 of this report.

28 2.2.2.4 SALADO FORMATION

29 The Salado Formation is about 600 m (1970 ft) thick at the WIPP and contains halite interbedded with
30 anhydrite, polyhalite, glauberite, and some thin mudstones (Adams, 1944; Bachman, 1981; Mercer, 1983).
31 Unlike the underlying Castile Formation, the Salado Formation overlaps the Capitan Limestone and extends
32 eastward beyond the reef for many kilometers into west Texas (Figure 2-3). Erosion has removed the Salado
33 Formation from the western portion of the basin (Figure 2-1).

34 Where the Salado Formation is intact and unaffected by dissolution, natural groundwater flow is negligible
35 because primary porosity and open fractures are lacking in the plastic salt (Mercer, 1983; Brinster, 1991). The
36 formation is not dry, however. Interstitial brine seeps into the repository at rates up to approximately 0.01

1 ℓ /day/for each m (in length) of excavation (Bredehoeft, 1988; Nowak et al., 1988), and the Salado is assumed to
2 be saturated (Brinster, 1991). Porosity is estimated to be approximately 0.01 (expressed as void volume per unit
3 volume of rock). Permeability of the formation is very low but measurable, with an average value of 0.05
4 microdarcies ($5 \times 10^{-20} \text{ m}^2$) reported by Powers et al. (1978a,b) from well tests. This value corresponds
5 approximately to a hydraulic conductivity $5 \times 10^{-13} \text{ m/s}$ ($1 \times 10^{-7} \text{ ft/d}$) (Freeze and Cherry, 1979, Table 2.3). In
6 situ testing of halite in the repository indicates lower permeabilities ranging from 1 to 100 nanodarcies (10^{-22} to
7 10^{-20} m^2) (Stormont et al., 1987; Beauheim et al., 1991). Additional information about the geology of the
8 Salado Formation at the repository is provided in Section 2.3.1, and in Volume 3, Section 2.3 of this report.

9 2.2.2.5 RUSTLER-SALADO CONTACT ZONE

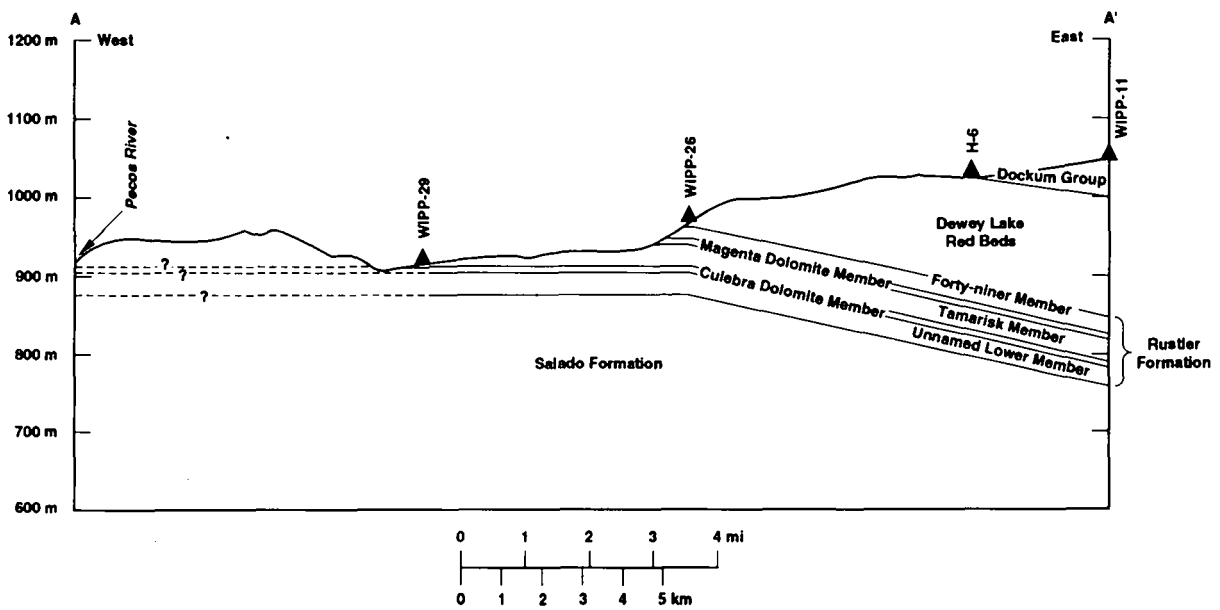
10 In the vicinity of Nash Draw, the contact between the Rustler and Salado Formations is an unstructured
11 residuum of gypsum, clay, and sandstone created by dissolution of halite. The residuum becomes thinner to the
12 east and intertongues with clayey halite of the unnamed lower member of the Rustler Formation. Mercer (1983)
13 concluded, on the basis of brecciation at the contact, that dissolution in Nash Draw occurred after deposition of the
14 Rustler Formation. In shafts excavated at the WIPP, the residuum shows evidence of channeling and filling,
15 fossils, and bioturbation, indicating that some dissolution occurred before Rustler deposition (Holt and Powers,
16 1988).

17 The residuum ranges in thickness in the vicinity of the WIPP from 2.4 m (7.9 ft) in P-14 east of Nash Draw
18 to 33 m (108 ft) in WIPP-29 within Nash Draw (Mercer, 1983). Measured hydraulic conductivity values for the
19 residuum are highest at Nash Draw (up to 10^{-6} m/s [10^{-1} ft/d]), and three to six orders of magnitude lower to the
20 east (Brinster, 1991). Porosity estimates range from 0.15 to 0.33 (Robinson and Lang, 1938; Hale and Clebsch,
21 1958; Geohydrology Associates, Inc., 1979; Mercer, 1983).

22 2.2.2.6 RUSTLER FORMATION

23 The Rustler Formation is of particular importance for WIPP PA because it contains the most transmissive
24 units above the repository and therefore provides the most likely pathway for the subsurface transport of
25 radionuclides to the accessible environment.

26 The Rustler Formation is 95 m (312 ft) thick at the WIPP (as measured in ERDA-9) and ranges in the area
27 from a minimum of 8.5 m (28 ft) where thinned by dissolution and erosion west of the repository to a maximum
28 of 216 m (709 ft) to the east (Brinster, 1991). Overall, the formation is composed of about 40 percent anhydrite,
29 30 percent halite, 20 percent siltstone and sandstone, and 10 percent anhydritic dolomite (Lambert, 1983). On the
30 basis of outcrops in Nash Draw west of the WIPP, the formation is divided into four formally named members and
31 a lower unnamed member (Vine, 1963). These five units (Vine, 1963; Mercer, 1983) are, in ascending order, the
32 unnamed lower member (oldest), the Culebra Dolomite Member, the Tamarisk Member, the Magenta Dolomite
33 Member, and the Forty-niner Member (youngest) (Figure 2-7, Table 2-1).



TRI-6342 262-3

Figure 2-7. East-west cross section showing stratigraphy of the Rustler Formation and the Dewey Lake Red Beds (modified from Brinster, 1991). Note vertical exaggeration. Location of cross section is shown on Figure 2-6.

1

2 Table 2-1. Properties of the Rustler Formation Units and Rustler-Salado Contact Zone. (Sources for data
3 provided in text.)

<u>Member Name</u>	<u>Thickness</u> (max/min) (m)	<u>Hydraulic</u> <u>Conductivity</u> (max/min) (m/s)	<u>Porosity</u> (max/min)
Forty-niner	20	5.0×10^{-9} 5.0×10^{-10}	—
Magenta	8 4	5.0×10^{-5} 5.0×10^{-10}	—
Tamarisk	84 8		—
Culebra	11.6 4	1×10^{-4} 2×10^{-10}	0.30 0.03
Unnamed	36	1×10^{-11} 6×10^{-15}	—
Rustler-Salado Contact Zone	33 2.4	1×10^{-6} 1×10^{-12}	0.33 0.15

4

5 The Unnamed Lower Member

6 The unnamed lower member is about 36 m (118 ft) thick at the WIPP and thickens slightly to the east. The
7 unit is composed mostly of fine-grained silty sandstones and siltstones interbedded with anhydrite (converted to
8 gypsum at Nash Draw) west of the WIPP. Increasing amounts of halite are present to the east. Halite is present
9 over the WIPP (Figure 2-8), but is absent north and south of the WIPP where the topographic expression of Nash
10 Draw extends eastward. Distribution of halite within this and other members of the Rustler Formation is
11 significant because, as is discussed in the following section, an apparent correlation exists between the absence of
12 halite and increased transmissivity in the Culebra Dolomite Member.

1 The basal interval of the unnamed lower member contains siltstone and sandstone of sufficient transmissivity
2 to allow groundwater flow. Transmissivities of 2.9×10^{-10} m²/s (2.7×10^{-4} ft²/d) and 2.4×10^{-10} m²/s
3 (2.2×10^{-4} ft²/d) were calculated from tests at H-16 that included this interval (Beauheim, 1987a). Assuming all
4 flow in the 34-m (112-ft) test interval came from the 20 m (64 ft) of the basal interval, these transmissivity
5 values correspond to hydraulic conductivities of 1.5×10^{-11} m/s (4.2×10^{-6} ft/d) and 1.2×10^{-11} m/s (3.4×10^{-6}
6 ft/d). Hydraulic conductivity in the lower portion of the unnamed member is believed to increase to the west in
7 and near Nash Draw, where dissolution in the underlying Rustler-Salado contact zone has caused subsidence and
8 fracturing of the sandstone and siltstone (Beauheim and Holt, 1990).

9 The remainder of the unnamed lower member contains mudstones, anhydrite, and variable amounts of halite.
10 Hydraulic conductivity of these lithologies is extremely low: tests of mudstones and claystones in the waste-
11 handling shaft gave hydraulic conductivity values ranging from 6×10^{-15} m/s (2×10^{-9} ft/d) to 1×10^{-13} m/s
12 (3×10^{-8} ft/d) (Saulnier and Avis, 1988; Brinster, 1991).

13 Culebra Dolomite Member

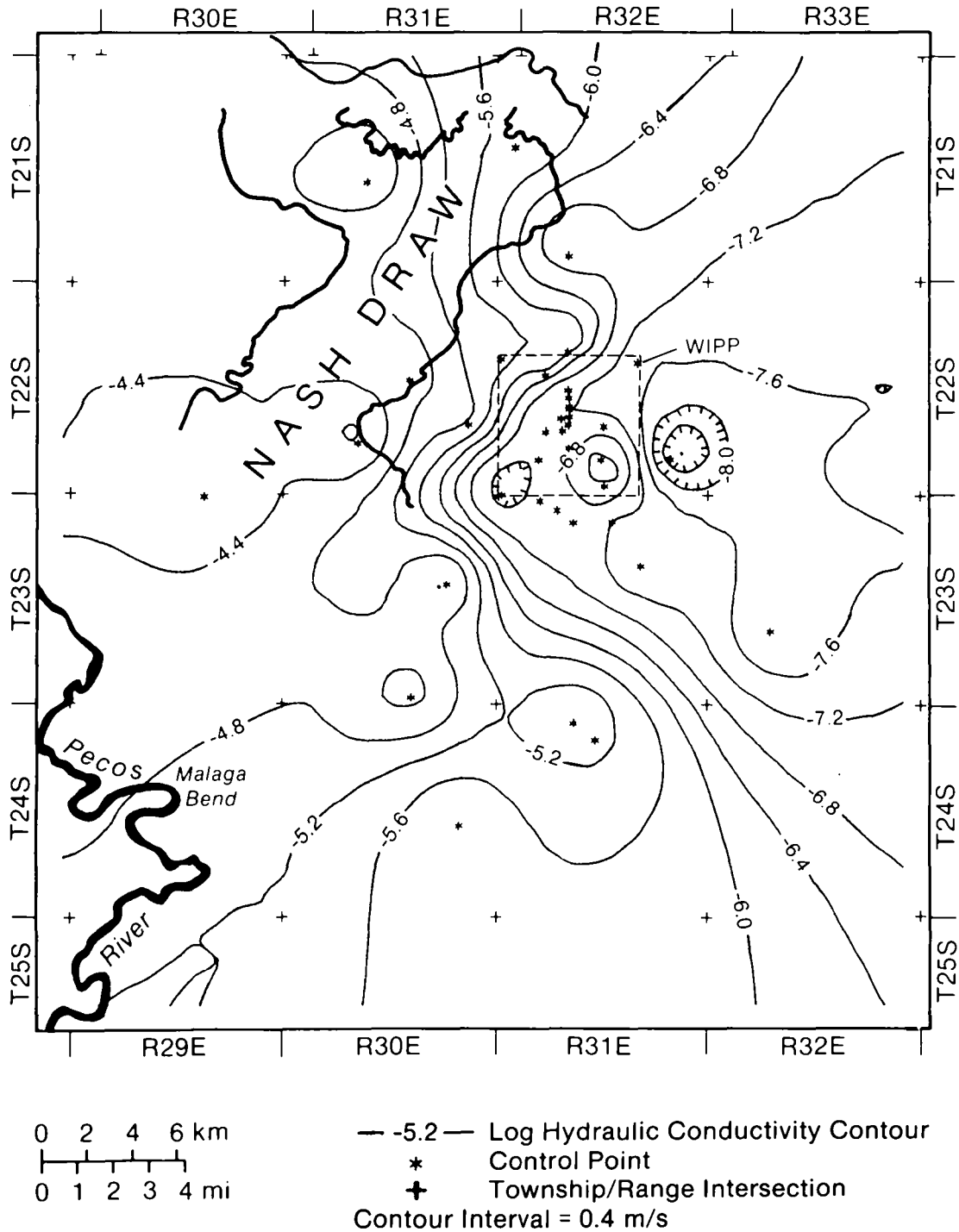
14 The Culebra Dolomite Member of the Rustler Formation is microcrystalline dolomite or dolomitic limestone
15 with solution cavities (Vine, 1963). In the vicinity of the WIPP, it ranges in thickness from 4 to 11.6 m (13 to
16 38.3 ft) and has a mean thickness of about 7 m (23 ft). Outcrops of the Culebra Dolomite occur in the southern
17 part of Nash Draw and along the Pecos River.

18 The Culebra Dolomite has been identified as the most likely pathway for release of radionuclides to the
19 accessible environment because of its relatively high hydraulic conductivity near the WIPP, and hydrologic
20 research has concentrated on the unit for over a decade (Mercer and Orr, 1977, 1979; Mercer, 1983; Mercer et al.,
21 1987; Beauheim, 1987a,b; LaVenue et al., 1988, 1990; Davies, 1989; Cauffman et al., 1990). Hydraulic data are
22 available from 41 well locations in the WIPP vicinity (Cauffman et al., 1990).

23 Hydraulic conductivity of the Culebra varies six orders of magnitude from east to west in the vicinity of the
24 WIPP (Figure 2-9), ranging from 2×10^{-10} m/s (6×10^{-5} ft/d) at P-18 east of the WIPP to 1×10^{-4} m/s
25 (6×10^1 ft/d) at H-7 in Nash Draw (Brinster, 1991). Present understanding of the geologic controls on this
26 variation in conductivity is based primarily on studies of core samples from 17 boreholes, exposures in the walls
27 of three shafts excavated at the WIPP, and approximately 600 geophysical logs from boreholes throughout the
28 vicinity (Figure 2-10) (Holt and Powers, 1988; Powers and Holt, 1990; Beauheim and Holt, 1990).

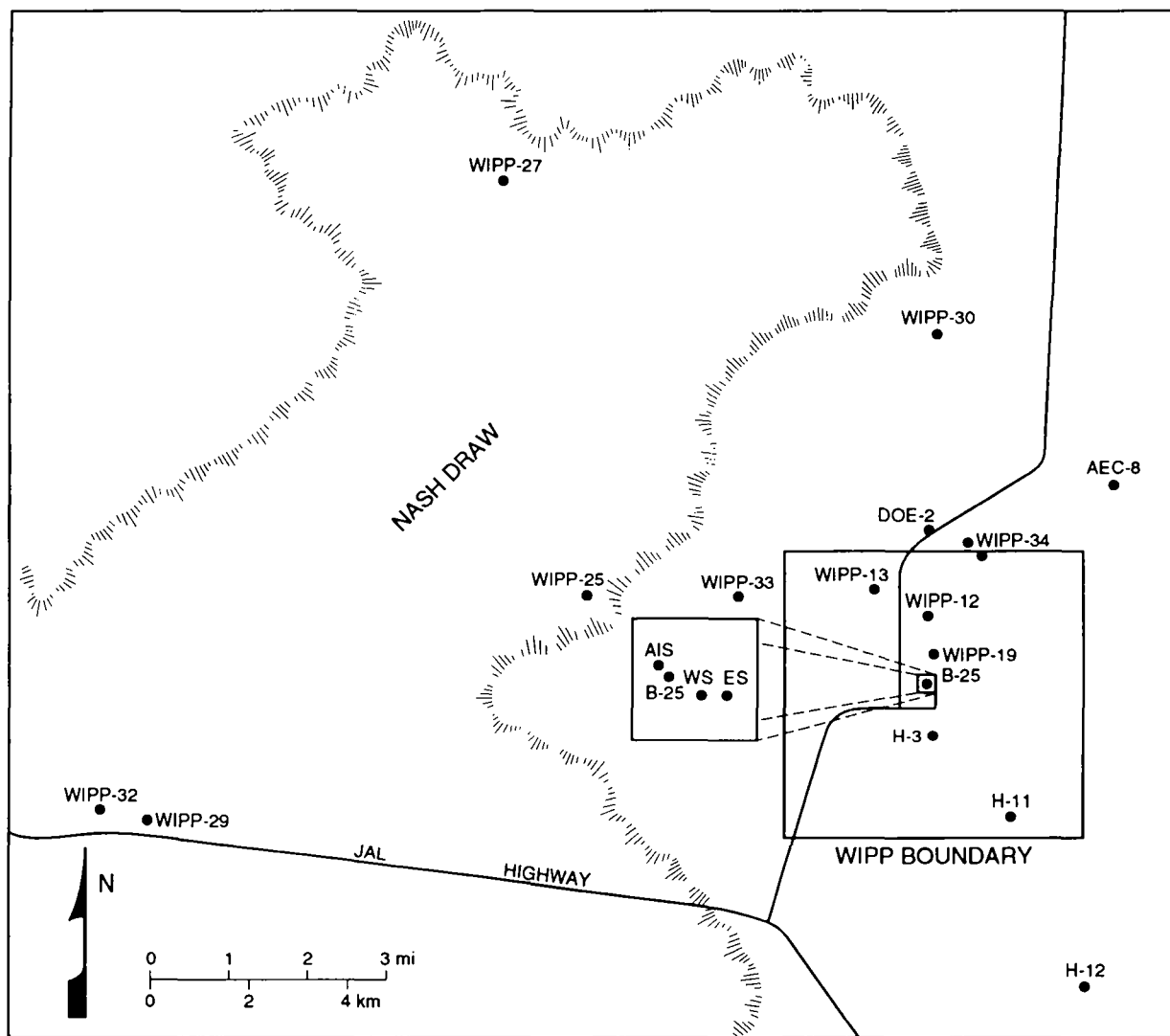
29 Measured matrix porosities of the Culebra Dolomite range from 0.03 to 0.30 (Lappin et al., 1989; Kelley and
30 Saulnier, 1990). Fracture porosity values have not been measured directly, but interpreted values from tracer tests
31 at the H-3 and H-11 hydropads are 2×10^{-3} and 1×10^{-3} , respectively (Kelley and Pickens, 1986). Data are
32 insufficient to map spatial variability of porosity.

33 Variations in hydraulic conductivity in the Culebra are believed to be controlled by the relative abundance of
34 open fractures (Snyder, 1985; Beauheim and Holt, 1990; Brinster, 1991) rather than by primary (i.e., depositional)
35 features of the unit. Lateral variations in depositional environments were small within the mapped region, and



TRI-6342-272-1

Figure 2-9. Log hydraulic conductivities (measured in m/s) of the Culobra Dolomite Member of the Rustler Formation (Brinster, 1991).



TRI-6342-3431-0

Figure 2-10. Sources of geologic information about the Culebra Dolomite, including boreholes from which core samples are available, and shafts studied during excavation. AIS, ES, and WS refer to the air intake, exhaust, and waste shafts, respectively.

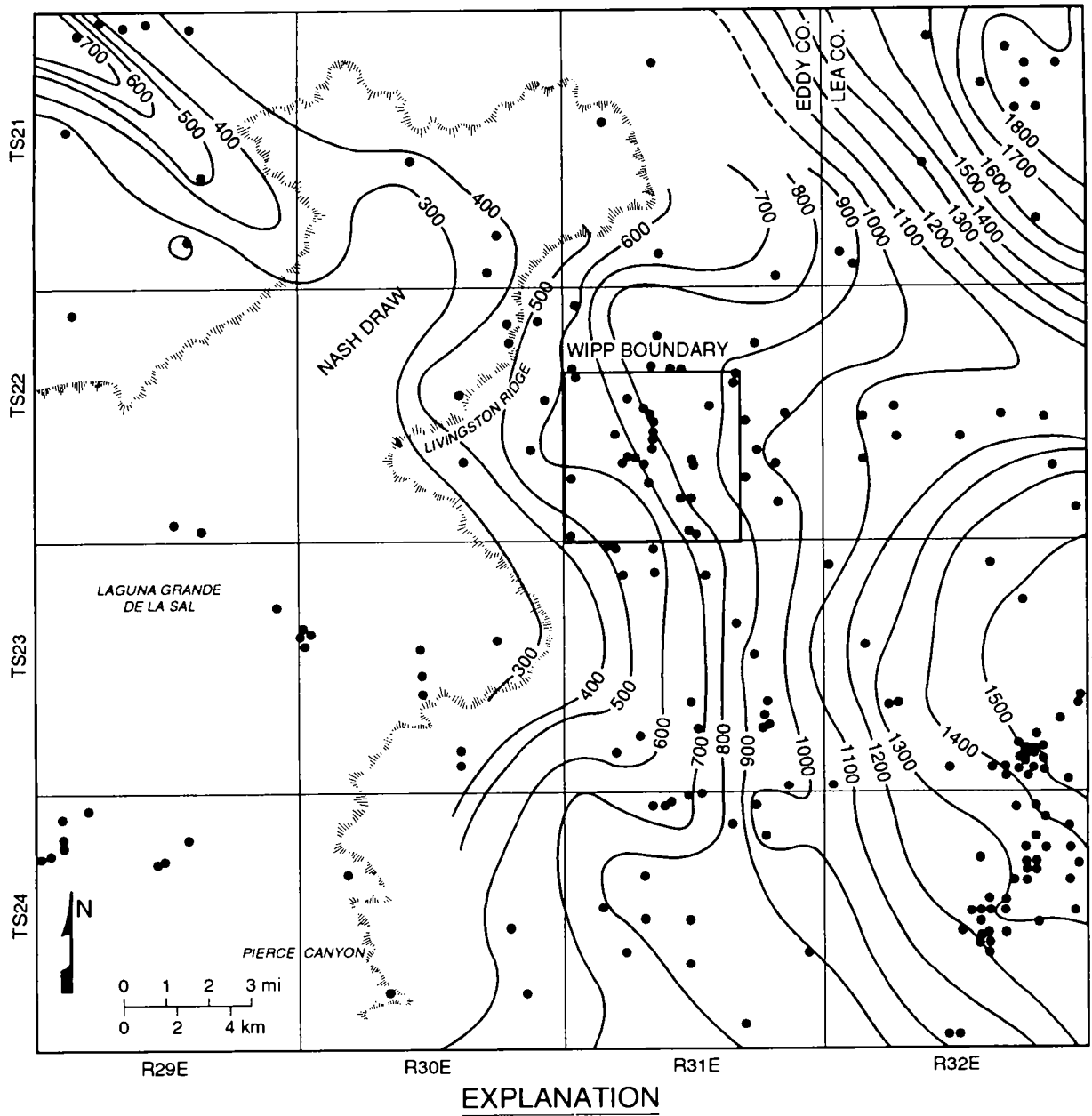
1 primary features of the Culebra show little map-scale spatial variability (Holt and Powers, 1988). Direct
2 measurements of the density of open fractures are not available from core samples because of incomplete recovery
3 and fracturing during drilling, but comparisons between highly fractured outcrops of the Culebra in southern Nash
4 Draw and the relatively unfractured exposures in the WIPP shafts suggests that density of open fractures in the
5 Culebra decreases to the east. Qualitative correlations have been noted between hydraulic conductivity and several
6 geologic features possibly related to open-fracture density, including (1) the distribution of overburden above the
7 Culebra (Figure 2-11) (Holt and Powers, 1988; Beauheim and Holt, 1990); (2) the distribution of halite in other
8 members of the Rustler Formation (compare Figures 2-8 and 2-9) (Snyder, 1985); (3) the dissolution of halite in
9 the upper portion of the Salado Formation (Figure 2-12) (Beauheim and Holt, 1990); and (4) the distribution of
10 gypsum fillings in fractures in the Culebra (Figure 2-13) (Beauheim and Holt, 1990).

11 Regional tilting of the Delaware Basin during the Late Pliocene and early Pleistocene (see Section 2.2.1) and
12 subsequent erosion have resulted in a westward decrease in overburden above the Culebra (Figure 2-13). The
13 decrease in confining stress during erosional unloading may have caused fracturing in the Culebra (Beauheim and
14 Holt, 1990), and may also have controlled the degree to which fractures opened. Locally, however, variations in
15 conductivity do not correlate precisely with variations in overburden thickness, and other geologic phenomena
16 must contribute (Beauheim and Holt, 1990).

17 Where the present distribution of halite in the Rustler Formation (Figure 2-8) results from post-depositional
18 dissolution, subsidence over areas of dissolution may have caused fracturing in the Culebra (Snyder, 1985).
19 Mapping of depositional environments in the Rustler Formation indicates, however, that the present limits of
20 halite in the formation coincide, in general, with a depositional transition from evaporites to mudstones near the
21 margins of a saline pan (Holt and Powers, 1988; Powers and Holt, 1990). Dissolution of the upper portion of the
22 Salado Formation (Figure 2-12), as inferred from stratigraphic thinning observed in geophysical logs, may also
23 have caused subsidence and fracturing in the Culebra (Beauheim and Holt, 1990).

24 Detailed examination of core samples from the Culebra shows that the percentage of fractures that are filled
25 with post-depositional gypsum crystals increases eastward across the site (Figure 2-13) (Beauheim and Holt,
26 1990). Furthermore, the crystalline structure of the fracture fillings changes across the site, suggesting that the
27 present conductivity distribution may reflect spatial variability in the processes that formed fracture fillings. East
28 of the WIPP, fracture-filling crystals have predominantly incremental growth forms, indicating gradual growth as
29 the fractures opened and no subsequent dissolution. Fractures with incremental fillings probably have had
30 relatively small apertures and little groundwater flow through them throughout their history. From the WIPP
31 west, fracture fillings, where present, are predominantly passive gypsum crystals that grew in pre-existing void
32 spaces. By implication, any early, incremental fillings in these fractures must have been dissolved at some time
33 in the past, and the fractures may have had relatively large groundwater flow through them before passive crystal
34 growth. In places where early, incremental fillings have been removed by dissolution and passive crystal growth
35 have not formed, or where they have been removed by further dissolution, conductivity is high. In places where
36 either passive or incremental crystals fill most fractures, conductivity is low.

37

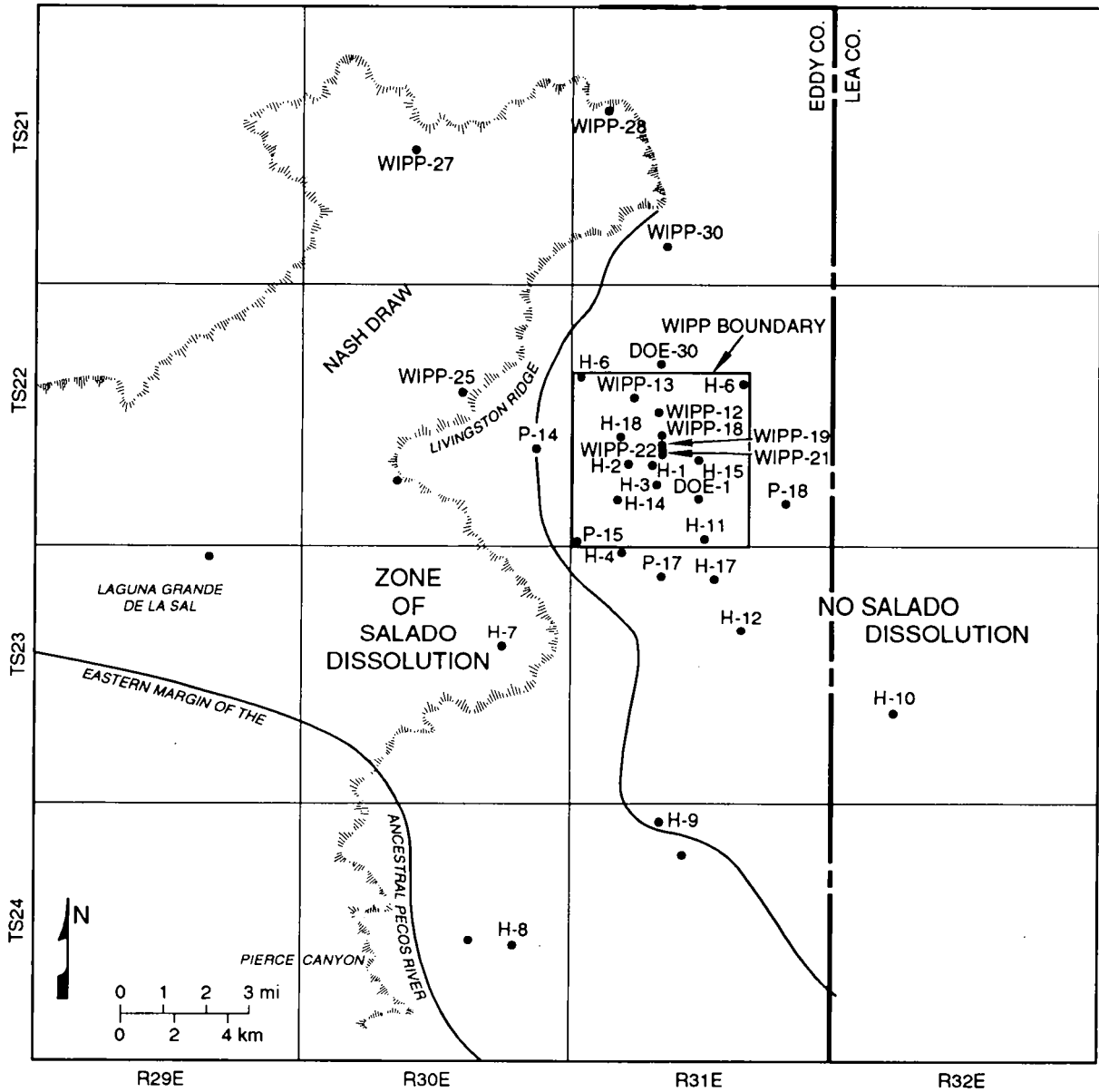


• DRILL HOLES

CONTOUR INTERVAL = 100 FEET

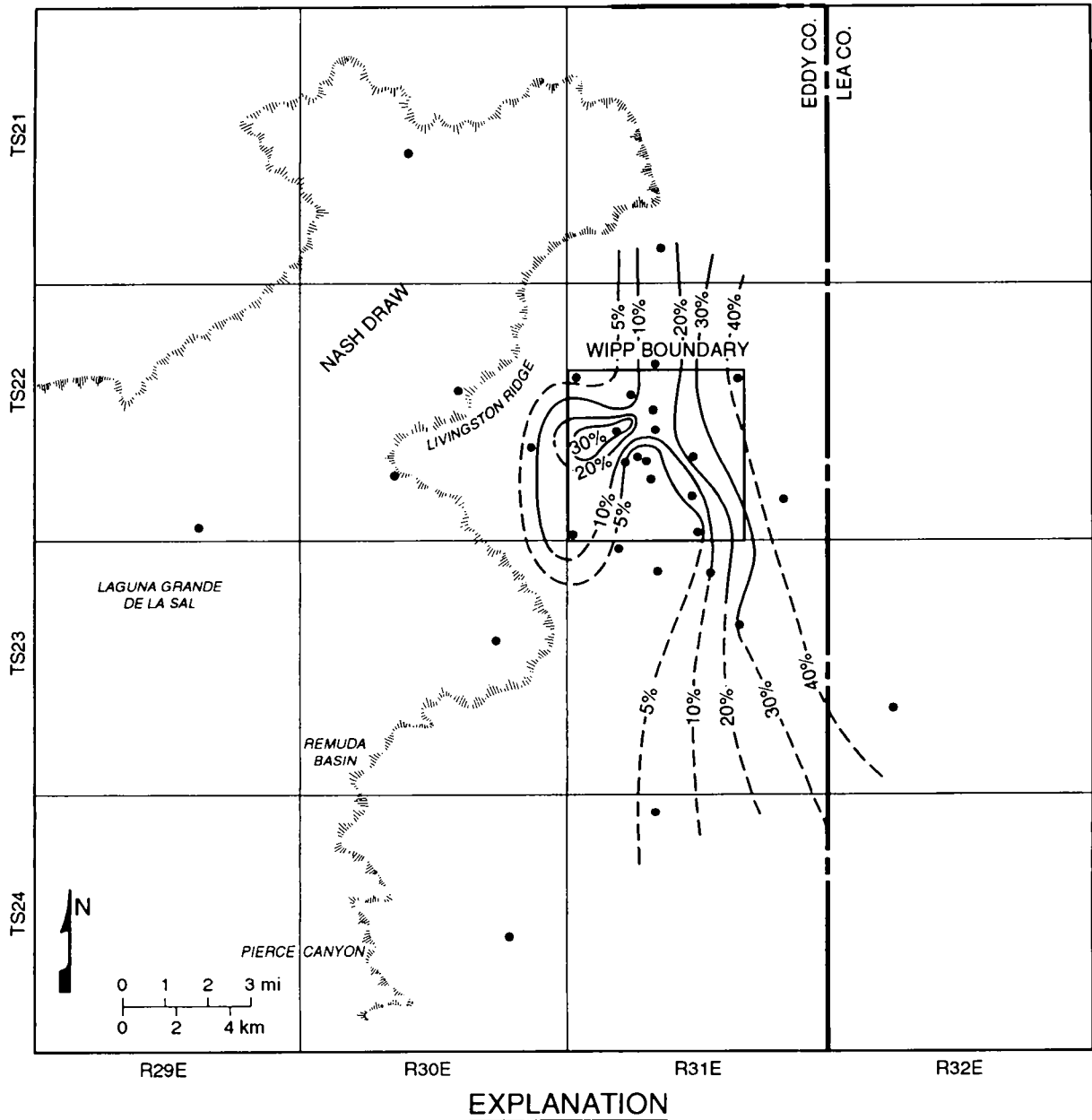
TRI-6342-3432-0

Figure 2-11. Isopach of overburden for the Culobra Dolomite Member (Beauheim and Holt, 1990).



TRI-63423433-0

Figure 2-12. Interpreted extent of Salado dissolution (Beauheim and Holt, 1990).



EXPLANATION

- WELLS EXAMINED
- CONTOUR INTERVAL = 10%
- 5% LINE SHOWN FOR CLARITY

TRI-6342-3434-0

Figure 2-13. Percentage of natural fractures in the Culobra Dolomite Member filled with gypsum (Beauheim and Holt, 1990).

1 As observed in core samples from the Culebra, clay minerals commonly occur on the surfaces of
2 subhorizontal fractures in dolomite (Sewards, 1991; Sewards et al., 1991a,b). Present distribution and
3 composition of clay in the Culebra (and other members of the Rustler Formation) reflect both depositional and
4 diagenetic processes (Sewards et al., 1992). Clays are most abundant in horizontal layers that represent original
5 bedding planes in the evaporite sequences. These clay-rich layers are found within the Culebra throughout the
6 WIPP vicinity. Because they are less competent than the dolomite above and below, clay-rich layers are
7 preferentially opened during fracturing, creating clay-lined subhorizontal fractures. Clay minerals identified by x-
8 ray diffraction analysis include corrensite (ordered mixed-layer chlorite/saponite) and illite, with minor amounts of
9 serpentine and chlorite. Corrensite is the most abundant of the clay minerals, usually constituting about 50
10 percent of the clay assemblage (Sewards et al., 1991a). Original detrital clays were illite and smectite; alternation
11 of smectite into corrensite occurred during early diagenesis as magnesium-rich pore waters migrated through the
12 formation (Sewards et al., 1992). Isotopic analyses (Rb/Sr) indicate that clay minerals reached their present
13 composition during the Late Permian (Brookins et al., 1990).

14 Because the cation exchange capacity of clay minerals in general and corrensite in particular is higher than that
15 of dolomite or gypsum, clay fracture-linings may play an important role in the chemical retardation of
16 radionuclides during potential transport (Siegel et al., 1990; Sewards et al., 1992). Clay fracture-linings may also
17 affect physical retardation of radionuclides by diffusion into the pore volume of both dolomite matrix and the clay
18 linings during transport (Section 7.6.2 of this volume; Volume 3, Section 2.6 of this report; memorandum by
19 Novak et al. in Volume 3, Appendix A of this report).

20 Tamarisk Member

21 Where present in southeastern New Mexico, the Tamarisk Member ranges in thickness from 8 to 84 m (26 to
22 276 ft) in southeastern New Mexico, and is about 36 m (118 ft) thick at the WIPP. The Tamarisk consists of
23 mostly anhydrite or gypsum interbedded with thin layers of claystone and siltstone. Near Nash Draw, dissolution
24 has removed evaporites from the Tamarisk Member, and the Magenta and Culebra Dolomites are separated only by
25 a few meters of residue (Brinster, 1991).

26 Unsuccessful attempts were made in two wells, H-14 and H-16, to test a 2.4-m (7.9-ft) sequence of the
27 Tamarisk Member that consists of claystone, mudstone, and siltstone overlain and underlain by anhydrite.
28 Permeability was too low to measure in either well within the time allowed for testing, but Beauheim (1987a)
29 estimated the transmissivity of the claystone sequence to be one or more orders of magnitude less than that of the
30 tested interval in the unnamed lower member, which yielded transmissivity values of 2.9×10^{-10} m²/s (2.7×10^{-4}
31 ft²/d) and 2.4×10^{-10} m²/s (2.2×10^{-4} ft²/d), corresponding to hydraulic conductivities in the basal siltstone of the
32 unnamed lower member of 1.5×10^{-11} m/s (4.2×10^{-6} ft/d) and 1.2×10^{-11} m/s (3.4×10^{-6} ft/d).

33 Magenta Dolomite Member

34 The Magenta Dolomite Member of the Rustler Formation is a fine-grained dolomite that ranges in thickness
35 from 4 to 8 m (13 to 26 ft) and is about 6 m (19 ft) thick at the WIPP. The Magenta is saturated except near

1 outcrops along Nash Draw, and hydraulic data are available from 14 wells. Hydraulic conductivity ranges over five
2 orders of magnitude from 5.0×10^{-10} to 5.0×10^{-5} m/s (1×10^{-4} to 1×10^1 ft/d).

3 A contour map of log hydraulic conductivities of the Magenta Dolomite Member based on sparse data (Figure
4 2-14) shows a decrease in conductivity from west to east, with slight indentations of the contours north and south
5 of the WIPP that correspond to the topographic expression of Nash Draw (Brinster, 1991). Comparison of Figures
6 2-9 and 2-14 show that in most locations conductivity of the Magenta is one to two orders of magnitude less than
7 that of the Culebra.

8 No porosity measurements have been made on the Magenta Dolomite Member. Beauheim (1987a) assumed a
9 representative dolomite porosity of 0.20 for interpretations of well tests.

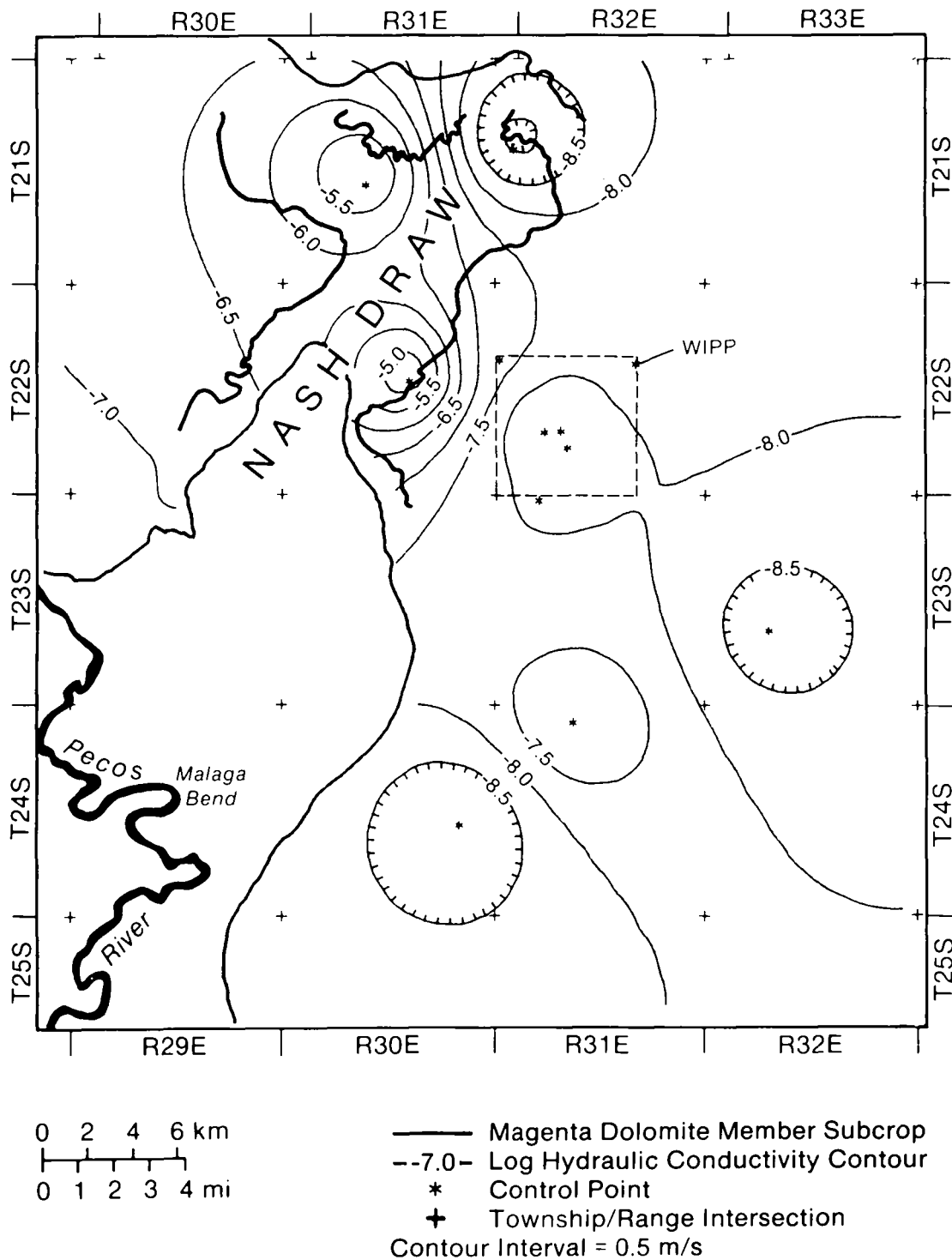
10 Forty-niner Member

11 The uppermost member of the Rustler Formation, the Forty-niner Member, is about 20 m (66 ft) thick
12 throughout the WIPP area and consists of low-permeability anhydrite and siltstone. Tests in H-14 and H-16
13 yielded hydraulic conductivities of about 5×10^{-9} m/s (1×10^{-3} ft/d) and 5×10^{-10} m/s (1×10^{-4} ft/d) respectively
14 (Beauheim, 1987a).

15 2.2.2.7 SUPRA-RUSTLER ROCKS

16 Strata above the Rustler Formation are not believed to represent a significant pathway for the migration of
17 radionuclides from the repository to the accessible environment because of relatively low transmissivities within
18 the saturated zone. These units are important to performance assessment, however, because vertical flux through
19 them may play an important role in the inflow and outflow of water from the Rustler Formation. Available
20 models of groundwater flow in the Culebra do not incorporate the effects of vertical flux.

21 Where present, the supra-Rustler units collectively range in thickness from 4 to 536 m (13 to 1758 ft).
22 Regionally, the supra-Rustler units thicken to the east and form a uniform wedge of overburden across the region
23 (Brinster, 1991). Fine-grained sandstones and siltstones of the Dewey Lake Red Beds (Pierce Canyon Red Beds of
24 Vine, 1963) conformably overlie the Rustler Formation at the WIPP and are the uppermost Permian rocks in the
25 region. The unit is absent in Nash Draw, is as much as 60 m (196 ft) thick where present west of the WIPP, and
26 can be over 200 m (656 ft) thick east of the WIPP (Figures 2-4, 2-7). East of the WIPP, the Dewey Lake Red
27 Beds are unconformably overlain by Mesozoic rocks of the Triassic Dockum Group. These rocks are absent west
28 of the repository and reach a thickness of over 100 m (328 ft) in western Lea County. East of the WIPP, Triassic
29 and, in some locations, Cretaceous rocks are unconformably overlain by the Pliocene Ogallala Formation. At the
30 WIPP, Permian strata are overlain by 8 m (25 ft) of the Triassic Dockum Group, discontinuous sands and gravels
31 of the Pleistocene Gatuña Formation, the informally named Pleistocene Mescalero caliche, and Holocene soils
32 (Holt and Powers, 1990).



TRI-6342-275-1

Figure 2-14. Log hydraulic conductivities (measured in m/s) of the Magenta Dolomite Member of the Rustler Formation (Brinster, 1991).

1 Drilling in the Dewey Lake Red Beds has not identified a continuous zone of saturation. Some localized
2 zones of relatively high permeability were identified by loss of drilling fluids at DOE-2 and H-3d (Mercer, 1983;
3 Beauheim, 1987a). Thin and apparently discontinuous saturated sandstones were identified in the upper Dewey
4 Lake Red Beds at H-1, H-2, and H-3 (Mercer and Orr, 1979; Mercer, 1983). Several wells operated by the J. C.
5 Mills Ranch (James Ranch) south of the WIPP produce sufficient quantities of water from the Dewey Lake Red
6 Beds to supply livestock (Brinster, 1991).

7 Hydrologic properties of supra-Rustler rocks are relatively poorly understood because of the lack of long-term
8 hydraulic tests and the difficulty of making those measurements. Hydraulic conductivity of the Dewey Lake Red
9 Beds, assuming saturation, is estimated to be 10^{-8} m/s (10^{-3} ft/d), corresponding to the hydraulic conductivity of
10 fine-grained sandstone and siltstone (Mercer, 1983; Davies, 1989). Porosity is estimated to be about 0.20, which
11 is representative of fine-grained sandstone (Brinster, 1991).

12 **2.2.3 Hydrology**

13 2.2.3.1 PRESENT CLIMATE

14 The present climate of southeastern New Mexico is arid to semi-arid (Swift, 1992). Annual precipitation is
15 dominated by a late summer monsoon, when solar warming of the continent creates an atmospheric pressure
16 gradient that draws moist air inland from the Gulf of Mexico (Cole, 1975). Winters are cool and generally dry.

17 Mean annual precipitation at the WIPP has been estimated to be between 28 and 34 cm/yr (10.9 and 13.5
18 in/yr) (Hunter, 1985). At Carlsbad, 42 km (26 mi) west of the WIPP and 100 m (330 ft) lower in elevation, 53-
19 year (1931-1983) annual means for precipitation and temperature are 32 cm/yr (12.6 in/yr) and 17.1°C (63°F)
20 (University of New Mexico, 1989). Freshwater pan evaporation in the region is estimated to be 280 cm/yr (110
21 in/yr) (U.S. DOE, 1980).

22 Short-term climatic variability can be considerable in the region. For example, the 105-year (1878 to 1982)
23 precipitation record from Roswell, 135 km (84 mi) northwest of the WIPP and 60 m (200 ft) higher in elevation,
24 shows an annual mean of 27 cm/yr (10.6 in/yr) with a maximum of 84 cm/yr (32.9 in/yr) and a minimum of 11
25 cm/yr (4.4 in/yr) (Hunter, 1985).

26 2.2.3.2 PALEOCLIMATES AND CLIMATIC VARIABILITY

27 Based on the past record, it is reasonable to assume that climate will change at the WIPP during the next
28 10,000 years, and the performance-assessment hydrologic model must allow for climatic variability. Presently
29 available long-term climate models are incapable of resolution on the spatial scales required for numerical
30 predictions of future climates at the WIPP (e.g., Hansen et al., 1988; Mitchell, 1989; Houghton et al., 1990), and
31 simulations using these models are of limited value beyond several hundreds of years into the future. Direct
32 modeling of climates during the next 10,000 years has not been attempted for WIPP performance assessment.

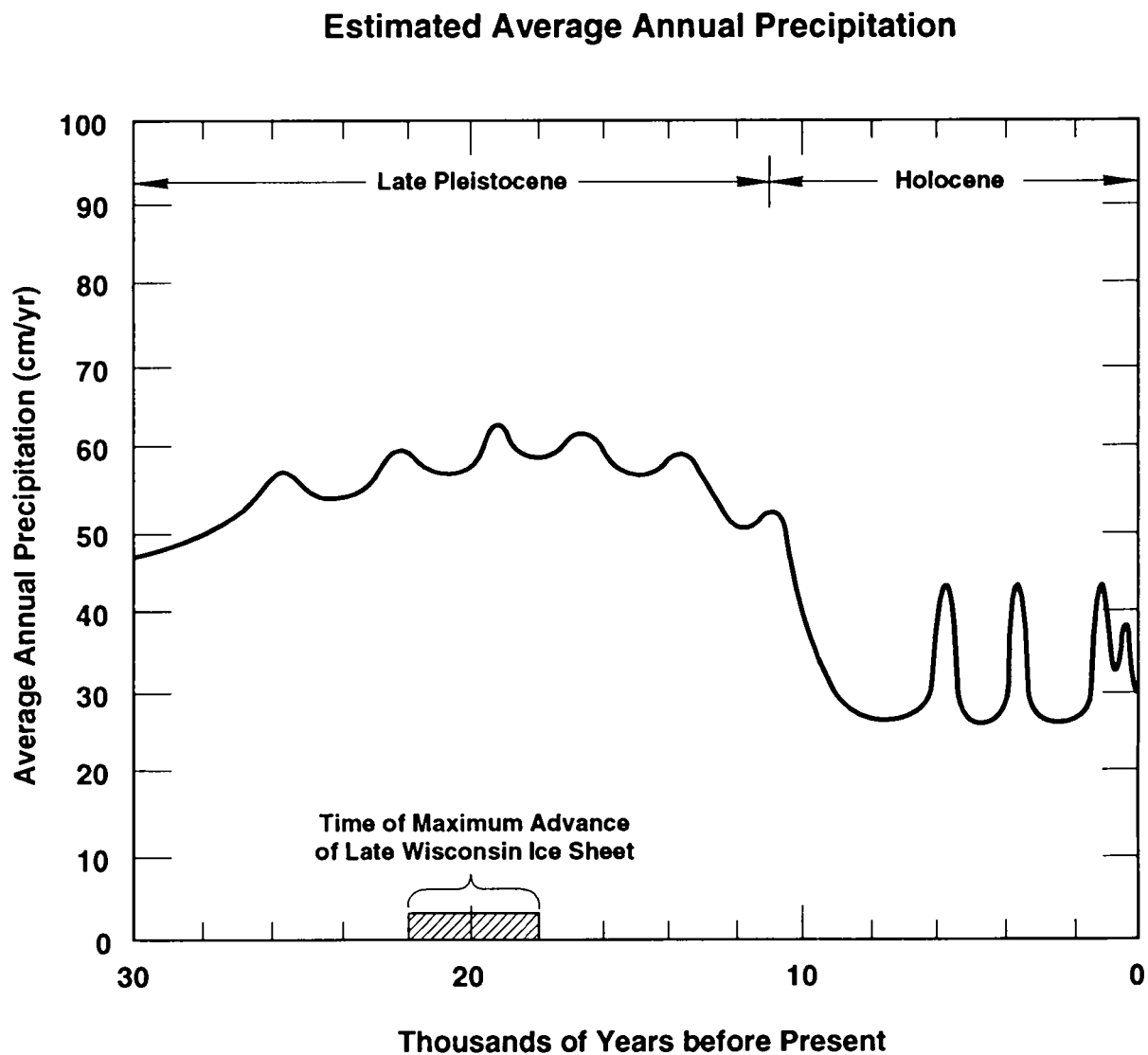
1 Instead, performance-assessment modeling uses past climates to set limits for future variability (Swift, 1991,
2 1992). The extent to which unprecedented climatic changes caused by human-induced changes in the composition
3 of the Earth's atmosphere may invalidate this assumption is uncertain. Presently available models of climatic
4 response to an enhanced greenhouse effect (e.g., Mitchell, 1989; Houghton et al., 1990) do not predict changes of
5 a larger magnitude than those of the Pleistocene (although predicted rates of change are greater), suggesting the
6 choice of a Pleistocene analog for future climatic extremes will remain appropriate.

7 Geologic data from the American Southwest show repeated alternations of wetter and drier climates
8 throughout the Pleistocene, which correspond to global cycles of glaciation and deglaciation (Swift, 1992).
9 Climates in southeastern New Mexico have been coolest and wettest during glacial maxima, when the North
10 American ice sheet reached its southern limit roughly 1200 km (750 mi) north of the WIPP. Mean annual
11 precipitation at these extremes was approximately twice that of the present. Mean annual temperatures may have
12 been as much as 5°C (9°F) cooler than at present. Modeling of global circulation patterns suggests these changes
13 resulted from the disruption and southward displacement of the winter jet stream by the ice sheet, causing an
14 increase in the frequency and intensity of winter storms throughout the Southwest (COHMAP Members, 1988).

15 Data from plant and animal remains and paleo-lake levels permit quantitative reconstructions of precipitation
16 in southeastern New Mexico during the advance and retreat of the last major ice sheet in North America. Figure
17 2-15 shows estimated mean annual precipitation for the WIPP for the last 30,000 years, based on an estimated
18 present precipitation of 30 cm/yr (11.8 in/yr). The precipitation maximum coincides with the maximum advance
19 of the ice sheet 22,000 to 18,000 years ago. Since the final retreat of the ice sheet approximately 10,000 years
20 ago, conditions have been generally dry, with intermittent and relatively brief periods when precipitation may have
21 approached glacial levels. Causes of these Holocene fluctuations are uncertain (Swift, 1992).

22 Glacial periodicities have been stable for the last 800,000 years, with major peaks occurring at intervals of
23 19,000, 23,000, 41,000 and 100,000 years, corresponding to variations in the Earth's orbit (Milankovitch, 1941;
24 Hays et al., 1976; Imbrie et al., 1984; Imbrie, 1985). Barring anthropogenic changes in the Earth's climate,
25 relatively simple modeling of the nonlinear climatic response to astronomically controlled changes in the amount
26 of solar energy reaching the Earth suggests that the next glacial maximum will occur in approximately 60,000
27 years (Imbrie and Imbrie, 1980). Regardless of anthropogenic effects, short-term, non-glacial climatic fluctuations
28 comparable to those of the last 10,000 years are probable during the next 10,000 years and must be included in
29 performance-assessment modeling.

30 Climatic variability will be incorporated into the modeling system conceptually by varying groundwater flow
31 into the Culebra Dolomite Member of the Rustler Formation as a scaled function of precipitation (Swift, 1991).
32 Short-term variability in precipitation is approximated with a periodic function that generates peaks of twice
33 present precipitation three times during the next 10,000 years and with a future climate that is wetter than that of
34 the present approximately one half of the time. Long-term, glacial increase in precipitation is approximated with
35 a periodic function that reaches a maximum of twice present precipitation in 60,000 years. For this performance
36 assessment, climatic variability has been included in the consequence analysis by varying boundary conditions of
37 the Culebra groundwater-flow model as a scaled function of future precipitation. Potentiometric heads along a
38 portion of the northern boundaries of the regional model domain were varied between present elevation and
39 approximately the ground surface, reaching maximum elevations at times of maximum precipitation.



TRI-6342-299-4

Figure 2-15. Estimated mean annual precipitation at the WIPP during the Late Pleistocene and Holocene (modified from Swift, 1992).

1 2.2.3.3 SURFACE WATER

2 The Pecos River, the principal surface-water feature in southeastern New Mexico, flows southeastward in
3 Eddy County approximately parallel to the axis of the Delaware Basin (Figure 2-1) and drains into the Rio Grande
4 in western Texas. In the vicinity of the WIPP, the drainage system includes small ephemeral creeks and draws and
5 has a drainage area of about 50,000 km² (20,000 mi²). At its closest point, the Pecos River is about 20 km
6 (12 mi) southwest of the WIPP (Brinster, 1991).

7 Very little, if any, of the surface water from Nash Draw reaches the Pecos River (Robinson and Lang, 1938;
8 Lambert, 1983). Several shallow, saline lakes in Nash Draw cover an area of about 16 km² (6 mi²) southwest of
9 the WIPP (Figure 2-6) and collect precipitation, surface drainage, and groundwater discharge from springs and
10 seeps. The largest lake, Laguna Grande de la Sal, has existed throughout historic time. Since 1942, smaller,
11 intermittent, saline lakes have formed in closed depressions north of Laguna Grande de la Sal as a result of effluent
12 from potash mining and oil-well development in the area (Hunter, 1985). Effluent has also enlarged Laguna
13 Grande de la Sal.

14 2.2.3.4 THE WATER TABLE

15 No maps of the water table are available for the vicinity of the WIPP. Outside of the immediate vicinity of
16 the Pecos River, where water is pumped for irrigation from an unconfined aquifer in the alluvium, near-surface
17 rocks are either unsaturated or of low permeability and do not produce water in wells. Tests of the lower Dewey
18 Lake Red Beds in H-14 that were intended to provide information about the location of the water table proved
19 inconclusive because of low transmissivities (Beauheim, 1987a). Livestock wells completed south of the WIPP in
20 the Dewey Lake Red Beds at the J. C. Mills Ranch (James Ranch) may produce from perched aquifers (Mercer,
21 1983; Lappin et al., 1989), or they may produce from transmissive zones in a continuously saturated zone that is
22 elsewhere unproductive because of low transmissivities.

23 Regionally, water-table conditions can be inferred for the more permeable units where they are close to the
24 surface and saturated. The Culebra Dolomite may be under water-table conditions in and near Nash Draw and near
25 regions of the Rustler Formation outcrop in Bear Grass Draw and Clayton Basin north of the WIPP (Figure 2-6).
26 The Magenta Dolomite is unsaturated and presumably above the water table at WIPP-28 and H-7 near Nash Draw.
27 Water-table conditions exist in the Rustler-Salado contact zone near where it discharges into the Pecos River at
28 Malaga Bend (Brinster, 1991).

29 2.2.3.5 REGIONAL WATER BALANCE

30 Hunter (1985) examined the overall water budget of approximately 5180 km² (2000 mi²) surrounding the
31 WIPP. Water inflow to the area comes from precipitation, surface-water flow in the Pecos River, groundwater
32 flow across the boundaries of the region, and water imported to the region for human use. Outflow from the
33 water-budget model occurs as stream-water flow in the Pecos River, groundwater flow, and evapotranspiration.
34 Volumes of water gained by precipitation and lost by evapotranspiration are more than one order of magnitude
35 larger than volumes gained or lost by other means.

1 Uncertainties about precipitation, evapotranspiration, and water storage within the system limit the usefulness
2 of estimates of groundwater recharge based on water-budget analyses. Regionally, Hunter (1985) concluded that
3 approximately 96 percent of precipitation was lost directly to evapotranspiration, without entering the surface or
4 groundwater flow systems. Within the 1000 km² (386 mi²) immediately around the WIPP, where no surface
5 runoff occurs and all precipitation not lost to evapotranspiration must recharge groundwater, a separate analysis
6 suggested evapotranspiration may be as high as 98 to 99.5 percent (Hunter, 1985). Direct measurements of
7 infiltration rates are not available from the WIPP vicinity.

8 2.2.3.6 GROUNDWATER FLOW ABOVE THE SALADO FORMATION

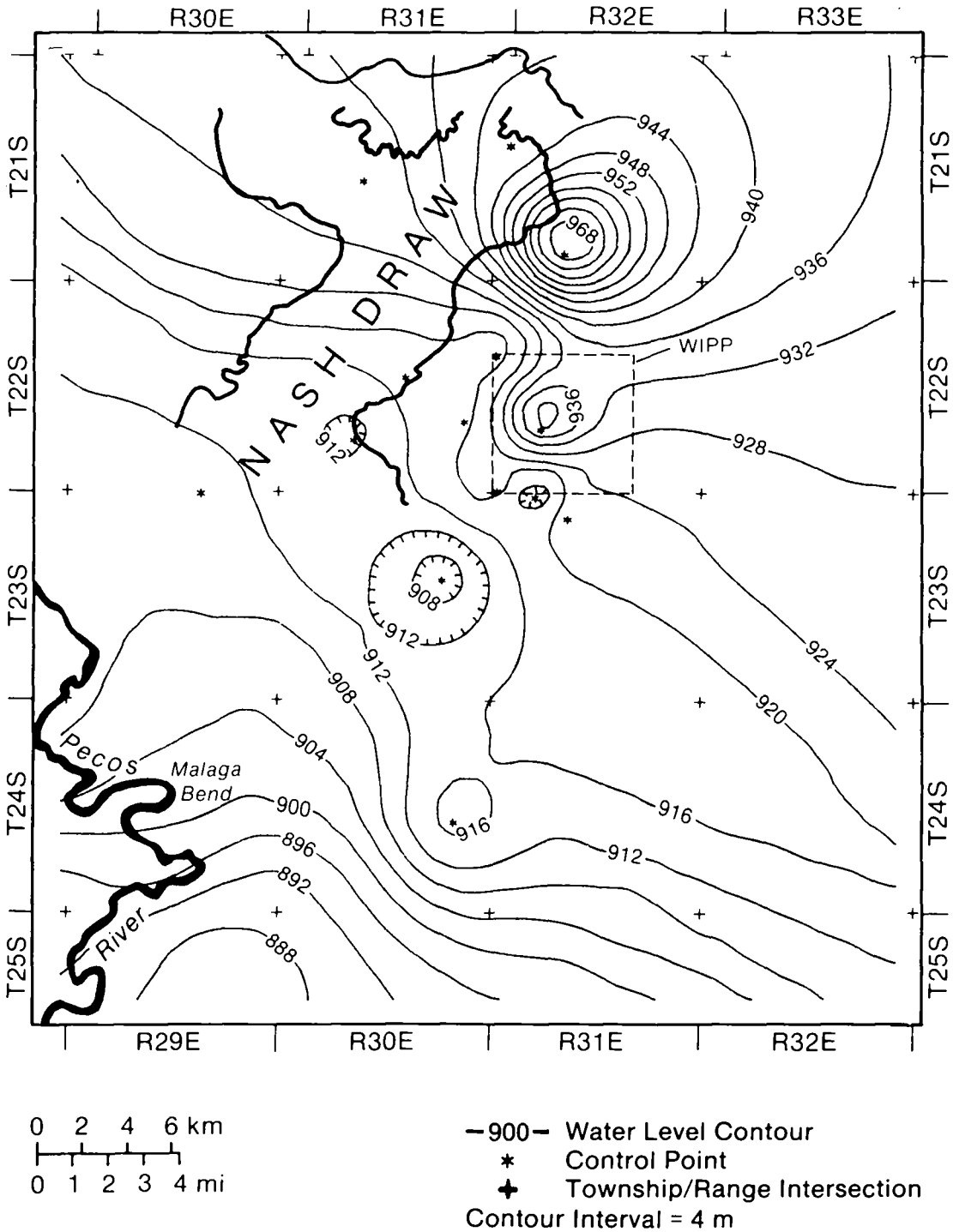
9 Well tests indicate that the three most permeable units in the vicinity of the WIPP above the Salado
10 Formation are the Culebra Dolomite and Magenta Dolomite Members of the Rustler Formation and the residuum
11 at the Rustler-Salado contact zone. The vertical permeabilities of the strata separating these units are not known,
12 but lithologies and the potentiometric and geochemical data summarized below suggest that for most of the
13 region, vertical flow between the units is very slow. Although preliminary hydrologic modeling indicates that
14 some component of vertical flow between units can be compatible with observed conditions (Haug et al., 1987;
15 Davies, 1989), the Culebra is assumed to be perfectly confined for the 1992 performance-assessment calculations.

16 Potentiometric Surfaces

17 Mercer (1983) and Brinster (1991) have constructed potentiometric-surface maps for the Rustler-Salado residuum,
18 the Culebra Dolomite, and the Magenta Dolomite; Brinster's (1991) maps are reproduced here (Figures 2-16, 2-17,
19 and 2-18). These maps show the elevation above sea level to which fresh water would rise in a well open to each
20 unit. Contours are based on measured heads (water elevations in wells) that have been adjusted to freshwater-
21 equivalent heads (the level to which fresh water would rise in the same well). Maps for the Culebra and the
22 Magenta Dolomites are based on data from 31 and 16 wells, respectively. The map for the Rustler-Salado
23 residuum includes data from 14 wells and water elevations in the Pecos River, reflecting an assumption that water-
24 table conditions exist in the unit near the river.

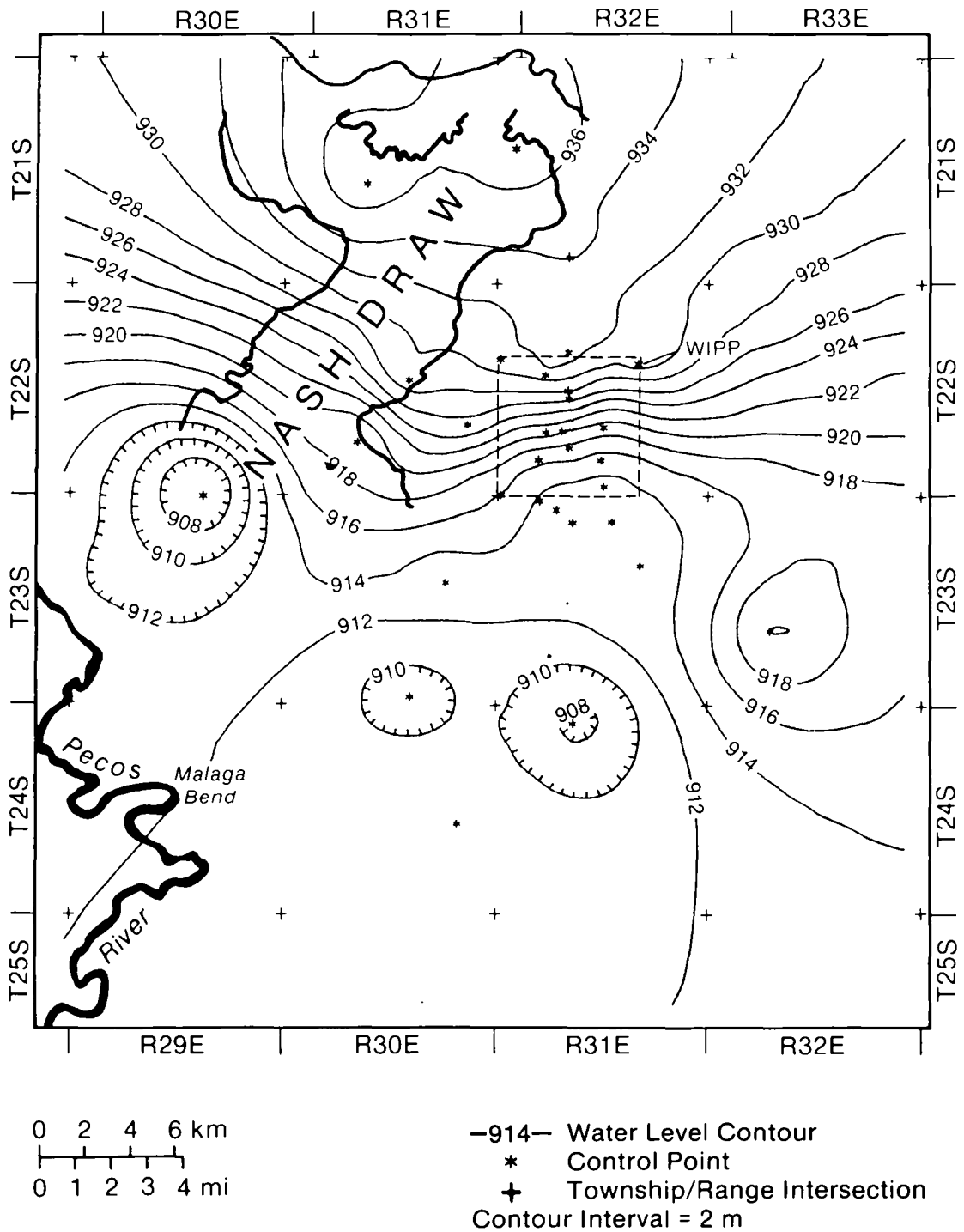
25 Because the data used to construct the potentiometric maps are sparse and unevenly distributed, interpretations
26 must be made with caution. For example, the "bull's-eye" patterns visible in all three maps are controlled by
27 single data points, and would probably disappear from the maps if sufficient data were available. Contours are
28 most reliable where data are closely spaced, particularly in the immediate vicinity of the WIPP, and are least
29 reliable where they have been extrapolated into areas of no data, such as the southeast portion of the mapped area.
30 With these caveats noted, however, the potentiometric maps can be useful in drawing conclusions about flow both
31 within and between the three units.

32 Flow of a constant-density liquid within an isotropic medium would be perpendicular to the potentiometric
33 contours. Near the WIPP, localized regions have been identified where variations in brine density result in non-
34 uniform gravitational driving forces and anomalous flow directions (Davies, 1989), and the effects of anisotropy
35 on flow patterns are not fully understood. In general, however, flow in the Rustler-Salado contact zone is from



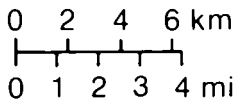
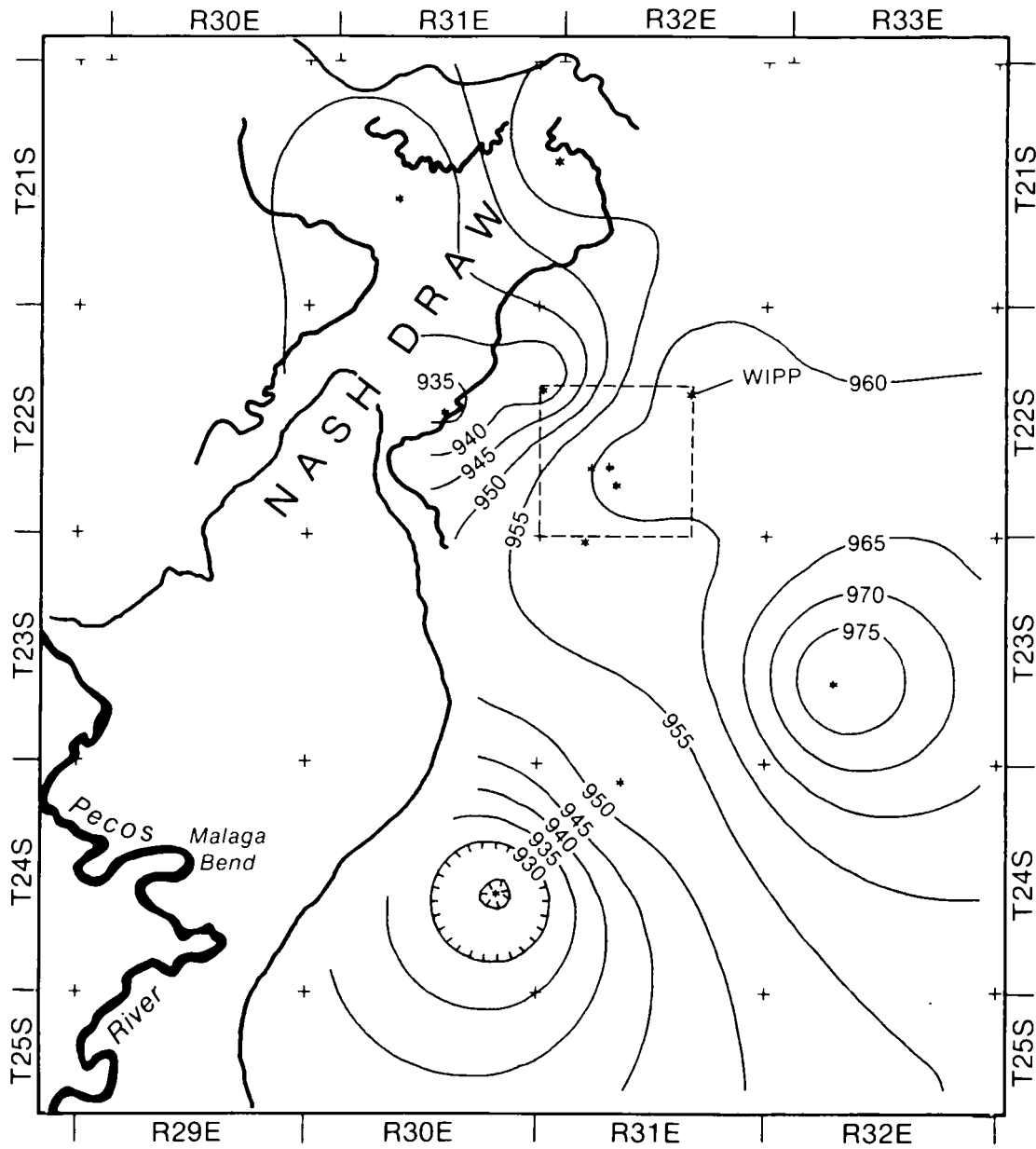
TRI-6342-295-1

Figure 2-16. Adjusted potentiometric surface of the Rustler-Salado contact zone in the WIPP vicinity (Brinster, 1991). Contours based on head data from indicated wells and water elevations in the Pecos River.



TRI-6342-293-1

Figure 2-17. Adjusted potentiometric surface of the Culebra Dolomite Member of the Rustler Formation in the WIPP vicinity (Brinster, 1991). Contours based on head data from indicated wells.



- Magenta Dolomite Member Subcrop
- 930- Water Level Contour
- * Control Point
- + Township/Range Intersection
- Contour Interval = 5 m

TRI-6342-285-1

Figure 2-18. Adjusted potentiometric surface of the Magenta Dolomite Member of the Rustler Formation in the WIPP vicinity (Brinster, 1991). Contours based on head data from indicated wells.

1 northeast to southwest. Flow in the Culebra is from north to south, and flow in the Magenta is from east to west
2 in that portion of the study area where data are sufficient to permit interpretation (i.e., near the WIPP).
3 Differences in flow directions may reflect long-term transient conditions (see "Recharge and Discharge" in Section
4 2.2.3.6) and indicate low permeability of the strata separating the three units; that is, if the three functioned as a
5 single aquifer, potentiometric maps would be similar.

6 Flow between units also is a function of hydraulic gradient and can be interpreted qualitatively from the
7 potentiometric maps. Like lateral flow within units, vertical flow between units is from higher potentiometric
8 levels to lower levels. Differences between the elevations of the potentiometric surfaces reflect low permeabilities
9 of the intervening strata and slow rates of vertical leakage relative to rates of flow within the aquifers. Brinster
10 (1991), and Beauheim (1987a) present analyses of vertical hydraulic gradients on a well-by-well basis. These
11 analyses suggest that, if flow occurs, the direction of flow between the Magenta and the Culebra is downward
12 throughout the WIPP area. Directly above the repository, flow may be upward from the Rustler-Salado residuum
13 to the Culebra Dolomite. Elsewhere in the region, both upward and downward flow directions exist between the
14 two units.

15 Groundwater Geochemistry

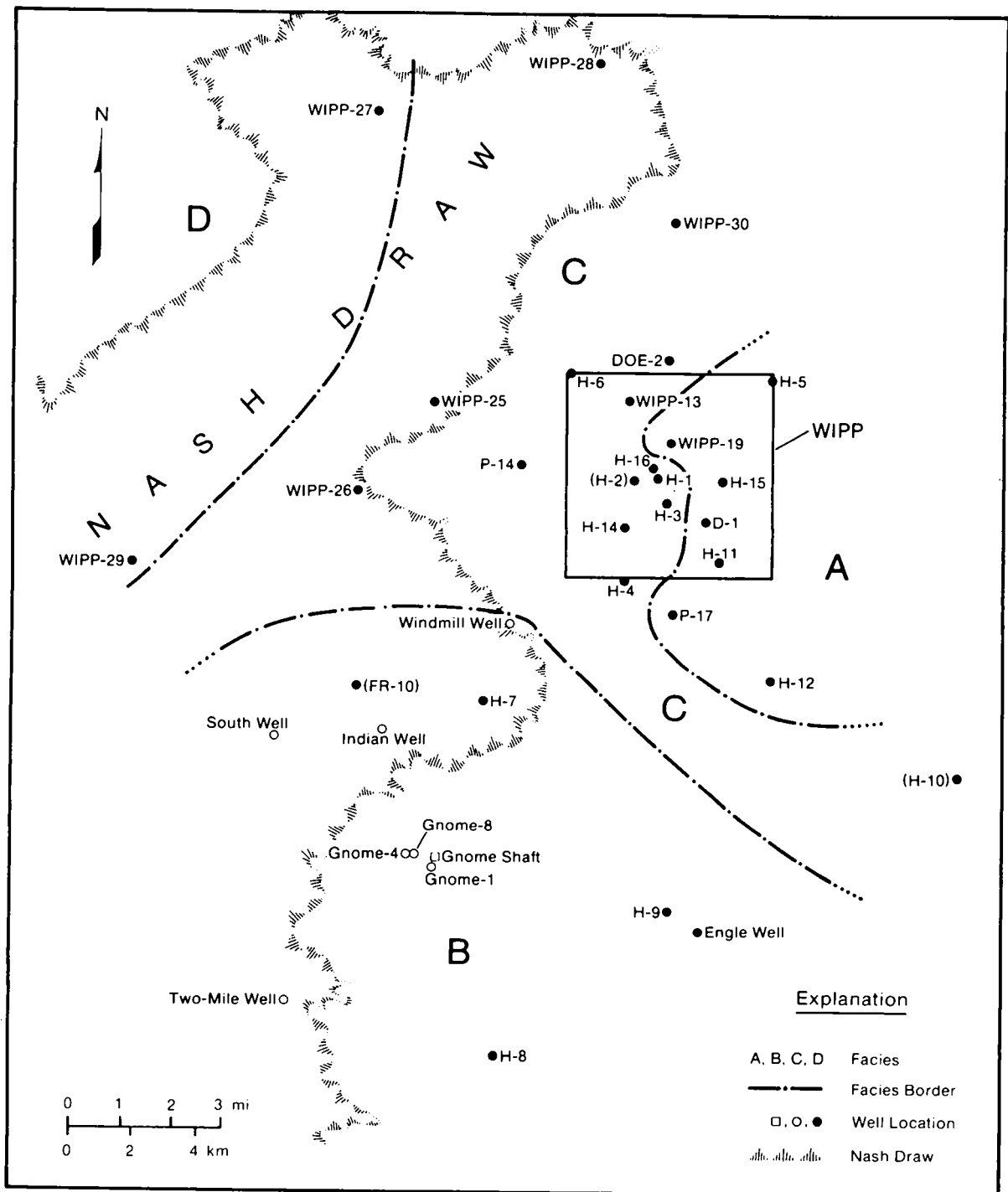
16 Major solute geochemical data are available for groundwater from the Rustler-Salado contact zone from 20
17 wells, from the Culebra Dolomite from 32 wells, and from the Magenta Dolomite from 12 wells (Siegel et al.,
18 1991). Groundwater quality in all three units is poor, with total dissolved solids (TDS) exceeding 10,000 mg/L
19 (the concentration specified for regulation by the Individual Protection Requirements of 40 CFR 191B) in most
20 locations.

21 Waters from the Rustler-Salado contact zone have the highest TDS concentrations of any groundwaters in the
22 WIPP area. The lowest concentration reported from the unit is 70,000 mg/L from H-7c southwest of the WIPP,
23 and the highest is 410,000 mg/L from H-5 at the northeast corner of the land-withdrawal area (Siegel et al., 1991).

24 Waters from the Magenta Dolomite are the least saline of those in the confined units. Within the land-
25 withdrawal area, TDS concentrations range from approximately 4000 to 25,000 mg/L. Higher values are reported
26 from H-10 southeast of the WIPP, where the sample is of uncertain quality, and from WIPP 27 in Nash Draw,
27 where groundwater chemistry has been altered by dumping of effluent from potash mines (Siegel et al., 1991).

28 Groundwater chemistry is variable in the Culebra Dolomite. A maximum TDS concentration of 324,100
29 mg/L is reported from WIPP-29 west of the repository in Nash Draw, and a minimum value of 2830 mg/L is
30 reported from H-8, 14 km (9 mi) southwest of the repository. Three other wells (H-7, H-9, and the Engle well),
31 all south of the WIPP, also contain water with less than 10,000 mg/L TDS (Siegel et al., 1991).

32 Relative concentrations of major ions vary spatially within the Culebra Dolomite. Siegel et al. (1991)
33 recognized four zones containing distinct hydrochemical facies (Figure 2-19) and related water chemistry to the
34 distribution of halite in the Rustler Formation. Zone A contains a saline (about 2 to 3 molal) sodium chloride
35 brine with a magnesium/calcium molar ratio greater than 1.2. Zone A waters occur eastward from the repository,



TRI-6331-78-0

Figure 2-19. Hydrochemical facies in the Culebra Dolomite Member of the Rustler Formation (Siegel et al., 1991).

1 in a region that corresponds roughly with the area of lowest transmissivity in the Culebra Dolomite. Halite is
2 present in the unnamed lower member of the Rustler Formation throughout Zone A, and in the eastern portion of
3 the region halite occurs in the upper members as well. Zone B is an area of dilute, calcium sulfate-rich water
4 (ionic strength less than 0.1 molal) south of the repository. This region generally has high transmissivity in the
5 Culebra Dolomite, and halite is absent from all members of the Rustler Formation. Zone C, extending from the
6 repository west to Nash Draw, contains waters of variable composition with low to moderate ionic strength (0.3
7 to 1.6 molal), with magnesium/calcium molar ratios less than 1.2. Transmissivity is variable in this region, and
8 halite is present in the Rustler Formation only to the east, in the unnamed lower member. Salinities are highest
9 near the eastern edge of the zone. Zone D waters, found only in two wells in Nash Draw, are anomalously saline
10 (3 to 6 molal) and have high potassium/sodium ratios that reflect contamination by effluent from potash mines.

11 Distribution of the hydrochemical facies may not be consistent with the inferred north-to-south flow of
12 groundwater in the Culebra Dolomite. Specifically, less saline waters of Zone B are down-gradient from more
13 saline waters in Zones A and C. Chapman (1988) suggested that direct recharge of fresh water from the surface
14 could account for the characteristics of Zone B. As discussed in more detail below ("Recharge and Discharge"
15 section), the inconsistency between chemical and potentiometric data could also result from a change in location
16 and amount of recharge since the wetter climate of the last glacial maximum (Lambert, 1991). Present flow in
17 the Culebra could be transient, reflecting gradual drainage of a groundwater reservoir filled during the Pleistocene
18 (Lambert and Carter, 1987; Davies; 1989; Lambert, 1991). Regional hydrochemical facies may not have
19 equilibrated with the modern flow regime and instead may reflect geographic distribution of halite during a past
20 flow regime (Siegel and Lambert, 1991).

21 Recharge and Discharge

22 The only documented points of naturally occurring groundwater discharge in the vicinity of the WIPP are the
23 saline lakes in Nash Draw and the Pecos River, primarily near Malaga Bend (Hunter, 1985; Brinster, 1991).
24 Discharge into the lakes from Surprise Spring was measured at a rate of less than 0.01 m³/s (0.35 ft³/s) in 1942
25 (Hunter, 1985). Estimated total groundwater discharge into the lakes is 0.67 m³/s (24 ft³/s) (Hunter, 1985).
26 Based on chemical and potentiometric data, Mercer (1983) concluded that discharge from the spring was from
27 fractured and more transmissive portions of the Tamarisk Member of the Rustler Formation, and that the lakes
28 were hydraulically isolated from the Culebra Dolomite and lower units. Lambert and Harvey's (1987) analysis of
29 stable isotopes in water from Surprise Spring supports the conclusion that Surprise Spring and Laguna Grande de
30 la Sal are not discharge points for the Culebra Dolomite.

31 Groundwater discharge into the Pecos River is larger than discharge into the saline lakes. Based on 1980
32 stream-flow gage data, Hunter (1985) estimated that groundwater discharge into the Pecos River between Avalon
33 Dam north of Carlsbad and a point south of Malaga Bend was no more than approximately 0.92 m³/s (33 ft³/s).
34 Most of this gain in stream flow occurs near Malaga Bend and is the result of groundwater discharge from the
35 residuum at the Rustler-Salado contact zone (Hale et al., 1954; Kunkler, 1980; Hunter, 1985; Brinster, 1991).

36 The only documented point of groundwater recharge is also near Malaga Bend, where an almost immediate
37 water-level rise has been reported in a Rustler-Salado residuum well following a heavy rainstorm (Hale et al.,

1 1954). This location is hydraulically down-gradient from the repository, and recharge here has little relevance to
 2 flow near the WIPP. Examination of the potentiometric-surface map for the Rustler-Salado contact zone (Figure
 3 2-16) indicates that some inflow may occur north of the WIPP, where freshwater-equivalent heads are highest.
 4 Additional inflow to the contact zone may occur as leakage from overlying units, particularly where the units are
 5 close to the surface and under water-table conditions. Brinster (1991) proposed that inflow to the contact zone (and
 6 other units in the Rustler Formation) could also come from below, upward through breccia pipes from the Capitan
 7 aquifer north and east of the repository.

8 No direct evidence exists for the location of either recharge to or discharge from the Culebra Dolomite. The
 9 potentiometric-surface map (Figure 2-17) implies inflow from the north and outflow to the south. Mercer (1983)
 10 suggested that recharge from the surface probably occurred 15 to 30 km (9 to 19 mi) northwest of the WIPP in and
 11 north of Clayton Basin (Figure 2-6), where the Rustler Formation crops out. An undetermined amount of inflow
 12 may also occur as leakage from overlying units throughout the region.

13 The potentiometric-surface map (Figure 2-17) indicates that flow in the Culebra Dolomite is toward the
 14 south. Some of this southerly flow may enter the Rustler-Salado contact zone under water-table conditions near
 15 Malaga Bend and ultimately discharge into the Pecos River. Additional flow may discharge directly into the Pecos
 16 River or into alluvium in the Balmorhea-Loving Trough to the south (Figure 2-6) (Brinster, 1991).

17 Recharge to the Magenta Dolomite may also occur north of the WIPP in Bear Grass Draw and Clayton Basin
 18 (Mercer, 1983). The potentiometric-surface map indicates that discharge is toward the west in the vicinity of the
 19 WIPP, probably into the Tamarisk Member and the Culebra Dolomite near Nash Draw. Some discharge from the
 20 Magenta Dolomite may ultimately reach the saline lakes in Nash Draw. Additional discharge probably reaches the
 21 Pecos River at Malaga Bend or alluvium in the Balmorhea-Loving Trough (Brinster, 1991).

22 Isotopic data from groundwater samples suggest that groundwater travel time from the surface to the Dewey
 23 Lake Red Beds and the Rustler Formation is long and rates of flow are extremely slow. Low tritium levels in all
 24 WIPP-area samples indicate minimal contributions from the atmosphere since 1950 (Lambert and Harvey, 1987).
 25 Four modeled radiocarbon ages from Rustler Formation and Dewey Lake Red Beds groundwater are between
 26 12,000 and 16,000 years (Lambert, 1987). Observed uranium isotope activity ratios require a conservative
 27 minimum residence time in the Culebra Dolomite of several thousands of years and more probably reflect
 28 minimum ages of 10,000 to 30,000 years (Lambert and Carter, 1987). Stable-isotope data are more ambiguous:
 29 Lambert and Harvey (1987) concluded that compositions are distinct from modern surface values and that the
 30 contribution of modern recharge to the system is slight, whereas Chapman (1986, 1988) concluded that available
 31 stable-isotope data do not permit interpretations of groundwater age. Additional stable-isotope research is in
 32 progress and may resolve some uncertainty about groundwater age.

33 Potentiometric data from four wells support the conclusion that little infiltration from the surface reaches the
 34 transmissive units of the Rustler Formation. Hydraulic head data are available for a claystone in the Forty-niner
 35 Member from DOE-2, H-3, H-4, H-5, and H-6. Comparison of these heads to Magenta heads in surrounding
 36 wells shows that flow between the units at all four wells may be upward (Beauheim, 1987a). This observation
 37 offers no insight into the possibility of infiltration reaching the Forty-niner Member, but it rules out the
 38 possibility of infiltration reaching the Magenta Dolomite or any deeper units at these locations.

1 Location and amount of groundwater recharge and discharge in the area may have been substantially different
2 during wetter climates of the Pleistocene. Gypsiferous spring deposits on the east side of Nash Draw are of late
3 Pleistocene age and reflect discharge from an active water table in the Rustler Formation (Bachman, 1981, 1987;
4 Davies, 1989; Brinster, 1991). Coarse sands and gravels in the Pleistocene Gatuña Formation indicate deposition
5 in high-energy, through-going drainage systems unlike those presently found in the Nash Draw area (Bachman,
6 1987). Citing isotopic evidence for a Pleistocene age for Rustler Formation groundwater, Lambert and Carter
7 (1987) and Lambert (1991) have speculated that during the late Pleistocene, Nash Draw may have been a principal
8 recharge area, and flow in the vicinity of the WIPP may have been eastward. In this interpretation, there is
9 essentially no recharge at the present, and the modern groundwater-flow fields reflect the gradual draining of the
10 strata. Preliminary modeling of long-term transient flow in a two-dimensional, east-west cross section indicates
11 that, although the concept remains unproven, it is not incompatible with observed hydraulic properties (Davies,
12 1989). As the performance-assessment groundwater-flow model is further developed and refined, the potential
13 significance of uncertainty in the location and amount of future recharge will be re-evaluated.

14 **2.2.4 Radionuclide Transport in the Culebra Dolomite**

15 Hydraulic tests using nonreactive tracers have been conducted in the Culebra Dolomite Member of the Rustler
16 Formation near the WIPP at the H-2, H-3, H-4, H-6, and H-11 hydropad well locations (Kelley and Pickens,
17 1986; Saulnier, 1987; Beauheim, 1987b,c; Jones et al., 1992) (see Figures 2-6 and 2-8 for well locations). At the
18 H-2 and H-4 hydropads, transmissivity in the Culebra is low, and tracer test results are best explained by
19 characterizing the Culebra as a single-porosity, matrix-only medium in which interconnected open fractures are not
20 present (see Section 2.2.2.6 for a discussion of fractures in the Culebra). At the H-3, H-6, and H-11 hydropads, a
21 dual-porosity, fracture-plus-matrix model for transport provides the best agreement with the tracer test data.
22 Neither a single-porosity, fracture-only nor a single-porosity, matrix-only model provides a suitable interpretation
23 of the tracer test data at these locations (Jones et al., 1992). The H-3 and H-11 hydropad locations lie south and
24 southeast of the waste panels, within the predicted flow paths from the panels (LaVenue and RamaRao, 1992), and
25 the WIPP PA Department therefore believes that a dual-porosity transport model provides the most realistic
26 estimate of subsurface releases at the accessible environment boundary. Alternative conceptual models for both
27 single-porosity, fracture-only transport (believed to be an unrealistic but known endpoint of a continuum of
28 models on which a realistic endpoint is uncertain) and dual-porosity, matrix-plus-fracture transport (believed to be
29 realistic) were used in the 1992 PA. Results are compared in Volume 1, Chapter 5 of this report.

30 Unlike the nonreactive materials used in tracer tests, radionuclides may be retarded during transport by
31 chemical interactions with the rock. Distribution coefficients (K_d s, mL/g), defined for a given element as the
32 concentration sorbed per gram of rock divided by the concentration per a milliliter of solution, are used to describe
33 the partitioning of radionuclides between groundwater and rock. As described in Section 7.6, K_d s are then used to
34 derive retardation factors, defined as mean fluid velocity divided by mean radionuclide velocity, which take into
35 account pore space geometry and the thickness of clay linings that line pores and fractures as well as K_d values.
36 Distribution coefficients may be determined experimentally for individual radionuclides in specific water/rock
37 systems (e.g., Lappin et al., 1989), but because values are strongly dependent on water chemistry and rock
38 mineralogy and the nature of the flow system, experimental data cannot be extrapolated directly to a complex
39 natural system. For the 1992 (and 1991) preliminary performance assessments, cumulative distribution functions

1 (cdfs) for K_{ds} were based on judgment elicited from an expert panel as described in the following section. In
2 keeping with the agreement between the DOE and the State of New Mexico (U.S. DOE and the State of New
3 Mexico, 1981, as modified), K_{ds} used in final compliance evaluations will be based on experimentally justified
4 data.

5 Sensitivity analyses performed as part of the 1990 PA indicated that, conditional on the models and
6 distributions used in the 1990 calculations, variability in distribution coefficients was one of the most important
7 contributors to overall variability in cumulative releases through groundwater transport (Helton et al., 1991), and
8 that overall performance was sensitive to the choice of conceptual model (single porosity versus dual porosity) for
9 transport (Bertram-Howery et al., 1990). Sensitivity analyses performed as part of the 1991 PA confirmed the
10 importance of both chemical retardation and physical retardation (Helton et al., 1992). The potential impact of
11 uncertainty in the conceptual model for transport is examined again in the 1992 PA.

12 2.2.4.1 EXPERT JUDGMENT ELICITATION FOR K_{ds}

13 Unlike other expert panels organized for WIPP performance assessment, which consisted of experts with no
14 formal affiliation with SNL (e.g., the future intrusion and markers panels discussed in Chapter 5 of this volume
15 and the source term panel discussed later in this chapter), the Radionuclide Retardation Expert Panel consisted of
16 SNL staff members who are currently working or have worked on retardation in the Culebra. In other regards,
17 procedures for the presentation of the issues and the elicitation of results were as suggested by Hora and Iman
18 (1989) and Bonano et al. (1990).

19 The Radionuclide Retardation Expert Panel was requested to provide probability distributions for distribution
20 (sorption) coefficients for eight elements (americium, curium, uranium, neptunium, plutonium, radium, thorium,
21 and lead) that represent a spatial average over the total area of concern (from a hypothetical intrusion borehole to
22 the boundary of the accessible environment). This was to be done for two separate cases: (1) the coefficients that
23 result from the clay that lines the fractures in the Culebra Dolomite, and (2) the coefficients that result from the
24 matrix pore space of the Culebra Dolomite. During the meetings, the panelists decided to further break down the
25 problem by examining the coefficients that would result from the particular rock species and two different
26 transport fluids: (1) transport fluid that is predominantly relatively low-salinity Culebra brine, or (2) transport
27 fluid that is predominantly high-salinity Salado brine. Probability distributions were thus provided for four
28 situations for each radionuclide.

29 Two short meetings were held in April 1991 to discuss the physical situation and the issue statement. The
30 period between the second and third meetings (approximately one month) was available for the panelists to
31 examine the existing data base and discuss the results with each other. The third meeting, held at the end of May
32 1991, involved the expert judgment elicitation training, a discussion among the panelists as to the cases and
33 assumptions to be used during the elicitation, and the actual elicitation sessions. At the request of one of the
34 panelists, judgments were elicited separately from the experts. Each panelist provided distributions where they
35 were able. Incompleteness resulted in some cases from a lack of knowledge about a particular radionuclide.
36 Specific distributions provided by each panelist are presented in Volume 3 of the 1991 edition of this report

1 (Section 2.6.10 of WIPP PA Division [1991c]). The composite distributions used in the 1992 performance-
2 assessment calculations are provided in Volume 3 of this report (Section 2.6.4).

3 The panelists judgments were based on a body of data generated largely by experiments with rock samples
4 taken from boreholes in the vicinity of the WIPP (Trauth et al., 1992):

5 • plutonium K_d s (Dosch and Lynch, 1978; Lynch and Dosch, 1980; Dosch, 1980; Nowak, 1980; Serne et
6 al., 1977; Tien et al., 1983)

7 • americium K_d s (Dosch and Lynch, 1978; Lynch and Dosch, 1980; Nowak, 1980; Serne et al., 1977; Tien
8 et al., 1983)

9 • curium K_d s (Dosch and Lynch, 1978; Serne et al., 1977; Tien et al., 1983)

10 • neptunium K_d s (Dosch and Lynch, 1978; Serne et al., 1977; Tien et al., 1983)

11 • uranium K_d s (Dosch, 1981; Dosch, 1980; Serne et al., 1977; Tien et al., 1983)

12 • strontium K_d s (as analog for radium) (Dosch and Lynch, 1978; Lynch and Dosch, 1980; Dosch, 1980;
13 Serne et al., 1977)

14 • radium and lead K_d s (Tien et al., 1983)

15 • thorium K_d s (Tien et al., 1983).

16 The K_d values reported in these references were calculated by indirect means: Measurements were not taken of the
17 activity sorbed to the rock. Rather, measurements were taken as to the activity lost from the solution contacting
18 the rock.

19 Tien et al. (1983) differed in their experimental approach from the other experimenters cited above. Tien et al.
20 (1983) compiled experimental distribution coefficients from open literature that might be applicable to
21 investigations of a potential repository site in bedded salt in the Palo Duro Basin of Texas.

22 2.2.4.2 PLANNED AND ONGOING EXPERIMENTAL WORK RELATED TO RADIONUCLIDE 23 TRANSPORT IN THE CULEBRA

24 The WIPP Test Phase Plan (U.S. DOE, 1990a, currently in revision) contains experimental programs that
25 will provide additional information on both chemical and physical retardation.

26 Chemical retardation will be addressed through laboratory experiments that will measure adsorption of
27 radionuclides as a function of water composition to characterize adsorption in the wide range of groundwater
28 compositions expected in the Culebra. Batch sorption experiments, in which crushed Culebra rock will be placed

1 in a brine solution containing the radionuclides of interest, will provide K_d values for many different conditions,
2 but will provide little information about retardation in natural fractures. K_d s based on these experiments will
3 provide an upper bound on the amount of sorption that can be expected. A set of column-flow experiments is
4 therefore in progress that will measure radionuclide sorption in columns of intact Culebra rock (core samples from
5 the Air Intake Shaft at the WIPP), thus providing a more direct determination of natural (both chemical and
6 physical) retardation in the Culebra (see U.S. DOE, 1992, and references cited therein for additional information
7 about these experiments).

8 Retardation could also be addressed through tracer tests at a proposed new seven-well hydropad, to be called H-
9 19 (Beauheim and Davies, 1992). The test may be conducted at the site of an existing well (e.g., H-3), or a new
10 location may be selected. In either case H-19 will be in a region of relatively high transmissivity south or
11 southeast of the waste panels, within the envelope of predicted flow paths to the accessible environment. Tests
12 with both conservative and reactive (but not radioactive) tracers will examine transport along various paths
13 between a central well and six outer wells drilled at different radii from the central location. Specific objectives of
14 these tests are to: address questions about vertical heterogeneity in the Culebra (tests will isolate specific
15 horizontal layers within the Culebra in different wells to examine vertical flow and transport between layers); to
16 provide data to allow evaluation of alternative conceptual models for transport in the Culebra, including
17 anisotropic, heterogeneous, and channeling models; to provide information about chemical retardation processes on
18 a field scale; to provide additional evidence that matrix diffusion is an important process in retardation; and to
19 provide core samples for additional laboratory tests from the region of predicted flow paths to the accessible
20 environment. Results of the field tracer tests are anticipated to be available for use in performance assessment
21 beginning in 1995 (Beauheim and Davies, 1992).

22 **2.3 Engineered Barrier System**

23 The WIPP disposal system includes engineered barriers that minimize the rate at which radionuclides may
24 migrate through the hydrogeologic setting to the accessible environment. As presently designed, the repository
25 relies on seals in panels, drifts, and shafts to prevent migration through the excavated openings. If performance
26 assessments indicate additional barriers are needed to reduce potential radionuclide transport up an intrusion
27 borehole, modifications can be made to the form of the waste and backfill or to the design of the waste-
28 emplacement areas that will enhance long-term performance. Section 2.3 contains descriptions of the repository
29 and seal design, the waste, the radionuclide source term, and the room/waste interactions. Because the performance
30 of engineered barriers is dependent on the properties of the surrounding strata, Section 2.3 also contains additional
31 information about the Salado Formation at the repository horizon.

32 **2.3.1 The Salado Formation at the Repository Horizon**

33 Depositional processes that created the Salado Formation were laterally persistent over large areas, and
34 individual stratigraphic horizons within the formation can be recognized in potash mines and boreholes throughout
35 the WIPP region (Lowenstein, 1988). Forty-four anhydrite and polyhalite "marker beds" in the Salado Formation
36 have been identified and numbered within the approximately 2700 km² (1050 mi²) of the Carlsbad potash mining

1 district (Jones et al., 1960). Thinner interbeds of anhydrite, clay, and polyhalite occur throughout the formation,
2 and are also laterally persistent.

3 Lithologic layers in the Salado Formation dip less than 1° to the southeast at the WIPP, and the waste-
4 emplacement area is being excavated at a constant stratigraphic horizon rather than at a constant elevation so that
5 all waste panels will share the same local stratigraphy. This slight slope of the repository will result in a
6 difference in floor elevation between the highest and lowest panels of less than 10 m.

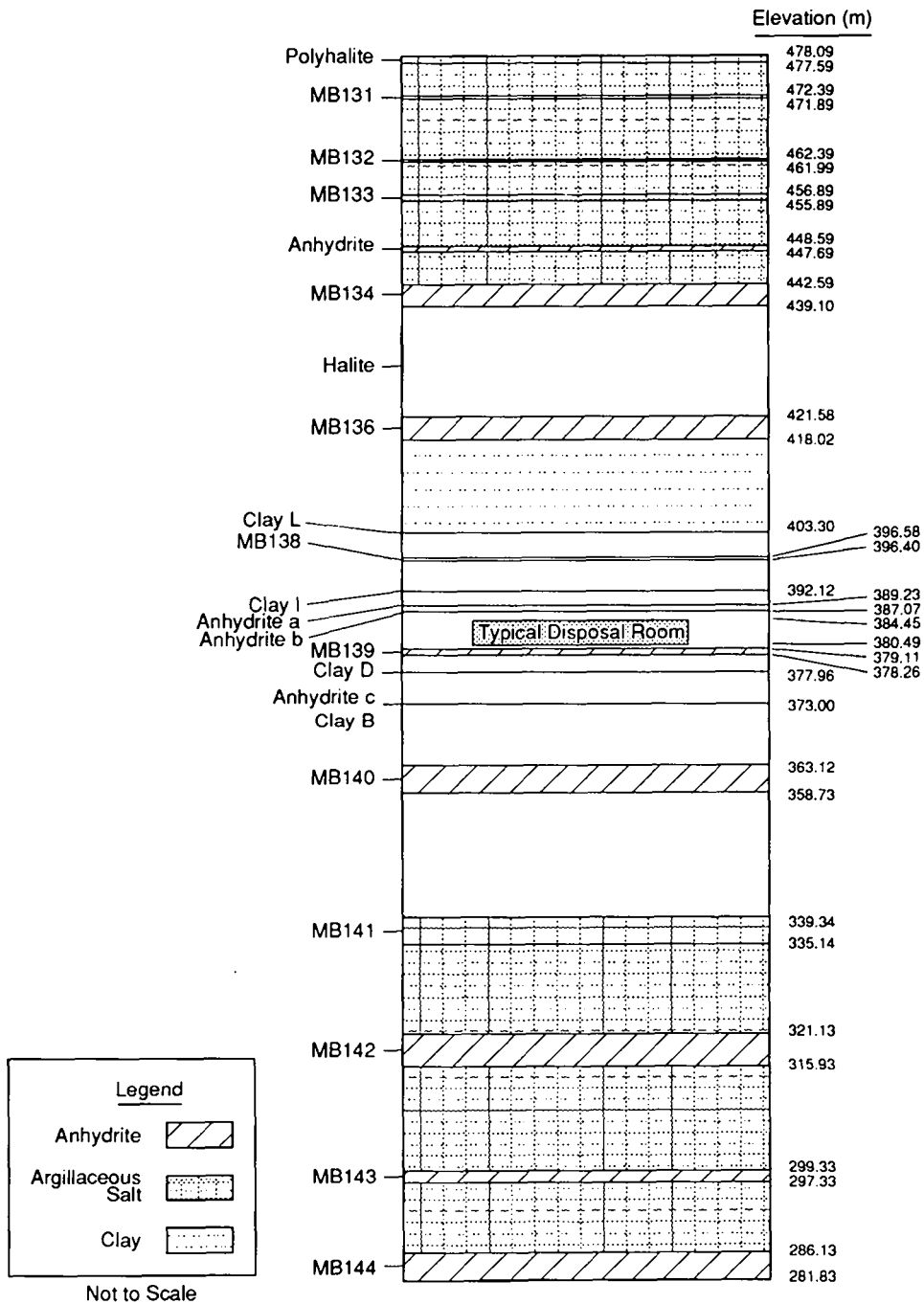
7 Panels are excavated entirely within a 7.3-m (24-ft) thick section of halite and polyhalite between anhydrite
8 marker beds 138 (MB138) and 139 (MB139), approximately 380 m (1250 ft) below the top of the Salado
9 Formation (Figure 2-20a). Waste-emplacement panels are excavated in the lower portion of this section,
10 approximately 1.4 m (4.6 ft) above MB139 (Figure 2-20b). Excavation has penetrated MB139 in sumps of all
11 four shafts, and in other locations. Experimental rooms, located in a separate part of the repository north of the
12 waste-emplacement area (see Section 2.3.2), have been excavated at a stratigraphic level higher than that of the
13 waste-emplacement panels, in part, so that borehole tests can be conducted beneath the room floors in undisturbed
14 strata of the waste-emplacement horizon.

15 Anhydrite interbeds are of importance for performance assessment because they are more permeable than the
16 halite layer containing the disposal room, and therefore provide the dominant pathway for fluid migration. As
17 discussed in more detail in Volume 3, presently available WIPP test data indicate undisturbed permeabilities
18 ranging between 10^{-16} and 10^{-21} m^2 for anhydrite and between 10^{-19} and 10^{-24} m^2 for halite (Gorham et al.
19 memo in Volume 3, Appendix A of this report). Interbeds included in the 1992 performance assessment are
20 MB139, and anhydrites A and B and MB138 located above the waste-emplacement panels (Figures 2-20a and 2-
21 20b).

22 Excavation of the repository and the consequent release of lithostatic stress has created a disturbed rock zone
23 (DRZ) around the underground openings. The DRZ at the WIPP has been confirmed by borehole observations,
24 geophysical surveys, and gas-flow tests, and varies in extent from 1 to 5 m (3.3 to 16.4 ft) (Stormont et al.,
25 1987; Peterson et al., 1987; Lappin et al., 1989). Fractures and microfractures within the DRZ have increased
26 porosity and permeability of the rock and increased brine flow from the DRZ to the excavated openings (Borns and
27 Stormont, 1988, 1989). Fracturing has occurred in MB139 below the waste-emplacement panels and in both
28 anhydrites A and B above the waste-emplacement panels. It is not known how far fracturing in the anhydrite
29 interbeds extends laterally from the excavations at this time, nor is the ultimate extent of the DRZ known. Most
30 deformation related to development of the DRZ is believed to occur in the first five years after excavation (Lappin
31 et al., 1989).

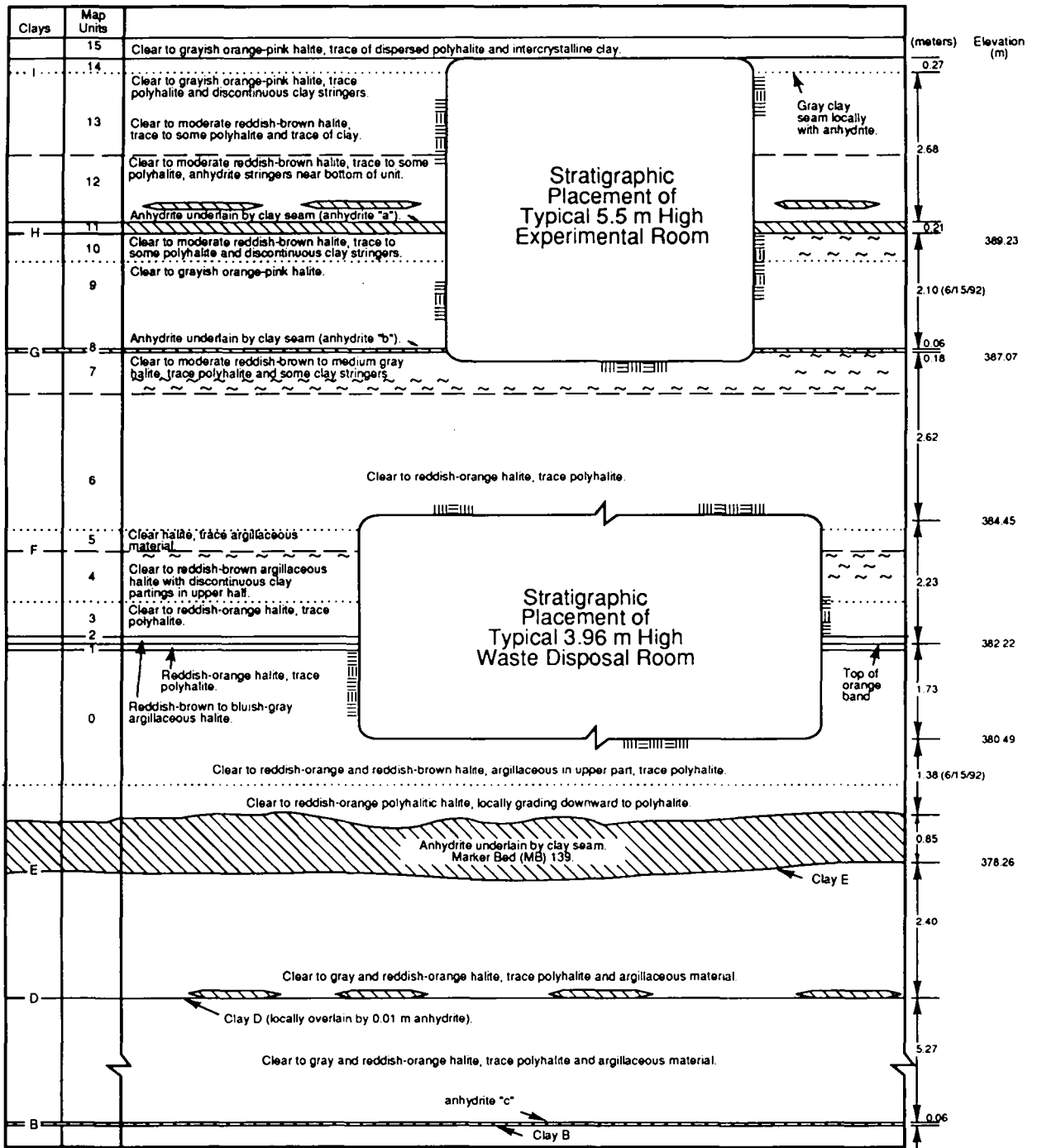
32 Fracturing in the DRZ, particularly in the anhydrite interbeds, may provide an enhanced pathway for fluid
33 migration out of the repository and possibly around panel and drift seals. Characterization of fracture-related
34 permeability in these layers is essential to modeling of two-phase (gas and brine) fluid flow into and out of the
35 repository. Work is in progress on modeling the possible pressure dependency of fracture permeability in
36 anhydrite interbeds, and results will be incorporated in future PAs.

Engineered Barrier System
The Salado Formation at the Repository Horizon



TRI-6342-1070-0

Figure 2-20a. Reference local stratigraphy near repository (after Munson et al., 1989a, Figure 3-3).



TRI-6334-257-3

Figure 2-20b. Stratigraphy at the repository horizon (after Bechtel National, Inc., 1986, Figures 6-2, 6-3, and Lappin et al., 1989, Figure 4-12). Units in the disposal area dip slightly to the south, but disposal excavations are always centered about the orange marked band (reddish-orange halite).

1 Borehole observations of pore-fluid pressure and permeability suggest that there may be a transition zone
2 extending outward beyond the DRZ. Within this transition zone pore-fluid pressures have dropped from their
3 undisturbed, pre-excavation level, apparently without irreversible rock damage and large permeability changes
4 (Gorham et al. memo in Volume 3, Appendix A of this report). The full extent of the transition zone is
5 uncertain, as are its material properties. Properties of the transition zone used in the 1992 PA calculations are
6 discussed in a memorandum of July 14, 1992 by Davies et al. in Volume 3, Appendix A of this report.

7 **2.3.2 Repository and Seal Design**

8 Major components of repository design that affect performance assessment are the waste itself, the
9 underground waste-emplacement area and its access drifts and shafts, and the seals that will be used to isolate the
10 emplacement area when the repository is decommissioned. The underground workings will ultimately consist of
11 eight waste-emplacement panels, access drifts and shafts, and an experimental area (Figure 2-21). Drifts in the
12 central portion of the repository will also be used for waste emplacement, providing the equivalent of an additional
13 two panels for waste emplacement. A more detailed discussion of repository design is available in Volume 3 of
14 this report.

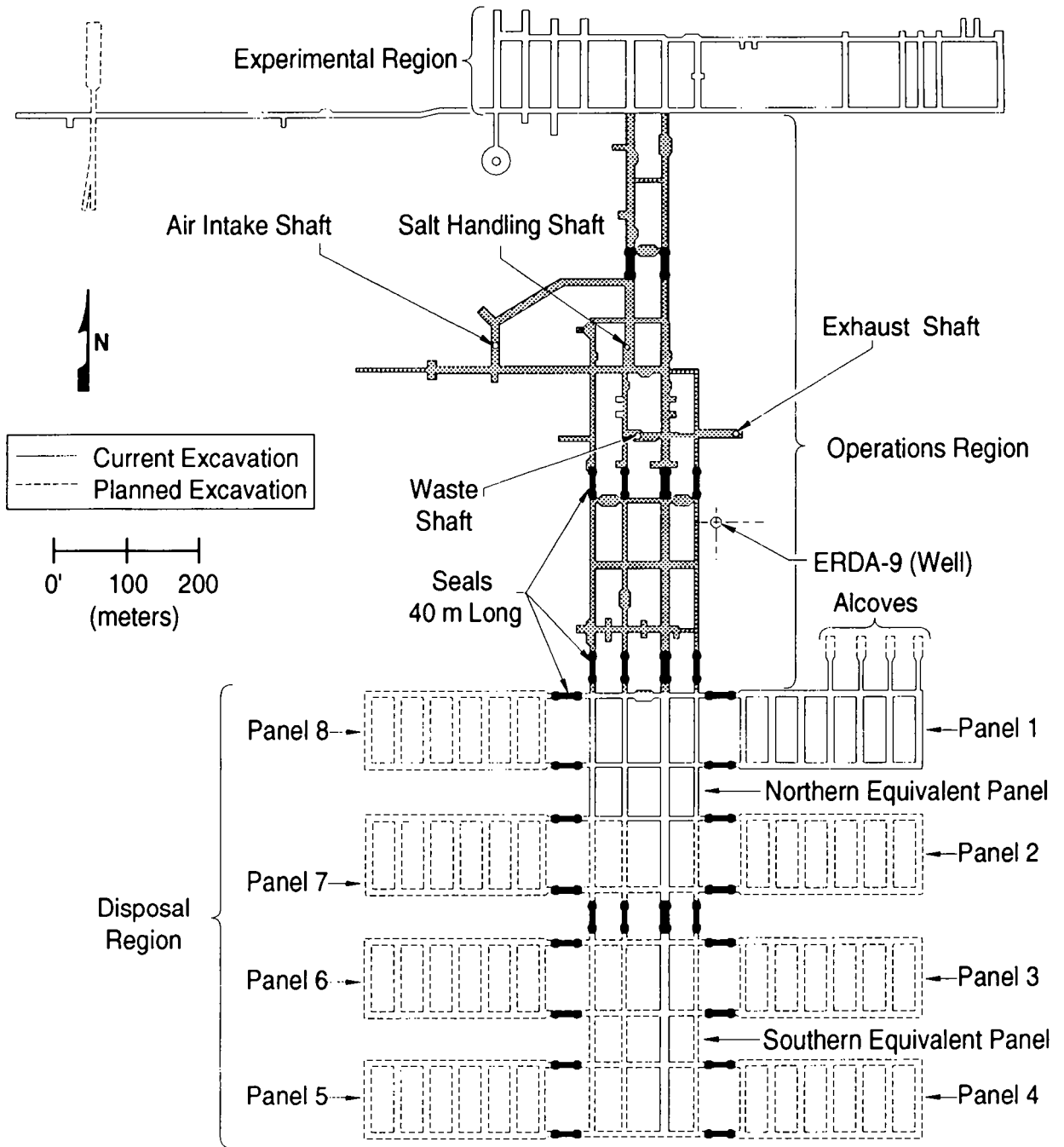
15 All underground horizontal openings are rectangular in cross section. The emplacement area drifts are 4.0 m
16 (13 ft) high by 7.6 m (25 ft) wide; the disposal rooms are 4.0 m (13 ft) high, 10.1 m (33 ft) wide, and 91.4 m
17 (300 ft) long. Pillars between rooms are 30.5 m (100 ft) wide. The eight waste-emplacement panels will each
18 have an initial volume of 46,000 m³ (1.6 × 10⁶ ft³). The northern drift emplace area will have an initial volume
19 of 34,000 m³ (1.2 × 10⁶ ft³), and the southern drift emplacement area will have an initial volume of 33,000 m³
20 (1.2 × 10⁶ ft³) (Rechard et al., 1990a). Overall, the waste-emplacement areas will have an initial volume of about
21 435,000 m³ (1.5 × 10⁷ ft³).

22 The four vertical access shafts are cylindrical and range in diameter from 5.8 m (19 ft) to 3.0 m (10 ft).
23 Shafts are lined in the units above the Salado Formation to prevent groundwater inflow and provide stability; they
24 are unlined in the salt.

25 Excavation of the first waste-emplacement panel is complete; the remaining panels will be excavated as
26 needed. Waste will be emplaced within the panels in drums or metal boxes, and panels will be backfilled and
27 sealed as they are filled. Seals will be installed in panels, drifts, and the vertical shafts before the repository is
28 decommissioned. Waste, backfill, and seals will be consolidated by creep closure after decommissioning.

29 **2.3.2.1 WASTE CHARACTERIZATION**

30 The waste that will be emplaced in the WIPP must meet the Waste Acceptance Criteria for the Waste
31 Isolation Pilot Plant (U.S. DOE, 1991a) as explained in Volume 1 of this report (Chapter 3). These acceptance
32 criteria specify that waste material containing particulates in certain size and quantity ranges will be immobilized,



TRI- 6334-206-7

Figure 2-21. Plan view of waste-disposal horizon showing shaft, drift, and panel seal locations (after Nowak et al., 1990).

1 that waste liquid content be restricted to that remaining in well-drained containers and be less than one volume
2 percent of the waste container, and that radionuclides in phyrophoric form be limited to less than one percent by
3 weight of the external container. The requirements also prohibit disposal at the WIPP of wastes containing
4 explosives, compressed gases, and ignitable, corrosive or reactive materials.

5 The current design of the WIPP has a total emplacement volume for contact-handled transuranic (CH-TRU)
6 waste of $6.2 \times 10^6 \text{ ft}^3$ (approximately $175,600 \text{ m}^3$) (U.S. DOE, 1980; Public Law 102-579, 1992). The
7 estimated volume of CH-TRU waste supplied by the 10 waste-generator and/or storage sites for the 1991
8 Integrated Data Base (IDB, US DOE 1991b) was approximately $53,700 \text{ m}^3$ of stored waste and an additional
9 $42,800 \text{ m}^3$ of waste to be generated by 2013. Estimates of the volume of waste to be generated may change in
10 the future. Rather than revise the volume of waste emplaced in the WIPP each year, the current performance-
11 assessment calculations are based on an initial CH-TRU-waste volume of approximately $175,600 \text{ m}^3$, the design
12 volume. This is mostly for modeling convenience and will not have a significant effect on comparisons to 40
13 CFR 191B.

14 The current estimate of the stored and projected waste total about $96,500 \text{ m}^3$. Therefore, an additional
15 $79,000 \text{ m}^3$ of waste could be emplaced in the WIPP. The characteristics of the additional $79,000 \text{ m}^3$ of waste
16 were estimated from the characteristics of the projected waste of the five largest future generators. Because of
17 changes that are occurring in weapons production and waste processing the waste that has not been generated
18 cannot be characterized precisely. Estimates of waste characterization currently used in performance assessment
19 have the potential for a large uncertainty. As discussed in Section 3.3.5 of Volume 3 of this report, uncertainty in
20 the constituents that affect gas generation from corrosion of iron-based materials and from biodegradation of
21 cellulose and rubbers have been included in the 1992 preliminary performance assessment.

22 Characterization of the CH-TRU waste for the current performance-assessment calculations was based on a
23 scale-up of masses estimated from expanded waste-characterization information. Based on $175,600 \text{ m}^3$ of CH-
24 TRU waste emplaced in the WIPP, estimates of a total of about 12,000,000 kg of combustibles, 20,000,000 kg
25 of metals and glass, and 25,000,000 kg of sludges were calculated. The total masses of iron-based metals,
26 cellulose, and rubbers were also calculated, and are provided in the memorandum by Peterson in Volume 3,
27 Appendix A of this report. The masses of these materials are required for performance assessment because they
28 influence gas generation and potential radionuclide transport.

29 The weight of the waste containers, drums and boxes, and of container liners were estimated because they also
30 effect gas-generation potential. It was assumed in the estimation of the container weights that only steel 55-
31 gallon drums and standard waste boxes (SWBs) will be emplaced in the WIPP. Other than test bins, these are the
32 only containers that can currently be transported in a TRUPACT-II (NuPac, 1989). Based on emplacing $175,600$
33 m^3 of CH-TRU-waste in drums and SWBs, it was estimated that about 518,000 drums and 35,600 SWBs would
34 be disposed of in the WIPP. The total weight of the low-carbon steel in the drums and SWBs is larger than the
35 estimated weight of corrodible iron-based materials in the waste.

36 The estimates of the total weight of the metals and glass and combustibles were nearly the same as were
37 estimated for the 1991 PA analyses (WIPP PA Division, 1991a). The weight of sludge decreased significantly
38 from the 1991 estimate. The weight of sludge in 1991 was based on the total weight of waste and average

1 weights of combustibles and metals and glass. The current estimate of the weight of sludge was based on
2 expanded input from the sites. The estimates of the weights of iron-based corrodible metals and biodegradable
3 materials were slightly decreased from the 1991 estimates.

4 2.3.2.2 SEALS

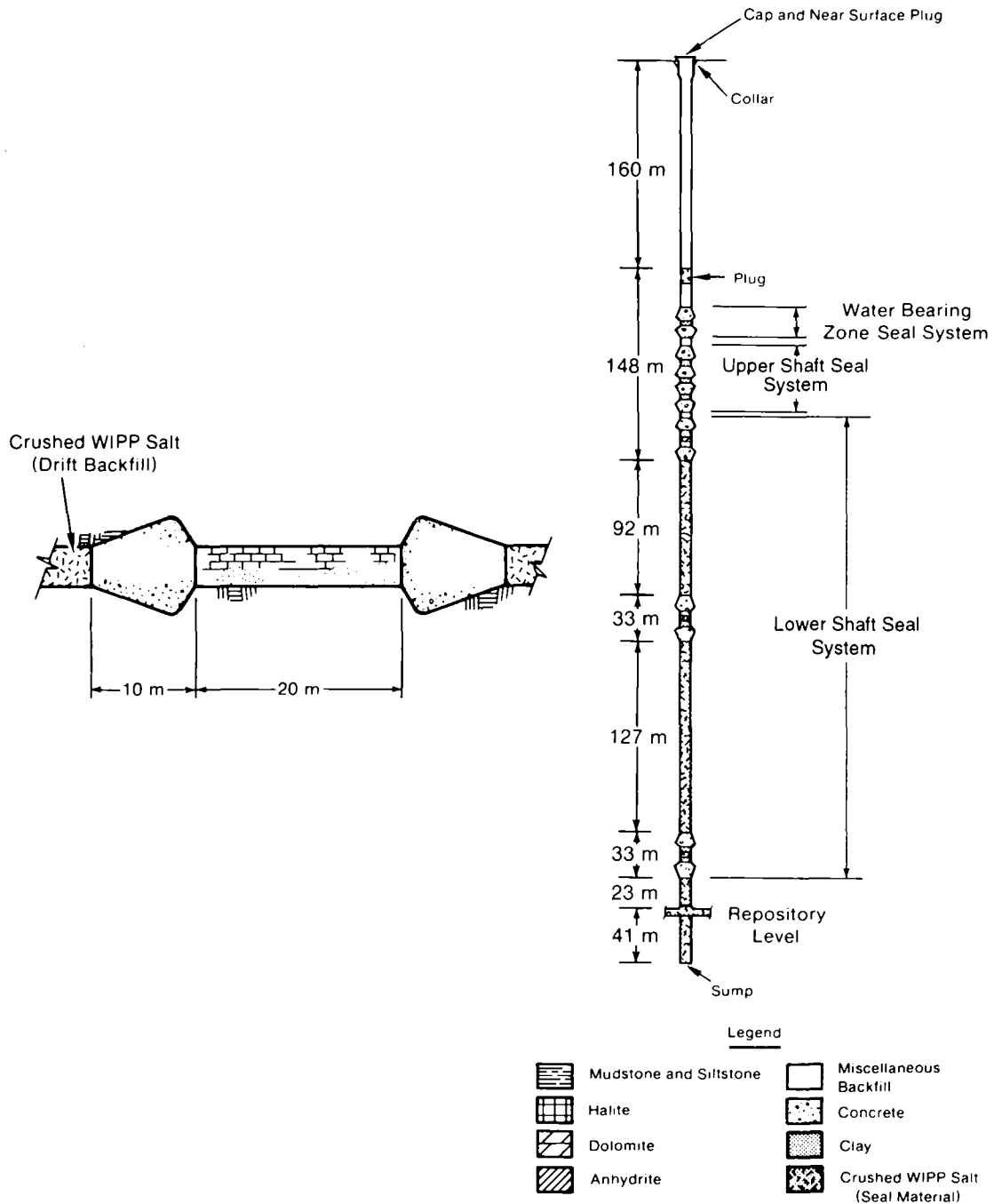
5 Seals will be emplaced in the entrance to each panel, in two locations within the drifts between the panels and
6 the vertical shafts in the drifts between the experimental area and the vertical shafts, and in each of the four vertical
7 shafts (Figure 2-21, 2-22) (Nowak et al., 1990). Design of these seals reflects specific functions for each type of
8 seal. Seals in the upper portion of the shafts must prevent groundwater flow from the transmissive units of the
9 Rustler Formation from reaching the lower portions of the shafts and the waste-emplacment areas. Seals in the
10 lower portion of the shafts must provide a long-term, low-permeability barrier that will prevent Salado Formation
11 brine and gas from migrating up the shaft. Panel seals (and drift seals) will inhibit long-term migration of
12 radionuclide-contaminated brine through the drifts to the base of the shafts and must also provide safe isolation of
13 radionuclides during the operational phase of the repository.

14 The primary long-term component of both lower shaft and panel seals will be crushed salt, confined between
15 short-term rigid bulkheads until creep closure reconsolidates it to properties comparable to those of the intact
16 Salado Formation. The short-term seals will be concrete in the panels and drifts, and composite barriers of
17 concrete, bentonite, and consolidated crushed salt in the shafts. Crushed salt in the long-term portion of the seals
18 will be preconsolidated to approximately 80% of the density of the intact formation and will compact further to
19 approximately 95% of initial density within 100 years, at which time permeabilities are expected to be comparable
20 to those of the undisturbed rock (Nowak and Stormont, 1987). Panel seals will be 40 m (131 ft) long, with 20 m
21 (66 ft) of preconsolidated crushed salt between two 10-m (33-ft) concrete barriers. Shaft-seal systems will extend
22 from the repository horizon in the Salado Formation to the surface, and will include composite barriers at the
23 appropriate depths for individual lithologic units, including the Culebra Dolomite Member of the Rustler
24 Formation (Nowak et al., 1990). Additional information about seal design is presented in Volume 3 of this report.

25 Marker Bed 139 will be sealed below each panel and drift seal by grouting, either with crushed-salt-based
26 grout, cementitious material, bitumen, or other appropriate materials. Other anhydrite layers will be sealed
27 similarly. Salt creep is expected to close fractures in halite in the DRZ over time, and engineered seals are not
28 planned for the DRZ outside of MB139 and other interbeds.

29 2.3.2.3 BACKFILL

30 Void space between waste containers and elsewhere in the underground workings will be backfilled before
31 sealing and decommissioning (Tyler et al., 1988; Lappin et al., 1989). The primary function of backfill will be
32 to reduce initial void space in the excavated regions and to accelerate the entombment of the waste by creep
33 closure. Consolidation of backfill by salt creep may reduce permeability in the waste-emplacment regions and
34 limit brine flow through the waste; long-term properties of the backfill are uncertain, however, and will depend on



TRI-6342-1281-1

Figure 2-22. Representative shaft and plug seals (after Nowak et al., 1990). Vertical distances based on stratigraphy in ERDA-9.

1 fluid pressures within the panels. As discussed in Section 2.3.5, the pressure history of the repository will depend
2 on the complexly coupled processes of salt creep, gas generation within the waste, and brine inflow from the
3 surrounding Salado Formation. Performance-assessment calculations for 1992 assume a backfill of pure,
4 unconsolidated crushed salt, with a relatively high permeability that provides little resistance to fluid flow. Pure
5 salt will not sorb radionuclides, and retardation of radionuclides within the repository environment is not
6 simulated. Design alternatives for backfill that contains bentonite as an additional barrier to retard radionuclides
7 have been examined (U.S. DOE, 1990b, 1991c; Butcher et al., 1991; Pfeifle and Brodsky, 1991; Brodsky and
8 Pfeifle, 1992) and will be available if needed.

9 2.3.2.4 ENGINEERED ALTERNATIVES

10 The WIPP has been designed to dispose of waste in the form in which it is shipped from the TRU-waste-
11 generator and/or storage sites. Preliminary performance-assessment calculations indicate that modifications to the
12 waste form that limit dissolution of radionuclides in brine have the potential to improve predicted performance of
13 the repository (Marietta et al., 1989; Bertram-Howery and Swift, 1990). Modifications to the backfill and design
14 of the room could also reduce radionuclide releases. Modifications could also, if needed, mitigate the effects of gas
15 generated within the repository. Present performance assessments are not complete enough to determine whether
16 or not such modifications will be needed for regulatory compliance, but the DOE has investigated engineered
17 alternatives to waste form and repository design so that alternatives will be available if needed (U.S. DOE,
18 1990b). The Engineered Alternatives Task Force (EATF) has identified 19 possible modifications to waste form,
19 backfill, and room design that merit additional investigation (U.S. DOE, 1990b, 1991c). The 1992 performance-
20 assessment calculations do not include simulations of these alternatives. Selected alternatives may be examined in
21 future performance-assessment calculations, however, to provide guidance to DOE on possible effectiveness of
22 modifications.

23 2.3.3 Radionuclide Inventory

24 As described in additional detail in Volume 3, Chapter 3 of this report, the radionuclide inventory for the 1992
25 performance assessment is estimated from input to the 1991 Integrated Data Base (IDB, U.S. DOE, 1991b). The
26 1991 IDB inventory of contact-handled transuranic (CH-TRU) waste (defined as transuranic waste with a surface
27 dose rate not greater than 200 mrem/hr [Public Law 102-579, 1992]) identifies approximately 53,700 m³ of waste
28 as currently stored at generator sites, and projects an additional volume of 42,800 m³ that will be generated in the
29 future. The design volume of the WIPP (175,600 m³) will accommodate an additional approximately 79,100 m³
30 of waste that is not described in the IDB. Performance assessments use an inventory in which the amount of CH-
31 TRU is scaled up from the IDB volume to the design volume. CH-TRU activity of the initial design-volume
32 inventory, expressed in curies, is estimated by scaling the curie inventory of the projected CH-TRU waste from
33 each of the five sites that will generate the most waste in the future by a factor of 1.89 (the ratio of design volume
34 to IDB volume) (Volume 3, Sections 3.3 and 3.4 of this report). This scaling of the inventory to a standard
35 volume is done for modeling convenience, primarily to ensure the commensurability of analysis results from one
36 iteration of performance assessment to the next. Because the releases allowed by the EPA are normalized using a
37 waste unit factor based on the total inventory of transuranic waste (U.S. EPA, 1985; see Volume 1, Appendix A,

1 and Volume 3, Section 3.3.4 of this report), scaling of the inventory does not have a proportional effect on the
2 location of the CCDF used for preliminary comparison with 40 CFR 191.13 (Volume 1, Section 5.1 of this
3 report).

4 The initial design-volume inventory of CH-TRU waste used in the 1992 performance assessment contains
5 8.2×10^6 Ci (memorandum by Peterson in Volume 3, Appendix A of this report). Uncertainty in this inventory
6 is large, particularly given the potential changes in the sources of CH waste due to changes in weapons
7 production. Existing legislation, regulations, and agreements do not limit the total curie inventory of CH-TRU
8 waste that may be emplaced, but do limit the total volume of waste that may be emplaced in the WIPP (6.2×10^6
9 ft^3 , or $175,600 \text{ m}^3$) (Public Law 102-579, 1992).

10 Remotely-handled transuranic waste (RH-TRU), defined to have a surface dose rate greater than 200 mrem/hr
11 but less than 1,000 rem/hr, will also be emplaced in the WIPP. The total RH-TRU inventory is limited to
12 5.1×10^6 Ci; no more than five percent of the RH-TRU canisters emplaced at the WIPP may have surface dose
13 rates that exceed 100 rem/hr, and the activity of the RH-TRU waste shall not exceed 23 Ci/liter averaged over the
14 volume of a canister (Public Law 102-579, 1992). Existing and projected RH-TRU waste in the IDB (US DOE,
15 1991b) has a volume of $6,667 \text{ m}^3$. This is slightly less than the WIPP design volume for RH-TRU waste (7080
16 m^3), but is predicted by the IDB to require 8071 canisters, somewhat more than the design capacity of 7950
17 canisters. The discrepancy occurs because the volume of waste placed in each canister differs depending on the
18 generator site, and not all canisters will be filled to the capacity assumed for the WIPP design criteria. The 1991
19 IDB also indicates that there may be a considerable volume of uncharacterized waste that will probably be
20 classified as RH-TRU. Given these uncertainties, the RH-TRU inventory is not scaled to design volume, and is
21 used in the 1992 PA as reported in the 1991 IDB. The total remotely-handled inventory for 1992 is approximately
22 3.5×10^6 Ci, of which 1.8×10^6 Ci result from transuranic radionuclides and isotopes of uranium (i.e.,
23 radionuclides with atomic number greater than or equal to 92) (memorandum from Peterson, Volume 3, Appendix
24 A of this report).

25 Radioactive decay within the repository is simulated with a simplified set of decay chains, provided in
26 Volume 3, Section 3.3.3 of this report. Of the 70 radionuclides identified as present either in the initial WIPP
27 inventory or as decay products, 26 are considered explicitly in PA analyses of direct releases from the repository to
28 the ground surface. (See Section 4.2 of this volume for a discussion of human intrusion scenarios and Section 7.7
29 of this volume for a discussion of modeling of releases during drilling.) Radionuclides omitted from the
30 simplified decay chains are those that have very short half-lives, very low activities, or both. Subsurface transport
31 within the Culebra Dolomite Member of the Rustler Formation (see Sections 4.2 and 7.6 of this volume) is
32 simulated for the nine most important radionuclides, identified in Volume 3, Section 3.3.3 of this report.

33 The only radioactive gas expected in the repository is radon-222, created from decay of radium-226. Decay of
34 thorium-230 will cause the activity of radium-226 in a panel to increase from about 0 Ci at the time of
35 emplacement to 8 Ci at 10,000 years. Because radon-222, with a half-life of only 3.8 days, will exist in secular
36 equilibrium (equal activity) with radium-226, with a half-life of 1600 years, its activity will also be insignificant
37 throughout the 10,000-year period. At 100,000 years the activity of radium-226 would increase to about 58 Ci in
38 a panel, and the activity of radon-222 would still not be significant. Not including release of volatile radionuclides
39 does not significantly affect the total radionuclide release.

2.3.4 Radionuclide Solubility and the Source Term for Transport Calculations

Before 1991, WIPP performance assessments calculated the source term for transport modeling* using the same estimated range and distribution (loguniform from 10^{-9} to 10^{-3} M) for the solubility limit of all radionuclide species in repository brine (Lappin et al., 1989; Brush and Anderson, 1989a). A fixed distribution was applied to all radionuclides for PA calculations before 1991 because, as is explained below, the state of knowledge at that time did not allow for the differentiation of radionuclides.

During the first meeting of the WIPP PA Source Term Group (in June of 1988), Choppin reported that estimates of the speciation and solubilities of americium, neptunium, plutonium, uranium, and thorium in both the Salado and Castile brines for expected concentrations of organic ligands were not possible because there are no thermodynamic data (solubility products for solid phases, or stability constants for dissolved organic or inorganic complexes) for these elements in solutions with ionic strengths equal to those of the Salado and Castile brines (Brush and Anderson, 1989b). In addition, Choppin observed that data reported by different groups using different experimental techniques are often contradictory, making the use of subjective expert judgment necessary for preliminary data selection for PA use until data from WIPP-specific experimental programs are available (see Section 2.3.4.2).

In lieu of data from laboratory experiments, the Source Term Group recommended a “best estimate” of 10^{-6} M for the concentration of plutonium and americium in any brine that resaturates the WIPP disposal rooms (Brush and Anderson, 1989a). This is the intermediate value (on a logarithmic scale) of the range of dissolved radionuclide concentrations (10^{-9} to 10^{-3} M) that have been used for sensitivity studies of the source term. Because the PA calculations require the input of a probability distribution, the entire range discussed above was used as a loguniform distribution. Because of the lack of applicable experimental data, there was no differentiation between the concentrations of various radionuclides in the 1989 PA. The 1990 estimated range in effective radionuclide solubilities was intended to include the effects of possible colloid formation within the repository (Rechard et al., 1990a). The conservative assumption was that colloidal materials would be completely transportable (i.e., that they would not be sorbed or precipitated within the repository).

2.3.4.1 EXPERT JUDGMENT ELICITATION

Since the beginning of the WIPP PA effort, it has been recognized that assuming a fixed solubility distribution for all radionuclides does not adequately capture the considerable uncertainty in radionuclide concentrations expected in the repository. The need for a better understanding of the source term was further highlighted by sensitivity analyses performed as part of the 1990 preliminary performance assessment. These sensitivity analyses indicated that, conditional on the models and distributions used in the 1990 calculations, uncertainty in the solubility limit was the most important single contributor to variability in total cumulative releases to the accessible environment resulting from groundwater transport (Helton et al., 1991).

* The source term for transport modeling for the PA is based on an analytical model that calculates the equilibrium concentration of the radionuclide species in the repository brine. See Section 7.4 and Appendix A.

1 Because of the paucity of experimental data for the conditions and solutions expected specifically at the WIPP,
2 a panel of experts external to the WIPP Project, called the Source Term Expert Panel, was convened in the spring
3 of 1991 to provide the performance-assessment team with judgment about both dissolved and suspended
4 radionuclides* for specific elements under variable Eh and pH conditions. Their judgments have been used to
5 develop radionuclide solubilities that vary by radionuclide and type of brine solution. The resulting solubility
6 ranges have been used in the 1991 and 1992 PA calculations.

7 Selection of the Source Term Expert Panel and elicitation of their judgment on solubility limits followed the
8 procedure suggested by Hora and Iman (1989). Candidates for the expert panel on source term were gathered by a
9 two-tiered nomination process. Initial nominations were solicited from an SNL staff member and an external
10 consultant, as well as from members of the Performance Assessment Peer Review Panel and the National
11 Research Council's WIPP Panel. Additional nominations were requested from all those contacted. Curricula vitae
12 from those who were interested in participating in such a panel and available during the entire study period were
13 reviewed by a two-member selection committee external to SNL. Some individuals removed themselves from
14 consideration because of prior time commitments, current contracts with SNL, a self-determined lack of expertise,
15 or involvement in an oversight organization. Nominees were evaluated on the basis of expertise and professional
16 reputation; four experts were selected whose complementary areas of specialization provided the needed breadth and
17 balance to the panel.**

18 During the first meeting of the Source Term Expert Panel (March 1991), the Panel members were presented
19 with published papers and reports identified from a comprehensive literature search that focused on radionuclide
20 solubility in high-ionic-strength solutions in salt formations, covering the United States repository program as
21 well as experiments conducted in Germany, Canada, Finland, Sweden, and at the Commission of the European
22 Communities, Joint Research Center at Ispra, Italy. Other issues discussed in these publications were speciation,
23 colloids, the leaching of radionuclides from high-level waste (HLW) glass, and the impact of backfill materials.

24 A summary of the expert judgment elicitation procedure and results, presented in detail in Trauth et al. (1992),
25 follows. A final report on this effort by the members the Source Term Expert Panel will be available in 1993.

26 As stated above, the Source Term Expert Panel was selected to include a balance in the required areas of
27 expertise (experience in actinide chemistry and with high-ionic-strength solutions). At the first meeting, the
28 panelists divided the problem into areas of specific responsibility and provided a structure for assembling the
29 individual judgments to obtain a single distribution codifying the collective judgment of the panel. In addition,
30 the group of experts decided to be elicited together to produce one set of results. A consequence of the group
31 elicitation is that the uncertainty expressed by specific experts could not be assessed. However, many of the inter-
32 expert differences were captured during the elicitation process resulting in more widely dispersed probability
33 functions.

* Because of the limited state of knowledge regarding colloids, the Source Term Expert Panel chose to limit their judgments to dissolved radionuclides (solubility).

** In the case of the Source Term Expert Panel, expertise was required in actinide chemistry and high-ionic-strength chemistry. Therefore, experts from both these disciplines were selected. These individuals used their complementary expertise to arrive at judgments that satisfy all the pertinent constraints of the solubility problem.

1 In addition to a literature review (discussed above), preparation for elicitation involved computer calculations
2 by the panel members using a standard brine that simulates the brine in the Salado Formation as the solvent
3 (WIPP Brine A) (Lappin et al., 1989). These efforts resulted in the determination of the oxidation state(s) in
4 which the radionuclides would exist in the WIPP rooms and drifts. Moreover, the solution and solid species that
5 would coexist with that particular oxidation state were identified using two regimes: (1) one regime based on solid
6 species with the highest solubility and therefore highest radionuclide concentration, and (2) another regime based
7 on solid species with the lowest solubility and therefore lowest radionuclide concentration. Which regime
8 predominates depends on the chemical properties within the repository, which in turn may depend on pH and ionic
9 strength of the brine and the presence of carbonates and/or sulfates. Furthermore, the factors controlling each
10 regime may differ for different radionuclides.

11 The experts' judgments on the solubility distributions were elicited at the second meeting (in April of 1991).
12 The assessment for each distribution began by establishing the upper and lower solubility regimes and the
13 calculated solubility of each radionuclide within each regime. The resulting probability distributions for the
14 radionuclides used in the 1992 calculations are presented in Volume 3 of this report (Section 3.3.5). Because the
15 calculated solubility is a single number that does not incorporate any uncertainty, it was necessary to account for
16 uncertainty in both the calculated value and the underlying conditions, such as pH.

17 Typically, the calculated value would be used to establish a fractile, often either the 0.10 or 0.90 fractile, of
18 the distribution. The absolute lower limit of the distribution was obtained by considering the sensitivity of
19 solubility to the underlying brine chemistry. The interior fractiles were obtained after the 0.10 and 0.90 fractiles
20 and the endpoints were established. Where possible, concentration data from well water from the Nevada Yucca
21 Mountain site (J-13) was used with a correction for the ionic-strength difference between the J-13 water and the
22 WIPP Brine A to determine the 0.50 fractile. For the determination of the 0.25 and 0.75 fractiles, one speciation
23 was thought in some cases to be more likely, resulting in a skewed distribution. In other cases, both speciations
24 were thought to be likely, resulting in a more symmetrical distribution.

25 The Source Term Expert Panel had considerable difficulty dealing with colloids because of a lack of
26 experimental data and limited knowledge of the physical principles governing their formation. Some diversity of
27 opinion existed about the significance of colloids. The panel did not believe that they could make judgments
28 about suspended-solids concentrations at the present time. They planned to include recommendations for future
29 experiments related specifically to colloids in a final panel report. Transport of radionuclides in colloids has not
30 been included in the 1992 PA.

31 Correlations between the concentrations assigned to the radionuclides were discussed briefly by the panel. The
32 consensus was that correlations do exist, possibly between americium(III) and curium(III), and between
33 neptunium(IV) and plutonium(IV). The panel is expected to address this issue in a forthcoming report on their
34 findings.

1 2.3.4.2 EXPERIMENTAL WORK

2 Future WIPP performance assessments will rely increasingly on data from planned solubility tests of actual
3 waste. These tests will complement the laboratory studies of radionuclide chemistry. The laboratory program is
4 currently determining solubilities and sorption coefficients of plutonium and its oxidation state analogues in
5 synthetic brines under various conditions of pH, and will soon examine actinide speciation and measure stability
6 constants for complex ions (Brush, 1990). As currently planned, the actinide source-term program will involve
7 filling test containers with a mixture of natural and synthetic brines with compositions chemically similar to
8 those of intergranular brines found in the Salado Formation. Container size will depend on waste homogeneity;
9 heterogeneous waste types such as combustibles will use "drum scale" vessels of 210 L volume, while more
10 homogeneous types such as process sludges will use "liter scale" test containers. The containers will permit
11 regular brine sampling, and gas monitoring and venting.

12 **2.3.5 Creep Closure, Fluid Flow, and Room/Waste Interactions**

13 When the repository is decommissioned, free brine initially will not be present within the emplacement area,
14 and void space above the backfilled waste will be air-filled. Brine seepage from the Salado Formation will have
15 filled fractures in anhydrite interbeds above and below the emplacement area (Lappin et al., 1989; Rechar et al.,
16 1990b).

17 Following excavation salt creep will begin to close the repository. In the absence of elevated gas pressures
18 within the repository, modeling of salt creep indicates that consolidation of the waste in unreinforced rooms would
19 be largely complete within 100 years (Tyler et al., 1988; Munson et al., 1989a,b). Brine will seep into the
20 emplacement area from the surrounding salt, however, and gas will be generated in the humid environment by
21 corrosion of metals, radiolysis of brine, and microbial decomposition of organic material. Some gas will disperse
22 into the surrounding anhydrite layers. Continued gas generation could increase pressure within the repository
23 sufficiently to reverse brine inflow and partially or completely desaturate the waste-emplacement area. Pressure
24 may be high enough to open fractures in the anhydrite interbeds above and below the repository, allowing
25 additional lateral migration of gas from the waste-emplacement area. High pressure may also halt and partially
26 reverse closure by salt creep. In the undisturbed final state, the emplacement area could be incompletely
27 consolidated and gas-filled rather than brine-filled.

28 All of the major processes active in the waste-emplacement area are linked, and all are rate- and time-
29 dependent. For example, creep closure will be, in part, a function of pressure within the repository. Pressure will
30 be in turn a function of the amount of gas generated and the volume available within the repository and the
31 surrounding Salado Formation for gas storage. Gas-storage volume will be a function of closure rate and time,
32 with storage volume decreasing as consolidation continues. Time and rate of gas generation, therefore, will
33 strongly influence repository pressurization and closure. Gas-generation rates will be dependent on specific
34 reaction rates and the availability of reactants, including water. Some water can be generated by microbial activity
35 (Brush and Anderson, 1989b). Additional water will be provided by brine inflow, which, is assumed to occur
36 according to two-phase immiscible flow through a porous medium and which will depend in large part on
37 repository pressure, so that some gas-generation reactions could be partially self-buffering.

1 Responses of the disposal system to human intrusion are equally complicated. Consequences will depend on
2 the time of intrusion, the degree to which the repository has closed, and the amount of gas generated. If intrusion
3 occurs into a fully pressurized, dry, and partially unconsolidated waste-emplacment area, venting of gas up the
4 borehole will permit brine to resaturate available void space. Following eventual deterioration of plugs in an
5 intrusion borehole, brine may flow from the emplacement area into the borehole, transporting radionuclides
6 upward toward the accessible environment. Upward flow from a pressurized brine pocket in the Castile Formation
7 may contribute to flow and radionuclide transport.

3. PERFORMANCE ASSESSMENT METHODOLOGY

This chapter contains an overview of WIPP performance-assessment methodology. Additional information about this subject is provided in other published sources (Helton et al., 1991; WIPP PA Division, 1991a).

3.1 Conceptualization of Risk for the WIPP Performance Assessment

The WIPP performance assessment uses a conceptualization for risk similar to that developed for risk assessments for nuclear power plants. This conceptualization characterizes risk in terms of what can go wrong, how likely things are to go wrong, and what the consequences are of things going wrong. This description provides a structure on which both the representation and calculation of risk can be based.

Kaplan and Garrick (1981) have presented this representation of risk as a set of ordered triples. The WIPP performance assessment uses their representation, and defines risk to be a set \mathcal{R} of the form

$$\mathcal{R} = \{(S_i, pS_i, \mathbf{cS}_i), i = 1, \dots, nS\}, \quad (3-1)$$

where

S_i = a set of similar occurrences,

pS_i = probability that an occurrence in set S_i will take place,

\mathbf{cS}_i = a vector of consequences associated with S_i ,

nS = number of sets selected for consideration,

and the sets S_i have no occurrences in common (i.e., the S_i are disjoint sets). This representation formally decomposes risk into what can happen (the S_i), how likely things are to happen (the pS_i), and the consequences of what can happen (the \mathbf{cS}_i). The S_i are scenarios in the WIPP performance assessment, the pS_i are scenario probabilities, and the vector \mathbf{cS}_i contains the normalized EPA releases and other performance measures associated with scenario S_i . Other performance measures of interest are dose and health effects for safety assessments, and concentrations of heavy metals and volatile organic compounds (VOCs) for hazardous waste assessments.

Risk results in \mathcal{R} can be summarized with complementary cumulative distribution functions (CCDFs). These functions provide a display of the information contained in the probabilities pS_i and the consequences \mathbf{cS}_i . With the assumption that a particular consequence result cS in the vector \mathbf{cS} has been ordered so that $cS_i \leq cS_{i+1}$ for $i = 1, \dots, nS$, the CCDF for this consequence result is the function F defined by

$F(x)$ = probability that cS exceeds a specific consequence value x

$$1 \quad = \sum_{j=i}^{nS} pS_j \quad (3-2)$$

2 where i is the smallest integer such that $\mathbf{cS}_i > x$. As illustrated in Figure 3-1, F is a step function that
 3 represents the probabilities that consequence values on the abscissa will be exceeded. To avoid a broken
 4 appearance, CCDFs are usually plotted with vertical lines added at the discontinuities.

5 The steps in the CCDFs shown in Figure 3-1 result from the discretization of all possible occurrences into
 6 the sets S_1, \dots, S_{nS} . Unless the underlying processes are inherently disjoint, the use of more sets S_i will tend to
 7 reduce the size of these steps and, in the limit, will lead to a smooth curve.

8 3.1.1 Calculation of Risk

9 The calculation of risk and its associated uncertainty begins with the determination of the sets S_i , which are
 10 the scenarios to be analyzed. Once these sets are determined, their probabilities pS_i and associated consequences
 11 \mathbf{cS}_i must be determined. In practice, development of the S_i is an iterative process that must take into account
 12 the procedures required to determine the probabilities pS_i and the consequences \mathbf{cS}_i . For the WIPP performance
 13 assessment, the overall process is organized so that pS_i and \mathbf{cS}_i are calculated by various models, the
 14 configuration of which depends on the individual S_i .

15 Use of these models requires values for imprecisely known variables that can be represented by a vector

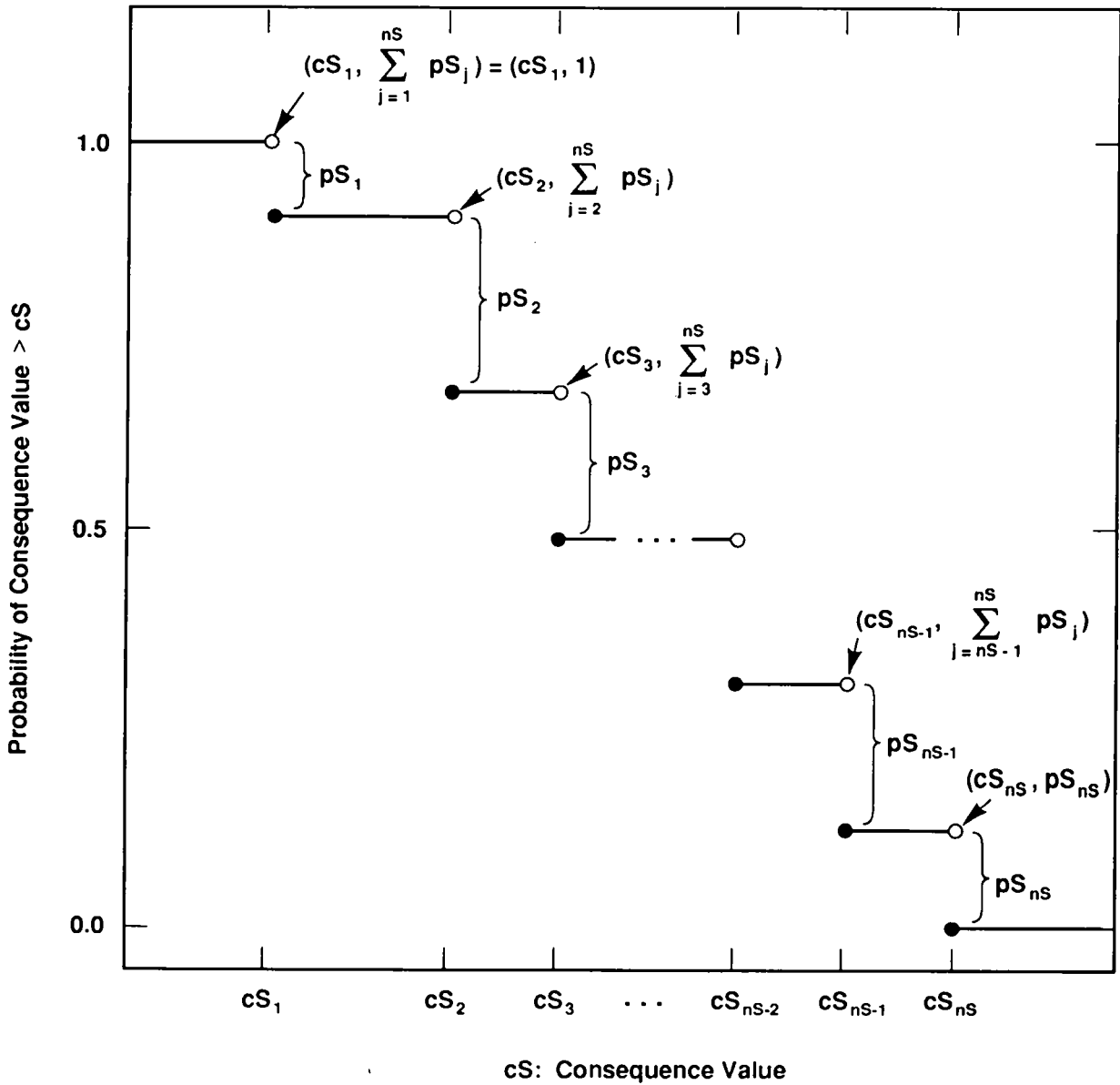
$$16 \quad \mathbf{x} = [x_1, x_2, \dots, x_{nV}], \quad (3-3)$$

17 where each x_j is an imprecisely known input required in the analysis and nV is the total number of such inputs. If
 18 the analysis has been developed so that each x_j is a real-valued quantity for which the overall analysis requires a
 19 single value, the representation for risk in Equation 3-1 can be restated as a function of \mathbf{x} :

$$20 \quad \mathcal{R}(\mathbf{x}) = \{[S_i(\mathbf{x}), pS_i(\mathbf{x}), \mathbf{cS}_i(\mathbf{x})], i = 1, \dots, nS(\mathbf{x})\} \quad (3-4)$$

21 As \mathbf{x} changes, so will $\mathcal{R}(\mathbf{x})$ and all summary measures that can be derived from $\mathcal{R}(\mathbf{x})$. Thus, rather than a
 22 single CCDF for each consequence contained in the vector \mathbf{cS} shown in Equation 3-1, a distribution of CCDFs
 23 results from the possible values that \mathbf{x} can represent (Figure 3-2).

24 The distribution assigned to the individual variables x_j in \mathbf{x} reflect uncertainty in the modeling system.
 25 Factors that affect uncertainty in risk results can be subdivided into those that affect imprecisely known variables,
 26 those related to the selection of conceptual and computational models, and those related to scenario selection.
 27 Factors related to scenario selection can be further subdivided into completeness, aggregation, and stochastic



TRI-6342-730-5

Figure 3-1. Estimated CCDF for consequence result cS (Helton et al., 1991; Helton, in press). The open and solid circles at the discontinuities indicate the points included on (solid circles) and excluded from (open circles) the CCDF.

1 variation. Uncertainty about imprecisely known variables may result from incomplete data or measurement
 2 uncertainty, and can affect all three elements of the triple introduced in Equation 3-1. Uncertainty about the
 3 appropriate choices of models can affect both pS_i and cS_i . Due to the complex nature of risk assessments, model
 4 selection can also affect the definition of the S_i . Completeness refers to the extent that a performance assessment
 5 includes all possible occurrences for the system under consideration. In terms of the risk representation in
 6 Equation 3-1, completeness deals with whether or not all possible occurrences are included in the union of the sets
 7 S_i . Aggregation refers to the division of the possible occurrences into the sets S_i . Resolution is lost if the S_i
 8 are defined too coarsely (e.g., nS is too small) or in some other inappropriate manner. Computational efficiency
 9 is lost if nS is too large. Model selection refers to the actual choice of the models used in a risk assessment.
 10 Uncertainty about the appropriate model choice can affect both pS_i and cS_i . Due to the complex nature of risk
 11 assessments, model selection can also affect the definition of the S_i . Uncertainty about imprecisely known
 12 variables, which may result from incomplete data or measurement uncertainty, can also affect all three elements of
 13 the risk triple. Stochastic variation is represented by the probabilities pS_i , which are functions of the many
 14 factors that affect the occurrence of the individual sets S_i .

15 Individual variables x_j may relate to each of these different types of uncertainty. For example, individual
 16 variables might relate to completeness uncertainty (e.g., the value for a cutoff used to drop low-probability
 17 occurrences from the analysis), aggregation uncertainty (e.g., a bound on the value for nS), model uncertainty
 18 (e.g., a 0-1 variable that indicates which of two alternative models should be used), variable uncertainty (e.g., a
 19 solubility limit or a retardation for a specific element), or stochastic uncertainty (e.g., a variable that helps define
 20 the probabilities for the individual S_i).

21 3.1.2 Characterization of Uncertainty in Risk

22 Characterization of the uncertainty in the results of a performance assessment requires characterization of the
 23 uncertainty in \mathbf{x} , the vector of imprecisely known variables. This uncertainty can be described with a sequence of
 24 probability distributions

$$25 \quad D_1, D_2, \dots, D_{nV}, \quad (3-5)$$

26 where D_j is the distribution developed for the variable $x_j, j=1, 2, \dots, nV$, contained in \mathbf{x} . The definition of these
 27 distributions may also be accompanied by the specification of correlations and various restrictions that further
 28 define the possible relations among the x_j . These distributions and other restrictions probabilistically characterize
 29 where the appropriate input to use in the performance assessment might fall, given that the analysis is structured
 30 so that only one value can be used for each variable under consideration.

31 Once the distributions in Equation 3-5 have been developed, Monte Carlo techniques can be used to determine
 32 the uncertainty in $\mathcal{R}(\mathbf{x})$ from the uncertainty in \mathbf{x} . First, a sample

$$33 \quad \mathbf{x}_k = [x_{k1}, x_{k2}, \dots, x_{k,nV}], \quad k = 1, \dots, nK \quad (3-6)$$

1 is generated according to the specified distributions and restrictions, where nK is the size of the sample.
2 Performance-assessment calculations are then performed for each sample element \mathbf{x}_k , which yields a sequence of
3 risk results of the form

$$4 \quad \mathcal{R}(\mathbf{x}_k) = \left\{ \left[\mathcal{S}_i(\mathbf{x}_k), p\mathcal{S}_i(\mathbf{x}_k), \mathbf{c}\mathcal{S}_i(\mathbf{x}_k) \right], i = 1, \dots, n\mathcal{S}(\mathbf{x}_k) \right\}, \quad (3-7)$$

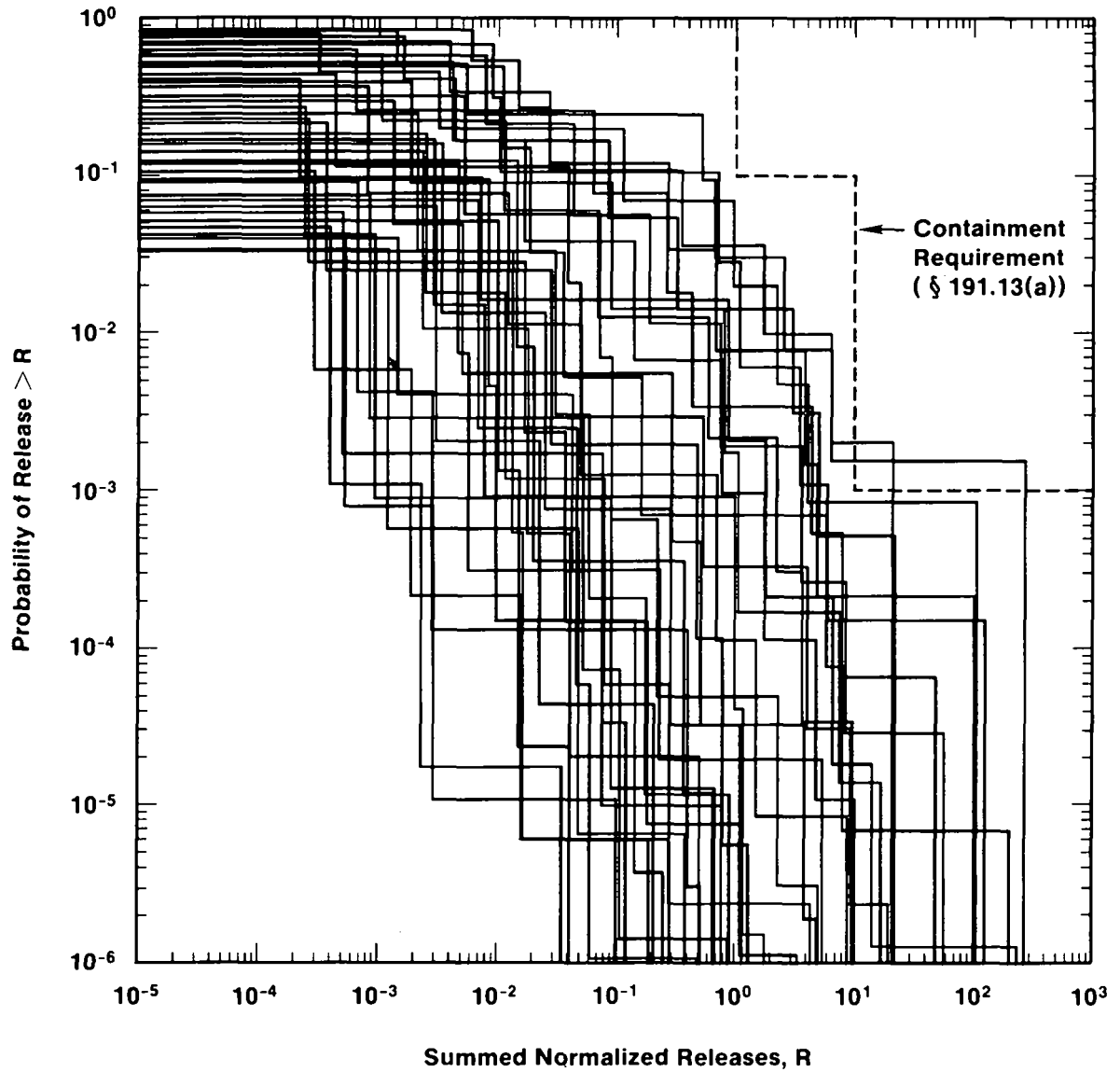
5 for $k = 1, \dots, nK$. Each set $\mathcal{R}(\mathbf{x}_k)$ is the result of one complete set of calculations performed with a set of
6 inputs (i.e., \mathbf{x}_k) that the review process producing the distributions in Equation 3-5 concluded was possible.
7 Further, associated with each risk result $\mathcal{R}(\mathbf{x}_k)$ in Equation 3-7 is a probability or weight* that can be used in
8 making probabilistic statements about the distribution of $\mathcal{R}(\mathbf{x})$.

9 A single CCDF can be produced for each set $\mathcal{R}(\mathbf{x}_k)$ of results shown in Equation 3-7, yielding a family of
10 CCDFs of the form shown in Figure 3-2. This distribution of CCDFs can be summarized by plotting the mean
11 value and selected percentile values of the exceedance probabilities shown on the ordinate for each consequence
12 value on the abscissa. For example, the mean plus the 10th, 50th (i.e., median), and 90th percentile values might
13 be used (Figure 3-3). The mean and percentile values can be obtained from the exceedance probabilities associated
14 with the individual consequence values and the weights or "probabilities" associated with the individual sample
15 elements.

16 Consideration of a family of CCDFs allows a distinction between the uncertainty that controls the shape of a
17 single CCDF and the uncertainty that results in a distribution of CCDFs. The stepwise shape of a single CCDF
18 reflects the fact that a number of different occurrences have a real possibility of taking place. This type of
19 uncertainty is referred to as stochastic variation in this report. A family of CCDFs arises from the fact that fixed,
20 but unknown, quantities are needed in the estimation of a CCDF. The distributions that characterize what the
21 values for these fixed quantities might be lead to a distribution of CCDFs, with each single CCDF reflecting a
22 specific sample element \mathbf{x}_k .

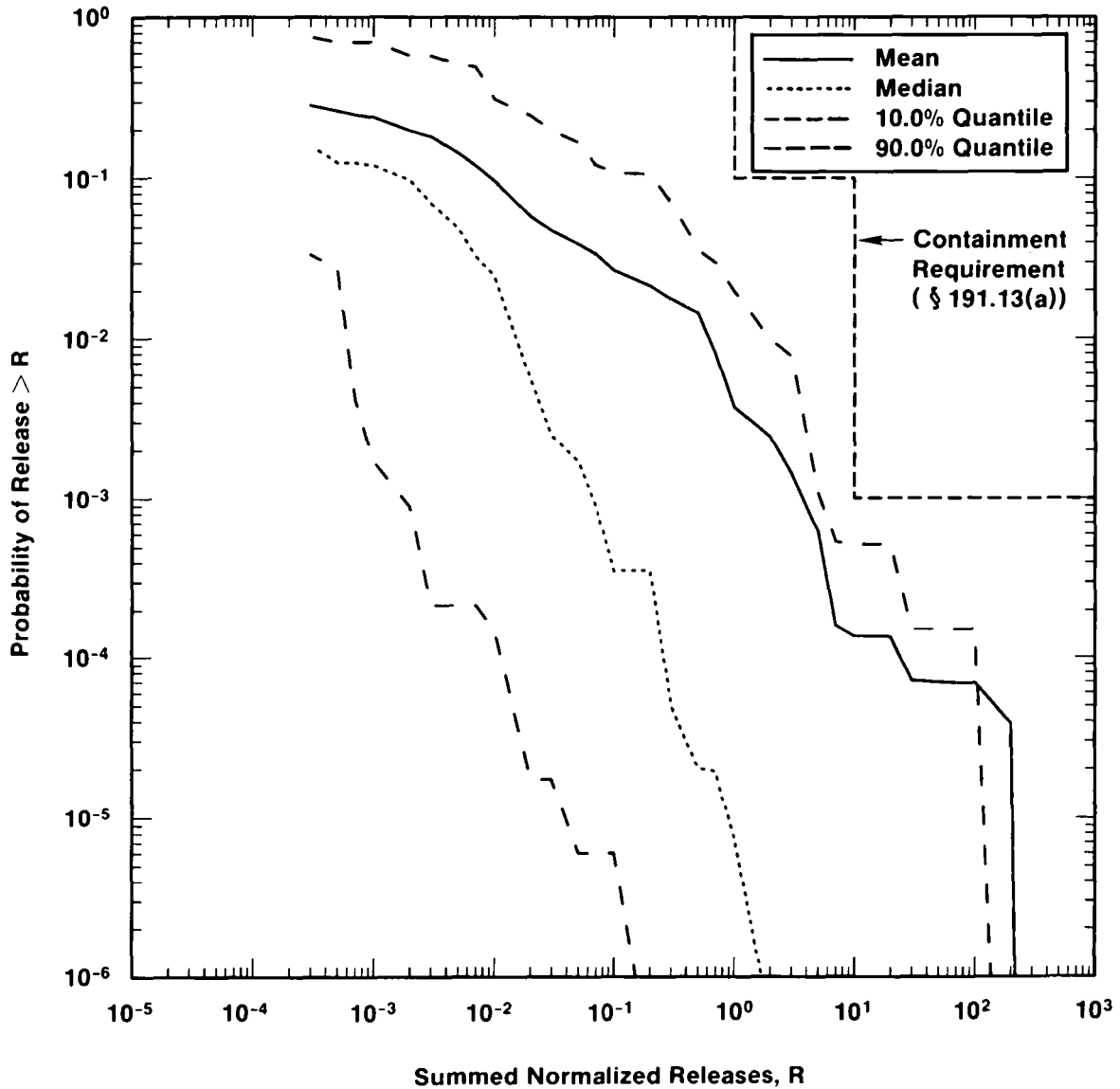
23 Both Kaplan and Garrick (1981) and the International Atomic Energy Agency (IAEA, 1989) distinguish
24 between these two types of uncertainty. Specifically, Kaplan and Garrick distinguish between probabilities derived
25 from frequencies and probabilities that characterize degrees of belief. Probabilities derived from frequencies
26 correspond to the probabilities $p\mathcal{S}_i$ in Equation 3-1, while probabilities that characterize degrees of belief (i.e.,
27 subjective probabilities) correspond to the distributions indicated in Equation 3-5. The IAEA report distinguishes
28 between what it calls Type-A uncertainty and Type-B uncertainty. The IAEA report defines Type-A uncertainty to
29 be stochastic variation; as such, this uncertainty corresponds to the frequency-based probability of Kaplan and
30 Garrick and the $p\mathcal{S}_i$ of Equation 3-1. Type-B uncertainty is defined to be uncertainty that is due to lack of
31 knowledge about fixed quantities; thus, this uncertainty corresponds to the subjective probability of Kaplan and

* In random or Latin hypercube sampling, this weight is the reciprocal of the sample size (i.e., $1/nK$) and can be used in estimating means, cumulative distribution functions, and other statistical properties. This weight is often referred to as the probability for each observation (i.e., sample \mathbf{x}_k). However, this association is not technically correct. If continuous distributions are involved, the actual probability of each observation is zero.



TRI-6342-1299-0

Figure 3-2. Example distribution of CCDFs obtained by sampling imprecisely known variables.



TRI-6342-1501-0

Figure 3-3. Example summary curves derived from an estimated distribution of CCDFs. The curves in this figure were obtained by calculating the mean and the indicated percentiles for each consequence value on the abscissa in Figure 3-2. The 90th-percentile curve crosses the mean curve due to the highly skewed distributions for exceedance probability. This skewness also results in the mean curve being above the median curve.

1 Garrick and the distributions indicated in Equation 3-5. This distinction has also been made by other authors,
2 including Vesely and Rasmuson (1984), Paté-Cornell (1986), and Parry (1988).

3 For a given conceptual model in the WIPP performance assessment, subjective uncertainty enters the analysis
4 due to lack of knowledge about quantities such as solubility limits, retardation factors, and flow fields. Stochastic
5 uncertainty enters the analysis through the assumption that future exploratory drilling will be random in time and
6 space (i.e., follows a Poisson process). However, the rate constant λ in the definition of this Poisson process is
7 assumed to be imprecisely known. Thus, subjective uncertainty exists in a quantity used to characterize stochastic
8 uncertainty.

9 **3.1.3 Risk and the EPA Limits**

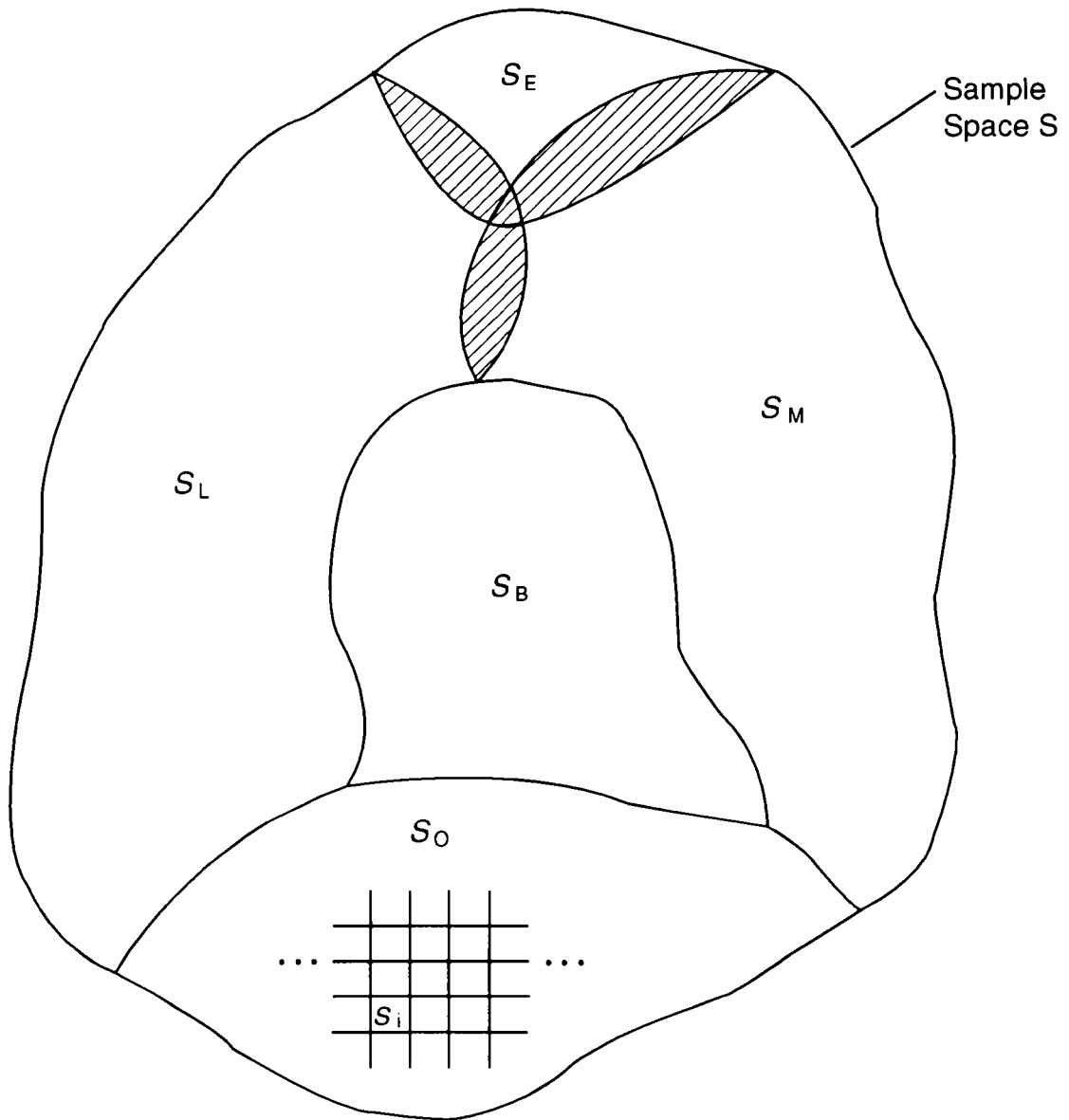
10 The EPA expressly identifies the need to consider the impact of uncertainties in calculations performed to
11 show compliance with the Containment Requirements. Specifically, Appendix B of 40 CFR 191 suggests that

12 ...whenever practicable, the implementing agency will assemble all of the results of the performance
13 assessments to determine compliance with § 191.13 into a "complementary cumulative distribution function"
14 that indicates the probability of exceeding various levels of cumulative release. When the uncertainties in
15 parameters are considered in a performance assessment, the effects of the uncertainties considered can be
16 incorporated into a single such distribution function for each disposal system considered. The Agency
17 assumes that a disposal system can be considered to be in compliance with [section] 191.13 if this single
18 distribution function meets the requirements of [section] 191.13(a) (U.S. EPA, 1985, p. 38088).

19 The representation for risk in Equation 3-1 provides a conceptual basis for the calculation of the
20 complementary cumulative distribution function (CCDF) for normalized releases specified in 40 CFR 191B.
21 Further, this representation provides a structure that can be used for both the incorporation of uncertainties and the
22 representation of the effects of uncertainties.

23 Each CCDF in the family of CCDFs that results from Eq. 3-7 would be the appropriate choice for
24 comparison against the EPA requirements, *if* \mathbf{x}_k contained the correct variable values for use in determining the
25 pS_i and cS_i and *if* the assumed conceptual models correctly characterize the disposal system. Increasing the
26 sample size nK will, in general, produce a better approximation of the true distribution of CCDFs, but will not
27 alter the fact that the distribution of CCDFs is conditional on the assumptions of the analysis.

28 If nK is large, displays of the complete family of CCDFs can be difficult to interpret. As discussed in the
29 previous section, mean and percentile curves can be used to summarize the information contained in the family.
30 Appendix B of 40 CFR 191 suggests that "the effects of the uncertainties considered can be incorporated into a
31 single [CCDF]" (U.S. EPA, 1985; p. 38088), but 40 CFR 191 does not contain specific guidance on which curve
32 should be compared to the Containment Requirements. In previous work, the mean curve has generally been
33 proposed for showing compliance with § 191.13(a) (e.g., Cranwell et al., 1987, 1990; Hunter et al., 1986). Only
34 mean curves are shown in Volume 1 of this report. Complete families of curves and the associated summary
35 curves are presented in Volume 4 of this report.



TRI-6342-3402-0

Figure 3-4. Decomposition of the sample space S into high-level subsets, where S_B designates the base-case subset, S_M designates a minimal disruption subset, S_E designates a regulatory exclusion subset, S_L designates a low-probability subset, and S_O designates $(S_B \cup S_M \cup S_E \cup S_L)^c$.

1 10,000 years, and represents the undisturbed performance of the disposal system. Second, a minimal disruption
 2 subset S_M consists of all elements in S that involve disruptions that result in no significant perturbation to the
 3 consequences associated with the corresponding elements in the base-case subset S_B . Third, a regulatory
 4 exclusion subset S_E consists of all elements in S that are excluded from consideration by regulatory directive
 5 (e.g., human intrusions more severe than the drilling of exploratory boreholes). Fourth, a low-probability subset
 6 S_L consists of elements of S not contained in S_B whose collective probability is small (e.g., the probability of
 7 S_L is less than 0.0001) regardless of their potential consequences. Everything that remains in S after the
 8 identification of S_B , S_M , S_E , and S_L now becomes a fifth subset S_O , where the subscript O represents
 9 "Other." In set notation,

$$S_O = (S_B \cup S_M \cup S_E \cup S_L)^c \quad (3-8)$$

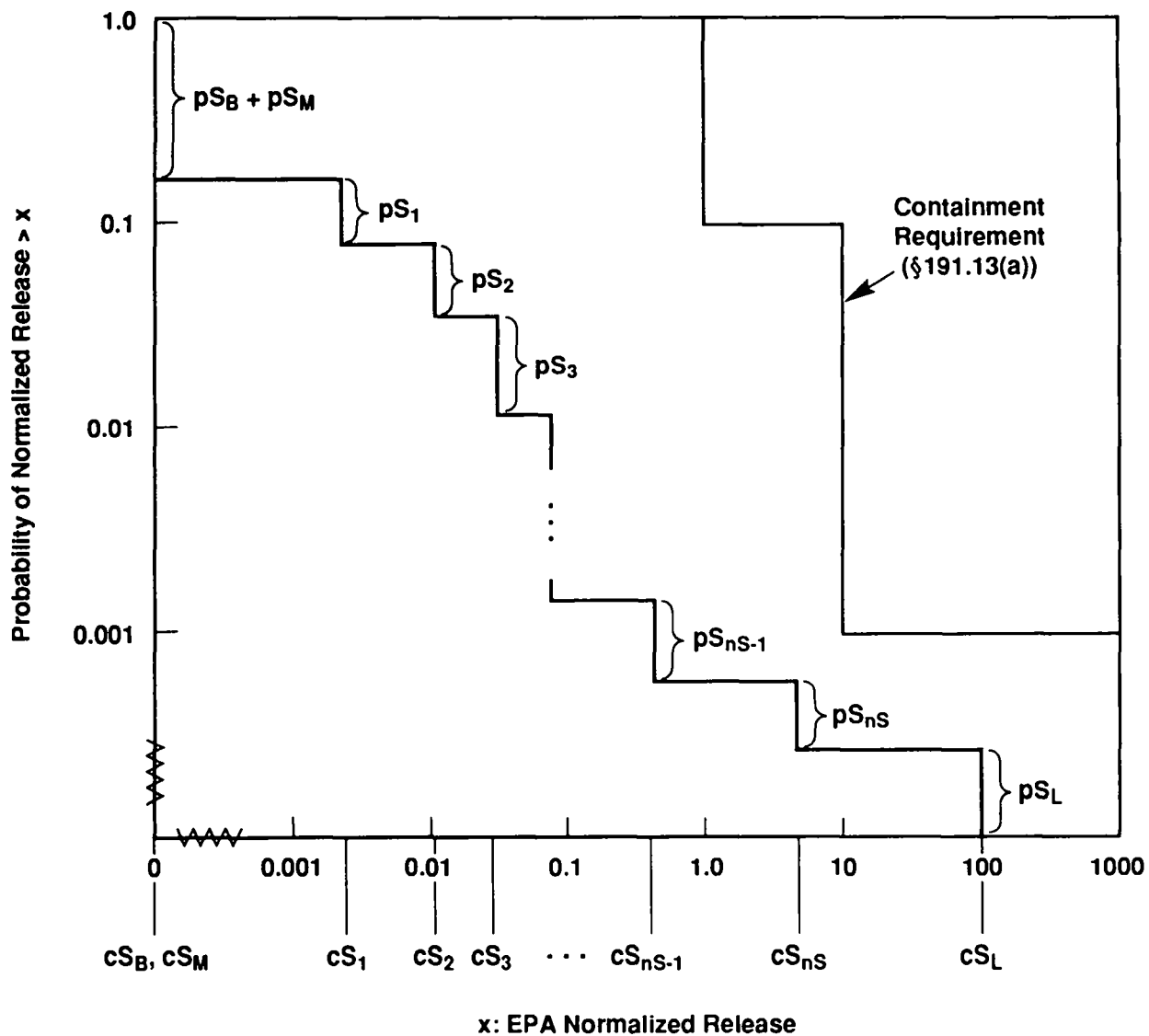
11 where the superscript c is used to designate the complement of a set.

12 Evaluation of compliance with the Containment Requirements of 40 CFR 191B does not depend equally on
 13 each of the five subsets of S . By definition, elements of S_E are excluded from consideration. The relative
 14 contributions of the other four subsets to a hypothetical CCDF for the WIPP are shown in Figure 3-5. Releases
 15 associated with the base case S_B for the WIPP are zero for this analysis (see Chapter 5 of Volume 1 and references
 16 cited there), and the consequences of both S_B and S_M therefore plot well below the EPA limits, at the extreme
 17 upper left of the CCDF. Consequences of S_L are by definition of sufficiently low probability (less than 10^{-4} in
 18 10^4 years) that they plot below the EPA limits. High-consequence elements of S_L plot at the lower right of the
 19 CCDF. Compliance depends primarily therefore on the examination of S_O , and specifically on a set of additional
 20 scenarios $S_i, i=1, \dots, nS$, obtained by further refining (i.e., subdividing) the subset S_O . S_E, S_L , and S_M could
 21 be defined to be mutually exclusive, but this distinction is not important here so they are represented in Figure 3-4
 22 with non-empty intersections. As described in Section 4.2.1, S_B and S_O are constructed to be mutually
 23 exclusive and to have empty intersections with S_M and S_L .

24 Although the scenarios that affect compliance for the WIPP come from the set S_i , performance assessments
 25 must also include S_B . The overall pattern of Figure 3-5 can be seen in the results of the WIPP preliminary
 26 performance assessments, with S_B determining the upper left of the CCDF and the remainder being determined by
 27 the S_i .

28 This analysis does not exclude S_L from consideration in the comparison with the EPA release limits. The
 29 contribution from S_L would always plot to the lower right of the CCDF, well below the EPA probability limits,
 30 and therefore would not matter in a compliance decision. S_M is not included in WIPP PA so the probability of
 31 S_M is not accumulated as shown in Figure 3-5, i.e., only the probability of S_B is included. The net effect of
 32 excluding S_M is to raise the CCDF toward the probability limits; therefore, including S_M would not negate a
 33 compliance decision.

34 Consequences of S_M cannot be seen on the CCDF for the WIPP because releases from S_B are zero.
 35 Consequences of S_L , which, if calculated, would appear as an extension on the extreme lower right of the CCDF,
 36 are also not displayed directly in the results of the WIPP performance assessments.



Notation: $pS_B, pS_M, pS_1, pS_2, \dots, pS_{nS}, pS_L$ probability for corresponding scenario

$cS_B, cS_M, cS_1, cS_2, \dots, cS_{nS}, cS_L$ consequence for corresponding scenario

S_1, S_2, \dots, S_{nS} assumed to be ordered so that $cS_1 \leq cS_2 \leq \dots \leq cS_{nS}$

TRI-6342-1278-0

Figure 3-5. Construction of a CCDF for comparison with the EPA release limits. Note that the location of cS_B at the lower left of the plot is correct for the WIPP—where no releases are predicted from the undisturbed base case—but is not a generic requirement for all sites.

1 The WIPP performance assessment does not follow the exact EPA guidance in defining S_L . Appendix B of
 2 40 CFR 191 suggests that "... performance assessments need not consider categories of events or processes that
 3 are estimated to have less than one chance in 10,000 of occurring over 10,000 years" (U.S. EPA, 1985,
 4 p. 38088). By suitably defining the events and processes selected for consideration (i.e., by making nS
 5 sufficiently large), all probabilities can theoretically be made less than the specified bound. Conceptually, the
 6 WIPP performance assessment avoids the potential problems raised by the wording of the guidance by placing a
 7 bound on the total probability of all occurrences that are removed from detailed consideration (i.e., the probability
 8 pS_L for S_L) rather than the individual probabilities for a number of different scenarios. In practice, the distinction
 9 has little impact because, as discussed later in Chapter 4 of this volume, probabilities estimated for elements of
 10 S_L are substantially below the suggested cutoff.

11 **3.2.2 WIPP Performance-Assessment Approach to Scenario Development**

12 Recognition of the five subsets of S provides the basis for the WIPP performance assessment's approach to
 13 scenario development. Because S_B , S_E , S_L , and S_M may account for a large part of the sample space S and
 14 also have readily predicted effects on the CCDF used for comparison with the EPA release limits, S_B , S_E , S_L ,
 15 and S_M are determined in the first stage of development before S_O is subdivided into the scenarios S_i shown in
 16 Figure 3-4.

17 The WIPP performance assessment uses a two-stage procedure for scenario development and the determination
 18 of scenario probabilities. The purpose of the first stage is to develop a comprehensive set of scenarios that
 19 includes all occurrences that might reasonably take place at the WIPP, and to determine the probabilities of these
 20 scenarios. The result of this stage is a set of scenarios that summarize what might happen at the WIPP. These
 21 scenarios provide a basis for discussing the future behavior of the WIPP and a starting point for the second stage
 22 of the procedure, which is the definition of scenarios S_i and the determination of the probabilities pS_i at a level of
 23 detail that is appropriate for use with the conceptual and computational models employed in the performance
 24 assessment.

25 The first stage of the analysis focuses on the determination of the sample space S and the subsets S_B , S_E ,
 26 S_L , S_M and S_O . Major groupings of scenarios within S_O are also recognized at this time, and defined for
 27 reference purposes as summary scenarios. This stage of the analysis uses a scenario-selection procedure suggested
 28 by Cranwell et al. (1990) that consists of the following five steps: (1) compiling or adopting a "comprehensive"
 29 list of events and processes that potentially could affect the disposal system, (2) classifying the events and
 30 processes to aid in completeness arguments, (3) screening the events and processes to identify those that can be
 31 eliminated from consideration in the performance assessment, (4) developing scenarios by combining the events
 32 and processes that remain after screening, and (5) screening scenarios to identify those that have little or no effect
 33 on the shape or location of the mean CCDF.

34 The purpose of the first step is to develop the sample space S , which consists of all possible 10,000-year
 35 time histories that involve the identified events and processes. The sample space S is subdivided into the subsets
 36 S_B , S_E , S_L , S_M , and S_O in Steps 2 and 3. The screening associated with Steps 2 and 3 also removes time

1 histories from \mathcal{S} that are physically unreasonable. In Step 4, a preliminary subdivision of the subset \mathcal{S}_O into
 2 additional summary scenarios is accomplished through a two-part process. In the first part, subsets of \mathcal{S}_O (i.e.,
 3 scenarios) are defined that involve specific events or processes. However, these scenarios are not mutually
 4 exclusive. In the second part, a subdivision of \mathcal{S}_O into mutually exclusive scenarios \mathcal{S}_i is accomplished by
 5 forming all possible intersections of the single event/process scenarios and their complements. The fifth and final
 6 step in the process is a screening of the scenarios \mathcal{S}_i on the basis of probability, consequence, and physical
 7 reasonableness. The purpose of this screening is to determine if some of the \mathcal{S}_i can be removed from the
 8 analysis.

9 A second stage of scenario development is necessary because the summary scenarios developed in the first
 10 stage are, in general, not defined at sufficiently fine levels of resolution for use in the construction of a CCDF that
 11 adequately displays the effects of stochastic, or Type-A, uncertainty (Section 3.1.2). The computational scenarios
 12 described in Section 4.4 of this volume represent a substantially finer subdivision of \mathcal{S}_O than that used to
 13 construct the summary scenarios, but they are based on the same screening of events and processes conducted
 14 during the first stage of scenario development. As in previous scenario construction for preliminary performance
 15 assessments of the WIPP, inadvertent intrusion into the repository during exploratory drilling is the only
 16 disruptive event considered in the 1992 assessment, and the computational scenarios reflect subdivisions based on
 17 time and number of intrusion, the activity of the waste intersected, and whether or not pressurized brine is
 18 encountered in the Castile Formation below the repository.

19 The determination of both scenarios and scenario probabilities is a complex process with significant
 20 uncertainties. To help assure that the WIPP performance assessment brings a broad perspective to this task,
 21 expert panels have been formed to provide a diversity of views with respect to possible futures at the WIPP and
 22 the probability of human intrusion. The formation of these panels and the results obtained from their
 23 deliberations are documented in Hora et al. (1991) and the memorandum by Hora in Volume 3, Appendix A of this
 24 report.

25 No inherently correct grouping exists of the possible time histories into scenarios; the probabilities associated
 26 with individual scenarios \mathcal{S}_i can always be reduced by using a finer grouping. As long as low-probability \mathcal{S}_i are
 27 not discarded, the use of more but lower probability \mathcal{S}_i will improve the resolution in the estimated CCDF shown
 28 in Figure 3-1. Because a consequence must be calculated for each scenario \mathcal{S}_i , the use of more \mathcal{S}_i results in more
 29 detailed specification of the calculations that must be performed for each scenario.

30 For example, a scenario \mathcal{S}_i for the WIPP might be defined by

31
$$\mathcal{S}_i = \{x : x \text{ a single 10,000-year time history beginning at decommissioning of the facility under}$$

 32
$$\text{consideration in which a single borehole occurs}\}. \quad (3-9)$$

 33

34 A more refined definition would be

3.4 Calculation of Scenario Consequences

The third element of the ordered triples shown in Equation 3-1 is the scenario consequence, cS_i . Estimation of cS_i is done using a linked system of computational models described in greater detail in Chapters 7 and 8 of this volume.

The models used in the WIPP performance assessment, as in other complex analyses, exist at four different levels. First, conceptual models provide a framework in which information about the disposal system can be organized and linked to processes that can be simulated with quantitative models. An adequate conceptual model is essential for both the development of the sample space S_0 appearing in Equation 3-8 and the division of S_0 into the scenarios S_i appearing in Equation 3-1. As defined in Chapter 2, alternative conceptual models may exist that are equally consistent with the available information. Consequences for each scenario must be estimated separately for each alternative conceptual model included in the analysis.

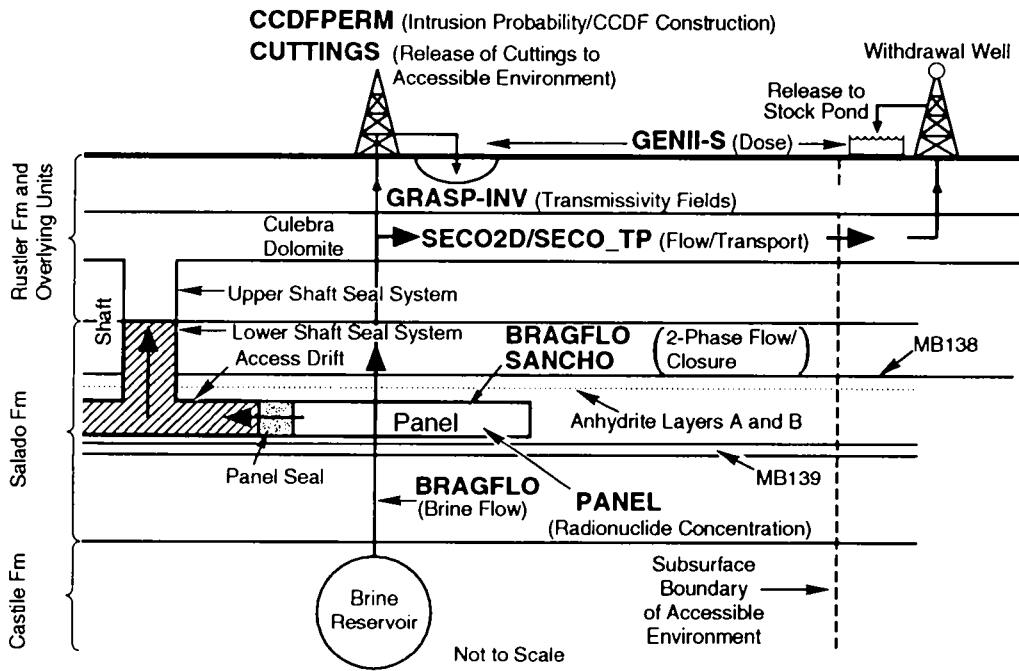
Second, mathematical models are developed to represent the processes at the site. The conceptual models provide the context within which these mathematical models must operate and define the processes they must characterize. The mathematical models are predictive in the sense that, given known properties of the system and possible perturbations to the system, they predict the response of the system. Among the processes represented by these mathematical models are fluid flow, mechanical deformation, radionuclide transport in groundwater, removal of waste through intruding boreholes, and human exposure to radionuclides released to the surface environment. Mathematical models for these processes, and others, are described in Chapter 7 of this volume.

Third, numerical models are developed to approximate the mathematical models. Most mathematical models do not have closed-form solutions, and numerical procedures must be developed to provide approximations to the solutions of the mathematical models. In essence, these approximations provide "numerical models" that calculate results that are close to the solutions of the original mathematical models. For example, Runge-Kutta procedures are often used to solve ordinary differential equations, and finite difference and finite element methods are used to solve partial differential equations. In practice, it is unusual for a mathematical model to have a solution that can be determined without the use of an intermediate numerical model. Numerical models used in the WIPP performance assessment are described in appendices to this volume.

Fourth, the complexity of the system requires the use of computer codes to implement the numerical models. Figure 3-6 illustrates the sequence of linked codes used in the 1992 WIPP performance assessment. Each of the models appearing in this figure is briefly described in Table 3-1; more information is available in Chapter 7 and appendices to this volume, and in references cited there.

3.5 Monte Carlo Analysis Techniques

As discussed in more detail by Helton et al. (1991) and in Volume 4 of this report, the WIPP performance assessment uses Monte Carlo techniques for uncertainty and sensitivity analyses. In the context of this report, uncertainty analyses evaluate uncertainty in performance estimates that results both from the existence of alternative conceptual models and from the uncertainty about imprecisely known input variables. Sensitivity anal-



TRI-6342-3401-0

Figure 3-6. Models used in 1992 WIPP performance assessment. The names for computer models (i.e., computer codes) are shown in capital letters.

Table 3-1. Summary of Computer Models Used in the 1992 WIPP Performance Assessment

Model	Description
BRAGFLO	Describes the multiphase flow of gas and brine through a porous, heterogenous reservoir. BRAGFLO solves simultaneously the coupled partial differential equations that describe the mass conservation of gas and brine along with appropriate constraint equations, initial conditions, and boundary conditions (Chapter 7).
CCDFPERM	Constructs probabilities for various computational scenarios associated with human intrusion by exploratory drilling (Section 1.4.2 of Volume 3).
CUTTINGS	Calculates the quantity of radioactive material (in curies) brought to the surface as cuttings and cavings generated by an exploratory drilling operation that penetrates a waste panel (Chapter 7).
GENII-S	Estimates potential radiation doses to humans from radionuclides in the environment (Leigh et al., in review).
GRASP-INV	Automatically generates simulations of transmissivity fields (estimates of transmissivity values) conditioned on measured transmissivity values and calibrated to steady-state and transient pressure data at well locations using an adjoint sensitivity and pilot-point technique (LaVenue and RamaRao, 1992).
PANEL	Calculates rate of discharge and cumulative discharge of radionuclides from a repository panel through an intrusion borehole. Discharge is a function of fluid flow rate, nuclide solubility, and remaining inventory (Chapter 7).
SANCHO	Finite element program that solves quasistatic, large deformation, inelastic response of two-dimensional solids (Stone et al., 1985). Used in the 1992 performance assessment to determine porosity of the waste as a function of time and moles of gas generated (Section 1.4.7 of Volume 3).
SECO2D	Calculates single-phase Darcy flow for groundwater-flow problems in two dimensions. The formulation is based on a single partial differential equation for hydraulic head using fully implicit time differencing (Chapter 7).
SECOTP	Simulates fluid flow and transport of radionuclides in fractured porous media (Chapter 7).

yses determine the contribution of individual input variables to the uncertainty in model predictions. As used here, both these types of analyses provide information about the effects of subjective, or Type-B, uncertainty. The effects of stochastic, or Type-A, uncertainty are incorporated into the performance assessment through the scenario probabilities pS_i appearing in Equation 3-1.

Monte Carlo analyses involve five steps: (1) selection of the variables to be examined and the ranges and distributions for their possible values; (2) generation of the samples to be analyzed; (3) propagation of the samples through the analysis; (4) uncertainty analysis; and (5) sensitivity analysis. These steps are described briefly in the following sections. A more complete discussion can be found in Helton et al. (1991).

3.5.1 Selection of Variables and Their Ranges and Distributions

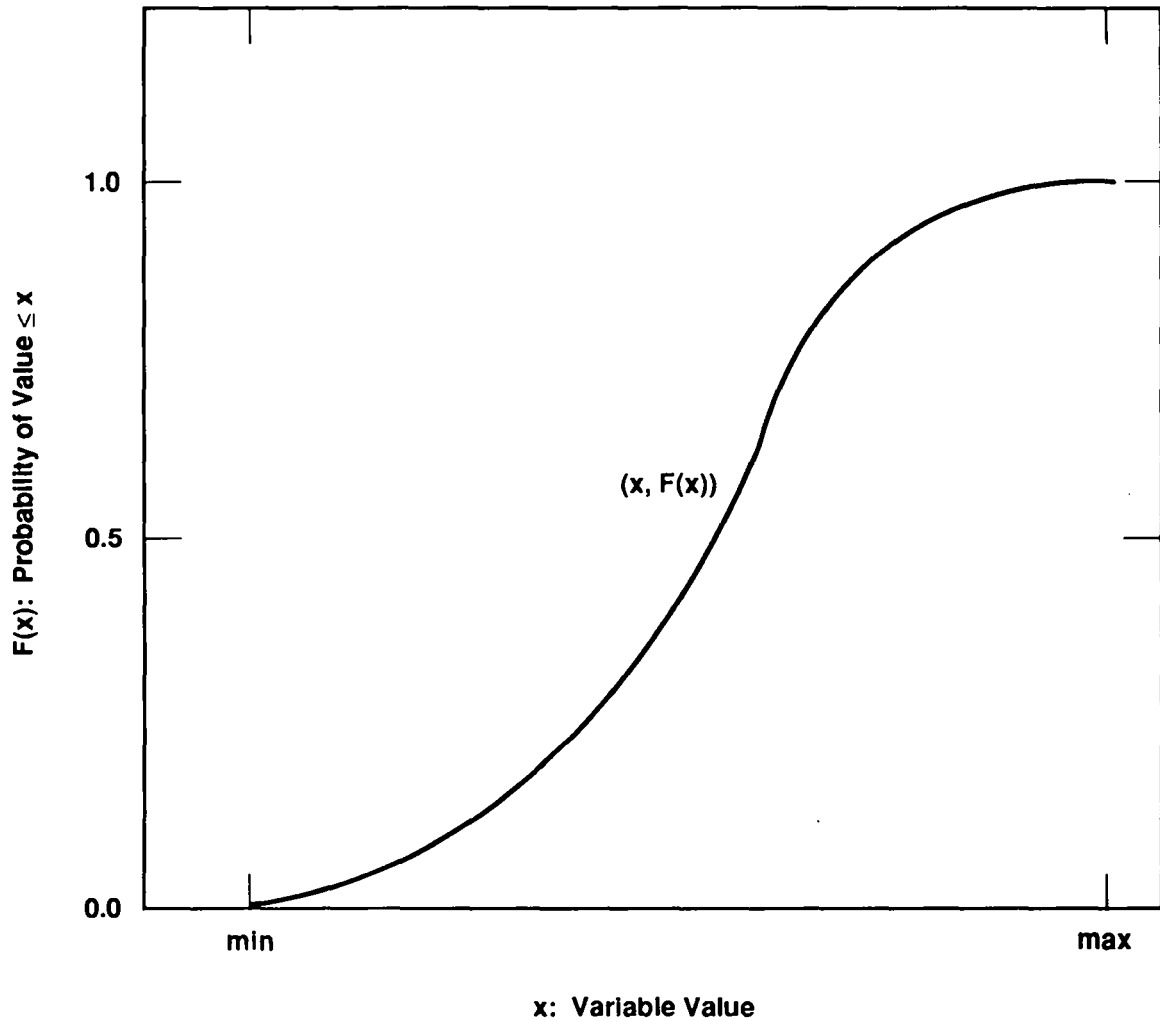
Monte Carlo analyses use a probabilistic procedure for the selection of model input. Therefore, the first step in a Monte Carlo analysis is the selection of uncertain variables and of ranges and distributions that characterize the uncertainty in their possible values. These variables are typically input parameters to computer models, and the impact of the assigned ranges and distributions can be great: analysis results are controlled in large part by the choice of input. Results of uncertainty and sensitivity analyses, in particular, strongly reflect the characterization of uncertainty in the input data.

As discussed in detail in Volume 3 of this report, information about the ranges and distributions of possible values is drawn from a variety of sources, including field data, laboratory data, literature, and, in instances where significant uncertainty exists and site-specific information is unavailable or insufficient at the time of the analyses, subjective expert judgment. In general, data from these sources cannot be examined statistically and incorporated directly in performance-assessment analyses, because data are rarely gathered with the specific model application in mind. Spatial and temporal scales over which the data are valid often do not match those of the models' applications, and in many cases, real site-specific data are simply not available. Data may be sparse or unavailable because measurements are infeasible (e.g., drilling sufficient boreholes to determine the regional heterogeneity of transmissivity in overlying aquifers), because direct measurements would in themselves create risk (e.g., drilling of boreholes through the repository to determine the extent of an underlying brine reservoir), because measurements are impossible (e.g., measuring future drilling technology), or for other reasons.

The review process that leads from the available data to the construction of the cumulative distribution functions (cdfs) used in the performance-assessment analyses is described in detail in Volume 3 of this report. Because of the nature of the available data and the type of analysis, this review process is unavoidably subjective, and involves the expert judgment of the investigators and performance-assessment analysts.

The ultimate outcome of the review process is a distribution function $F(x)$ of the form shown in Figure 3-7 for each independent variable of interest. For a particular variable x_j , the function F is defined such that

$$\text{prob}(x < x_j \leq x + \Delta x) = F(x + \Delta x) - F(x) \quad (3-12)$$



TRI-6342-666-3

Figure 3-7. Distribution function for an imprecisely known analysis variable. For each value x on the abscissa, the corresponding value $F(x)$ on the ordinate is the probability that the appropriate value to use in the analysis is less than or equal to x (Helton et al., 1991).

1 That is, $F(x+\Delta x) - F(x)$ is equal to the probability that the appropriate value to use for x_j in the particular analysis
2 under consideration falls between x and $(x + \Delta x)$.

3 **3.5.2 Generation of the Sample**

4 Various techniques are available for generating samples from the assigned distribution functions for the
5 variables (McGrath et al., 1975; McGrath and Irving, 1975a,b), including random sampling, stratified sampling,
6 and Latin hypercube sampling. As discussed in more detail in Helton et al. (1991), the WIPP performance
7 assessment uses stratified sampling and Latin hypercube sampling.

8 Stratified sampling is a modification of random sampling in which a systematic coverage of the full range of
9 possible values is forced by subdividing the sample space into strata with assigned probabilities. The
10 decomposition of the subset S_O shown in Equation 3-8 into scenarios S_i as indicated in Equation 3-1 is a form
11 of stratified sampling in which the scenario probabilities pS_i are the strata probabilities. Stratified sampling
12 forces the inclusion of low-probability, but possibly high-consequence, scenarios, and is used to incorporate
13 stochastic, or Type-A, uncertainty into the WIPP performance assessment.

14 Latin hypercube sampling (McKay et al., 1979), in which the full range of each variable is subdivided into
15 intervals of equal probability and samples are drawn from each interval, is used to incorporate subjective, or Type-
16 B, uncertainty, into the WIPP performance assessment. Specifically, a Latin hypercube sample of size 70 was
17 generated from the 49 variables in Tables 6.0-1, -2, and -3 in Volume 3 of this report. The restricted pairing
18 technique of Iman and Conover (1982) was used to prevent spurious correlations within the sample. The resultant
19 sample is listed in Volume 4 of this report.

20 **3.5.3 Propagation of the Sample through the Analysis**

21 The next step is the propagation of the sample through the analysis. Each element of the sample is supplied
22 to the model as input, and the corresponding model predictions are saved for use in later uncertainty and sensitivity
23 studies. The Compliance Assessment Methodology Controller (CAMCON) has been developed to facilitate the
24 complex calculations and storage of the input and output files from each program (Rechard, 1989, 1992). This
25 methodology incorporates data bases, sampling procedures, model evaluations, data storage, uncertainty and
26 sensitivity analysis procedures, and plotting capabilities into a unified structure. The structure and operation of
27 CAMCON is illustrated in Figure 1-1.

28 Additional information on CAMCON and its use in the 1992 WIPP performance assessment is given in
29 Chapter 1 of this volume and in Rechard (1992).

3.5.4 Uncertainty Analysis

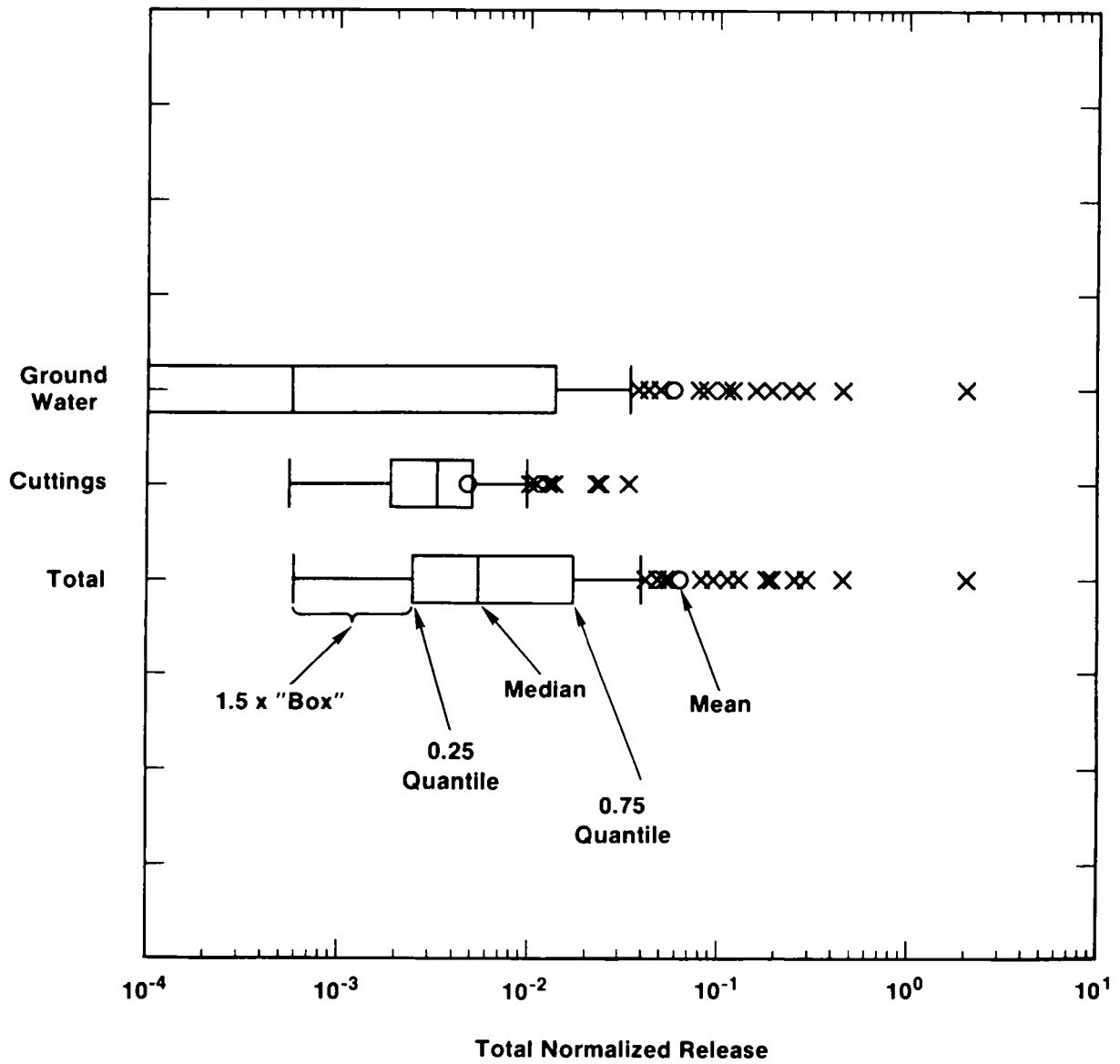
Once a sample has been generated and propagated through a model, uncertainty in the model predictions can be interpreted directly from the CCDF. Stochastic, or Type-A, uncertainty, is represented by the steps in an individual CCDF. Subjective, or Type-B, uncertainty, can be represented either with a family of CCDFs or with a summary diagram showing mean and quantile curves, as shown in Figures 3-2 and 3-3.

Uncertainty in a predicted performance measure can be characterized with an estimated distribution function, which can be displayed either as the above CCDF, a density function, a cumulative distribution function, or as box plots (Iman and Conover, 1982), as shown in Figure 3-8. The endpoints of the boxes in Figure 3-8 are formed by the lower and upper quartiles of the data, that is, $x_{.25}$ and $x_{.75}$. The vertical line within the box represents the median, $x_{.50}$. The sample mean is identified by the large dot. The bar on the right of the box extends to the minimum of $x_{.75} + 1.5(x_{.75} - x_{.25})$ and the maximum observation. In a similar manner, the bar on the left of the box extends to the maximum of $x_{.25} - 1.5(x_{.75} - x_{.25})$ and the minimum observation. The observations falling outside of these bars are shown with x 's. Box plots display the same information as a distribution function in a reduced form (without explicit probabilities). They are convenient for presenting and comparing different distributions in a single figure, especially for displaying outliers (high consequence values).

3.5.5 Sensitivity Analysis

The final step in a Monte Carlo study is sensitivity analysis, which provides information about the sensitivity of the modeling system to uncertainty in specific input parameters. Sensitivity analyses can identify those parameters for which reductions in uncertainty (i.e., narrowing of the range of values from which the sample used in the Monte Carlo analysis is drawn) have the greatest potential to increase confidence in the estimate of disposal-system performance. Identification of sensitive parameters can help set priorities for additional research; however, because results of these analyses are inherently conditional on the models, data distributions, and techniques used to generate them, the analyses cannot provide insight about the correctness of the conceptual models and data distributions used. Qualitative judgment about the modeling system must be used in conjunction with sensitivity analyses to set priorities for performance-assessment data acquisition and model development.

Sensitivity analysis techniques used in the WIPP performance assessment include scatterplots and regression analysis, and are described in detail by Helton et al. (1991). Results of the 1992 sensitivity analyses are presented in Volume 4 of this report.



TRI-6342-801-0

Figure 3-8. Example of box plots (hypothetical results).

4. SCENARIO CONSTRUCTION

4.1 Evaluation of Events and Processes

The selection of scenarios for consideration in WIPP PA is based on the formal five-step procedure described by Cranwell et al. (1990). The five steps are (1) compiling or adopting a comprehensive set of events and processes* that potentially could affect the disposal system, (2) classifying the events and processes to aid in completeness arguments, (3) screening the events and processes to identify those that can be eliminated from consideration in the PA, (4) developing scenarios by combining the events and processes that remain after screening, and (5) screening scenarios to identify those that have little or no effect on the shape or location of the CCDFs. Section 4.1 summarizes work done on the first three of these steps: the identification, classification, and screening of events and processes, referred to jointly as "evaluation of events and processes." Evaluation of events and processes has not been significantly revised since 1991, and more complete discussions of specific events and processes are available elsewhere (Guzowski, 1990; WIPP PA Division, 1991a). Additional work is in progress on evaluation of events and processes in response to reviewers' comments (e.g., Appendix B of Volume 1 of this report), and will be incorporated in future PAs.

4.1.1 Identifying Events and Processes

The WIPP PA uses the list of potentially disruptive events and processes provided by Cranwell et al. (1990) as a starting point for scenario development (Table 4-1). This list was developed by a panel of experts that met in 1976 and again in 1977 under the auspices of the U.S. Nuclear Regulatory Commission to identify events and processes that could compromise the performance of an engineered disposal system for nuclear waste constructed in deep geologic media.** Concerns raised during the development of the WIPP have led to the inclusion of three additional events and processes not identified by the panel: gas generation by the degradation of the waste, waste-related explosions, and nuclear criticality.

* Note that classification of a phenomenon as an event rather than a process, or vice versa, has no effect on scenario development. The distinction in terminology is based on 40 CFR 191B (§191.13(a)), and has been interpreted to describe the time interval over which a phenomenon occurs relative to the time interval of interest. Events are relatively brief whereas processes may occur during a large portion of the time interval of interest. The distinction is not rigid, however, and the terms are functionally interchangeable in scenario development.

** As listed in Cranwell et al. (1990), the Scenario Identification Panel Members and their affiliations were William S. Twenhofel, United States Geological Survey (USGS), Denver, CO; William W. Dudley, USGS, Denver, Co; Randolph Stone, Lawrence Livermore National Laboratory, Livermore, CA; Frederick J. Pearson, USGS, Reston, VA; Herbert R. Shaw, USGS, Menlo Park, CA; Donald Caldwell, United States Nuclear Regulatory Commission (USNRC), Washington, DC; Ben Ross, The Analytical Sciences Corp., Reading, MA; Edward Hawkins, USNRC, Washington, DC; and Martin Tierney, Sandia National Laboratories, Albuquerque, NM. Working sessions of this panel were held on December 7-8, 1976, at Grand Canyon, AZ, and again on April 13, 1977, in Carlsbad, NM.

Table 4-1. Potentially Disruptive Events and Processes

Natural Events and Processes	
Celestial Bodies	Metcorite Impact
Surficial Events and Processes	Erosion/Sedimentation Glaciation Pluvial Periods Sea-Level Variations Hurricanes Seiches Tsunamis Regional Subsidence or Uplift Mass Wasting Flooding
Subsurface Events and Processes	Diapirism Seismic Activity Volcanic Activity Magmatic Activity Formation of Dissolution Cavities Formation of Interconnected Fracture Systems Faulting
Human-Induced Events and Processes	
Inadvertent Intrusions	Explosions Drilling Mining Injection Wells Withdrawal Wells
Hydrologic Stresses	Irrigation Damming of Streams and Rivers
Repository- and Waste-Induced Events and Processes	Caving and Subsidence Shaft and Borehole Seal Degradation Thermally Induced Stress Fracturing in Host Rock Excavation-Induced Stress Fracturing in Host Rock Gas Generation Explosions Nuclear Criticality

Source: Modified from Cranwell et al., 1990.

1 4.1.2 Classifying Events and Processes

2 This step is optional, and has not been carried out explicitly for WIPP PA. Cranwell et al. (1990) included
3 classification in the procedure to assist in organizing the events and processes, to assist in completeness
4 arguments, and to provide insights when developing conceptual models of the disposal system.

5 4.1.3 Screening Events and Processes

6 Events and processes are screened using three criteria developed by Cranwell et al. (1990): probability of
7 occurrence, consequence, and physical reasonableness; and a fourth criteria specific to PAs conducted for 40 CFR
8 191B, regulatory requirements. All four are applied in the context of the 1985 version of 40 CFR 191B (U.S.
9 EPA, 1985), and screening will be reexamined when the regulation is repromulgated.

10 The “probability of occurrence” and “consequence” criteria are based directly on guidance provided in Appendix
11 B of 40 CFR 191:

12 The [EPA] assumes that . . . performance assessments need not consider categories of events or
13 processes that are estimated to have less than one chance in 10,000 of occurring over 10,000 years.
14 Furthermore, the performance assessments need not evaluate in detail the releases from all events and
15 processes estimated to have a greater likelihood of occurrence. Some of these events and processes may
16 be omitted from the performance assessments if there is a reasonable expectation that the remaining
17 probability distribution of cumulative releases would not be significantly changed by such omissions
18 (U.S. EPA, 1985, p. 38088).

19 As interpreted by the WIPP PA Department, individual events and processes (as well as “categories of events
20 and processes”) that have a probability of more than 1 chance in 10,000 of occurring over 10,000 years will be
21 retained for further evaluation. Lower-probability phenomena are identified but not considered further. Low-
22 consequence phenomena (i.e., those that would not significantly change the CCDF) are identified qualitatively in
23 the WIPP PA methodology and are eliminated regardless of probability (WIPP PA Division, 1991a).
24 Consequences of these phenomena can be evaluated quantitatively if uncertainties warrant.

25 The final screening criterion described by Cranwell et al. (1990), “physical reasonableness,” is not explicitly
26 described in 40 CFR 191B. As used in WIPP PA, this criterion distinguishes between those phenomena to which
27 a meaningful probability can be assigned (e.g., meteorite impacts) and those phenomena for which scientific
28 understanding is insufficient to assign meaningful and defensible quantitative probabilities (e.g., the occurrence of
29 volcanic activity in a geologic setting where such an event is unprecedented). The distinction between “physical
30 reasonableness” and “probability of occurrence” is not rigid, and phenomena identified as “physically unreasonable”
31 could also be eliminated on the basis of extremely low probability.

32 The “regulatory requirements” criterion is used only to screen events related to human activities, and is based
33 directly on guidance in Appendix B of 40 CFR 191:

1 . . . inadvertent and intermittent intrusion by exploratory drilling for resources (other than any provided
2 by the disposal system itself) can be the most severe intrusion scenario assumed by the implementing
3 agencies (U.S. EPA, 1985, p. 38089).

4 As interpreted by the WIPP PA Department, this allows the exclusion of all deliberate human activities that
5 disrupt the repository, as well as those inadvertent human activities that could result in consequences (e.g., EPA
6 normalized cumulative releases to the accessible environment, or other performance measures) greater than those of
7 exploratory drilling. Specifically, this criterion is used to screen acts of war, direct mining of the waste,
8 systematic drilling of multiple boreholes for resource production or other purposes, and modes of intrusion other
9 than exploratory drilling identified by an expert panel on inadvertent human intrusion into the WIPP (Hora et al.,
10 1991; memorandum by Hora in Volume 3, Appendix A of this report).

11 **4.1.4 Summary of Screened Events and Processes**

12 The following summary is taken from the 1991 PA (WIPP PA Division, 1991a), where each of the events
13 and processes listed in Table 4-1 are described in detail. As shown in Table 4-2, events and processes are either
14 retained for consideration in PA or screened out on the basis of the four criteria described in the previous section.
15 Events and processes retained for consideration are either included in the base-case scenario for the system or used
16 for developing scenarios describing disturbed performance.

17 All of the natural events and processes listed in Table 4-1 that have been retained are part of the undisturbed
18 performance of the system, and none are included in the development of disturbed-performance scenarios.
19 Phenomena such as erosion, sedimentation, climatic change (pluvial periods), seismic activity, and some shallow
20 dissolution are certain to occur during the next 10,000 years, and are part of the conceptual model for the base-case
21 scenario. Several other listed events (i.e., sea-level variations, hurricanes, seiches, and tsunamis) are restricted to
22 coastal areas, and are physically unreasonable at the WIPP location. Surficial geologic events, including regional
23 subsidence or uplift, mass wasting, glaciation, and flooding, and all subsurface events except seismic activity and
24 shallow dissolution of the Rustler-Salado contact are screened out as physically unreasonable or of low
25 probability.

26 Of the human-induced events and processes, inadvertent explosions at the location of the waste panels are
27 excluded by regulatory requirements; inadvertent explosions near the waste panels during warfare and nuclear
28 testing are screened out on the basis of low probability. Irrigation and damming of valleys close enough to the
29 WIPP to have an impact are low-probability events because of poor water and soil quality and limited water
30 supplies. Based on the geologic setting and previous resource evaluations, both exploratory drilling for resources
31 and the drilling of injection wells are realistic events for the WIPP, and are retained for scenario development.
32 Intrusion of injection wells into the waste-emplacement region is not modeled explicitly in PA, because drilling
33 technology and therefore consequences are assumed to be the same as for exploratory drilling. Expert judgment on
34 the probability of intrusion by injection wells is not available (Hora, memo in Appendix A of Volume 3).
35 Injection wells that do not penetrate the repository are screened out on the basis of low consequence.

Table 4-2. Summary of Screened Events and Processes (from WIPP PA Division, 1991a)

Events and Processes	RETAINED		SCREENED OUT			
	Base-Case Conditions	For Scenario Development	Low Probability	Physically Unreasonable	Low Consequence	Regulatory Requirements
Natural						
Meteorite Impact			X			
Erosion/Sedimentation	X					
Glaciation				X		
Pluvial Periods (Climate Change)	X					
Sea-Level Variations				X		
Hurricanes				X		
Seiches				X		
Tsunamis						
"Conventional"				X		
Meteorite Impact			X			
Regional Subsidence or Uplift				X		
Mass Wasting				X		
Flooding				X		
Diapirism				X		
Seismic Activity	X					
Volcanic Activity				X		
Magmatic Activity				X		
Formation of Dissolution Cavities						
Deep Dissolution				X		
Shallow Dissolution						
Rustler-Salado Contact	X					
Nash Draw*			X	X		
Formation of Interconnected						
Fracture Systems				X		
Faulting				X		
*Screening criterion depends on which possible mechanisms considered for origin of Nash Draw						

Table 4-2. Summary of Screened Events and Processes (from WIPP PA Division, 1991a) (continued)

Events and Processes	RETAINED		SCREENED OUT			
	Base-Case Conditions	For Scenario Development	Low Probability	Physically Unreasonable	Low Consequence	Regulatory Requirements
Human-Induced						
Explosions						
At Waste-Panels Location						×
Near Waste-Panels Location						
At Surface/Warfare			×			
Deep Testing			×			
Drilling (Exploratory)		×				
Mining						
At Waste-Panels Location						×
Near Waste-Panels Location		×				
Injection Wells						
Withdrawal Wells						
Water Wells		×				
Oil and Gas Wells						
At Waste-Panels Location						×
Near Waste-Panels Location					×	
Geothermal Wells					×	
Irrigation			×			
Damming of Streams and Rivers						
At Pecos River					×	
Near Nash Draw			×			
Repository- and Waste-Induced						
Subsidence and Caving					×	
Shaft & Borehole Seal Degradation	×					
Thermally Induced Fractures				×		
Excavation-Induced Fractures	×					
Gas Generation	×					
Explosions (Gas Ignition)					×	
Near Criticality						
Critical Mass (Explosion)			×			
Sustained Reaction**						

** Retained for additional evaluation

1 In the category of waste- and repository-induced events and processes, gas generation and shaft-seal degradation are
2 part of the conceptual model of the base-case scenario. Borehole seal degradation is addressed through parameter
3 uncertainty during modeling. Excavation-induced fracturing in the host rock is handled by including the disturbed
4 zone surrounding mined openings in the conceptual model of the base-case scenario. Caving into the rooms or
5 drifts may occur in the short term after decommissioning, but this process has no long-term consequences on
6 performance because of the mechanical behavior of salt. Thermally induced fracturing of the host rock is not a
7 physically reasonable phenomenon because of the low thermal output of WIPP waste. Subsidence caused by the
8 mined openings and explosions caused by the ignition of gases created by waste degradation have no effect on the
9 long-term performance of the disposal system and can be eliminated from scenario development. Nuclear
10 criticality requires additional evaluation before a screening decision is made.

11 As shown in Table 4-2, a total of 10 events and processes are retained for consideration following screening.
12 Seven of these are essentially certain to occur, and are included in the conceptual model for the base-case scenario
13 (see Section 4.2.3.1). The other three—exploratory drilling, potash mining near the waste panels, and water
14 wells—are used to develop summary scenarios describing disturbed performance of the system. Exploratory
15 drilling is subdivided into two possibilities: drilling into a waste-filled room or drift and a brine reservoir in the
16 underlying Castile Formation (Event E1), and drilling into a waste-filled room or drift without penetrating a brine
17 reservoir (Event E2). Mining (Event TS) is limited to potash extraction by either conventional or solution
18 methods in areas beyond the boundaries of the waste panels; drilling of withdrawal wells (Event E3) is limited to
19 water wells in areas where water quantity and quality will permit water use. Both mining and water wells will be
20 evaluated in future performance assessments for their effects on groundwater flow in the WIPP area.

21

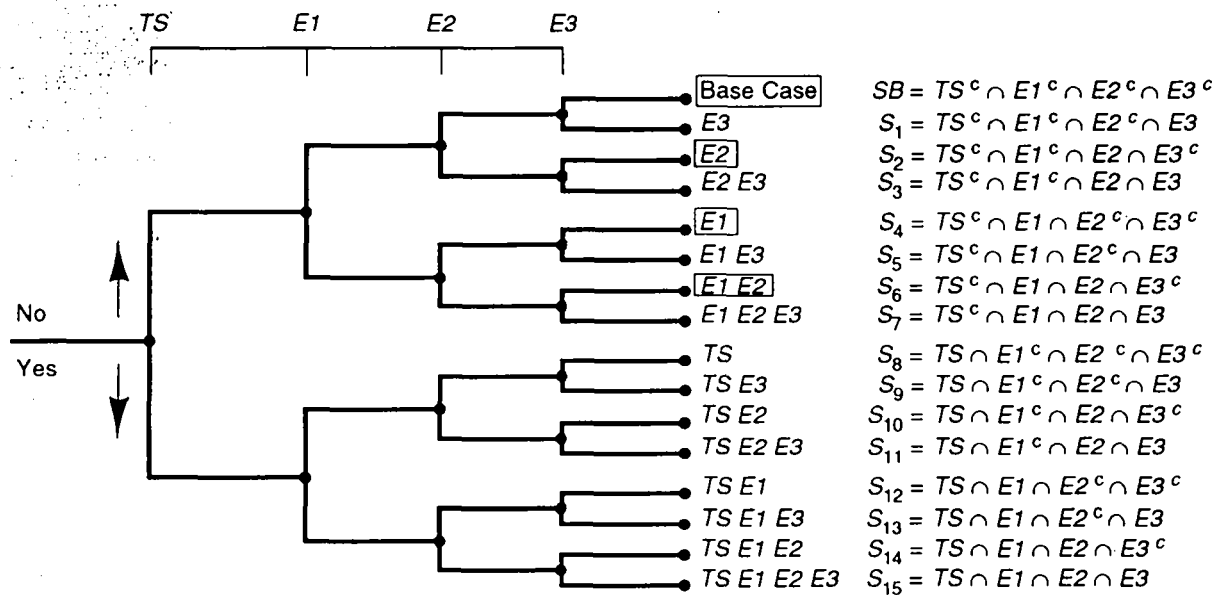
22

4.2 Summary Scenarios

23 4.2.1 Development of Summary Scenarios

24 As explained in the 1991 PA documentation (WIPP PA, 1991a, Section 4.1.7), logic diagrams based on the
25 approach defined by Cranwell et al. (1990) are used to combine events and processes that remain after screening
26 into summary scenarios. As the logic diagram for the WIPP performance assessment (Figure 4-1) shows, no
27 temporal relationship between events and processes is implied by their sequence across the top of the diagram; at
28 each junction within the diagram a yes/no decision is made as to whether the next event or process is added to the
29 scenario. As a result, each scenario consists of a combination of occurrence and nonoccurrence of all events and
30 processes that survive screening (Cranwell et al., 1990). To simplify scenario notation, only the events and
31 processes that occur are used to identify the scenario. Based on the assumption that the events and processes
32 remaining after screening define all possible futures of the disposal system that are important for a probabilistic
33 assessment, the logic diagram produces scenarios that are comprehensive and mutually exclusive because all
34 possible combinations of events and processes are developed, and each scenario is a unique set of events and
35 processes.

36 Figure 4-1 shows all of the scenarios (the possible combinations of the four events) that survived the
37 screening process for the WIPP (Section 4.1.4):



- x = 10,000 yr Time History
- TS = {x: Subsidence Resulting from Solution Mining of Potash}
- E1 = {x: One or More Boreholes Pass Through a Waste Panel and into a Brine Pocket}
- E2 = {x: One or More Boreholes Pass Through a Waste Panel Without Penetrating a Brine Pocket}
- E3 = {x: One or More Withdrawal Wells near Repository Where Water Quality Will Permit Water Use}
- Superscript c (e.g., TS^c) Denotes Set Complement

TRI-6342-3436-0

Figure 4-1. Potential scenarios for the WIPP disposal system.

- 1 • E1, the inadvertent drilling of an exploratory borehole into a waste-filled room or drift and a brine reservoir
2 in the underlying Castile Formation,
- 3 • E2, the inadvertent drilling of an exploratory borehole into a waste-filled room or drift that does not
4 intersect a brine reservoir in the underlying Castile Formation,
- 5 • E3, drilling of water withdrawal wells in areas where water quality will permit water use, and
- 6 • TS, mining for potash by either conventional or solution methods in areas beyond the boundaries of the
7 waste panels.

8 For the 1992 PA calculations, only the base-case scenario and scenarios containing the E1 and E2 events were
9 considered; therefore, only four summary scenarios were evaluated this year: the base case (expected behavior of
10 the disposal system without disruption by human intrusion), E1, E2, and E1E2. The TS event will be added to
11 later PA calculations for 40 CFR 191B. The E3 event will be evaluated in safety assessments because it provides
12 a potential pathway through which human doses could occur.

13 4.2.2 Screening of Summary Scenarios

14 The purpose of scenario screening is to identify those scenarios that will have no or a minimal impact on the
15 shape and/or location of the mean CCDF. The criteria used to screen combinations of events and processes
16 (scenarios) are similar to those criteria used to screen individual events and processes (Section 4.1.3). These
17 criteria are physical reasonableness of the combinations of events and processes, probability of occurrence of the
18 scenario, and consequence.

19 The probability of occurrence for a scenario is determined by combining the probabilities of occurrence and
20 nonoccurrence from the events and processes that make up the scenario. A mechanical approach to determining
21 scenario probabilities can be implemented by assigning the probability of occurrence and nonoccurrence for each
22 event and process to the appropriate "yes" and "no" legs at each bifurcation in the logic diagram (Figure 4-1). The
23 probability of a scenario is the product of the probabilities along the pathway through the logic diagram that
24 defines that scenario. Based on the probability criterion in Appendix B of 40 CFR 191 for screening out
25 individual events and processes, scenarios with probabilities of occurrence of less than 1 chance in 10,000 in
26 10,000 years need not be considered in determining compliance with 40 CFR 191B, and therefore, consequence
27 calculations are not necessary.

28 Consequence in this step of the procedure means integrated discharge to the accessible environment for 10,000
29 years. By inferring that the guidance in Appendix B of 40 CFR 191 for individual events and processes also
30 applies to scenarios, scenarios whose probability of occurrence is greater than the cutoff in Appendix B can be
31 eliminated from further consideration if their omission would not significantly change the remaining probability
32 distribution of cumulative releases. Because the degree to which the mean CCDF will be affected by omitting
33 such scenarios is difficult to estimate prior to constructing CCDFs, only those scenarios that have no releases or
34 very small, low-probability releases should be screened out from additional consequence calculations. If

1 significant changes are made to the data base, the conceptual models, or mathematical models of the disposal
2 system, the omitted scenarios should be rescreened.

3 In implementing this step of the procedure for this preliminary WIPP performance assessment, no scenarios
4 were screened out. Because parameter values did not define the events, all combinations of events in the scenarios
5 are physically reasonable. Because final scenario probabilities have not been estimated, no scenarios were screened
6 out on the basis of low probability of occurrence. Final calculations of consequences have not been completed, so
7 no scenarios were screened out on the basis of this criterion.

8 **4.2.3 Retained Summary Scenarios**

9 This section describes the scenarios retained for consequence analysis that are considered in the 1992 PA
10 calculations.

11 **4.2.3.1 UNDISTURBED SUMMARY SCENARIO (S_B)**

12 **Guidance from 40 CFR 191**

13 The Individual Protection Requirements of 40 CFR 191B (§191.15) call for a reasonable expectation that the
14 disposal system will limit annual doses to individuals for 1,000 years after disposal, assuming undisturbed
15 performance of the disposal system. Undisturbed performance is defined in 40 CFR 191B to mean “the predicted
16 behavior of a disposal system, including consideration of the uncertainties in predicted behavior, if the disposal
17 system is not disrupted by human intrusion or the occurrence of unlikely natural events” (§191.12(p)). Duration
18 of this performance is not limited by the definition.

19 Although undisturbed performance is not mentioned in the Containment Requirements (§191.13), undisturbed
20 performance is not precluded from the containment calculations and, for the WIPP, is the base case of the scenario-
21 development methodology (Cranwell et al., 1990; Guzowski, 1990). The base-case scenario describes the disposal
22 system from the time of decommissioning and incorporates all expected changes in the system and associated
23 uncertainties for the 10,000 years of concern for §191.13. Subpart B of 40 CFR 191 does not provide a definition
24 of unlikely natural events to be excluded from undisturbed performance nor, by implication, likely natural events
25 to be included. Because of the relative stability of the natural systems within the region of the WIPP disposal
26 system, all naturally occurring events and processes that will occur are part of the base-case scenario and are
27 nondisruptive. These conditions represent undisturbed performance (Marietta et al., 1989; Bertram-Howery et al.,
28 1990). They include the events and processes retained for undisturbed conditions, which are listed in Table 4-2.

1 Base-Case Description

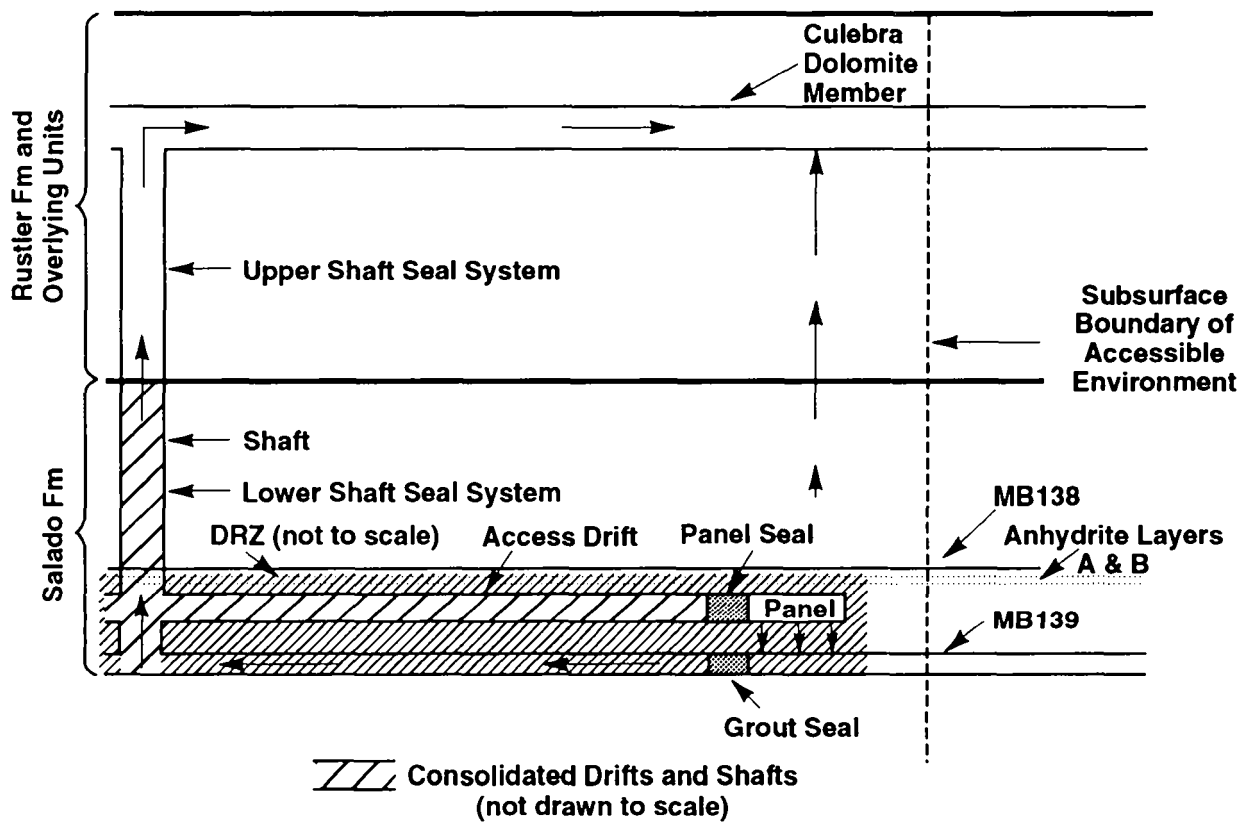
2 After the repository is filled with waste, the disposal rooms and drifts in the panels are backfilled and seals are
3 emplaced in the shafts and access drifts to the panels (Figure 4-2). While excavations are open, the salt creeps
4 inward because of the decrease in confining pressure on the salt around the rooms. Portions of the access drifts and
5 the lower parts of shafts are filled with preconsolidated, crushed salt (Stormont et al., 1987; Borns and Stormont,
6 1988; Nowak et al., 1990). Because of the high lithostatic pressures at the repository depth, salt creep is expected
7 to exert sufficient pressure on the crushed salt to consolidate the material into low-conductivity seals with
8 properties similar to those of the host rock. Portions of the upper parts of the shafts are also filled with salt, but
9 pressure is not expected to be sufficient here to cause the same degree of consolidation as is expected in lower
10 portions of the shafts.

11 Gas generation is an important process for the undisturbed case. Some waste and some waste containers will
12 be composed of organic material. Because microbes transported into the repository with the waste are expected to
13 be viable under sealed-repository conditions (Brush and Anderson, 1989b), organic material in the repository will
14 biodegrade with concomitant generation of gases. In addition, moisture in the repository, either brought in with
15 waste or seeping in from the Salado Formation, can corrode metals in the waste and metallic waste containers
16 themselves, with gas generated as a by-product. Radiolysis also will generate gases.

17 Sufficient quantities of gas will be generated to result in elevated pressures in the repository, approaching and
18 perhaps exceeding lithostatic pressure (approximately 15 MPa). Elevated pressures may open fractures in
19 anhydrite layers above and below the waste-disposal panels, which are relatively more brittle than the plastic
20 halite.

21 Two potential pathways for groundwater flow and radionuclide transport dominate the undisturbed disposal
22 system (Figure 4-2):

- 23 • In the first path, the pressure gradient between the waste-disposal panels and the Culebra causes brine and
24 radionuclides to migrate from the waste-disposal panels to the base of the shafts and up the shafts toward
25 the Culebra. This migration may occur directly through panel seals and the backfill in access drifts, but is
26 more likely to occur through anhydrite interbeds (primarily MB139 below the panels, but possibly also
27 MB138 and interbeds A and B above the panels). Contaminated brine may enter the interbeds either
28 through fractures in salt in the DRZ, or directly as a result of rooms and drifts intersecting the interbeds
29 during construction or room closure. Migration to the base of the shafts could then occur in fractures in the
30 anhydrite layers. Migration up the shafts occurs through the shaft-seal system.
- 31 • The second major path for brine and radionuclide migration from the undisturbed repository is laterally
32 through anhydrite interbeds toward the subsurface boundary of the accessible environment in the Salado
33 Formation. Brine enters the interbeds as described for the first path, and is driven outward from the panels
34 by elevated pressures in the waste resulting from gas generation.



TRI-6342-200-9

Figure 4-2. Conceptual model used in simulating undisturbed performance.

1 A third pathway for radionuclide transport from the undisturbed disposal system was considered in previous
2 analyses (Lappin et al., 1989), in which brine migrated vertically from the panels through the intact Salado
3 Formation toward the Culebra. Although this pathway has a larger pressure decline over the shortest distance than
4 either of those discussed above, and also has the largest cross-sectional area through which migration could occur,
5 low permeabilities of the intact halite result in extremely long travel times (400,000 years for the first arrival of
6 radionuclides at the Culebra, as calculated by Lappin et al. [1989]). Because of the improbability of developing
7 interconnected, vertical fractures in the plastic halite, this pathway is not modeled in performance assessment.

8 4.2.3.2 HUMAN-INTRUSION SUMMARY SCENARIOS

9 Guidance from 40 CFR 191

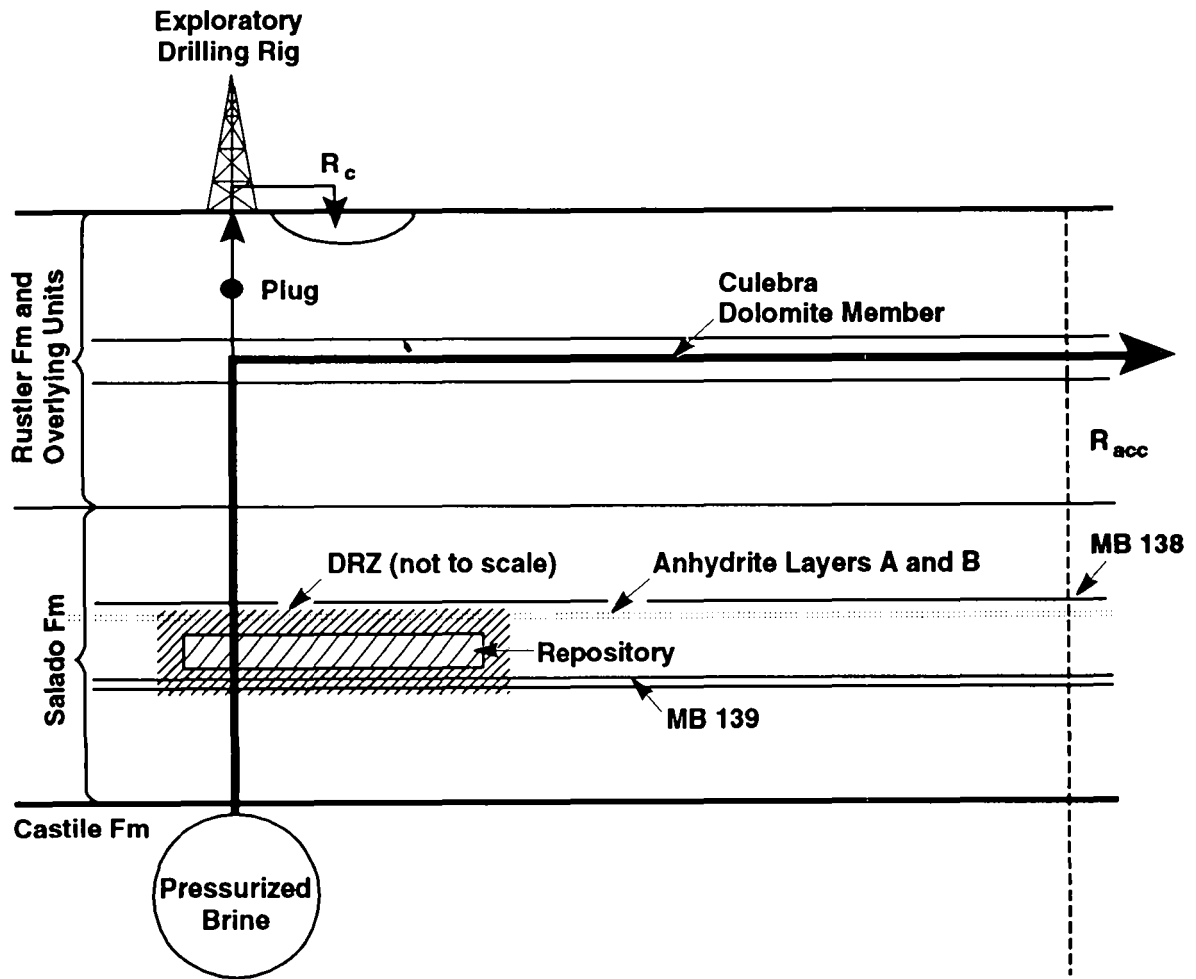
10 Appendix B of 40 CFR 191 provides guidance on a number of factors concerning human intrusion. Active
11 controls cannot be assumed to prevent or reduce radionuclide releases for more than 100 years after disposal (U.S.
12 EPA, 1985, p. 38088). Passive institutional controls can be assumed to deter systematic and persistent
13 exploitation and to reduce the likelihood of inadvertent intrusion, but these controls cannot eliminate the chance of
14 inadvertent intrusion. As discussed in Section 4.1.3, Appendix B (U.S. EPA, 1985, p. 38088) also suggests that
15 exploratory drilling for resources can be the most severe form of human intrusion considered, and that the
16 likelihood and consequence of drilling should be based on site-specific factors. In keeping with the guidance, this
17 assessment includes scenarios that contain human-intrusion events.

18 Intrusion Borehole through a Room or Drift into Pressurized Brine in the Castile Formation 19 (Summary Scenario E1)

20 Scenario E1 (Figure 4-3) consists of one or more boreholes that penetrate through a waste-filled room or drift
21 and continue into or through a brine reservoir in the underlying Castile Formation in which brine pressure is
22 between hydrostatic and lithostatic for that depth (Marietta et al., 1989). Radionuclides may be released to the
23 accessible environment in two ways: some radionuclides will be brought to the ground surface during drilling as
24 particulate material entrained in drilling fluid; additional radionuclides may reach the subsurface boundary of the
25 accessible environment following long-term groundwater transport up the borehole and laterally down a
26 potentiometric gradient in the Culebra Dolomite Member of the Rustler Formation.

27 Radionuclides released during drilling result from the drill bit directly intersecting waste. Material ground up
28 by the drill bit (cuttings) is transported to the surface by the circulating drilling fluid. Additional material may be
29 eroded from the walls of the borehole by the circulating drilling fluid (cavings) or by the spalling of solid material
30 into the hole as the panel depressurizes. Cuttings, cavings, and spillings are collectively referred to as cuttings in
31 performance-assessment documentation.

32 After drilling is complete, the hole is assumed to be plugged and abandoned. All borehole plugs and drilling
33 mud remaining in the borehole, except for a plug above the Culebra, are assumed to degrade into material with



TRI-6342-215-2

Figure 4-3. Conceptual model for scenario E1. Arrows indicate assumed direction of flow. Exploratory borehole penetrates pressurized brine below the repository horizon. R_c is the release of material directly from the drilling operation. R_{acc} is the release at the subsurface boundary of the accessible environment. A plug above the Culebra Dolomite Member is assumed to remain intact for 10,000 years.

1 properties similar to those of silty sand. Plug degradation is in keeping with guidance provided by Appendix B of
2 40 CFR 191: "consequences of ... inadvertent drilling need not be more severe than ... creation of a groundwater
3 flow path with a permeability typical of a borehole filled by the soil or gravel that would normally settle into an
4 open hole over time—not the permeability of a carefully sealed borehole" (U.S. EPA, 1985, p. 38089). The
5 borehole is assumed to remain propped open by the material filling it, preventing closure of the hole by salt creep
6 in the Salado Formation. A single plug above the Culebra is assumed to remain intact for Scenario E1, diverting
7 all upward flow into the Culebra and maximizing radionuclide transport into that unit and toward the subsurface
8 boundary of the accessible environment. Rate of flow depends on the head difference between the Culebra and the
9 injected brine and on the hydraulic properties of the borehole fill. Radionuclides from the room may be
10 incorporated into the Castile brine if it circulates through the waste adjacent to the borehole.

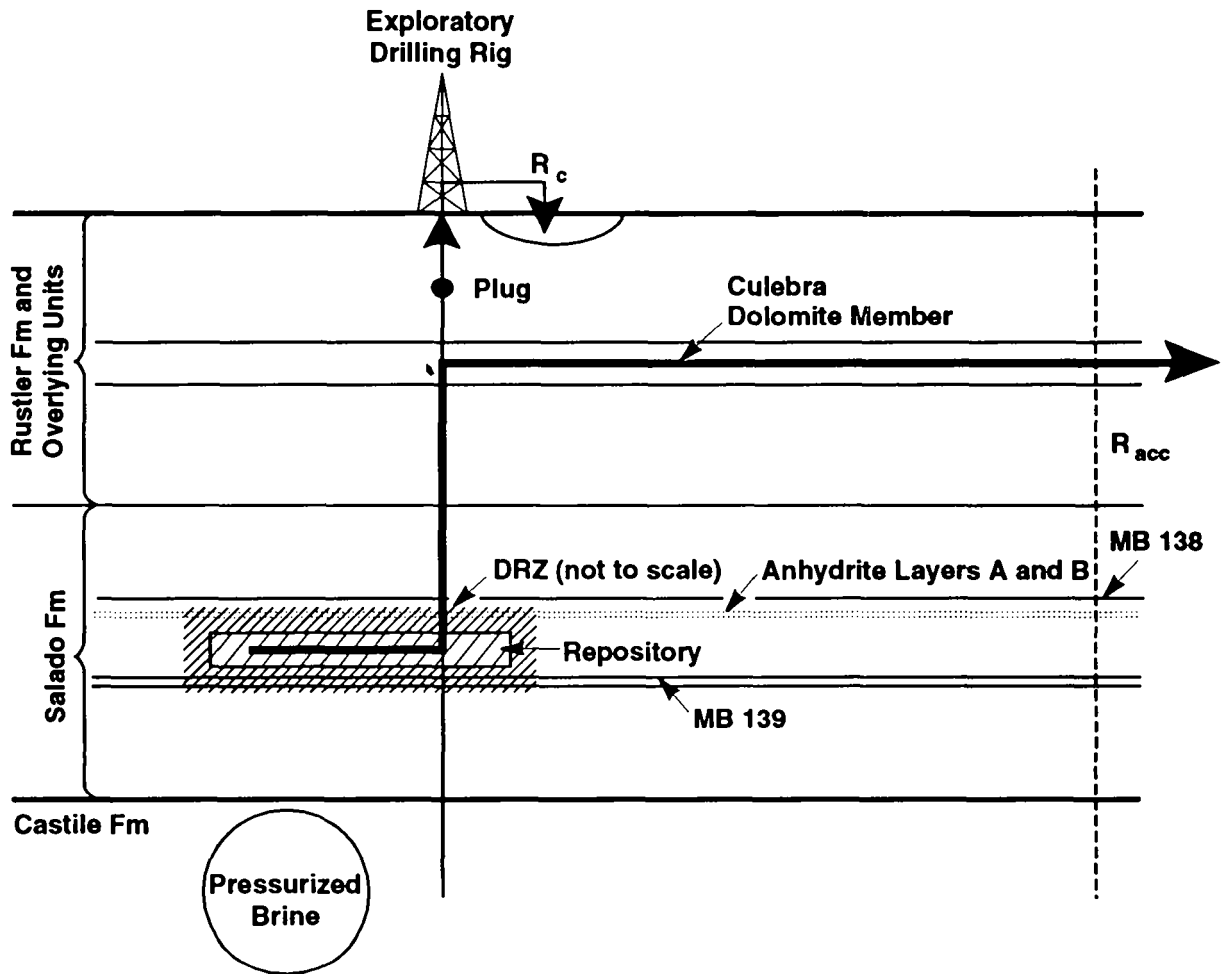
11 Intrusion Borehole into a Room or Drift (Summary Scenario E2)

12 Scenario E2, like Scenario E1 (described above), also consists of one or more boreholes that penetrate to or
13 through a waste-filled room or drift (Figure 4-4). Unlike Scenario E1, however, the borehole does not intersect
14 pressurized brine or any other important source of water (Marietta et al., 1989). Releases of cuttings at the ground
15 surface during drilling are identical to those described for Scenario E1, as are the assumptions about borehole
16 plugging. Rate of flow into the Culebra is determined in Scenario E2 by the head gradient between the repository
17 and the Culebra and the hydraulic properties of the borehole fill.

18 Intrusion Borehole through a Room or Drift into Pressurized Brine in the Castile Formation and 19 Another Intrusion Borehole into the Same Panel (Summary Scenario E1E2)

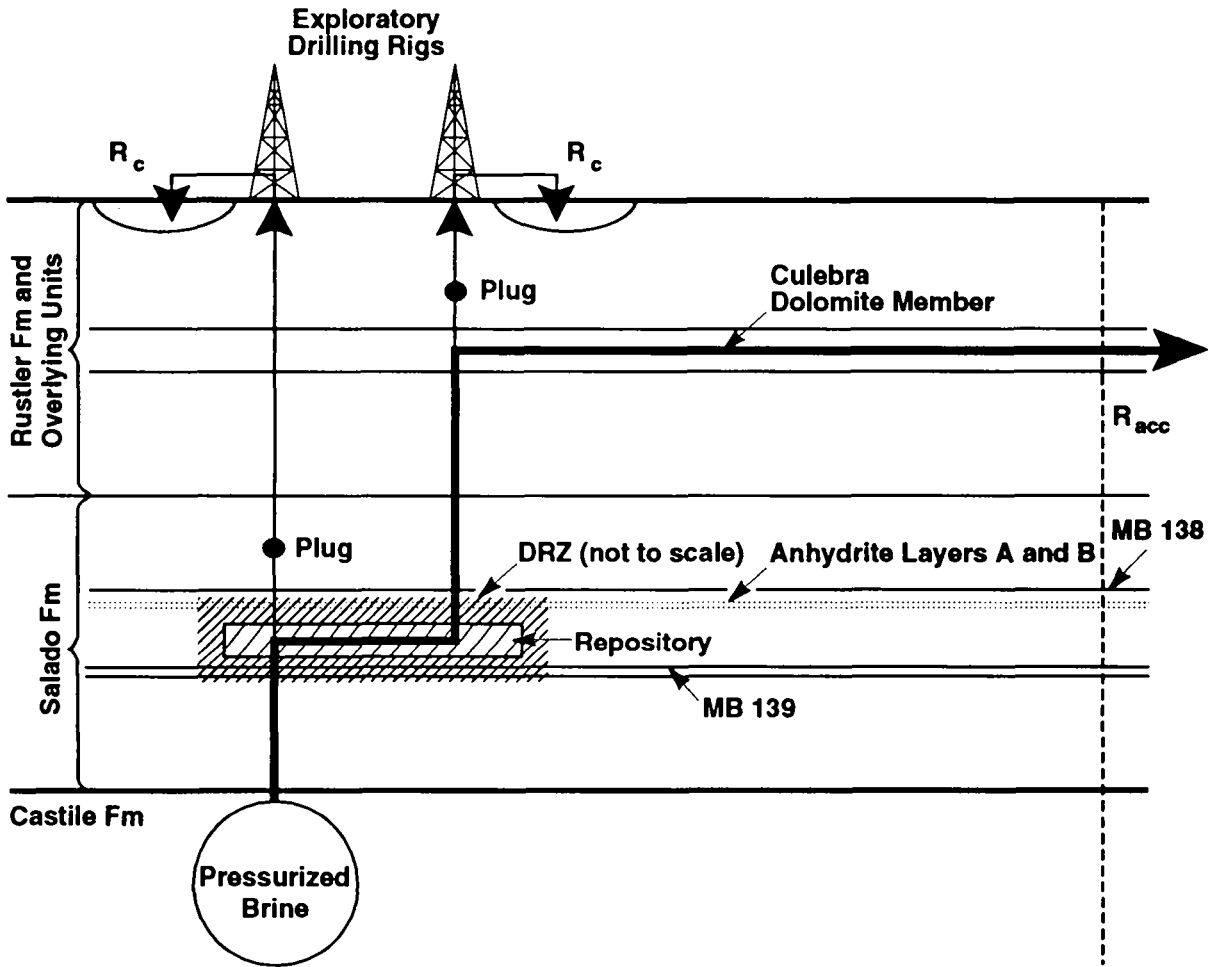
20 Scenario E1E2 consists of exactly two boreholes that penetrate waste-filled rooms or drifts in the same panel
21 (Figure 4-5) (Marietta et al., 1989). One borehole also penetrates pressurized brine in the Castile Formation,
22 whereas the other borehole does not. Assumptions about the degradation of borehole plugs are the same as those
23 described for Scenarios E1 and E2, except that in this case specific plugs are assumed to remain intact so as to
24 maximize flow from the Castile brine reservoir through the waste and into the Culebra. The borehole that
25 penetrates the pressurized brine (the E1-type borehole) remains plugged between the waste and the Culebra; the
26 other borehole (the E2-type borehole) remains plugged above the Culebra. Brine flow in Scenario E1E2 is driven
27 by the head difference between the Castile brine reservoir and the Culebra.

28 Radionuclides are released directly to the surface during drilling of the two holes as described with E1 and E2;
29 additional releases from this system are dependent on the sequence in which the holes are drilled. The plug in the
30 borehole that penetrates the pressurized brine reservoir allows brine flowing up the hole to enter the repository but
31 not leave the repository until the second hole penetrates the same panel. Once the second hole is drilled, a
32 pathway is formed for brine and gas from the pressurized brine reservoir to flow through waste panels and nearby
33 members to this new hole and up to the Culebra Dolomite Member. If the hole that does not penetrate pressurized
34 brine is drilled first, gas and/or fluid pressure is relieved; this is followed by brine flow and radionuclide transport
35 up the hole as a result of brine inflow into the panel from the host rock, possibly enhanced by creep



TRI-6342-216-2

Figure 4-4. Conceptual model for scenario E2. Arrows indicate assumed direction of flow. Exploratory borehole does not penetrate pressurized brine below the repository horizon. R_c is the release of material directly from the drilling operation. R_{acc} is the release at the subsurface boundary of the accessible environment. A plug above the Culebra Dolomite Member is assumed to remain intact for 10,000 years.



TRI-6342-217-2

Figure 4-5. Conceptual model for scenario E1E2. Arrows indicate assumed direction of flow. One exploratory borehole penetrates pressurized brine below the repository horizon a plug between the repository and the Culebra Dolomite Member is assumed to remain intact for 10,000 years. The second borehole does not penetrate pressurized brine below the repository; a plug above the Culebra Dolomite Member is assumed to remain intact for 10,000 years. R_c is the release of material directly from the drilling operation. R_{acc} is the release at the subsurface boundary of the accessible environment.

1 closure of rooms and drifts. Flow is diverted into the Culcra by the plug located above this unit. The
2 subsequent drilling and plugging of the borehole that penetrates the pressurized brine reservoir results in flow
3 through the repository and up the other borehole. If driving pressure is depleted, Scenario E1E2 reverts to
4 Scenario E2, because the borehole that penetrates the pressurized brine no longer contributes to flow and transport
5 (Marietta et al., 1989). For modeling convenience, analyses of Scenario E1E2 assume that both boreholes are
6 drilled at or close to the same time.

7 **4.2.4 Computational Approximations of Scenarios E1, E2, and E1E2**

8 The 1992 PA calculations use the same conceptual approximations for Scenarios E1, E2, and E1E2 that were
9 used in the 1991 calculations (WIPP PA Division, 1991b, Sections 5.1.1 and 5.1.2). E2-type intrusions are
10 simulated explicitly using the BRAGFLO, SANCHO, and PANEL codes (Sections 7.2, 7.3, and 7.4, and
11 Appendices A and B of this volume).

12 E1E2-type intrusions are not simulated explicitly because the axisymmetric cylindrical geometry used for
13 BRAGFLO cannot readily accommodate two intrusion boreholes (WIPP PA Division, 1991b, Section 5.1.1).
14 E1E2-type boreholes are simulated therefore using a single borehole and the assumption that all brine in the panel
15 mixes with all Castile brine flowing up the borehole. This assumption duplicates the primary feature of Scenario
16 E1E2—all radionuclides in a single panel are potentially available for transport up the borehole. Because the flow
17 path between the two boreholes is omitted, the simplification may somewhat overestimate both the amount of
18 waste dissolved and the rate at which flow occurs through the waste and up the borehole.

19 E1-type intrusions are also not simulated explicitly, in this case for computational efficiency. Consequences
20 of E1-type intrusions are instead assumed to be the same as the consequences for E2-type intrusions occurring at
21 the same time. Probabilities are determined separately for the two types of intrusions (Section 5.3 of this
22 volume); the contributions of Scenarios E1 and E2 to the overall CCDF are therefore not identical.

23 Justification for this approximation is based on the assumption that brine flowing up the E1 borehole from
24 the Castile reservoir does not circulate through the waste. All radionuclides entering the borehole are assumed to
25 be dissolved in brine that entered the waste from the far field of the Salado Formation or that was initially present
26 in the panels. Comparison in the 1991 PA (WIPP PA Division, 1991b, Section 5.1.2) of the consequences of
27 E1- and E2-type intrusions for 60 realizations indicates that cumulative flow of brine from the panel into the
28 borehole is in most (but not all) realizations greater for the E2 borehole than for the E1 borehole. Larger brine
29 flows from the waste (and therefore larger potential radionuclide releases) occur for the E2 borehole because the
30 elevated Castile brine pressure present in the E1 borehole retards brine inflow into the waste from the far field of
31 the Salado Formation. Brine flows from the waste into the E1 borehole exceed those into the E2 borehole only
32 for those realizations in which total flow is small because the panel was not brine-saturated at the time of
33 intrusion. These small total flows make only a small contribution to the total radionuclide release, and do not
34 invalidate the approximation.

5. DRILLING INTRUSION PROBABILITIES

5.1 Introduction

Representation of a performance assessment as a set of ordered triples and the construction of CCDFs (Section 3.1) both involve the idea of scenario probabilities; in turn, the idea of scenario probabilities makes sense only if an underlying sample space is defined. Current performance assessments that address the EPA release limits use a sample space \mathcal{S} defined by

$$\mathcal{S} = \{x : x \text{ a single 10,000-year history of the facility under consideration, beginning at decommissioning}\}. \quad (5-1a)$$

Each history, x , is assumed to be complete in the sense that it provides a full specification, including time of occurrence, for everything of importance to performance assessment. The summary scenarios (base case, E1, E2, and E1E2) are then defined as subsets of \mathcal{S} . Specifically,

$$E1 = \{x : x \text{ a single 10,000-year history in which at least one borehole penetrates a waste-filled room or drift and a pressurized brine reservoir}\}, \quad (5-1b)$$

$$E2 = \{x : x \text{ a single 10,000-year history in which at least one borehole penetrates a waste-filled room or drift without penetrating a pressurized brine reservoir}\}, \text{ and} \quad (5-1c)$$

$$E1E2 = \{x : x \text{ a single 10,000-year history in which at least one pair of boreholes penetrates waste-filled rooms or drifts in the same panel; one of the boreholes in this pair penetrates a pressurized brine reservoir while the other does not}\}. \quad (5-1d)$$

Each summary scenario is further divided into disjoint subset \mathcal{S}_i called computational scenarios. For example,

$$E1 \doteq \bigcup_i \mathcal{S}_i, \quad (5-2)$$

where the \mathcal{S}_i appear in the ordered-triple representation in Equation (3-1). In the terminology of probability theory, the \mathcal{S}_i are events (as are the summary scenarios: base case, E1, E2, and E1E2), and the $p\mathcal{S}_i$ are probabilities for these events. However, to avoid confusion engendered by the different disciplines' use of the word "event," the \mathcal{S}_i will be called scenarios and the $p\mathcal{S}_i$ s will simply be called probabilities. The purpose of this chapter is to show how the $p\mathcal{S}_i$ s are calculated in the 1992 performance-assessment exercise; but before proceeding, it is important to recognize several properties of the \mathcal{S}_i s (computational scenarios) and the $p\mathcal{S}_i$ s (computational scenario probabilities).

1 It is the discretization of the sample space \mathcal{S}_i into the sets \mathcal{S}_i that leads to the steps in the estimated CCDFs
 2 (Section 3.2). To construct CCDFs of the form shown in Section 3.2, the time histories associated with a given
 3 summary scenario must be sorted into disjoint sets such that

- 4 • each \mathcal{S}_i is sufficiently homogeneous that it is reasonable to use the same consequence result \mathbf{cS}_i for all
 5 elements of \mathcal{S}_i
- 6 • a probability $p\mathcal{S}_i$ can be determined for each \mathcal{S}_i
- 7 • the computational costs for estimation of $p\mathcal{S}_i$ s and \mathbf{cS}_i s are acceptable.

8 5.2 Probability Computations

9 This section describes a decomposition of summary scenarios involving drilling intrusions into
 10 computational scenarios on the basis of number of intrusions and their times of occurrence and derives formulas
 11 necessary to convert from drilling rates to scenario probabilities. For these derivations, the occurrence of
 12 individual drilling intrusions is assumed to be random in time and space, although the drilling rate need not be
 13 assumed constant or, for that matter, continuous through time.

14 The symbol $\mathcal{S}_k(a, b)$ will be used to denote subsets of the sample space defined by

$$15 \mathcal{S}_k(a, b) = \{x: x \text{ an element of } \mathcal{S} \text{ that involves exactly } k \text{ drilling intrusions in the time interval} \\ 16 [a, b]\}. \quad (5-3)$$

17 One objective of this section is to present the probability $p[\mathcal{S}_k(a, b)]$ for $\mathcal{S}_k(a, b)$. Membership in $\mathcal{S}_k(a, b)$
 18 only places a restriction on intrusions in the time interval $[a, b]$ and thus does not preclude intrusions in other
 19 time intervals. As a result, an additional objective will be to present the probability $p[\bigcap_{i=1}^n \mathcal{S}_{n(i)}(t_{i-1}, t_i)]$ for the
 20 set $\bigcap_{i=1}^n \mathcal{S}_{n(i)}(t_{i-1}, t_i)$, where $t_0 < t_1 < \dots < t_n$ and each $n(i), i = 1, 2, \dots, n$, is a nonnegative integer. This
 21 corresponds to determining the present of a scenario in which exactly $n(1)$ intrusions occur in time interval
 22 $[t_0, t_1]$, exactly $n(2)$ intrusions occur in time interval $[t_1, t_2]$, and so on. Helton (in press) has suggested a
 23 general form for these intrusion probabilities; the core of ideas behind his suggestion is outlined below.

24 The probability of having exactly one intrusion in the time interval $[u, v]$ is approximated by a function F
 25 such that

$$26 p[\mathcal{S}_1(u, v)] = F(u, v) + O[(v - u)^2], \quad (5-4)$$

27 where the preceding notation is a shorthand for the statement that the ratio

$$28 \frac{p[\mathcal{S}_1(u, v)] - F(u, v)}{(v - u)^2} \quad (5-5)$$

1 is bounded as $v - u$ approaches zero. More precisely, the statement in Equation 5-4 is satisfied on a time interval
 2 $[a, b]$ if there exists a number B and a sequence of times $a = t_0 < t_1 < \dots < t_n = b$ such that, if $1 \leq i \leq n$ and
 3 $t_{i-1} \leq u < v \leq b$, then

$$4 \quad \left| \frac{p[S_1(u, v)] - F(u, v)}{(v - u)^2} \right| < B. \quad (5-6)$$

5 The expressions in Equations 5-4 and 5-6 are providing a mathematical form for the statement " $F(u, v)$ is a good
 6 approximation to $p[S_1(u, v)]$ when $v - u$ is small."

7 The function F in Equation 5-4 can be defined in a number of ways. The simplest definition is

$$8 \quad F(u, v) = \lambda(v - u). \quad (5-7)$$

9 In this case, F corresponds to a Poisson process with a time-independent rate constant λ (i.e., a homogeneous
 10 Poisson process) and

$$11 \quad p[S_k(a, b)] = \frac{[\lambda(b - a)]^k}{k!} \exp[-\lambda(b - a)]. \quad (5-8)$$

12 The probability of intrusion by drilling was modeled as a homogeneous Poisson process in the 1991 series of PA
 13 calculations. The constant λ was taken as an imprecisely known parameter with upper bound equal to the
 14 maximum drilling rate required by EPA standards; i.e., λ was uniformly distributed between zero and λ_{\max} , with

$$15 \quad \lambda_{\max} = \left(\frac{30}{\text{km}^2 \cdot 10,000 \text{ yr}} \right) \cdot (\text{area of waste panels}) \quad (5-9)$$

$$= 3.28 \times 10^{-4} \text{ yr}^{-1}$$

16 The next step in generalizing beyond Equation 5-7 is

$$17 \quad F(u, v) = \lambda(u)(v - u), \quad (5-10)$$

18 in which case F corresponds to a Poisson process with a time-dependent rate constant (i.e., a nonhomogeneous
 19 Poisson process) and

$$20 \quad p[S_k(a, b)] = \frac{1}{k!} \left(\int_a^b \lambda(s) ds \right)^k \exp \left[- \int_a^b \lambda(s) ds \right]. \quad (5-11)$$

21

1 This result can be used to compute the probability of a general scenario in which exactly $n(1)$ intrusions occur in
 2 time interval $[t_0, t_1]$, exactly $n(2)$ intrusions occur in time interval $[t_1, t_2]$, and so on. If this general scenario is
 3 denoted by $\mathcal{S}(\mathbf{n})$, where

$$4 \quad \mathbf{n} = [n(1), n(2), \dots, n(n)] \text{ and } t_0 = a, t_n = b,$$

5 then

$$6 \quad p[\mathcal{S}(\mathbf{n})] = \prod_{i=1}^n \left[\frac{1}{n(i)!} \left(\int_{t_{i-1}}^{t_i} \lambda(s) ds \right)^{n(i)} \right] \exp \left[- \int_a^b \lambda(s) ds \right]. \quad (5-12)$$

7 Computational scenarios and corresponding probabilities for summary scenarios E1 and E2 can be generated by
 8 specification of the time intervals $[t_{i-1}, t_i]$ and the $n(i)$ appearing in Equation 5-12, and by suitably defining the
 9 function $\lambda(t)$ appearing in that equation.

10 In the preferred conceptual model for the 1992 series of PA calculations, probability of intrusion by drilling is
 11 modeled as an inhomogeneous Poisson process using Equations 5-11 and 5-12; for comparison, the 1992 PA also
 12 uses a homogeneous Poisson process (Equation 5-9) as an alternative conceptual model for drilling intrusions.
 13 For the preferred conceptual model, the time-dependent drilling rates, $\lambda(t)$, are calculated with an algorithm
 14 proposed by Hora (see Section 5.2; also Hora's memo in Appendix A of Volume 3 of this report) using
 15 information obtained in an expert judgment process concerning effects of human intrusion into the WIPP. Note
 16 that Hora's algorithm gives drilling rates in units of

$$17 \quad \frac{\text{number of boreholes}}{\text{km}^2 \cdot 10,000 \text{ yr}}$$

18 and the time-dependent drilling rates used in Equations 5-11 and 5-12 are scaled from Hora's values by multiplying
 19 by area of the waste panels (Equation 5-9). As stated above, $\lambda(t)$ may also have to be scaled to reflect, for
 20 example, the fraction of the area of waste panels that overlaps brine pockets.

21 Computational scenarios for the E1E2 summary scenario can be defined in a manner similar to the ones
 22 employed for the E1 and E2 scenarios. Once defined, the probabilities of these computational scenarios are best
 23 calculated using the basic result in Equation 5-11 together with the scenario

$$24 \quad \mathcal{BP}^{+-}(t_{i-1}, t_i) = \{x : x \text{ an element of } \mathcal{S} \text{ in which a waste panel is penetrated by one or more} \\ 25 \quad \text{boreholes that pass through a pressurized brine pocket in the time interval } (t_{i-1}, t_i) \\ 26 \quad \text{and by one or more boreholes that do not pass through a pressurized brine pocket in} \\ 27 \quad \text{the time interval } (t_{i-1}, t_i)\}.$$

28 Then, in extension of the derivations on pages 2-23 to 2-27 of the 1991 Volume 2 (WIPP PA Division, 1991b),

$$p[BP^{+-}(t_{i-1}, t_i)] = \sum_{\ell=1}^{nP} \left\{ 1 - \exp \int_{t_{i-1}}^{t_i} \lambda_{\ell}^{+}(t) dt \right\} \left\{ 1 - \exp \int_{t_{i-1}}^{t_i} \lambda_{\ell}^{-}(t) dt \right\}, \quad (5-13)$$

2 where

3 nP = the number of waste panels

$$4 \quad \lambda_{\ell}^{+}(t) = \left(\frac{aBP}{nP \cdot aTOT} \right) \lambda(t)$$

$$5 \quad \lambda_{\ell}^{-}(t) = \left(\frac{aTOT(\ell) - aBP / nP}{aTOT} \right) \lambda(t)$$

6 aBP = area of pressurized brine pocket under waste panels (m^2)

7 $aTOT(\ell)$ = area of ℓ^{th} waste panel (m^2)

8 $aTOT$ = total area of waste panels (m^2).

9 Variable activity loading in the repository was described using the same representation used in the 1991 PA
 10 (Helton et al., 1992, Chapter 2). Intrusion probabilities were calculated using the code CCDFPERM (Volume 3,
 11 Section 1.4.2 of this report).

12 5.3 Lambda Function Generation

13 The 1992 performance assessment is the first to incorporate the judgments of experts on possible future
 14 modes of intrusion into the WIPP and on how markers may mitigate the effects of these intrusions; 40 CFR 191,
 15 Subpart B, (U.S. EPA, 1985) requires consideration of both these questions. Specifically, 40 CFR 191, Subpart
 16 B, indicates that the DOE “should consider the effects of each particular disposal system’s site, design, and passive
 17 institutional controls in judging the likelihood and consequence of . . . inadvertent human intrusion” (Appendix B
 18 of U.S. EPA, 1985). The discussion that follows in Sections 5.3.1, 5.3.2, and 5.3.3 describes WIPP PA’s
 19 methodology for addressing the mitigating effect of passive markers. This approach may be refined and modified
 20 as the performance assessment process matures. The following material, largely excerpted from Hora (memo in
 21 Appendix A, Volume 3 of this report), is intended to give an overview of the expert-judgment processes and
 22 reasoning that entered into the construction of a probabilistic model of inadvertent intrusion by exploratory
 23 drilling.

24 5.3.1 The Expert Judgment Process

25 During 1990-1992, experts external to SNL were assembled to study the likelihood of potential inadvertent
 26 human intrusion into the WIPP. These experts formed two groups—one group (called the Futures Panel) studied

1 what future societies might be like and how they might inadvertently intrude into nuclear waste (Hora et al.,
2 1991). The second group (called the Markers Panel), after considering the findings of the first group, studied how
3 markers might be used to warn future societies about the presence and danger of the buried waste (memorandum by
4 Hora in Volume 3, Appendix A of this report). Both groups provided probabilities and probability distributions
5 for critical aspects of the human intrusion problem.

6 The Futures Panel was divided into four teams. Each team was composed of four experts from various fields
7 of social and physical science. Each team was asked to address the same set of questions. The results of their
8 work suggests that future societies may undertake activities that could lead to inadvertent intrusion into the WIPP.
9 These teams judged that a number of factors (such as level of technology, demand for resources, population level,
10 and ability to retain knowledge about nuclear waste) would influence the likelihood of inadvertent intrusion.
11 Because the teams used different structures for analysis and considered different factors that would influence the
12 likelihood of inadvertent intrusion, the results of their endeavors had to be interpreted individually in order to be
13 used in the construction of Lambda Functions.

14 As the Futures Panel was completing its effort, the Markers Panel, consisting of 13 experts, was organized
15 into two teams to study markers for the WIPP site. These markers may be incorporated into the repository design
16 to serve as warnings to future societies about the presence of nuclear waste. Each team was asked to consider the
17 findings of the Futures teams, to suggest design characteristics for a marker system, and to assess the efficacy of
18 such a system of markers in deterring inadvertent human intrusion. Based on the assumption that the ability of a
19 marker system to deter intrusions rests on the survival of the marker system over an extended period of time and
20 the ability of potential intruders to detect the markers and to understand the messages that they carry, the Markers
21 Panel members were asked to provide estimates of probabilities for several events:

- 22 • First, the probability that a marker and its message(s) would remain intact. (This first probability estimate
23 was requested for various times in the future.)
- 24 • Second, if the marker and its messages remain intact, the probability that the potential intruders are able to
25 understand the message and thus become forewarned of the inherent dangers of intrusion. (This second
26 probability estimate was requested for several different types of intrusion.)

27 The above two probability estimates were made under various assumptions about the state of technology in the
28 future.

29 As noted above, the Futures Panel posed several types of activities that could lead to inadvertent intrusion
30 into the WIPP (drilling, mining, archaeological investigation); but on the basis of guidance in Appendix B of 40
31 CFR Part 191 (U.S. EPA, 1985), it was concluded that the preliminary performance assessment need not consider
32 intrusion modes such as mining or archaeological investigation that may result in more severe consequences than
33 exploratory drilling for resources. Moreover, the guidance also provides an upper bound for the drilling intensity
34 to be used in the performance assessment. Three modes of exploratory drilling were identified by the experts
35 examining human intrusion issues. These modes are exploratory drilling for mineral resources (primarily fossil
36 fuels), drilling water wells, and drilling for injection disposal wells. Because the repository is well below the
37 water table in an area where water quality is poor, drilling for water was judged to be an insignificant threat when

1 compared to drilling for mineral resources (see Section 4.1.3 of this volume). Drilling for disposal wells was
2 identified as a possible threat by one of the four Futures teams, but probabilities were not provided. Thus,
3 exploratory drilling for resources is the only mode of intrusion considered in the 1992 preliminary comparison.

4 **5.3.2 Algorithm for Generating Lambda Functions**

5 The time-dependent drilling rates, or lambda functions, that arise in modeling the probability of drilling
6 (Section 5.2 of this volume) were calculated in the 1992 PA exercise using an algorithm constructed by Hora
7 (memo in Volume 3, Appendix A of this report). The purpose of this algorithm was to assemble quantitative
8 expert judgments concerning future human intrusion into the WIPP.

9 The existence of markers and the ability of a society to interpret the warnings left at the WIPP may depend
10 upon the state of development of that society. In this exercise, the state of development of the society was
11 represented by the level of the technological development of the society. The level of technological development
12 (high, medium, or low) was randomly generated from probability distributions provided by the Futures teams.
13 Prior to this step, however, the Futures team whose level of technology was to be sampled had to be chosen.
14 This was necessary because the four teams studying potential futures developed analyses independently and in
15 different ways and there was no simple way to combine their findings. For this reason, a team was randomly
16 selected on each generation of a lambda function. The assessments from each team represent their collective
17 judgment. In contrast, members of one of the Markers teams individually provided probability assessments while
18 the other team provided a consensus set of probability distributions. Thus, when one of the two Markers teams
19 was randomly chosen, it could also be necessary to select randomly one of the team members for that iteration.
20 This procedure avoided making unfounded assumptions about how to combine disparate distributions.

21 Next, using a given level of technology, the frequency (f) at which attempted inadvertent intrusion occurs in
22 the absence of markers or monuments was elicited from the Futures experts. This time-dependent frequency is
23 called the raw drilling intensity; it does not take into account deterrence by markers. Thus, to gain an estimate of
24 the effective drilling intensity λ , the raw drilling intensity was modified in the following way: For each of the
25 several points in time that the raw drilling intensity was evaluated, the probability of the markers existing (p_1)
26 and the probability of the markers deterring an intrusion attempt given that the markers exist (p_2) were evaluated.
27 These two probabilities modify the raw drilling intensity to give the effective drilling intensity,

$$28 \quad \lambda = f(1 - p_1 p_2).$$

29 The algorithm for generating inadvertent intrusion can then be succinctly described by the following steps:

30 1. Randomly select one of the four Futures teams.

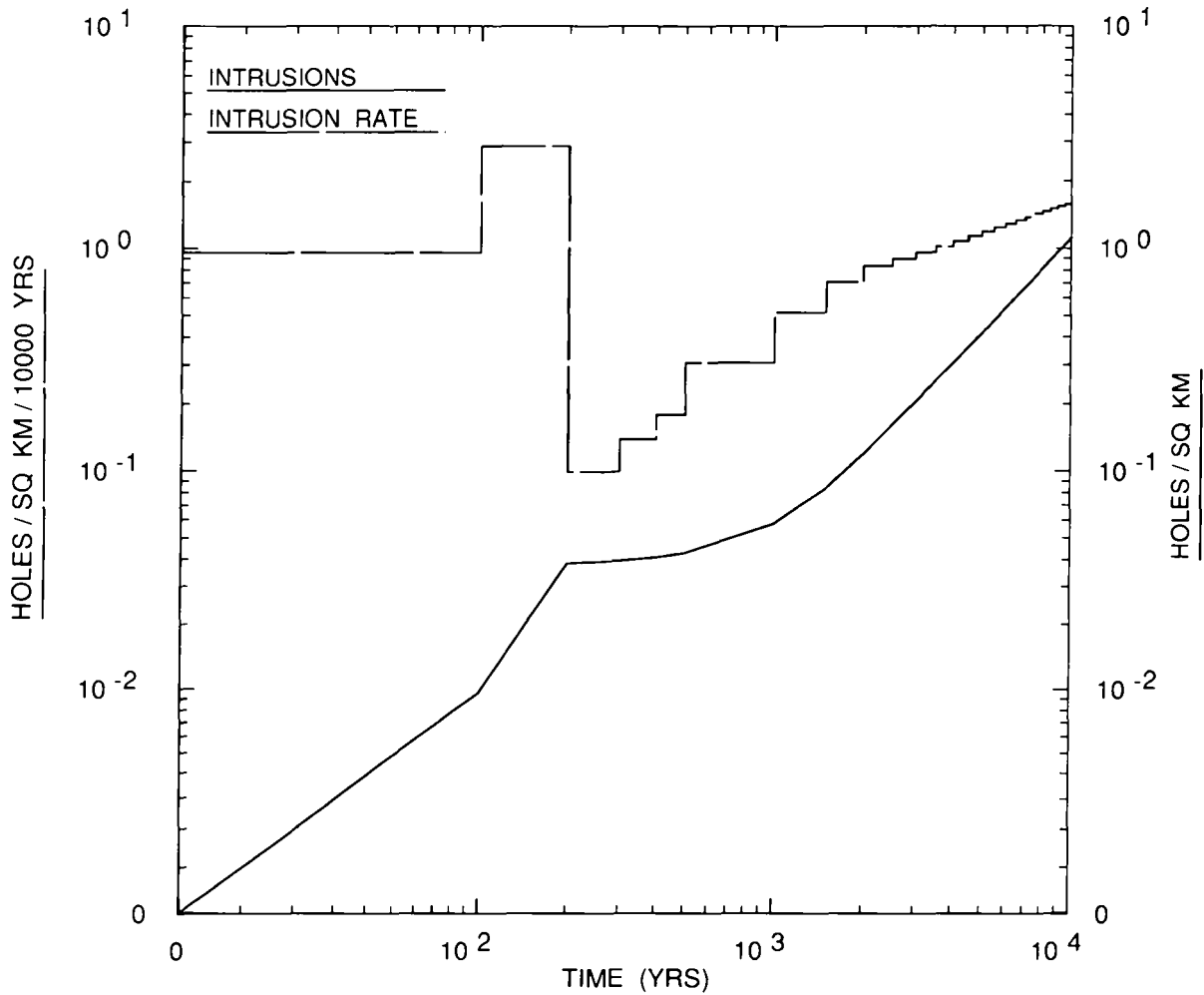
31 The following steps use distributions conditional on the outcome of step 1:

- 1 2. Randomly select a level of technology in the future. When probabilities of levels of technology are
2 time-dependent, a rank correlation of 1 will be used to generate the level of technology in the several time
3 periods.
- 4 3. Generate a random variable to determine the intrusion intensity. When intrusion intensities vary with
5 time periods, a rank correlation of 1 will be used to generate the intrusion intensities in the several time
6 periods.
- 7 4. Randomly select one of the Markers teams and a Marker team member, if necessary.
- 8 5. For each time period generate the probability that markers are extant given the level of technology.
- 9 6. For each time period, generate the probability that the markers deter intrusion given that the markers are
10 extant, the level of technology, and the mode of intrusion.
- 11 7. Compute the effective drilling intensity for each time period.

12 Note that in step 3, a single random number is used to select an intrusion intensity for all periods. This
13 assumption results in the variability of the performance measure being maximized among the Monte Carlo
14 iterations.

15 **5.3.3 Use of the Lambda Functions**

16 The effective drilling intensity, $\lambda(t)$, is used to generate probabilities of computational scenarios for human
17 intrusion by drilling in the manner described in Section 5.2. However, the algorithm described in Section 5.3.2
18 does not provide direct input to sensitivity and uncertainty analyses; instead, the code implementing the algorithm
19 is run many times in order to generate a family of equally likely realizations of the lambda functions, and it is this
20 family of realizations that is sampled in the Monte Carlo calculations (see Section 5.2, Volume 3 of this report).
21 A family of 70 realizations was generated for the 1992 series of calculations; one of these realizations is shown on
22 Figure 5-1 and the remainder are displayed in Appendix D of Volume 3. The realizations of $\lambda(t)$ can be regarded
23 as a random sample from an effectively infinite population of drilling intensities implicitly defined by the expert-
24 judgment data and the reasoning that went into the construction of Hora's algorithm (Section 5.3.2). The
25 variability shown by members of this artificial population (see Appendix D, Volume 3) represents the assessed
26 uncertainty in future drilling intensities and the effectiveness of markers.



TRI-6342-2057-0

Figure 5-1. A realization of effective drilling intensity $\lambda(t)$ (dashed line) and its associated integrated effective drilling intensity (solid line) as functions of time. This is one of 70 realizations used in 1992 sensitivity and uncertainty analyses.

6. DATA AND CDFS

6.1. Conventions

Volume 3 of this report provides distribution functions for parameter values used as input to the 1992 PA calculations, and references for the primary data sources on which the distributions are based. Volume 3 uses standard terms of probability theory and statistics or nonstandard terms to characterize model parameters. Very brief explanations of these terms are provided below; more detailed explanations are provided in Section 1.2 of Volume 3.

6.1.1 Probability Distribution Functions

For a continuous, uncertain parameter, say X , the *probability density function* (pdf) is a function $f(x) \geq 0$ with the properties

$$\int_a^b f(x)dx = \text{probability that uncertain parameter } X \text{ lies in interval } (a,b):$$

$$\int_{-\infty}^{+\infty} f(x)dx = 1$$

The *cumulative distribution function* (cdf) associated with $f(x)$ is defined by

$$F(x) = \int_{-\infty}^x f(s)ds = \text{probability that uncertain parameter } X \text{ is less than or equal to } x.$$

Uncertain parameters may also be called “imprecisely known parameters” elsewhere in this series of reports.

Probability density functions (pdfs) and cdfs can be similarly defined for uncertain parameters that take on a denumerable number of values, $x_i, i = 1, 2, \dots$. The sequence $\{f_i\}, i = 1, 2, \dots$, such that $f_i > 0$ and

$$\sum_i f_i = 1,$$

is the discrete analogue of the continuous pdf, and

$$F(x) = \sum_{\text{all } x_j < x} f_j$$

is the discrete analogue of the continuous cdf.

1 6.1.2 Empirical Distribution Functions

2 *Empirical cdfs* are histograms or piecewise-constant functions that are based on percentiles derived from a set
 3 of measurements (data), or a set of subjective estimates of experts. For independent measurements (data) of some
 4 quantity, the empirical cdf is an unbiased estimator of the unknown population cdf of that quantity (Blom, 1989,
 5 p. 216); this property does not always apply to empirical cdfs derived from subjective estimates of experts.

6 6.1.3 Range

7 The *range* of a distribution is denoted by (a, b) , the pair of numbers in which a and b are respectively the
 8 minimum and maximum values that can reasonably be taken by the uncertain parameter X .

9 6.1.4 Mean and Sample Mean

10 The mean value (or, simply, *mean*) of a distribution is one measure of the central tendency of a distribution;
 11 it is analogous to the arithmetic average of a series of numbers. The population mean, μ , is defined by

$$12 \quad \mu = \int_{-\infty}^{\infty} xf(x)dx \text{ for continuous distributions, or}$$

$$13 \quad \sum_{\text{all } x_i} x_i f_i \text{ for discrete distributions.}$$

14 The sample mean, denoted by \bar{x} , is the arithmetic average of values in an empirical data set. A sample mean
 15 can also be assigned to empirical cdfs derived from subjective estimates of experts.

16 6.1.5 Median and Sample Median

17 The median value of a cdf is denoted by x_{50} and is that value in the range at which 50% of all values lie
 18 above and below (i.e., the 0.5 quantile). Sample medians, here denoted by \bar{x}_{50} , can be obtained directly from
 19 empirical cdfs.

20 6.1.6 Variance and Coefficient of Variation

21 The *variance* of a distribution, σ^2 , is the second moment of the distribution about its mean, i.e.,

$$22 \quad \sigma^2 = \int_{-\infty}^{\infty} (x - \mu)^2 f(x)dx \text{ for continuous distributions, or}$$

1
$$\sum_{\text{all } x_i} (x_i - \mu)^2 f_i \text{ for discrete distributions.}$$

2 The *standard deviation*, σ , is the positive square root of the variance. The coefficient of variation, the ratio
3 of standard deviation to mean, σ/μ , is a convenient measure of the relative width of a distribution.

4 The *sample variance*, S^2 , of a set of measurements of parameter X, say X_1, X_2, \dots, X_N is the sum

5
$$\frac{1}{N-1} \sum_{n=1}^N (X_n - \bar{x})^2.$$

6 The sample variance of independent measurements of some quantity is an unbiased estimator of the population
7 variance of that quantity (Blom, 1989, p. 197). (A variance can also be formally calculated for empirical cdfs
8 derived from subjective estimates of experts; this is not a sample variance, however.)

9 6.1.7 Categories of Distributions

10 Distributions used in the 1992 PA are grouped into five categories:

- 11 • continuous, analytical distributions (normal, lognormal, uniform, or loguniform)
- 12 • discrete, analytical distributions (Poisson, binomial)
- 13 • constructed empirical distributions based on measurements
- 14 • constructed empirical distributions based on expert judgment
- 15 • miscellaneous categories (null distributions; i.e., constants and tabular functions).

16 6.1.7.1 CONTINUOUS DISTRIBUTIONS

17 Four continuous, analytical distributions are frequently used in the 1992 PA:

- 18 • **Normal.** Normal designates the normal pdf, a good approximation to the distribution of many physical
19 parameters.
- 20 • **Lognormal.** Lognormal designates a lognormal pdf, a distribution of a variable whose logarithm follows
21 a normal distribution.
- 22 • **Uniform.** Uniform designates a pdf that is constant in the interval (a, b) and zero outside of that interval.

- 1 • **Loguniform.** Loguniform designates a loguniform pdf, a distribution of a variable whose logarithm
2 follows a uniform distribution.

3 6.1.7.2 DISCRETE DISTRIBUTIONS

4 A frequently used discrete distribution is the Poisson distribution. The Poisson pdf is often used to model
5 processes taking place over continuous intervals of time such as the arrival of telephone calls at a switch station
6 (queuing problem) or the number of imperfections per unit length produced in a bolt of cloth. The Poisson pdf
7 was used in the 1991 probability model for human intrusion by exploratory drilling. The 1992 probability model
8 for human intrusion incorporates effects of deterrence by markers; this model is based on generalized Poisson
9 distributions.

10 6.1.7.3 CONSTRUCTED DISTRIBUTIONS (DATA)

11 A *constructed distribution* of the *Data* type is simply an empirical cdf constructed from sets of measured data
12 points in the data base. For intrinsically discrete data, the empirical cdf is a piecewise-constant function
13 resembling a histogram. For intrinsically continuous data, the empirical cdf is always converted to a piecewise-
14 linear function by joining the empirical percentile points with straight lines; this is done to ensure that, in Monte
15 Carlo sampling, the distribution of sampled parameter values will cover all of the range of the distribution
16 (Tierney, 1990, p. II-5).

17 In some cases, the PA Department may modify constructed distributions of the *Data* type by extending the
18 range of the data set to include estimated 0.01 and 0.99 quantiles. Because the range of measurements in a data set
19 may not reflect the true range of the random variable underlying the measurements, the PA Department may
20 estimate the range by $\bar{x} + 2.33s$, where \bar{x} is the sample mean and s is the sample standard deviation.

21 6.1.7.4 CONSTRUCTED DISTRIBUTIONS (SUBJECTIVE)

22 *Constructed distributions* of the *Subjective* type are histograms based on subjective estimates of range (the 0
23 and 100 percentile) and at least one interior percentile point (usually the 50 percentile or median). The subjective
24 estimates of percentile points are usually obtained directly from experts in the subject matter of the parameter of
25 concern. Histograms for intrinsically continuous parameters are always converted to piecewise linear cdfs by
26 joining the subjective percentile points with straight lines.

27 6.1.7.5 MISCELLANEOUS CATEGORIES

28 *Null* categories of distributions are described below:

- 29 • **Constant.** When a distribution type is listed as constant, a distribution has not been assigned and a
30 constant value is used in all PA calculations.

- 1 • **Spatial.** The spatial category indicates that the parameter varies spatially. This spatial variation is
2 usually shown on an accompanying figure. The median value recorded is a typical value for simulations
3 that use the parameter as a lumped parameter in a model; however, the value varies depending upon the
4 scale of the model. The range of a spatially varying parameter is also scale dependent.

- 5 • **Table.** The table category indicates that the parameter varies with another property and the result is a
6 tabulated value. For example, relative permeability varies with saturation; its distribution type is listed as
7 table (also, the median value is not meaningful and is therefore omitted in the table).

8 6.2 Selection of Parameter Distributions

9 6.2.1 Requests for Data from Sandia Investigators and Analysts

10 The PA Department follows a well-defined procedure for acquiring and controlling the parameter distributions
11 used in consequence and probability models:

- 12 • **Identify Necessary Data.** Each year, the PA Department identifies data that are necessary to construct
13 parameter distributions for the preliminary performance assessment. Members of the department may
14 compile data from published reports, personal communications with investigators, and other sources.

- 15 • **Request Median Value and Distribution.** The PA Department then requests that the investigators
16 provide either new data or a median value and distribution for each parameter in a large subset of the
17 parameters. Some model parameters are specific to the PA calculations and so individuals in the PA
18 Department are considered the experts for these parameters (e.g., probability model parameters). Initially,
19 Sandia investigators are responsible for providing data, or if data are unavailable, distributions for all
20 parameters. As this procedure for acquiring data is repeated, a few parameters are evaluated through formal
21 elicitation.

- 22 • **Update Secondary Data Base.** The PA Department enters the endorsed or elicited data for all
23 parameters into the secondary data base. The PA Department then either constructs parameter distributions
24 or uses distributions provided by the investigator; the PA Department selects a subset of these parameters
25 to sample in each annual PA exercise, keeping all other values constant at their median values, unless
26 specifically noted.

- 27 • **Perform Consequence Simulations and Sensitivity Analyses.** The PA Department runs
28 consequence simulations and sensitivity analyses with selected subsets of parameters from the updated
29 secondary data base. The sensitivity analysis evaluates the sensitivity of a parameter in determining
30 variation of the result (i.e., CCDF).

- 31 • **Determine Whether Parameter Is Important in Analysis.** By means of the sensitivity analyses,
32 the PA Department can determine whether the parameter as specified is significant in the calculations.

1 **6.2.2 Construction of Distributions**

2 The PA Department follows the five-step procedure outlined below to construct probability distributions
3 (cdfs):

- 4 1. Determine whether site-specific data for the parameter in question exist. If data exist, go to step 3.
- 5 2. Request that the investigator supply a specific shape (e.g., normal, lognormal) and associated numerical
6 parameters for the distribution of the parameter. If specific shape and distribution parameters cannot be
7 supplied, go to step 4; otherwise go to step 5.
- 8 3. Determine the size of the combined data sets. If sample size is sufficiently large, PA staff constructs
9 distribution (go to step 5).
- 10 4. If sample size is small, or investigator cannot provide a specific distribution, request that the investigator
11 provide subjective estimates of the range and details on the distribution of the parameter.
- 12 5. Assign distribution.

13 **6.2.3 Some Limitations on Distributions**

14 The major limitations on the validity of the probability distributions assigned to parameters in the 1992 PA
15 are believed to be a consequence of two things:

- 16 • The equating of spatial variability with model parameter uncertainty, particularly for that class of
17 parameters called material-property parameters.
- 18 • The neglect of correlations between model parameters.

19 These limitations are discussed in detail in Volume 3 (Section 1.3.3).

7. CONSEQUENCE MODELING

7.1 Radioactive Decay

The quantity of radioactive material that reaches the accessible environment depends in part on the growth and decay of the component radionuclides in the waste. The Bateman equations (Wehr et al., 1984) are used to calculate this decay within the repository. The Bateman equations in terms of activity are:

$$\frac{dN_i}{dt} = -\lambda_i N_i + \lambda_i N_{i-1}, \quad (7-1)$$

where N_i is the activity of radionuclide i , t is time, and λ_i is the disintegration constant of radionuclide i .

For given initial inventories $N_i^{(0)}$, the solution can be written as

$$N_i(t) = \sum_{j=1}^i a_{i,j} e^{-\lambda_j t}, \quad (7-2)$$

where the coefficients $a_{i,j}$ are defined by the recurrence relations

$$a_{i,i} = N_i^{(0)} - \sum_{j=1}^{i-1} a_{i,j} \quad (7-3)$$

and

$$a_{i,j} = \frac{\lambda_i}{\lambda_i - \lambda_j} a_{i-1,j} \quad i > j. \quad (7-4)$$

7.2 Multiphase Flow Through Porous Media

A computational model called BRAGFLO (BRine And Gas FLOW) that simulates two-phase fluid flow through porous, heterogeneous reservoirs has been developed for WIPP PA. As discussed in Appendix A of this volume, BRAGFLO uses finite-difference methods to solve the coupled nonlinear partial differential equations (PDEs) describing the mass conservation of the gas and brine components distributed between the gas and liquid phases.

The PA Department uses BRAGFLO in Monte Carlo consequence analyses to quantify the flow of brine and gas through the repository and surrounding strata for both the undisturbed, base-case scenario and human-intrusion scenarios. For the 1992 PA, the code is used to model fluid flow within the Salado Formation and the repository, including a representation of the shaft system for undisturbed performance. The Culebra Dolomite Member of the

1 Rustler Formation and a hypothetical pressurized brine reservoir in the Castile Formation are included in the
2 model because of their potential roles as a sink and a source, respectively, for fluid flow.

3 **7.2.1 Features and Capabilities of BRAGFLO**

4 BRAGFLO is capable of describing three-phase (e.g., water, gas, and oil) fluid flow through porous media in
5 one, two, or three dimensions. Only two phases (brine and gas) are modeled for WIPP PA; calculations to date
6 have only been performed in one and two dimensions. The code uses spatially varying meshes and solves the
7 coupled nonlinear PDEs using nonlinear Newton-Raphson iteration, automatic time-stepping, and direct or
8 iterative solvers.

9 Additional features of BRAGFLO are the capability to incorporate the following: the effect of halite creep on
10 waste porosity using output from the SANCHIO code (see Section 7.3 and Appendix B of this volume);
11 anisotropic permeabilities; nonideal gas behavior (Redlich-Kwong-Soave); rock compressibility; and kinetic or
12 reactant-dependent gas generation as a function of fluid saturations.

13 Multiphase flow is simulated as simultaneous immiscible displacement in porous media. Regions within the
14 model domain (e.g., waste, seals, and lithologic units) are represented as solid continua of interconnected void
15 space, and porosity is expressed as the ratio of void volume to total volume for each region. Flow occurs
16 according to heuristic extensions of Darcy's Law, in that the rate of flow of a homogeneous fluid through a porous
17 medium is proportional to the hydraulic gradient and to the cross-sectional area normal to the direction of flow,
18 and inversely proportional to fluid viscosity (see Appendix A of this volume for additional discussion).
19 Permeability is the constant of proportionality in Darcy's law. Flow is assumed to be laminar, and fluids are
20 viscous and Newtonian. Forces that affect fluid flow are those due to pressure, gravity, capillarity, and viscous
21 shear. Fluid saturation is defined to be the ratio of fluid volume to void volume. At least one fluid phase is
22 present at all times, and all void volume is occupied by fluid.

23 Effects of capillary pressure and relative permeability occur when two (or more) fluid phases are present in a
24 porous medium. Curvature of the interface separating fluid phases and surface tension cause a capillary pressure
25 difference across the interface. During fluid flow, interference between the phases deforms the interface. Relative
26 permeability describes this interference on a macroscopic scale, and varies with fluid saturation. Relative
27 permeability is expressed as the ratio of the permeability of the rock (or other material) with the fluid in question
28 at a given saturation to the permeability of the rock when 100 percent saturated with the fluid.

29 Residual saturation of a fluid phase is defined as the smallest saturation of fluid required to form continuous
30 pathways through the medium. It is the minimum saturation at which the phase will flow in response to a
31 pressure gradient. Below residual brine saturation, brine exists as a thin film around rock grains or as isolated
32 pockets, and gas is present in sufficient volume to form an interconnected pathway. The relative permeability for
33 brine is zero. Above residual brine saturation and below residual gas saturation, both brine and gas form
34 continuous pathways through the porous network, and relative permeabilities for both phases are greater than zero.

1 When brine saturation is sufficiently high that gas saturation falls below residual, gas exists only as isolated
2 pockets surrounded by brine. Gas flow does not occur, and relative permeability for gas is zero.

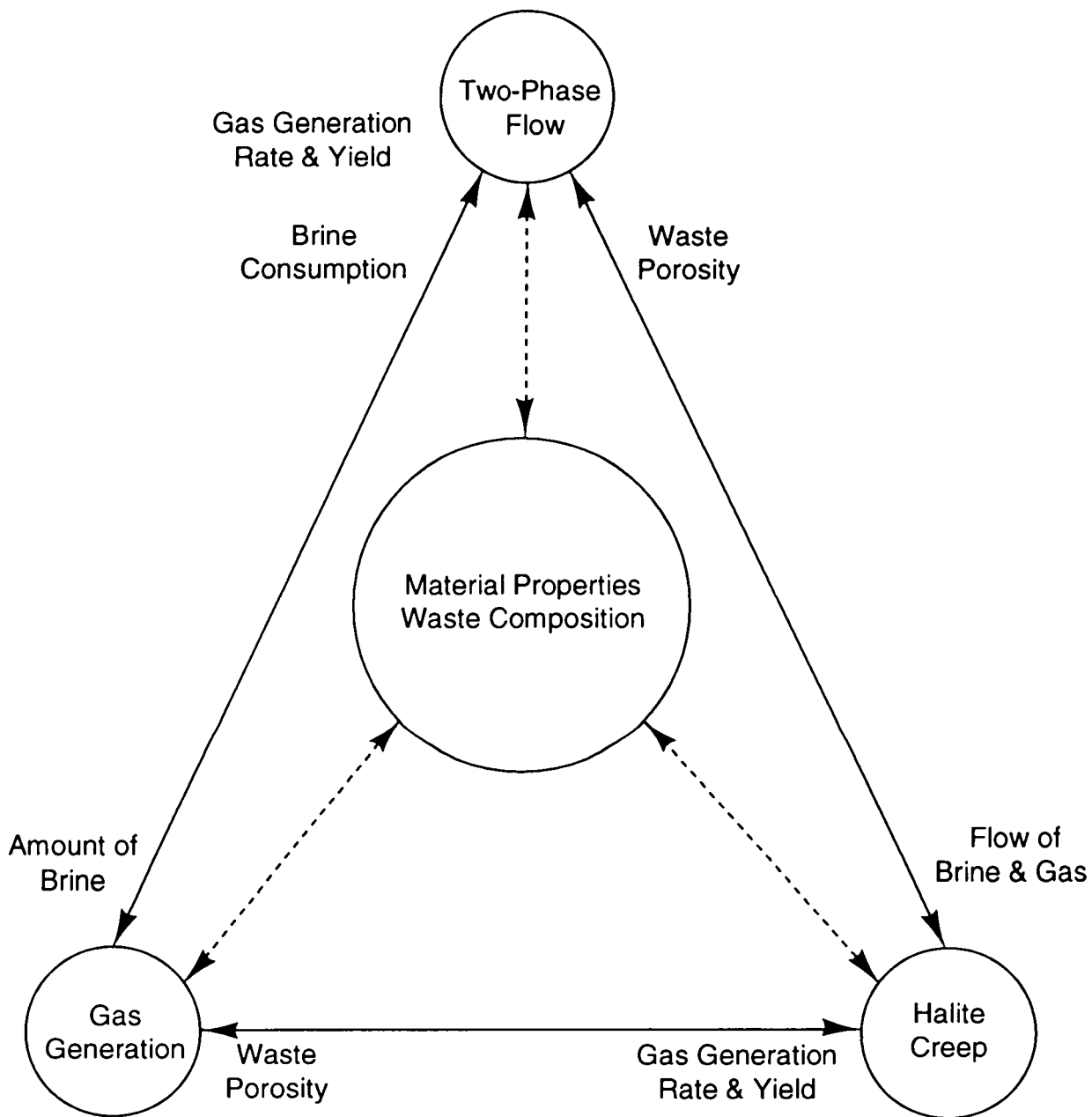
3 **7.2.2 Interaction of Important Repository Processes**

4 The coupling of processes simulated by BRAGFLO is illustrated schematically in Figure 7-1. The material
5 properties that describe the repository system are represented in the center of a triangle, the apices of which
6 represent the physical processes that operate within the system. Arrows indicate the major interactions. Thus, the
7 amount of brine present in the room is a function of two-phase flow, and is a contributing factor in the rate and
8 amount of gas generation. The rate and amount of gas generation are contributing factors to two-phase flow, as is
9 brine consumption by corrosion reactions that generate gas. Changes in waste porosity result from halite creep; it
10 affects both two-phase flow and, therefore, gas generation through its influence on brine solubility. Completing
11 the coupled interactions, both two-phase flow and gas generation affect halite creep (through their impact on
12 pressure within the panels) and therefore have an effect on changes in waste porosity.

13 **7.2.3 General Assumptions Used in 1992 PA Two-Phase Flow Modeling**

14 The following is a list of major assumptions used in two-phase flow modeling for the 1992 PA:

- 15 • Rock permeabilities (1) varied with material type, (2) were uniform within a material, and (3) did not vary
16 with time.
- 17 • Void volume of waste was estimated as a function of pressure using SANCHO (Section 7.3 of this
18 volume).
- 19 • Gas potential was based on an extrapolation of inventory volume fractions of combustibles and
20 metals/glasses to design capacity (Section 2.3.2.1 of this volume; Volume 3, Section 3.4 of this report).
- 21 • Gas generation occurs by corrosion of ferrous metals and biodegradation of combustible materials only, and
22 the contribution of radiolysis is assumed to be negligible (Volume 3, Section 3.3 of this report; WIPP PA
23 Division, 1991c, Section 3.3).
- 24 • All gas was assumed to have the physical properties of hydrogen, which will be a principal component
25 resulting from corrosion of ferrous metals (Volume 3, section 1.4.1 of this report).
- 26 • As long as corrodible or biodegradable waste remains, gas generation is a function only of brine saturation
27 (WIPP PA Division, 1991c, Section 3.3).



TRI- 6342-3435-0

Figure 7-1. Interaction of some important repository processes.

- 1 • Water is consumed during corrosion of ferrous metals; biodegradation reactions require the presence of water
2 to occur but have no effect on the net water balance (WIPP PA Division, 1991c, Section 3.3).
- 3 • No reactions affect gas after it is generated (WIPP PA Division, 1991c, Section 3.3).
- 4 • The solubility of gas in brine is assumed to be negligible.
- 5 • The Salado Formation is assumed to be initially 100 percent brine saturated.
- 6 • Initial pressures in the Salado Formation vary hydrostatically from a sampled pressure at the elevation of
7 MB139 (Volume 3, Section 2.4.3 of this report).

8 **7.3 Waste-Filled Room Deformation**

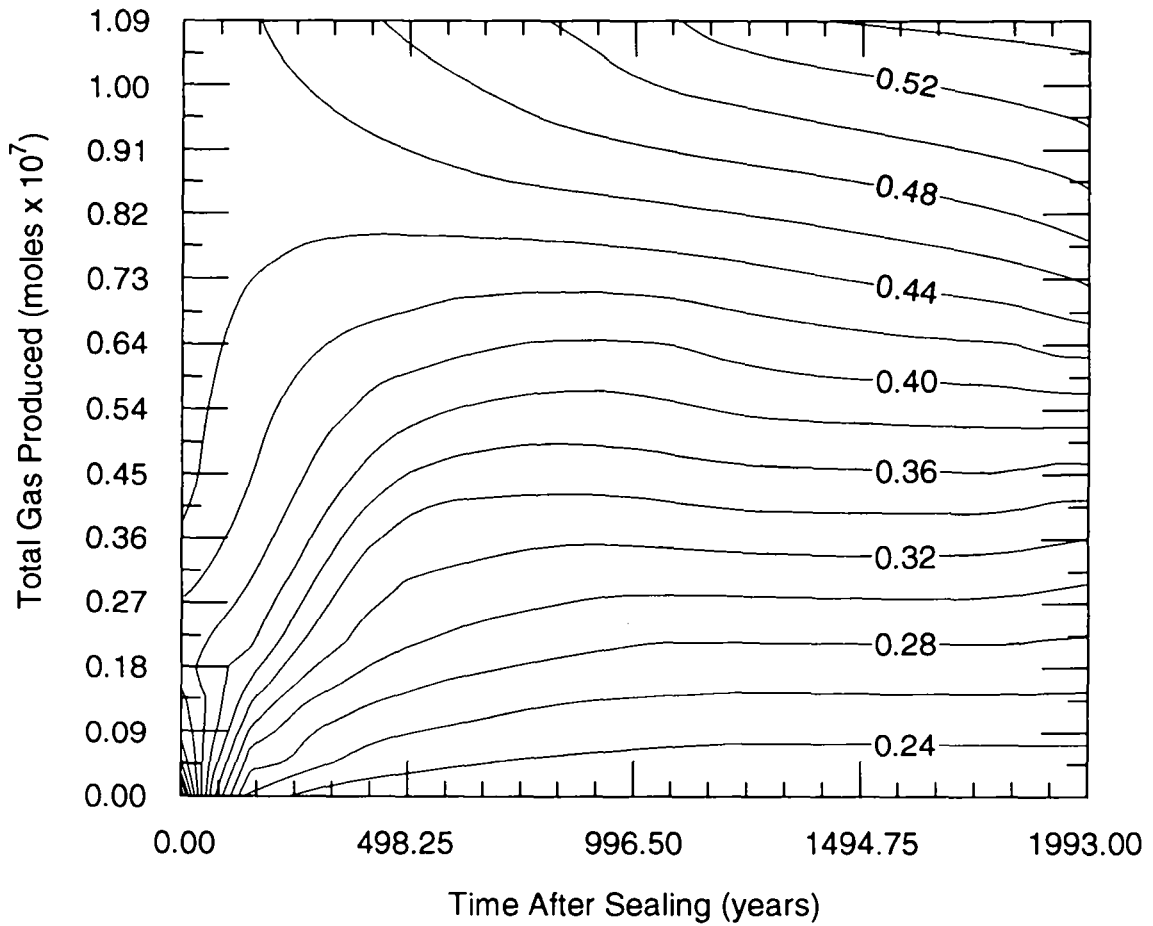
9 Consequence models of multiphase flows within a waste-filled room (Section 7.2) require that the effective
10 porosity and permeability of waste and backfill materials be specified. Realistic estimates of effective porosity and
11 permeability must in turn account for three phenomena:

- 12 • waste-material composition (metallics, sludges, combustibles)
- 13 • geomechanical closure of the room
- 14 • backpressure of gases generated in the room by chemical and biological degradation of waste materials.

15 Thus, the ideal model of multiphase flow within a waste-filled room would couple the two-phase flow model
16 described in Section 7.2 and Appendix A with a model that can simulate the geomechanical closure of the room.

17 This ideal model, however, is not practically achievable. Direct solution of the fully coupled equations of
18 two-phase flow and geomechanical closure in the repetitive manner required by the PA methodology is unrealistic
19 using present resources; the PA Department instead has chosen to examine the sensitivity of the system to closure
20 using simplifications of the coupling that capture closure approximately while keeping calculations of two-phase
21 flow manageable. In the 1991 series of PA calculations, a simple approximation was made: Effects of room
22 closure and gas pressure were ignored and room material-property parameters were assigned time-independent
23 values that were based on the assumed waste-material composition. (See Sections 3.4.7 and 3.4.8 of WIPP PA
24 Division [1991c]).

25 The present (1992) series of calculations includes effects of room closure and gas generation in an indirect
26 way. A *separate* (i.e., uncoupled) calculation of the effective porosity of a waste-filled room as a function of
27 time and total moles of gas generated was made (Mendenhall and Lincoln, February 28, 1992, memo in Appendix
28 A, Volume 3 of this report); data from this calculation were used to fit a porosity "surface" (Figure 7-2) that was
29 then used as a constraint on room porosity in the equations of two-phase flow (see Appendix A on BRAGFLO).



TRI-6342-2008-0

Figure 7-2. Surface giving porosity of waste-filled disposal room as a function of total volume of gas produced and time after sealing. Pore space is assumed to be fully saturated with gas. Porosity is expressed as void volume per unit volume of waste.

1 The room deformation component of the separate calculation was accomplished with SANCHO, a finite element
2 computer program for simulating the quasistatic, large-deformation, inelastic response of two-dimensional solids;
3 a brief description of the SANCHO code is provided in Appendix B. Details of room-deformation and gas-
4 generation components of the separate calculation and values of mechanical and material-property parameters used
5 in the separate calculation are provided in Volume 3 of this report.

6 **7.4 Waste Mobilization**

7 Following the occurrence of an E2 or E1E2 scenario (Section 4.2.3.2), flow of brine through a collapsed
8 WIPP panel and up an intrusion borehole may result in mobilization of dissolved, radionuclide-bearing compounds
9 and their transport towards the Culebra Dolomite Member of the Rustler Formation. The consequence model that
10 simulates the process of waste mobilization is currently implemented in part of a computer code called PANEL.
11 The mathematical model on which PANEL is based is described in Section 1.4.4 of Volume 3 of this series of
12 reports, and represents an extreme simplification of a potentially complex situation that in reality involves a
13 mixture of waste forms having widely varying physical and chemical compositions in contact with
14 inhomogeneous flows of brine. The discussion that follows (1) details the assumptions that were made in order to
15 arrive at the simplified mathematical model of waste mobilization (Section 7.4.1) and (2) briefly presents the
16 simplified model of waste mobilization (Section 7.4.2).

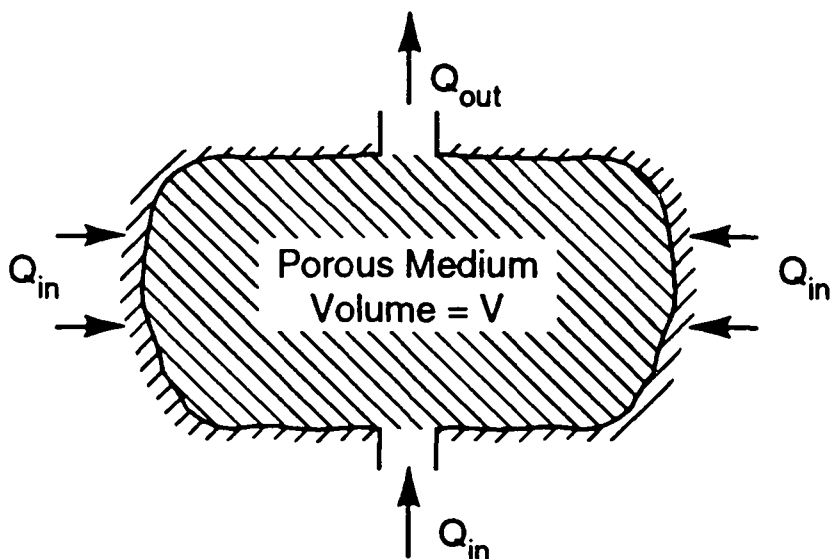
17 **7.4.1 Assumptions**

18 Eight assumptions about panel geometry, waste and backfill composition, brine discharge, and brine-waste
19 chemical reactions are implicit in the PA Department's current model of waste mobilization:

- 20 1. A collapsed WIPP panel (rooms and drifts) is idealized as a single, connected cavity of constant volume
21 (Figure 7-3).
- 22 2. Waste and backfill within the collapsed WIPP panel (cavity) are treated as a homogeneous porous
23 medium of constant porosity and infinite permeability; radionuclide-bearing compounds are uniformly
24 distributed throughout the cavity.
- 25 3. The idealized panel (cavity) is connected to sources and sinks for brine by one or more discrete inlets or
26 outlets (boreholes); brine may also flow across walls of the cavity (Figure 7-3).
- 27 4. Steady-state discharge of brine through the idealized panel is assumed to hold for all time; that is,

$$28 \quad \sum Q_{in} = \sum Q_{out} = Q(t),$$

29 where the net discharge, $Q(t)$, is calculated with the model for multiphase flow (Section 7.2).



TRI-6342-1435-0

Figure 7-3. Idealized collapsed WIPP panel in PANEL model.

5. The pore spaces of the idealized panel are fully saturated with brine at all times; that is, mobilization of radionuclide-bearing compounds in the gas phase is ignored.
6. Chemical equilibrium and uniform mixing of liquid-phase compounds throughout the idealized panel are achieved on time scales that are much smaller than the mean residence time of the brine in the cavity.
7. The solubility limit for a given isotope (e.g., U-234) of a given element (e.g., uranium) is assumed to be proportional to the solubility limit of the element; the constant of proportionality is taken as the ratio of the mass of the isotope that currently remains in the cavity to the sum of the masses of all currently remaining isotopes of the element.
8. Mobilization is limited to dissolved radionuclides; suspended radionuclides (colloids) are not considered to be mobilized by the brine.

Assumptions 1 and 2 imply that the total pore space in the idealized, collapsed WIPP panel is constant and equal to ϵV , where ϵ is the constant porosity and V is the cavity volume; assumption 5 implies that the total pore space is filled with brine at all times. Assumptions 3 and 4 imply that the mean residence time of brine in the repository is given by

$$\tau = \frac{\epsilon V}{Q}$$

1 regardless of the stated time dependence of Q . Assumption 6 implies that characteristic times to reach chemical
2 equilibrium and characteristic times for complete mixing of dissolved species by diffusion through cavity pore
3 spaces are always much smaller than τ . Because the rates of chemical reactions between dissolved and immobile
4 species are unknown, the validity of assumption 6 cannot be tested at this time; times for complete mixing by
5 diffusion can be estimated but have not yet been compared with mean residence times for brine.

6 Assumption 7 was made in order to simplify the equations that describe the masses of the various radioactive
7 isotopes of an element that remain in the cavity at any time after occurrence of an E2 or E1E2 scenario (see
8 Section 7.4.2 below and Section 1.4.4 of Volume 3). An alternative assumption would set isotope solubility
9 limits equal to the element solubility limit.

10 7.4.2 Simplified Mathematical Model

11 The simplified mathematical model of waste mobilization is expressed as a system of coupled, ordinary
12 differential equations, with each system applying to a radioactive decay chain:

$$13 \quad \dot{M}_i = -S_i \left(\frac{M_i}{\sum_j M_j} \right) Q(t) - \lambda_i M_i + (\lambda_{i-1} M_{i-1}) \left(\frac{\text{atomic wt}_i}{\text{atomic wt}_{i-1}} \right), \quad (7-5)$$

14 where $i = 1, 2, \dots, N$ numbers the N radionuclides in a given decay chain, a dot (\bullet) over a quantity means the time
15 derivative, and

16 $M_i(t)$ = mass of i^{th} radionuclide remaining in cavity at time $t > t_0$ (kg),

17 $Q(t)$ = discharge of brine through cavity at $t > t_0$ (m^3/s),

18 S_i = solubility limit for *element* associated with i^{th} radionuclide (kg/m^3),

19 λ_i = decay constant for i^{th} radionuclide (s^{-1}), and

20 t_0 = the time of initiation of a disruptive scenario (s).

21 In Equation 7-5, $\sum M_j$ signifies summation over the remaining masses of all radionuclides (including the i^{th}
22 radionuclide) associated with a given element. The initial conditions of Equation 7-5 are

$$23 \quad M_i(t_0) = M_{i0}(t_0), \quad (7-6)$$

24 where $M_{i0}(t_0)$ is the initial ($t = 0$) inventory of the i^{th} radionuclide (kg) aged by the Bateman equations (Section
25 7.1) to reflect mass remaining at $t_0 > 0$.

7.5 Groundwater Transmissivity Fields

The WIPP PA Department employs a multiple-realization technique to account for spatial variability of the transmissivity field within the Culebra Dolomite (LaVenue and RamaRao, 1992). The technique uses an automated inverse approach to calibrate a two-dimensional model to both steady-state and transient pressure data. The multiple-realization technique can be broken down into three steps:

1. **Unconditional Simulation.** An unconditional simulation of the WIPP transmissivity fields is generated. This is a random field that has the same spatial correlation structure as the transmissivity measurements, but does not necessarily match measured transmissivities at the location of their measurements.
2. **Conditional Simulation.** The random field produced in Step 1 is conditioned in this step so that it honors exactly the measured transmissivities at the locations of their measurements. The resulting field, called a “conditional simulation” of the transmissivity field, is used as the initial estimate of the Culebra transmissivity field.
3. **Automated Calibration.** The conditional simulation of the transmissivity field is then calibrated so that the pressures computed by the groundwater-flow model (both steady and transient state) agree closely (calibrated within the uncertainty in head measurements, i.e., between 1 and 2 m) with the measured pressures in a least-square sense. Calibration is achieved by placing synthetic transmissivity values (pilot points) automatically where the sensitivity of the difference between observed and calculated pressure to changes in the transmissivity field is greatest. When calibration is completed, a conditionally simulated transmissivity field is obtained that conforms with all head and transmissivity data at the WIPP site and may be regarded therefore as a plausible version of the true distribution of transmissivity.

This process is repeated to produce the desired number of calibrated, conditionally simulated fields. (Seventy of these fields were calculated in this manner for the 1992 PA calculations.) A description of this methodology, extracted from LaVenue and RamaRao (1992), follows. (A more complete discussion of the methodology is provided in Appendix D of this volume.)

7.5.1 Unconditional Simulation

The following methods have been used earlier in groundwater hydrology for generating unconditional simulations: nearest-neighbor method (Smith and Freeze, 1979; Smith and Schwartz, 1981), matrix decomposition (de Marsily, 1986), multidimensional spectral analysis (Shinozuka and Jan, 1972; Mejía and Rodríguez-Iturbe, 1974), turning-bands method (Matheron, 1971, 1973; Mantoglou and Wilson, 1982; Zimmerman and Wilson, 1990). Here the turning-bands method is used.

In the turning-bands method, a two-dimensional stochastic process is generated by the summation of a series of equivalent one-dimensional processes (Mantoglou and Wilson, 1982):

$$Z_s(N) = \frac{\sum_{i=1}^L Z_i(\zeta_{N_i})}{\sqrt{L}}, \quad (7-7)$$

where $Z_s(N)$ is the two-dimensional field to be simulated, $Z_i(\zeta_{N_i})$ is the one-dimensional process in the line interval (band) of line i measured by ζ_i and containing N_i (the projection of point N onto line i), and L is the number of lines selected. As in LaVenue et al. (1990), the 1992 calculations model the WIPP transmissivity data as a two-dimensional field with an intrinsic random function of order zero (IRF-0), making it possible to use the Weiner-Levy Process to generate the line process $Z_i(\zeta_{N_i})$ in Equation 7-7.

7.5.2 Conditional Simulation

The procedure for conditioning is based on the following relationship:

$$Z(x) \approx Z_{ok}(x) + [Z_{uc}(x) - Z_{uk}(x)], \quad (7-8)$$

where $Z(x)$ is the true (but unknown) value of the field at point x , $Z_{ok}(x)$ is the kriged estimate of Z at x based on the observed values of Z at the locations of the observations, $Z_{uc}(x)$ is the unconditionally simulated value of the field at point x , and $Z_{uk}(x)$ is value of the kriged estimate at x based on the unconditionally simulated values of Z_{uc} at the locations of the observations. Equation 7-8 clarifies the conditioning step as one of adding a simulated kriging error on a kriged field using the measured data. This step involves kriging twice, once with the measured transmissivities and another time with the unconditionally simulated transmissivities, both at the location of the observations. The simulated kriging error is rendered zero at all observation points.

7.5.3 Automated Calibration

In the 1992 calculations, model calibration is done by an indirect approach. Synthetic transmissivity values, referred to as pilot points, are automatically placed in regions of the conditionally simulated transmissivity field where an objective function (Equation 7-9) is most sensitive to changes in the this transmissivity field. This objective function is defined as the weighted sum of the squared deviations between the model computed pressures and the observed pressures, with the summation being extended in the spatial and temporal domain where pressure measurements are taken:

$$J(\underline{u}) = \sum_{k=1}^L \underline{e}_p^T(k) \underline{R}^{-1}(k) \underline{e}_p(k), \quad (7-9)$$

where $J(\underline{u})$ is the weighted least square (WLS) error criterion function, \underline{u} is the vector of parameters ($Y_p = \log_{10} T_p$), T_p is the pilot-point transmissivity, \underline{e}_p is the difference between the computed and observed pressures, \underline{R} is the covariance matrix of errors in the observed pressure, k is the time step number, L is the number of time steps, and T is the transpose.

1 Pilot points are added to the existing measured transmissivity data set during the course of calibration. After a
 2 pilot point is added to the transmissivity data set, the augmented data set is used to obtain a revised, conditionally
 3 simulated transmissivity field for a subsequent iteration in calibration. With the addition of a pilot point, the
 4 transmissivity distribution in the neighborhood of the pilot point gets modified with dominant modifications
 5 being closer to the pilot-point location.

6 Pilot points are placed at locations where their potential for reducing the objective function (Equation 7-9) is
 7 highest. This potential is quantified by the sensitivity coefficients (dJ/dY) of the objective function J with
 8 respect to Y , the logarithm (to base 10) of pilot-point transmissivity. Coupled adjoint sensitivity analysis and
 9 kriging are used to compute the required derivatives (RamaRao and Reeves, 1990). The transmissivities at pilot
 10 points are assigned by an unconstrained optimization algorithm and a subsequent imposition of constraints. The
 11 optimization algorithm, which belongs to a class of iterative search algorithms, involves the repeated application
 12 of the following equation until convergence is achieved:

$$13 \quad \underline{Y}_{i+1} = \underline{Y}_i + \beta_i \underline{d}_i, \quad (7-10)$$

14 where i is the iteration index, \underline{d}_i is the direction vector, β_i is the step length (a scalar), and \underline{Y}_i is a vector of
 15 parameters to be optimized (i.e., logarithms of pilot point transmissivities to base 10).

16 There are two levels of iteration used in the calibration process, designated as “inner” and “outer” iterations.
 17 An inner iteration relates to the iterations needed to optimize the transmissivities of the pilot points. When the
 18 convergence of an inner iteration is achieved, the pilot points are added to the transmissivity data set, and then the
 19 outer iteration may proceed. During the outer iteration, optimal location of the next set of pilot points is
 20 determined using coupled kriging and adjoint sensitivity analysis. Subsequently, their transmissivities are
 21 optimized by a sequence of inner iterations.

22 Convergence criteria for the inner iterations are as follows:

- 23 • The performance measure J drops below a prescribed minimum value.
- 24 • The number of iterations equals a prescribed maximum for the inner iterations.
- 25 • The ratio of the norm of the gradient to the initial gradient norm reduces below a prescribed value.
- 26 • The gradient norm is less than a prescribed minimum.
- 27 • The relative change in the objective function falls below a prescribed value.

28 Outer iterations cease once the performance measure J drops below a prescribed minimum value or the number of
 29 iterations equals a prescribed maximum for the outer iterations.

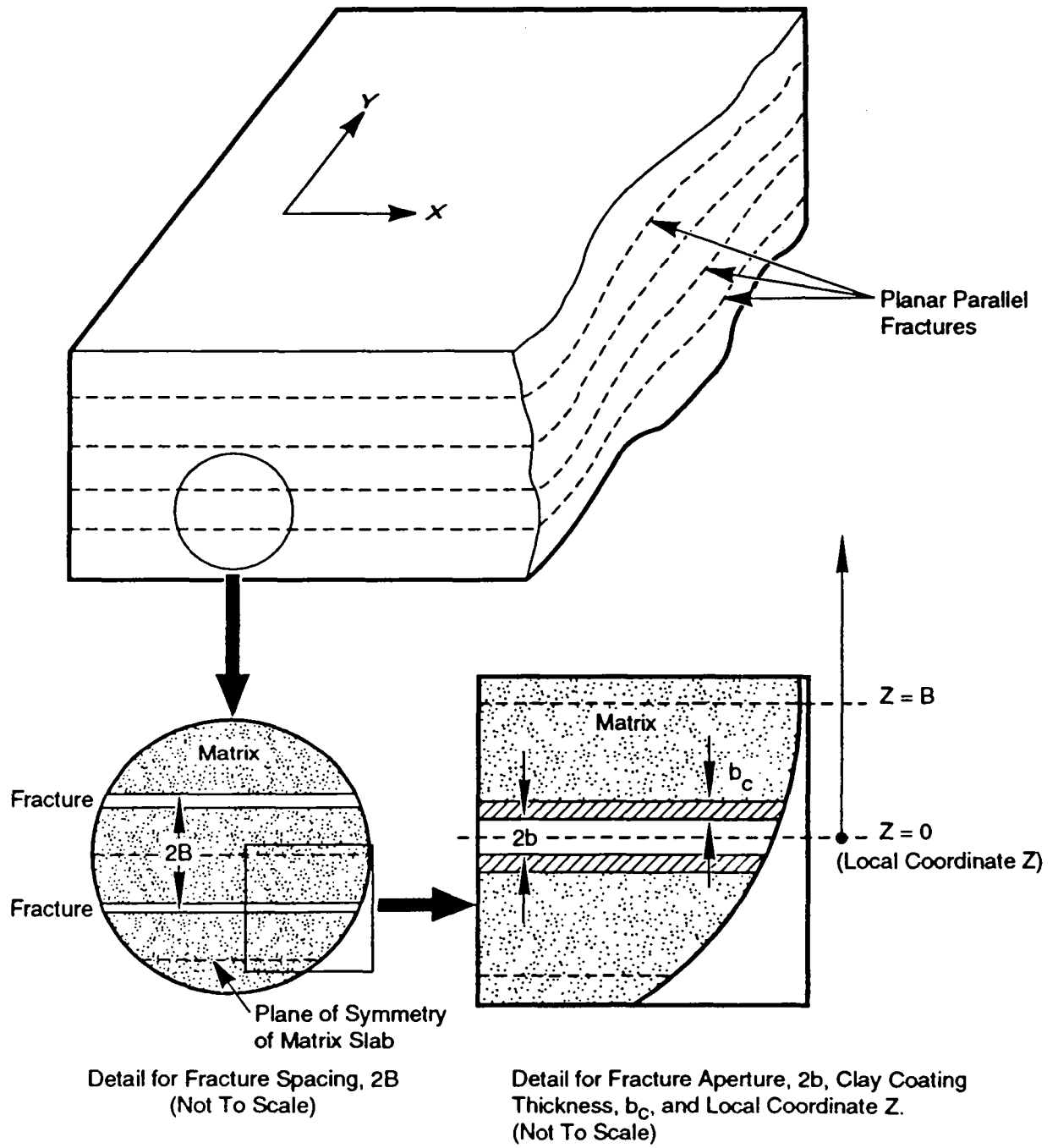
7.6 Groundwater Flow and Transport

Following the occurrence of an E2 or E1E2 scenario (Section 4.2.3.2), flow of brine through a collapsed WIPP panel may result in mobilization of dissolved, radionuclide-bearing compounds from waste (Section 7.4), the transport of these compounds up an intrusion borehole, and eventually their injection into the Culebra Dolomite Member of the Rustler Formation (Section 2.2.2.6). Dissolved compounds that reach the Culebra could then be carried to the accessible-environment boundary by advection and diffusion in groundwater flowing in the Culebra. Thus, to estimate consequences of certain disturbed-case scenarios, models of groundwater flow and solute transport through the Culebra are needed.

The consequence model that simulates groundwater flow in the Culebra is currently implemented by a computer code called SECO_2DH (Appendix C). The mathematical model on which SECO_2DH is based is described in Section 7.6.1 (below), which details assumptions that were made in order to arrive at the current model of groundwater flow; this section also contains discussions of modeling the effects of climate change on boundary conditions for the Culebra flow model.

Simulations of solute transport in groundwater flowing through the Culebra are currently implemented by a companion to the SECO_2DH code called SECO_TP (Appendix C). The mathematical model on which SECO_TP is based is described in Section 1.4.6 of Volume 3 of the present series of reports. Section 7.6.2 (following) contains discussion of the assumptions that were made in order to arrive at the current model of solute transport; it also contains discussion of the 1992 treatments of hydrodynamic dispersion (Section 7.6.2.1) and chemical sorption in fracture flows (Section 7.6.2.2).

The mathematical models of groundwater flow and solute transport are based on a common, highly simplified conceptual model of the Culebra Dolomite Member of the Rustler Formation: The Culebra Dolomite Member is imagined to be a sheet-like mass of rock having lateral dimensions of the order of tens of kilometers and uniform thickness of about 8 meters. Sets of planar fractures, all parallel to the plane of bedding, run continuously throughout the rock mass (Figure 7-4, top) and it is assumed that all water flow through the Culebra is sustained by the fracture sets, i.e., there is no flow through matrix blocks separating fractures (Figure 7-4, lower left) even though the matrix blocks are assumed to be saturated and have a finite kinematic porosity. The surfaces of fractures are assumed to be uniformly coated with layers of clay of constant thickness greater than or equal to 0 (Figure 7-4, lower right) that are never allowed to entirely fill the void space of a fracture; these clay layers are assumed to be saturated and to have finite kinematic porosity, but as in the matrix material, no advective flow is allowed through a clay layer.



TRI- 6342-1436-0

Figure 7-4. Conceptual hydrologic model of the Culebra Dolomite Member.

1 **7.6.1 Groundwater Flow in the Culebra**

2 Groundwater flow at regional and local scales within the Culebra Dolomite is simulated by solving the
3 following partial differential equation in two dimensions (x,y):

4
$$S_s \frac{\partial h}{\partial t} = \nabla \cdot (\bar{K} \cdot \nabla h) \quad (7-11)$$

5 where

6 $h = h(x,y,t)$, the hydraulic head(m),

7 $S_s = S_s(x,y,t)$, the specific storage of the Culebra (m⁻¹),

8 $\bar{K} = \bar{K}(x,y,t)$, the hydraulic conductivity tensor (m/s).

9 The specific storage and hydraulic conductivity tensors are obtained from more directly measurable quantities.

10
$$S_s = \frac{S(x,y)}{\Delta Z}, \quad \bar{K} = \frac{\bar{T}(x,y)}{\Delta Z}, \quad (7-12)$$

11 where

12 $S(x,y) =$ storage coefficient in the Culebra (dimensionless),

13 $\Delta Z = Z(x,y)$, Culebra thickness (m),

14 $\bar{T}(x,y) =$ one of a set of simulated transmissivity tensors (units: m²/s). See Section 2.6.9 of Volume 3
15 for a discussion of how transmissivity fields are generated. Also see Section 7.5 of this report.

16 Given appropriate initial and boundary conditions, the SECO_2DH code is used to solve Equation 7-11
17 numerically to yield a potentiometric head field, $h(x,y,t)$, which may be used to compute specific discharge (or
18 Darcy velocity) at any point in the Culebra:

19
$$\vec{q}(x,y,t) = -\bar{K} \cdot \nabla h \text{ (m / s)}. \quad (7-13)$$

20 The storage coefficients $S(x,y)$, and the Culebra thickness ΔZ are treated as constants (as opposed to functions
21 of position) in the 1992 series of calculations.

1 7.6.1.1 BOUNDARY CONDITIONS

2 Groundwater flow is modeled separately in regional and local grids (Figure 7-5) to provide increased resolution
 3 in the area of primary interest around the WIPP. In solving Equation (7-11), boundary conditions are specified on
 4 the outer edges of the regional grid; these boundary conditions may be a mix of the following kind, depending
 5 upon geological and hydrological conditions at a point on the regional boundary: (1) Dirichlet (specified h on
 6 boundary); (2) inhomogeneous Neuman (specified gradients of h on boundary); (3) Robin boundary conditions [a
 7 mixture of (1) and (2)]; and (4) adaptive boundary conditions, in which flux (\dot{q}) is specified at inflow boundaries
 8 and head (h) is specified at outflow boundaries. Boundary conditions for the local grid, in which radionuclide
 9 transport is modeled, are determined by the groundwater flow calculated for the regional grid. The actual problem
 10 geometry and specifications for boundary conditions that were used in the 1992 series of calculations can be found
 11 in Volume 4 of this report.

12 7.6.1.2 EFFECTS OF CLIMATE CHANGE

13 The effects of climate change are simulated through inclusion of time-dependent Dirichlet boundary
 14 conditions. Specifically, potentiometric heads on portions of the northwestern and northeastern edges of the
 15 regional grid (closest to the assumed recharge area for the Culebra) are set according to the formula (Swift, 1992,
 16 1991)

$$17 \quad h_f(x, y, t) = h_p(x, y) \left[\frac{3A_R + 1}{4} - \left(\frac{A_R - 1}{2} \right) \left(\cos \theta t - \sin \frac{\Phi}{2} t + \frac{1}{2} \cos \Phi t \right) \right] \quad (7-14)$$

18 where

19 h_f = future potentiometric head (m)

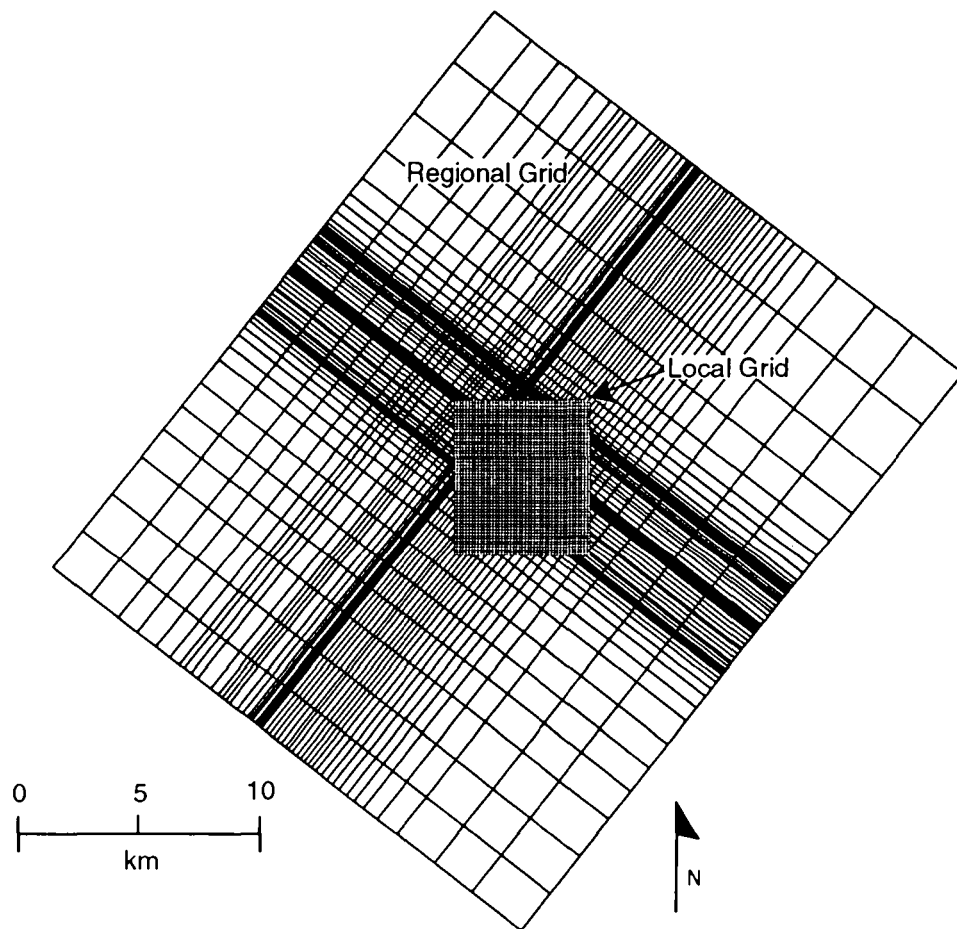
20 h_p = present potentiometric head (m)

21 A_R = Recharge amplitude factor (dimensionless)

22 θ = Pleistocene glaciation frequency (Hz)

23 Φ = frequency of Holocene-type climatic fluctuations (Hz).

24 The recharge amplitude factor, A_R , is a number to be chosen between 1 and $\gamma > 1$. If $A_R = 1$, it is seen that
 25 there are no effects of climatic change. If $A_R > 1$, the maximum future head, h_f , will be greater than the present
 26 head. The constant γ is a scaling factor that is chosen to ensure physically reasonable head values on the portion
 27 of the recharge boundary where boundary conditions are applied.



TRI-6342-2680-0

Figure 7-5. Example of regional and local grids used for disturbed fluid flow and transport calculations.

7.6.2 Solute Transport in the Culebra

The mathematical model of solute transport at the local scale is described in Section 1.4.6 of Volume 3 of the present series of reports. The physical assumptions and limitations of the 1992 version of the solute transport model are the same as those of the 1991 version (see 6.5.2.3 in WIPP PA Division, 1991b), namely:

1. The numerical solution is limited to two dimensions, reflecting the conceptual model of the Culebra Dolomite member (Figure 7-4).
2. Hydrodynamic dispersion is quantified with a Fick's law term.
3. Fracture flow is modeled as an equivalent porous medium of constant porosity.
4. No advective transport exists through the Culebra matrix; however, one-dimensional diffusion of solutes across fracture-matrix interfaces are allowed (Figure 7-4).
5. Adsorption of solutes on solid phases obeys a linear isotherm.
6. Local chemical equilibrium always exists between solutes and solid phases.
7. Material-property parameters are treated as constants over distinct material regions; in other words, intramaterial spatial variability is ignored.

The purpose of assumption 4 is to permit simple simulation of the phenomenon of dynamic solute storage within porous materials surrounding fractures. As solute concentration in fractures increases, solute will diffuse into and become immobilized within the matrix; if concentrations in fractures decreases with time, solute is returned to fractures by diffusion out of the matrix.

The major differences between the 1992 and 1991 versions of the solute transport model lie in the former's treatment of dispersivity parameters and adsorption effects in fracture flows. Details of changes in the way these important physical effects are implemented in the model are presented in the remainder of this section.

7.6.2.1 MODELING HYDRODYNAMIC DISPERSION

The components of the hydrodynamic dispersion tensor for the fracture system D_{ij} , are (Scheidegger, 1960)

$$D_{11} = \alpha_L \frac{(V_1)^2}{|V|} + \alpha_T \frac{(V_2)^2}{|V|} + D^*,$$

$$D_{22} = \alpha_L \frac{(V_2)^2}{|V|} + \alpha_T \frac{(V_1)^2}{|V|} + D^*,$$

$$D_{12} = D_{21} = (\alpha_L - \alpha_T) \frac{V_1 V_2}{|V|},$$

2 where V_i , $i = 1, 2$, are the components of the average linear velocity vector in the fracture system (m/s), α_L and
3 α_T are respectively longitudinal and transverse dispersivities (m), D^* is the molecular diffusion coefficient of the
4 "average" solute species (m^2/s), and

$$|V| = (V_1^2 + V_2^2)^{1/2}$$

6 The dispersivities, α_L and α_T , are measures of the dispersion of the true linear velocity vector about the
7 average value. Ideally, these parameters would be estimated by fitting transport model calculations to results of
8 tracer tests conducted in the Rustler Formation at an appropriate scale; but, in the absence of tracer-test results
9 suitable for parameter estimation, the PA Department has had to rely on subjective judgments and results from
10 stochastic transport theory to form the necessary estimates. In 1991, it was assumed that α_L , α_T were
11 imprecisely known constants (WIPP PA Division, 1991c, Section 2.6.2), with longitudinal dispersivity varying
12 between 50 and 300 meters and transverse dispersivity varying between 5 and 30 meters (i.e., one-tenth of
13 longitudinal dispersivity).

14 The treatment of Culebra dispersivity in the present (1992) series of PA calculations relies heavily on
15 stochastic transport theory, exemplified by the universal scaling approach used by Neuman (1990) to investigate
16 the compatibility of fractal transmissivity fields with the observed scale dependence of dispersivity. Neuman
17 provides an expression that relates longitudinal dispersivity to the mean value of the variogram of $\ln T$ variance at
18 the scale S and the travel distance L , namely

$$\alpha_L = C_o L \sigma_y^2(S), \quad (7-15)$$

20 where C_o is a constant ~ 1 in isotropic media; and

$$\sigma_y^2(S) = \bar{\gamma}(v, v) \approx \frac{1}{v^2} \int_v \int_v \gamma(x-y) dx dy, \quad (7-16)$$

22 where $\gamma(h)$ is the variogram of $\ln T$, $h = |x-y|$, and each integration in the above expression is carried over a
23 fixed area v , $\sim L^2$. In current (1992) PA calculations, $C_o = 1$ and L is taken to be the size of the model block in
24 which α_L is being evaluated.

1 The variogram, $\gamma(h)$, is taken to be the one used in the "local" scale generation of the 1992 random
2 transmissivity fields (Section 7.5 and Appendix D, Volume 3),

$$3 \qquad \qquad \qquad \gamma(h) = 1.2 \times 10^{-3} h. \qquad \qquad \qquad (7-17)$$

4 Here, the "local" scale is defined as that appropriate for the transmissivity measurements, i.e., a scale length
5 between slug tests radii of influence and pump tests radii of influence; such a scale length is of the order of 10
6 meters. Note that Equation (7-17) is a linear variogram, for which the concepts of "correlation length" and
7 "integral scale" have no meaning.

8 The integral in Equation (7-16) has been evaluated by Journel and Huijbregts (1978, p. 113) for a linear
9 variogram $\gamma(h) = h$ and a rectangular mesh with dimensions L and ℓ . Their result is analytically messy, but in
10 the case where $L = \ell$ ($v =$ area of a square of side L), their expression reduces to

$$11 \qquad \qquad \qquad \bar{\gamma}(v, v) = 0.5213 L.$$

12 Multiplying this expression by the constant in Equation (7-17), 1.2×10^{-3} , and substituting for $\bar{\gamma}(v, v)$ in
13 Equation (7-13) gives an expression for the longitudinal dispersivity in terms of the size of the model block in
14 which α_L is being evaluated:

$$15 \qquad \qquad \qquad \alpha_L \approx 6.2 \times 10^{-4} L^2 \text{ (m)}. \qquad \qquad \qquad (7-18)$$

16 In practice, a value of 1.5 meters is added to the α_L obtained by Equation (7-18) in order to account for microscale
17 dispersion that must occur below the "local" scale.

18 The ratio of longitudinal to transverse dispersivity does not seem to be scale dependent; data from Gelhar et al.
19 (1992) suggest that this ratio is almost always between 10 and 50. In the present (1992) series of calculations,
20 the fixed relation

$$21 \qquad \qquad \qquad \alpha_T = \frac{1}{10} \alpha_L \qquad \qquad \qquad (7-19)$$

22 was adopted.

23 Note that using model block size as travel distance in obtaining Equation (7-18) is equivalent to the
24 assumption that dispersivity reaches its asymptotic limit at the scale of a model block, and any other non-
25 asymptotic behavior is taken care of by variability of the simulated transmissivity fields (Section 7.5 and
26 Appendix D, Volume 3).

1 7.6.2.2 MODELING CHEMICAL SORPTION IN FRACTURE FLOWS

2 Chemical retardation of solutes by sorption on fracture surfaces was modelled in 1990-1991 PA calculations with
3 a formula proposed by M. D. Siegel (1990). Siegel suggested that the effective solute velocity in a clay-lined
4 fracture, V_{eff} , is related to the average linear velocity of groundwater in the fracture, V , by

5
$$\frac{V}{V_{eff}} = 1 + \rho_c K_{dc} (b_c / b), \quad (7-20)$$

6 where

7 ρ_c = density of clay liner (kg/m³),

8 K_{dc} = partition coefficient of solute in clay (m³/kg),

9 $2b_c$ = total thickness of clay layer in a fracture (m), and

10 $2b$ = fracture aperture (m).

11 The expression on the right side of Equation (7-20) is called R , the retardation factor; the partition coefficient K_{dc}
12 is also called the distribution coefficient.

13 Consideration of Equation (7-20) will show that it cannot generally describe retardation of solutes being
14 transported through an *open*, saturated fracture; in this case, retardation of solute molecules must proceed by
15 reactions between the mobilized species and stationary species located on the solid surface facing the fracture void
16 space. In contrast, Equation (7-20) turns out to be a "thin-skin" approximation to retardation of mobile solutes
17 *within* pore spaces of the clay layer, which is valid only after solute molecules have diffused or been advected into
18 the clay layer and concentrational equilibrium is nearly established. In other words, Equation (7-20) is appropriate
19 for concentrational equilibrium; note, however, that it may take a long time to reach concentrational equilibrium
20 by diffusion of solute through highly sorbing clay and that, by assuming instantaneous equilibrium, the
21 retardation of solutes in fracture flows may have been overestimated in the 1990-1991 calculations.

22 The PA Department abandoned use of Equation (7-20) in 1992 and, for reasons provided below, has set $R = 1$
23 in fracture flows (see Equation 1.4.6-1 in Section 1.4.6, Volume 3 of this report). An approximate, but
24 physically motivated expression for the retardation of solutes in fracture flows is derived in the remainder of this
25 subsection and used to justify the choice of $R = 1$.

26 Freeze and Cherry (1979, p. 411) give an expression for the retardation factor in solute transport through a
27 planar fracture of aperture $2b$:

28
$$R = 1 + \frac{1}{b} K_a, \quad (7-21)$$

1 where

$$2 \quad K_a = \frac{\text{mass of solute on solid phase per unit area of solid phase}}{\text{concentration of solute in solution}} \quad (\text{m}).$$

3 Equation (7-21) should be valid when time scales for (1) diffusion across a fracture aperture and (2) achievement of
4 equilibrium in surficial chemical reactions are always much smaller than other problem time scales (e.g., time
5 required to advect a solute molecule across a grid cell, time required to diffuse into clay layers).

6 The surficial distribution coefficient, K_a , can be related to the familiar mass-based distribution coefficient
7 (Freeze and Cherry, 1979, p. 405),

$$8 \quad K_d = \frac{\text{mass of solute on solid phase per unit mass of solid phase}}{\text{concentration of solute in solution}} \quad (\text{m}^3 / \text{kg}).$$

$$9 \quad \text{by} \quad K_a = K_d / \sigma_m,$$

10 where σ_m is the surface area per unit mass of the solid phase (m^2/kg). Obviously, σ_m depends upon the
11 physical nature of the solid phase, here a natural aggregation of clay grains on the surfaces of saturated fractures in
12 the Culebra Dolomite. No measurements or estimates of σ_m for these clays seem to be available, but an order-
13 of-magnitude estimate of this quantity can be rapidly made if the clay is visualized as an aggregation of regularly
14 packed spheres of radius a (i.e., spheres centered on vertices of a cubic lattice of elemental size $2a$). To begin
15 making this estimate, consider M kg of bulk clay having *grain-density* ρ_g ; then the number of spheres in this
16 mass is

$$17 \quad n_p \approx (3M) / (4\pi a^3 \rho_g),$$

18 and the surface area of the solid phase that is presented to the pore space of the M kg of clay is

$$19 \quad A \approx 4\pi a^2 n_p = \frac{3M}{a\rho_g}.$$

20 It follows that

$$21 \quad \sigma_m = \frac{A}{M} \approx \frac{3}{a\rho_g}, \quad \text{and so } K_a \approx \frac{a\rho_g K_d}{3}.$$

22 Substitution of this result in Equation (7-21) gives the promised order-of-magnitude estimate of the fracture
23 retardation factor:

$$24 \quad R \approx 1 + \frac{\rho_g}{3} K_d (a/b). \quad (7-22)$$

1 Note the superficial similarity of expressions in Equations (7-20) and (7-22). Their relative magnitudes are
2 nevertheless always different as can be seen by forming the ratio of ($R-1$)s from the respective formulas; for
3 instance, the ratio of ($R-1$) for Equation (7-22) to ($R-1$) for Equation (7-20) is of the order of a/b_c , the ratio of
4 clay particle size to clay layer thickness. In all but the narrowest of fracture apertures, a/b_c should be of the order
5 of 10^{-2} or less (take $a = 1 \mu\text{m}$, $b = 100 \mu\text{m}$). Thus, retardations computed from Equation (7-22) should be much
6 less than retardations computed from Equation (7-20), justifying the earlier claim that retardation in fracture flows
7 (i.e., "single porosity" model) may have been overestimated in the 1990-1991 series of PA calculations.

8 Clay layers on fracture surfaces actually played two roles in 1990-1991 PA models of solute transport in the
9 Culebra Dolomite: (1) the role described above, i.e., as agents of retardation of solutes in fracture flows, and (2) as
10 barriers to mass transfer of solutes across the matrix-fracture interface (the "matrix skin resistance" of Section
11 2.6.7 in WIPP PA Division, 1991c). The PA Department has also abandoned the second of these roles for clay
12 linings in 1992 versions of the solute-transport models. Clay linings are now treated as extensions of the matrix
13 and a single diffusion equation [Equation (1.4.6-5), Section 1.4.6, Volume 3 of this series] is used to model solute
14 mass transport in an effective porous media comprised of Culebra matrix blocks and their adjacent clay linings.

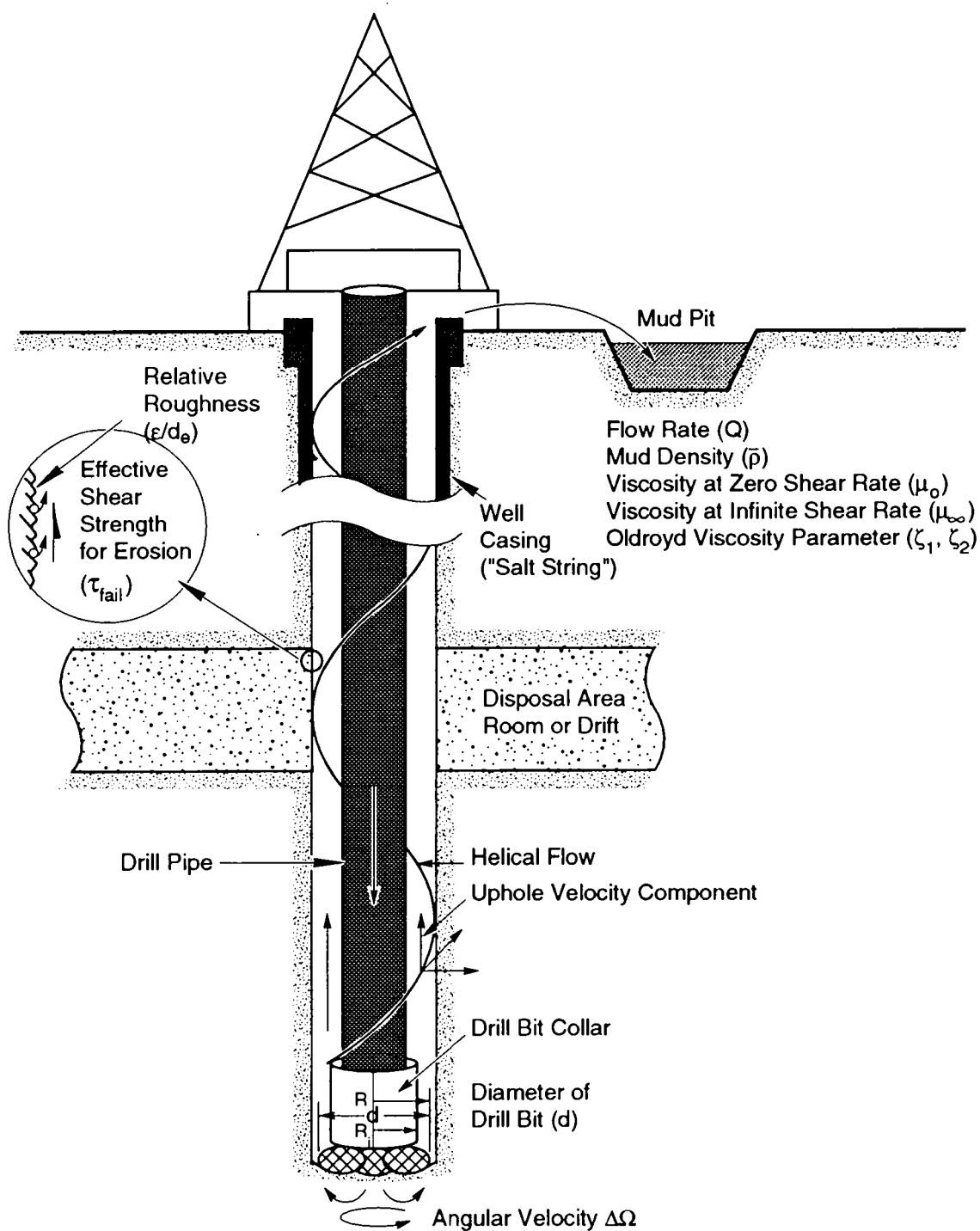
15 7.7 Direct Removal of Waste

16 Of the possible pathways for release during the 10,000-year regulatory period, one of the most important is
17 that caused by the direct removal of waste that would result when an exploratory drill bit inadvertently penetrates a
18 waste storage room. To quantify the extent of radioactive release resulting from direct removal of waste, the
19 model described below, extracted from Berglund (1992), has been developed. The current performance assessment
20 model assumes that future drilling techniques will be similar to those in use today. This assumption is necessary
21 to provide a basis on which predictions of release can be estimated.

22 In rotary drilling, a cutting bit attached to a series of hollow drill collars and drill pipes is rotated at a fixed
23 angular velocity and is directed to cut downward through underlying strata. To remove the material loosened by
24 the drilling action, a drilling fluid ("mud") is pumped down the drill pipe, through and around the drill bit, and up
25 to the surface within the annulus formed by the drill pipe and the borehole wall (Figure 7-6).

26 If an exploratory drill bit penetrates a waste-filled room, waste resulting from three separate physical processes
27 can mix with the drilling fluid and be transported to the surface:

- 28 • cuttings—waste contained in the cylindrical volume created by the cutting action of the drill bit through the
29 waste,
- 30 • cavings—waste that erodes from the borehole in response to the upward-flowing drilling fluid within the
31 annulus, and
- 32 • spillings—waste surrounding the eroded borehole that is transported by waste-generated gas escaping to the
33 lower-pressure borehole.



TRI-6330-51-3

Figure 7-6. Rotary drilling.

1 A discussion of these three processes follows.

2 **7.7.1 Cuttings**

3 For a gauge borehole, the volume of cuttings removed and transported to the surface is equal to the product of
4 the drill bit area and the drill depth. Thus, to estimate the total volume of waste removed due to the cutting action
5 of the drill bit (V), it is only necessary to know the compacted repository height (h) and the drill-bit area (A):

$$6 \qquad \qquad \qquad V = Ah. \qquad \qquad \qquad (7-23)$$

7 The cuttings volume calculated in this manner is a lower bound to the total quantity of waste removed by drilling.

8 **7.7.2 Cavings**

9 While a number of factors that influence drillhole wall erosion have been identified in the literature (Broc,
10 1982), industry opinion singles out fluid shear stress as the most important factor (Walker and Holman, 1971;
11 Darley, 1969). This analysis therefore assumes that borehole erosion is caused primarily by the magnitude of
12 fluid shear stress acting on the borehole wall. This analysis also assumes that erosion of wall material occurs
13 when the fluid shear stress at the wall exceeds the effective shear strength for erosion of the wall material (the
14 surrounding compacted repository wastes) and that the diameter of the bored hole increases until this condition no
15 longer exists. In this process, it is assumed that sufficient time is available to complete the erosion process. All
16 the eroded material is assumed to pass to the surface in the flowing drilling fluid.

17 Flow in the annulus between the drill pipe and borehole wall is usually laminar (Darley and Gray, 1988).
18 Adjacent to the collars, however, the smaller annular volume created by the larger collar diameter (Figure 7-6)
19 causes higher mud velocities, making flow either laminar or turbulent (Berglund, 1990; Pace, 1990). For laminar
20 flow, the analysis lends itself to classical solution methods. Turbulent flow, where the flow is assumed to be
21 axial with no rotational component, requires a more approximate approach.

22 **7.7.2.1 LAMINAR FLOW**

23 Below Reynolds numbers of about 2100 for Newtonian fluids and 2400 for some non-Newtonian fluids
24 (Walker, 1976), experiments have shown that the flow of a fluid in a circular pipe or annulus is well behaved and
25 can be described using a well-defined relationship between the velocity field and the fluid shear stress. This type of
26 flow is called laminar. Drilling fluids exhibit non-Newtonian fluid behavior, making it necessary to choose a
27 functional form for the variation of viscosity with shear rate for the fluid. Of the several different functional forms
28 that can be used to account for the varying viscosity, this analysis uses a form chosen by Oldroyd (1958) and
29 further developed by Savins and Wallick (1966).

1 Savins and Wallick (1966) have shown that the solution for laminar helical flow of a non-Newtonian fluid in
 2 an annulus could be written in terms of three nonlinear integral equations:

$$3 \quad F_1 = \int_{\alpha}^1 \left(\frac{\rho^2 - \lambda^2}{\rho} \right) \frac{d\rho}{\eta} = 0$$

$$4 \quad F_2 = C \int_{\alpha}^1 \frac{d\rho}{\rho^3 \eta} - \Delta\Omega = 0$$

$$5 \quad F_3 = \frac{4Q}{\pi R^3} + 4 \left(\frac{RJ}{2} \right) \int_{\alpha}^1 \left(\frac{\alpha^2 - \rho^2}{\eta} \right) \left(\frac{\rho^2 - \lambda^2}{\rho} \right) d\rho = 0, \quad (7-24)$$

6
 7 where Q is the drilling fluid (mud) flow rate; r is the radial coordinate; α is the ratio of the collar radius over the
 8 cutting radius (R_i/R) (Figure 7-6); $\Delta\Omega$ is the drill string angular velocity; η is the viscosity of the drilling fluid;
 9 ρ is the non-dimensional radial coordinate representing the ratio r/R ; and λ^2 , $RJ/2$, and C are parameters related
 10 to the fluid shear stresses. As long as annular flow remains in the laminar regime, the above three nonlinear
 11 integral equations can be solved numerically to determine the final eroded volume of the borehole (a function of
 12 the effective shear strength for erosion, τ_{fail}) and the resulting total cavings volume.

13 7.7.2.2 TURBULENT FLOW

14 At a Reynolds number of about 3000, flow becomes fully turbulent; momentum effects dominate and fluid
 15 viscosity is no longer as important in characterizing pressure losses. A far more important parameter is the
 16 surface roughness past which the fluid must flow.

17 The increased complexity of turbulent flow makes empirical procedures necessary. For axial flow in an
 18 annulus, the pressure loss under turbulent conditions can be approximated by (Broc, 1982)

$$19 \quad \Delta P = \frac{2fL\bar{\rho}\bar{V}^2}{(0.8165)D}, \quad (7-25)$$

20 where f is the coefficient of pressure head loss (Fanning friction factor), D is the hydraulic diameter, L is the
 21 borehole length, \bar{V} is the average fluid velocity, and $\bar{\rho}$ is the drill fluid density.

22 If the shear stress due to the flowing fluid is assumed to be uniformly distributed on the inner and outer
 23 surfaces of the annulus, it can be easily shown using Equation 7-25 that the shear stress is related to the average
 24 fluid velocity through the relation

$$\tau = \frac{f \bar{\rho} \bar{V}^2}{2(0.8165)}, \quad (7-26)$$

The Fanning friction factor is empirically related to the Reynolds number and relative roughness by the equation (Whittaker, 1985)

$$\frac{1}{\sqrt{f}} = -4 \log_{10} \left[\frac{\epsilon}{3.72D} + \frac{1.255}{R_e \sqrt{f}} \right], \quad (7-27)$$

where ϵ/D is the relative roughness and R_e is the Reynolds number. For circular pipes, D in this equation represents the inside diameter and ϵ is the absolute roughness or the average depth of pipe wall irregularities. In the absence of a similar equation for flow in an annulus, it is assumed that this equation also applies here, where D is the hydraulic diameter, and ϵ is the absolute roughness of the waste-borehole interface.

The above three equations can be used to obtain the final eroded borehole radius under turbulent flow conditions by forcing the fluid shear stress acting on the borehole wall to equal the shear strength for erosion of the repository waste (τ_{fail}).

7.7.3 Spallings

The spalling of borehole walls is a common occurrence in oil and gas drilling and can be caused by an encounter with a geopressurized formation; a similar event may occur if an exploratory drill bit penetrates a waste-filled, pressurized room at the WIPP. Corrosion and biodegradation of the waste will generate gas, raising the gas pore pressure in the waste to values approaching and perhaps exceeding the lithostatic level within the next 700 to 2,000 years. Because the permeability of the surrounding Salado Formation is expected to be 1 to 7 orders of magnitude less than that of the compacted waste, the Salado can be considered impermeable compared to the waste. The intrusion of a drill bit into the waste could therefore “suddenly” expose the waste with its high pore pressure (for example, 14.8 MPa) to the borehole hydrostatic pressure of 7.7 MPa (assuming a saturated salt solution is used while drilling), causing gas to escape to the borehole after flowing through the compacted waste. The escaping gas may compromise the stability of the borehole wall and contribute to the quantity of waste material that reaches the surface environment.

Spalling is a complex process that involves the flow of gas in a moving waste matrix, changing stress states, changing porosity and permeability of the waste, waste failure, and when the waste interacts with the drill bit, turbulent mixing of the three phases—solid waste, drilling fluid, and gas. The approach for modeling spalling caused by the intrusion of an exploratory drill bit is still being developed.

The current state of understanding for spall as related to WIPP is treated in Berglund (1992). In addition to a discussion of related literature, Berglund (1992) describes several types of calculations, each of which addresses a different aspect of gas flow and waste response from a penetrated, gas-pressurized, waste storage room. The waste response is found to be very dependent on the constitutive nature of the compacted composite waste, a feature

1 that is currently unknown. If the waste is assumed to behave as a granular, soil-like material with a nonlinear
2 constitutive character and a small cohesive strength, the behavior of the waste subject to gas flow indicates a
3 movement toward the borehole after penetration. In both the one- and two-dimensional computational models,
4 where an instantaneous borehole pressure drop is assumed, the inward motion of the waste-borehole boundary
5 would quickly (in milliseconds) be blocked by the presence of the drill string and would remain impressed against
6 the drill string while a sufficient pore pressure gradient is maintained.

7 What happens to the waste as it is impressed against the drill string is not known because the interface
8 between the waste and drill stem is very difficult to characterize without experimental verification. One
9 possibility is the compressed waste will completely block the flow of drilling mud. Whether the drilling
10 operation can proceed in such circumstances is unknown. Certainly the flow of gas out of the waste will be
11 further restricted if not completely blocked. Such a restriction would prolong the compressive stresses acting
12 between the drill string and the waste. Another possibility is that some drilling fluid may be able to channel its
13 way through the waste-drill string boundary carrying eroded waste up into the upper borehole.

14 The driller may, however, be able to detect the resistance afforded by the waste pressing against the drill stem
15 by the increase in torque, circulation pressure, and by a drop in mud flowrate (Austin, 1983). Under such
16 conditions the driller may raise the cutting bit and allow the "spall" to continue naturally, eventually proceeding
17 after the process diminishes (Short, 1982). Often under these conditions a repetitive process is undertaken of
18 cleaning out, drilling ahead a few feet of new hole, picking up the drill bit to check for fill, then cleaning out
19 again. This is repeated until spalling slows. The cleanout procedure can be used for 12 to 24 hours, or longer, if
20 it shows sign of becoming effective (Short, 1982).

21 If drilling can proceed with the waste impressed against the drilling equipment, erosion will probably occur at
22 the interface and could continue until a significant portion of the gas has leaked from the penetrated room or the
23 target drill depth is reached. Based on leakage rates from the waste with uniform permeabilities, significant
24 volumes of gas will be removed from the room only after several hours for the greatest waste permeability and
25 hundreds of days for the least permeability. Moreover, the decrease in waste permeability caused by the
26 compressive stress field at the drill string-waste interface is likely to decrease the gas leakage rates significantly.

27 In the analyses considered in Berglund (1992), actions to prevent a blowout taken by the driller after
28 encountering a gas-pressurized formation are also discussed. When formation gas flow into a borehole is detected
29 at the surface, such as by an increase in return mud volume, the driller usually will "close in" the well by
30 engaging blowout preventers (BOPs) to prevent serious injury to personnel and damage to equipment. This action
31 is usually taken within a minute or two after the "kick" is first observed, and the effect is that the gas flow from
32 the formation to the borehole is effectively curtailed (Mills, 1984). The well is then "killed" by increasing the
33 mud density in the borehole so that the formation (waste) pore pressure is in balance with the mud pressure. The
34 drilling can then safely continue. With the pressure gradient in the borehole wall thus reduced to zero, spallation
35 will cease and waste will be brought to the surface by erosion only. BOPs are engaged only if a blowout
36 condition is detected. For high-permeability wastes ($k = 1 \times 10^{-13} \text{ m}^2$), the rate of flow of gas to the borehole
37 will increase the mud volume in the annulus significantly, and it is very likely that the well will be "killed."
38 However, for lower permeabilities, the gas flowrate is much reduced; the driller may not engage BOPs but
39 continue drilling, thus allowing spall into the borehole to occur.

1 Estimating the amount of material that may eventually be passed into the borehole as the result of gas
2 generation in the repository is difficult and speculative. However, based upon the analysis performed and the
3 literature examined to date, it does not appear to be unreasonable that a volume of waste greater than the lower
4 bound cuttings volume ($\text{bit area} \times \text{waste depth}$) could eventually reach the ground surface. Currently, little data
5 are available that predict the constitutive nature of the compacted, decomposed waste at the time of intrusion, nor
6 have there been any experiments performed that could confirm the mechanisms for borehole spall as discussed.
7 These data are currently being developed.

1
2

8. REFERENCES

- 3 Adams, J.E. 1944. "Upper Permian Ochoa Series of Delaware Basin, West Texas and Southeastern New Mexico,"
4 *Bulletin of the American Association of Petroleum Geologists*. Vol. 28, no. 11, 1596-1625.
- 5 Anderson, R.Y. 1981. "Deep-Seated Salt Dissolution in the Delaware Basin, Texas and New Mexico,"
6 *Environmental Geology and Hydrology in New Mexico*. Eds. S. G. Wells and W. Lambert. New Mexico
7 Geological Society Special Publication No. 10. Roswell, NM: New Mexico Geological Society, 133-
8 145.
- 9 Apostolakis, G., R. Bras, L. Price, J. Valdes, K. Wahi, and E. Webb. 1991. *Techniques for Determining*
10 *Probabilities of Events and Processes Affecting the Performance of Geologic Repositories: Suggested*
11 *Approaches*. NUREG/CR-3964, SAND86-0196. Albuquerque, NM: Sandia National Laboratories. Vol.
12 2.
- 13 Austin, E.H. 1983. *Drilling Engineering Handbook*. Boston, MA: International Human Resources Development
14 Corporation.
- 15 Bachman, G.O. 1981. *Geology of Nash Draw, Eddy County, New Mexico*. U.S. Geological Survey Open-File
16 Report 81-31. Denver, CO: U. S. Geological Survey.
- 17 Bachman, G.O. 1984. *Regional Geology of Ochoan Evaporites, Northern Part of Delaware Basin*. New Mexico
18 Bureau of Mines and Mineral Resources Circular 184. Socorro, NM: New Mexico Bureau of Mines and
19 Mineral Resources.
- 20 Bachman, G.O. 1987. *Karst in Evaporites in Southeastern New Mexico*. SAND86-7078. Albuquerque, NM:
21 Sandia National Laboratories.
- 22 Beauheim, R.L. 1986. *Hydraulic-Test Interpretations for Well DOE-2 at the Waste Isolation Pilot Plant (WIPP)*
23 *Site*. SAND86-1364. Albuquerque, NM: Sandia National Laboratories.
- 24 Beauheim, R.L. 1987a. *Interpretations of Single-Well Hydraulic Tests Conducted At and Near the Waste*
25 *Isolation Pilot Plant (WIPP) Site, 1983-1987*. SAND87-0039. Albuquerque, NM: Sandia National
26 Laboratories.
- 27 Beauheim, R.L. 1987b. *Analysis of Pumping Tests of the Culebra Dolomite Conducted At the H-3 Hydropad at*
28 *the Waste Isolation Pilot Plant (WIPP) Site*. SAND86-2311. Albuquerque, NM: Sandia National
29 Laboratories.
- 30 Beauheim, R.L. 1987c. *Interpretation of the WIPP-13 Multipad Pumping Test of the Culebra Dolomite at the*
31 *Waste Isolation Pilot Plant (WIPP) Site*. SAND87-2456. Albuquerque, NM: Sandia National Laboratories.

References

- 1 Beauheim, R.L., and P.B. Davies. 1992. "Experimental Plan for Tracer Testing in the Culcra Dolomite at the
2 WIPP Site." Revision A. Albuquerque, NM: Sandia National Laboratories.
- 3 Beauheim, R.L., and R.M. Holt. 1990. "Hydrogeology of the WIPP Site," *Geological and Hydrological Studies*
4 *of Evaporites in the Northern Delaware Basin for the Waste Isolation Pilot Plant (WIPP), New Mexico.*
5 Geological Society of America 1990 Annual Meeting Field Trip #14 Guidebook. Dallas, TX: Dallas
6 Geological Society. 131-179.
- 7 Beauheim, R.L., G.J. Saulnier, Jr., and J. D. Avis. 1991. *Interpretation of Brine-Permeability Tests of the*
8 *Salado Formation at the Waste Isolation Pilot Plant Site: First Interim Report.* SAND90-0083.
9 Albuquerque, NM: Sandia National Laboratories.
- 10 Bechtel National, Inc. 1986. *Waste Isolation Pilot Plant Design Validation Final Report.* DOE/WIPP-86-010.
11 Prepared for U.S. Department of Energy. San Francisco, CA: Bechtel National, Inc.
- 12 Berglund, J.W. 1990. Appendix A, "Letter 1a: Bar Graphs Representing Range of Values for Drilling
13 Operations Near WIPP Site," *Data Used in Preliminary Performance Assessment of the Waste Isolation*
14 *Pilot Plant (1990).* R.P. Rechar, H. Iuzzolino, and J. S. Sandha (Report Authors). SAND89-2408.
15 Albuquerque, NM: Sandia National Laboratories. A-157 through A-164.
- 16 Berglund, J.W. 1992. *Mechanisms Governing the Direct Removal of Wastes from the Waste Isolation Pilot*
17 *Plant Repository Caused by Exploratory Drilling.* SAND92-7295. Albuquerque, NM: Sandia National
18 Laboratories.
- 19 Bertram-Howery, S.G., and R.L. Hunter, eds. 1989. *Preliminary Plan for Disposal-System Characterization*
20 *and Long-Term Performance Evaluation of the Waste Isolation Pilot Plant.* SAND89-0178.
21 Albuquerque, NM: Sandia National Laboratories.
- 22 Bertram-Howery, S.G., and P.N. Swift. 1990. *Status Report: Potential for Long-Term Isolation by the Waste*
23 *Isolation Pilot Plant Disposal System.* SAND90-0616. Albuquerque, NM: Sandia National Laboratories.
- 24 Bertram-Howery, S.G., M.G. Marietta, R.P. Rechar, P.N. Swift, D.R. Anderson, B.L. Baker, J.E. Bean, Jr.,
25 W. Beyeler, K.F. Brinster, R.V. Guzowski, J.C. Helton, R.D. McCurley, D.K. Rudeen, J.D. Schreiber,
26 and P. Vaughn. 1990. *Preliminary Comparison with 40 CFR Part 191, Subpart B for the Waste*
27 *Isolation Pilot Plant, December 1990.* SAND90-2347. Albuquerque, NM: Sandia National Laboratories.
- 28 Blom, G. 1989. *Probability and Statistics: Theory and Applications.* New York, NY: Springer-Verlag.
- 29 Bonano, E.J., S.C. Hora, R.L. Keeney, and D. von Winterfeldt. 1990. *Elicitation and Use of Expert Judgement*
30 *in Performance Assessment for High-Level Radioactive Waste Repositories.* NUREG/CR-5411,
31 SAND89-1821. Albuquerque, NM: Sandia National Laboratories.

- 1 Borns, D.J., and J.C. Stormont. 1988. *An Interim Report on Excavation Effect Studies at the Waste Isolation*
2 *Pilot Plant: The Delineation of the Disturbed Rock Zone*. SAND87-1375. Albuquerque, NM: Sandia
3 National Laboratories.
- 4 Borns, D.J., and J.C. Stormont. 1989. "The Delineation of the Disturbed Rock Zone Surrounding Excavations in
5 Salt," *Rock Mechanics as a Guide for Efficient Utilization of Natural Resources, Proceedings of the*
6 *30th U.S. Symposium, West Virginia University, Morgantown, WV. June 19-22, 1989*. Ed. A.W. Rhair.
7 Brookfield, VT: A.A. Balkema. 353-360.
- 8 Borns, D.J., L.J. Barrows, D.W. Powers, and R.P. Snyder. 1983. *Deformation of Evaporites Near the Waste*
9 *Isolation Pilot Plant (WIPP) Site*. SAND82-1069. Albuquerque, NM: Sandia National Laboratories.
- 10 Bredehoeft, J.D. 1988. "Will Salt Repositories Be Dry?" *EOS, Transactions, of the American Geophysical*
11 *Union*. Vol. 69, no. 9.
- 12 Brinster, K.F. 1991. *Preliminary Geohydrologic Conceptual Model of the Los Medanos Region Near the Waste*
13 *Isolation Pilot Plant for the Purpose of Performance Assessment*. SAND89-7147. Albuquerque, NM:
14 Sandia National Laboratories.
- 15 Broc, R., ed. 1982. *Drilling Mud and Cement Slurry Rheology Manual*. Houston, TX: Gulf Publishing
16 Company.
- 17 Brodsky, N.S., and T.W. Pfeifle. 1992. *Consolidation of the Waste Isolation Pilot Plant Crushed*
18 *Salt/Bentonite Mixtures as a Function of Confining Pressure and Moisture Content as Compared With*
19 *Constitutive Model Predictions*. SAND91-7071. Albuquerque, NM: Sandia National Laboratories.
- 20 Brookins, D.G., S.J. Lambert, and D.B. Ward. 1990. *Authigenic Clay Minerals in the Rustler Formation,*
21 *WIPP Site, New Mexico*. SAND89-1405. Albuquerque, NM: Sandia National Laboratories.
- 22 Brush, L.H. 1990. *Test Plan for Laboratory and Modeling Studies of Repository and Radionuclide Chemistry*
23 *for the Waste Isolation Pilot Plant*. SAND90-0266. Albuquerque, NM: Sandia National Laboratories.
- 24 Brush, L.H., and D.R. Anderson. 1989a. Appendix E: "Estimates of Radionuclide Concentrations in Brines,"
25 *Performance Assessment Methodology Demonstration: Methodology Development for Purposes of*
26 *Evaluating Compliance with EPA 40 CFR 191, Subpart B, for the Waste Isolation Pilot Plant*. M.G.
27 Marietta, S.G. Bertram-Howery, D.R. Anderson, K.F. Brinster, R.V. Guzowski, H. Iuzzolino, and R.P.
28 Rechar (Report Authors). SAND89-2027. Albuquerque, NM: Sandia National Laboratories. E-1
29 through E-14.

30

31

References

- 1 Brush, L.H., and D.R. Anderson. 1989b. Appendix A.2: "Effects of Microbial Activity on Repository Chemistry,
2 Radionuclide Speciation, and Solubilities in WIPP Brines," *Systems Analysis, Long-Term Radionuclide*
3 *Transport, and Dose Assessments, Waste Isolation Pilot Plant (WIPP), Southeastern New Mexico;*
4 *March 1989.* Eds. A.R. Lappin, R.L. Hunter, D.P. Garber, and P.B. Davies. SAND89-0462.
5 Albuquerque, NM: Sandia National Laboratories. A-31 through A-50.
- 6 Butcher, B.M., C.F. Novak, and M. Jercinovic. 1991. *The Advantages of a Salt/Bentonite Backfill for Waste*
7 *Isolation Pilot Plant Disposal Rooms.* SAND90-3074. Albuquerque, NM: Sandia National Laboratories.
- 8 Cauffman, T.L., A.M. LaVenue, and J.P. McCord. 1990. *Ground-Water Flow Modeling of the Culebra*
9 *Dolomite. Volume II: Data Base.* SAND89-7068/2. Albuquerque, NM: Sandia National Laboratories.
- 10 Chapman, J.B. 1986. *Stable Isotopes in the Southeastern New Mexico Groundwater: Implications for Dating*
11 *Recharge in the WIPP Area.* EEG-35. Santa Fe, NM: Environmental Evaluation Group, Environmental
12 Improvements Division, Health and Environment Department, State of New Mexico.
- 13 Chapman, J.B. 1988. *Chemical and Radiochemical Characteristics of Groundwater in the Culebra Dolomite,*
14 *Southeastern New Mexico.* EEG-39. Santa Fe, NM: Environmental Evaluation Group, Environmental
15 Improvement Division, Health and Environment Department, State of New Mexico.
- 16 Cheeseman, R.J. 1978. "Geology and Oil/Potash Resources of the Delaware Basin, Eddy and Lea Counties, New
17 Mexico," *Geology and Mineral Deposits of Ochoan Rocks in Delaware Basin and Adjacent Areas.* Ed.
18 G.S. Austin. New Mexico Bureau of Mines and Mineral Resources Circular 159. Socorro, NM: New
19 Mexico Bureau of Mines and Mineral Resources. 7-14.
- 20 COHMAP (Cooperative Holocene Mapping Project) Members. 1988. "Climatic Changes of the Last 18,000
21 Years: Observations and Model Simulations," *Science.* Vol. 241, no. 4869, 1043-1052.
- 22 Cole, F.W. 1975. *Introduction to Meteorology.* 2nd. ed. New York, NY: John Wiley and Sons, Inc.
- 23 Cranwell, R.M., J.E. Campbell, J.C. Helton, R.L. Iman, D.E. Longsine, N.R. Ortiz, G.E. Runkle, and M.J.
24 Shortencarier. 1987. *Risk Methodology for Geologic Disposal of Radioactive Waste: Final Report.*
25 NUREG/CR-2452, SAND81-2573. Albuquerque, NM: Sandia National Laboratories.
- 26 Cranwell, R.M., R.V. Guzowski, J.E. Campbell, and N.R. Ortiz. 1990. *Risk Methodology for Geologic*
27 *Disposal of Radioactive Waste: Scenario Selection Procedure.* NUREG/CR-1667, SAND80-1429.
28 Albuquerque, NM: Sandia National Laboratories.
- 29 Darley, H.C.H. 1969. "A Laboratory Investigation of Borehole Stability," *JPT, Journal of Petroleum*
30 *Technology.* Vol. 21, no. 7, 883-892.
- 31 Darley, H.C.H., and G.R. Gray. 1988. *Composition and Properties of Drilling and Completion Fluids.* Houston,
32 TX: Gulf Publishing Company. 243.

- 1 Davies, P.B. 1984. "Deep-Seated Dissolution and Subsidence in Bedded Salt Deposits." Ph.D. dissertation.
2 Stanford, CA: Department of Applied Earth Sciences, Stanford University.
- 3 Davies, P.B. 1989. *Variable-Density Ground-Water Flow and Paleohydrology in the Waste Isolation Pilot*
4 *Plant (WIPP) Region. Southeastern New Mexico.* U.S. Geological Survey Open-File Report 88-490.
5 Albuquerque, NM: U.S. Geological Survey.
- 6 de Marsily, G. 1986. *Quantitative Hydrogeology: Groundwater Hydrology for Engineers.* Orlando, FL:
7 Academic Press, Inc.
- 8 Dosch, R.G. 1980. *Assessment of Potential Radionuclide Transport in Site-Specific Geologic Formations.*
9 SAND79-2468. Albuquerque, NM: Sandia National Laboratories.
- 10 Dosch, R.G. 1981. *Solubility and Sorption Characteristics of Uranium (VI) Associated with Rock Samples and*
11 *Brines/Groundwaters from WIPP and NTS.* SAND80-1595. Albuquerque, NM: Sandia National
12 Laboratories.
- 13 Dosch, R.G., and A.W. Lynch. 1978. *Interaction of Radionuclides with Geomedia Associated with the Waste*
14 *Isolation Pilot Plant (WIPP) Site in New Mexico.* SAND78-0297. Albuquerque, NM: Sandia National
15 Laboratories.
- 16 Earth Technology Corporation. 1988. *Final Report for Time Domain Electromagnetic (TDEM) Surveys at the*
17 *WIPP Site.* SAND87-7144. Albuquerque, NM: Sandia National Laboratories.
- 18 Freeze, R.A., and J.A. Cherry. 1979. *Groundwater.* Englewood Cliffs, NJ: Prentice-Hall, Inc.
- 19 Gallegos, D.P., P.I. Pohl, and C.D. Updegraff. 1992. *An Investigation of the Impact of Conceptual Model*
20 *Uncertainty on the Estimated Performance of a Hypothetical High-Level Nuclear Waste Repository Site*
21 *in Unsaturated, Fractured Tuff.* SAND90-2882. Albuquerque, NM: Sandia National Laboratories.
- 22 Gelhar, L.W., C. Welty, and K.R. Rehfeldt. 1992. "A Critical Review of Data on Field-Scale Dispersion in
23 Aquifers," *Water Resources Research.* Vol. 28, no. 7, 1955-1974.
- 24 Geohydrology Associates, Inc. 1979. *Water-Resources Study of the Carlsbad Potash Area, New Mexico.*
25 Consultant Report for the U.S. BLM. Contract No. YA-S12-CT8-195. (Copy on file in the Waste
26 Management and Transportation Library, Sandia National Laboratories, Albuquerque, NM.)
- 27 Geological Society of America, Inc. 1984. *Decade of North American Geology Geologic Time Scale.*
28 Geological Society of America Map and Chart Series MCH050. Boulder, CO: Geological Society of
29 America, Inc.
- 30 Gilkey, A.P. 1986a. *SPLIT — A Distance-versus-Variable Plot Program for the Output of a Finite Element*
31 *Analysis.* SAND86-0882. Albuquerque, NM: Sandia National Laboratories.

References

- 1 Gilkey, A.P. 1986b. *TYPLOT — A Time History or X-Y Plot Program for the Output of a Finite Element*
2 *Analysis*. SAND86-0883. Albuquerque, NM: Sandia National Laboratories.
- 3 Gilkey, A.P. 1988. *ALGEBRA - A Program That Algebraically Manipulates the Output of a Finite Element*
4 *Analysis*. SAND88-1431. Albuquerque, NM: Sandia National Laboratories.
- 5 Gilkey, A.P., and D.P. Flanagan. 1987. *DETOUR — A Deformed Mesh/Contour Plot Program*. SAND86-
6 0914. Albuquerque, NM: Sandia National Laboratories.
- 7 Guzowski, R.V. 1990. *Preliminary Identification of Scenarios That May Affect the Escape and Transport of*
8 *Radionuclides From the Waste Isolation Pilot Plant, Southeastern New Mexico*. SAND89-7149.
9 Albuquerque, NM: Sandia National Laboratories.
- 10 Guzowski, R.V. 1991. *Evaluation of Applicability of Probability Techniques to Determining the Probability of*
11 *Occurrence of Potentially Disruptive Intrusive Events at the Waste Isolation Pilot Plant*. SAND90-
12 7100. Albuquerque, NM: Sandia National Laboratories.
- 13 Hale, W.E., and A. Clebsch, Jr. 1958. *Preliminary Appraisal of Ground-Water Conditions in Southeastern*
14 *Eddy County and Southwestern Lea County, New Mexico*. Trace Elements Memorandum Report 1045.
15 United States Department of the Interior, Geological Survey. (Copy on file in the Waste Management and
16 Transportation Library, Sandia National Laboratories, Albuquerque, NM.)
- 17 Hale, W.E., L.S. Hughes, and E.R. Cox. 1954. *Possible Improvement of Quality of Water of the Pecos River by*
18 *Diversion of Brine at Malaga Bend, Eddy County, New Mexico*. Carlsbad, NM: Pecos River
19 Commission, New Mexico and Texas, in cooperation with United States Department of the Interior,
20 Geological Survey, Water Resources Division.
- 21 Hansen, J., I. Fung, A. Lacis, D. Rind, S. Lebedeff, R. Ruedy, and G. Russell. 1988. "Global Climate Changes
22 as Forecast by Goddard Institute for Space Studies Three-Dimensional Model," *Journal of Geophysical*
23 *Research*. Vol. 93, no. D8, 9341-9364.
- 24 Harms, J.C., and C.R. Williamson. 1988. "Deep-Water Density Current Deposits of Delaware Mountain Group
25 (Permian), Delaware Basin, Texas and New Mexico," *American Association of Petroleum Geologists*
26 *Bulletin*. Vol. 72, no. 3, 299-317.
- 27 Haug, A., V.A. Kelley, A.M. LaVenue, and J.F. Pickens. 1987. *Modeling of Ground-Water Flow in the*
28 *Culebra Dolomite at the Waste Isolation Pilot Plant (WIPP) Site: Interim Report*. SAND86-7167.
29 Albuquerque, NM: Sandia National Laboratories.
- 30 Hays, J.D., J. Imbrie, and N.J. Shackleton. 1976. "Variations in the Earth's Orbit: Pacemaker of the Ice Ages,"
31 *Science*. Vol. 194, no. 4270, 1121-1132.

- 1 Helton, J.C. In press. "Drilling Intrusion Probabilities for Use in Performance Assessment for Radioactive
2 Waste Disposal," *Reliability Engineering and System Safety*. (Copy on file as SAND93-7001J in Waste
3 Management and Transportation Library, Sandia National Laboratories, Albuquerque, NM.)
- 4 Helton, J.C., J.W. Garner, R.D. McCurley, and D.K. Rudeen. 1991. *Sensitivity Analysis Techniques and
5 Results for Performance Assessment at the Waste Isolation Pilot Plant*. SAND90-7103. Albuquerque,
6 NM: Sandia National Laboratories.
- 7 Helton, J.C., J.W. Garner, R.P. Rechar, D.K. Rudeen, and P.N. Swift. 1992. *Preliminary Comparison with
8 40 CFR Part 191, Subpart B for the Waste Isolation Pilot Plant, December 1991—Volume 4: Uncertainty
9 and Sensitivity Analysis Results*. SAND91-0893/4. Albuquerque, NM: Sandia National Laboratories.
- 10 Hills, J.M. 1984. "Sedimentation, Tectonism, and Hydrocarbon Generation in Delaware Basin, West Texas and
11 Southeastern New Mexico," *American Association of Petroleum Geologists Bulletin*. Vol. 68, no. 3,
12 250-267.
- 13 Hiss, W.L. 1975. "Stratigraphy and Ground-Water Hydrology of the Capitan Aquifer, Southeastern New Mexico
14 and West Texas." Ph.D. dissertation. Boulder, CO: University of Colorado.
- 15 Holt, R.M., and D.W. Powers. 1988. *Facies Variability and Post-Depositional Alteration Within the Rustler
16 Formation in the Vicinity of the Waste Isolation Pilot Plant, Southeastern New Mexico*. DOE/WIPP-88-
17 004. Carlsbad, NM. Westinghouse Electric Corporation.
- 18 Holt, R.M., and D.W. Powers. 1990. *Geologic Mapping of the Air Intake Shaft at the Waste Isolation Pilot
19 Plant*. DOE-WIPP 90-051. Carlsbad, NM: Westinghouse Electric Corporation.
- 20 Hora, S.C., and R.L. Iman. 1989. "Expert Opinion in Risk Analysis: The NUREG-1150 Methodology." *Nuclear
21 Science and Engineering*. Vol. 102, no. 4, 323-331.
- 22 Hora, S.C., D. von Winterfeldt, and K.M. Trauth. 1991. *Expert Judgment on Inadvertent Human Intrusion into
23 the Waste Isolation Pilot Plant*. SAND90-3063. Albuquerque, NM: Sandia National Laboratories.
- 24 Houghton, J.T., G.J. Jenkins, and J.J. Ephraums. 1990. *Climate Change: The IPCC Scientific Assessment*. New
25 York, NY: Cambridge University Press.
- 26 Hunter, R.L. 1985. *A Regional Water Balance for the Waste Isolation Pilot Plant (WIPP) Site and Surrounding
27 Area*. SAND84-2233. Albuquerque, NM: Sandia National Laboratories.
- 28 Hunter, R.L., R.M. Cranwell, and M.S.Y. Chu. 1986. *Assessing Compliance with the EPA High-Level Waste
29 Standard: An Overview*. SAND86-0121, NUREG/CR-4510. Albuquerque, NM: Sandia National
30 Laboratories.

References

- 1 IAEA (International Atomic Energy Agency). 1989. *Evaluating the Reliability of Predictions Made Using*
2 *Environmental Transfer Models*. Safety Series Report No. 100. Vienna: International Atomic Energy
3 Agency.
- 4 Iman, R.L., and W.J. Conover. 1982. "A Distribution-Free Approach to Inducing Rank Correlation Among
5 Input Variables," *Communications in Statistics: Simulation and Computation*. Vol. B11, no. 3, 311-334.
- 6 Iman, R.L. and W.J. Conover. 1983. *A Modern Approach to Statistics*. New York, NY: John Wiley & Sons,
7 Inc.
- 8 Imbrie, J. 1985. "A Theoretical Framework for the Pleistocene Ice Ages," *Journal of the Geological Society*.
9 Vol. 142, pt. 3, 417-432.
- 10 Imbrie, J., and J.Z. Imbrie. 1980. "Modeling the Climatic Response to Orbital Variations," *Science*. Vol. 207,
11 no. 4334, 943-953.
- 12 Imbrie, J., J.D. Hays, D.G. Martinson, A. McIntyre, A.C. Mix, J.J. Morley, N.G. Pisias, W.L. Prell, and N.J.
13 Shackleton. 1984. "The Orbital Theory of Pleistocene Climate: Support from a Revised Chronology of the
14 Marine $\delta^{18}\text{O}$ Record," *Milankovitch and Climate, Proceedings of the NATO Advanced Research*
15 *Workshop on Milankovitch, Palisades, NY, November 30-December 4, 1982*. Eds. A.L. Berger,
16 J. Imbrie, J. Hays, G. Kukla, and B. Saltzman. Boston, MA: D. Reidel Publishing Co. Pt. 1, 269-305.
- 17 Jones, C.L., C.G. Bowles, and K.G. Bell. 1960. *Experimental Drill Hole Logging in Potahs Deposits of the*
18 *Carlsbad District, New Mexico*. U.S. Geological Survey Open File Report 60-84. Denver, CO: U.S.
19 Geological Survey.
- 20 Jones, T.L., V.A. Kelley, J.F. Pickens, D.T. Upton, R.L. Beauheim, and P.B. Davies. 1992. *Integration of*
21 *Interpretation Results of Tracer Tests Performed in the Culebra Dolomite at the Waste Isolation Pilot Plant*
22 *Site*. SAND92-1579. Albuquerque, NM: Sandia National Laboratories.
- 23 Journel, A.G., and Ch.J. Huijbregts. 1978. *Mining Geostatistics*. Orlando, FL: Academic Press, Inc.
- 24 Kaplan, S., and B.J. Garrick. 1981. "On the Quantitative Definition of Risk," *Risk Analysis*. Vol. 1, no. 1,
25 11-27.
- 26 Kelley, V.A., and J.F. Pickens. 1986. *Interpretation of the Convergent-Flow Tracer Tests Conducted in the*
27 *Culebra Dolomite at the H-3 and H-4 Hydropads at the Waste Isolation Pilot Plant (WIPP) Site*. SAND86-
28 7161. Albuquerque, NM: Sandia National Laboratories.
- 29 Kelley, V.A., and G.J. Saulnier, Jr. 1990. *Core Analyses for Selected Samples from the Culebra Dolomite at*
30 *the Waste Isolation Pilot Plant*. SAND90-7011. Albuquerque, NM: Sandia National Laboratories.

- 1 Kunkler, J.L. 1980. *Evaluation of the Malaga Bend Salinity Alleviation Project, Eddy County, New Mexico.*
2 U.S. Geological Survey Open-File Report 80-1111. Albuquerque, NM: U.S. Geological Survey/Water
3 Resources Division and the Pecos River Commission.
- 4 Lambert, S.J. 1983. *Dissolution of Evaporites in and Around the Delaware Basin, Southeastern New Mexico*
5 *and West Texas.* SAND82-0461. Albuquerque, NM: Sandia National Laboratories.
- 6 Lambert S.J. 1987. *Feasibility Study: Applicability of Geochronologic Methods Involving Radiocarbon and*
7 *Other Nuclides to the Groundwater Hydrology of the Rustler Formation, Southeastern New Mexico.*
8 SAND86-1054. Albuquerque, NM: Sandia National Laboratories.
- 9 Lambert, S.J. 1991. Chapter 5: "Isotopic Constraints on the Rustler and Dewey Lake Groundwater Systems,"
10 *Hydrogeochemical Studies of the Rustler Formation and Related Rocks in the Waste Isolation Pilot Plant*
11 *Area, Southeastern New Mexico.* Eds. M.D. Siegel, S.J. Lambert, and K.L. Robinson. SAND88-0196.
12 Albuquerque, NM: Sandia National Laboratories. 5-1 through 5-79.
- 13 Lambert, S.J., and J.A. Carter. 1984. *Uranium-Isotope Disequilibrium in Brine Reservoirs of the Castile*
14 *Formation, Northern Delaware Basin, Southeastern New Mexico, I: Principles and Methods.* SAND83-
15 0144. Albuquerque, NM: Sandia National Laboratories.
- 16 Lambert, S.J., and J.A. Carter. 1987. *Uranium-Isotope Systematics in Groundwaters of the Rustler Formation,*
17 *Northern Delaware Basin, Southeastern New Mexico. I. Principles and Preliminary Results.* SAND87-
18 0388. Albuquerque, NM: Sandia National Laboratories.
- 19 Lambert, S.J., and D.M. Harvey. 1987. *Stable-Isotope Geochemistry of Groundwaters in the Delaware Basin of*
20 *Southeastern New Mexico.* SAND87-0138. Albuquerque, NM: Sandia National Laboratories.
- 21 Lambert, S.J., and J.W. Mercer. 1978. *Hydrologic Investigations of the Los Medaños Area, Southeastern New*
22 *Mexico, 1977.* SAND77-1401. Albuquerque, NM: Sandia National Laboratories.
- 23 Lappin, A.R. 1988. *Summary of Site-Characterization Studies Conducted from 1983 through 1987 at the*
24 *Waste Isolation Pilot Plant (WIPP) Site, Southeastern New Mexico.* SAND88-0157. Albuquerque, NM:
25 Sandia National Laboratories.
- 26 Lappin, A.R., R.L. Hunter, D.P. Garber, P.B. Davies, R.L. Beauheim, D.J. Borns, L.H. Brush, B.M. Butcher,
27 T. Cauffman, M.S.Y. Chu, L.S. Gomez, R.V. Guzowski, H.J. Iuzzolino, V. Kelley, S.J. Lambert, M.G.
28 Marietta, J.W. Mercer, E.J. Nowak, J. Pickens, R.P. Rechard, M. Reeves, K.L. Robinson, and M.D.
29 Siegel. 1989. *Systems Analysis, Long-Term Radionuclide Transport, and Dose Assessments, Waste*
30 *Isolation Pilot Plant (WIPP), Southeastern New Mexico; March 1989.* SAND89-0462. Albuquerque, NM:
31 Sandia National Laboratories.

References

- 1 LaVenue, A.M., and B.S. RamaRao. 1992. *A Modeling Approach to Address Spatial Variability within the*
2 *Culebra Dolomite Transmissivity Field*. SAND92-7306. Albuquerque, NM: Sandia National
3 Laboratories.
- 4 LaVenue, A.M., A. Haug, and V.A. Kelley. 1988. *Numerical Simulation of Groundwater Flow in the Culebra*
5 *Dolomite at the Waste Isolation Pilot Plant (WIPP) Site; Second Interim Report*. SAND88-7002.
6 Albuquerque, NM: Sandia National Laboratories.
- 7 LaVenue, A.M., T.L. Cauffman, and J.F. Pickens. 1990. *Ground-Water Flow Modeling of the Culebra*
8 *Dolomite: Volume 1 - Model Calibration*. SAND89-7068/1. Albuquerque, NM: Sandia National
9 Laboratories.
- 10 Leigh, C.D., B.M. Thompson, J.E. Campbell, D.E. Longsine, R.A. Kennedy, and B.A. Napier. (In review).
11 *User's Guide for GENII-S: A Code for Statistical and Deterministic Simulations of Radiation Doses to*
12 *Humans from Radionuclides in the Environment*. SAND91-0561. Albuquerque, NM: Sandia National
13 Laboratories. (Copy on file in the Waste Management and Transportation Library, Sandia National
14 Laboratories, Albuquerque, NM.)
- 15 Lowenstein, T.K. 1988. "Origin of Depositional Cycles in a Permian "Saline Giant": The Salado (McNutt
16 Zone) Evaporites of New Mexico and Texas," *Geological Society of America Bulletin*. Vol. 100, no. 4,
17 592-608.
- 18 Lynch, A.W., and R.G. Dosch. 1980. *Sorption Coefficients for Radionuclides on Samples from the Water-*
19 *Bearing Magenta and Culebra Members of the Rustler Formation*. SAND80-1064. Albuquerque, NM:
20 Sandia National Laboratories.
- 21 Mantoglou, A., and J.L. Wilson. 1982. "Turning Bands Method for Simulation of Random Fields Using Line
22 Generation by a Spectral Method," *Water Resources Research*. Vol. 18, no. 5, 1379-1394.
- 23 Marietta, M.G., S.G. Bertram-Howery, D.R. Anderson, K.F. Brinster, R.V. Guzowski, H. Iuzzolino, and R.P.
24 Rechard. 1989. *Performance Assessment Methodology Demonstration: Methodology Development for*
25 *Evaluating Compliance With EPA 40 CFR Part 191, Subpart B, for the Waste Isolation Pilot Plant*.
26 SAND89-2027. Albuquerque, NM: Sandia National Laboratories.
- 27 Matheron, G. 1971. *The Theory of Regionalized Variables and its Applications*. Fontainebleau, France: École
28 National Supérieure des Mines.
- 29 Matheron, G. 1973. "The Intrinsic Random Functions and Their Applications," *Advances in Applied*
30 *Probability*. Vol. 5, no. 3, 439-468.
- 31 McGrath, E.J., and D.C. Irving. 1975a. *Techniques for Efficient Monte Carlo Simulation. Volume II. Random*
32 *Number Generation for Selected Probability Distributions*. ORNL-RSIC-38 (Vol. 2). Oak Ridge, TN:
33 Oak Ridge National Laboratory.

- 1 McGrath, E.J., and D.C. Irving. 1975b. *Techniques for Efficient Monte Carlo Simulation. Volume III.*
2 *Variance Reduction.* ORNL-RSIC-38 (Vol. 3). Oak Ridge, TN: Oak Ridge National Laboratory.
- 3 McGrath, E.J., S.L. Basin, R.W. Burton, D.C. Irving, and S.C. Jaquette. 1975. *Techniques for Efficient*
4 *Monte Carlo Simulation. Volume I. Selecting Probability Distributions.* ORNL-RSIC-38. (Vol. 1). Oak
5 Ridge, TN: Oak Ridge National Laboratory.
- 6 McKay, M.D., R.J. Beckman, and W.J. Conover. 1979. "A Comparison of Three Methods for Selecting Values
7 of Input Variables in the Analysis of Output from a Computer Code," *Technometrics.* (Vol. 21). no. 2,
8 239-245.
- 9 Mejía, J.M., and I. Rodríguez-Iturbe. 1974. "On the Synthesis of Random Fields From the Spectrum: An
10 Application to the Generation of Hydrologic Spatial Processes," *Water Resources Research.* Volume 10,
11 no. 4, 705-711.
- 12 Mercer, J.W. 1983. *Geohydrology of the Proposed Waste Isolation Pilot Plant Site, Los Medaños Area,*
13 *Southeastern New Mexico.* U.S. Geological Survey Water-Resources Investigations Report 83-4016.
14 Albuquerque, NM: U.S. Geological Survey.
- 15 Mercer, J.W., and B.R. Orr. 1977. *Review and Analysis of Hydrogeologic Conditions Near the Site of a*
16 *Potential Nuclear-Waste Repository, Eddy and Lea Counties, New Mexico.* U.S. Geological Survey
17 Open-File Report 77-123. Albuquerque, NM: U.S. Geological Survey.
- 18 Mercer, J.W., and B.R. Orr. 1979. *Interim Data Report on Geohydrology of the Proposed Waste Isolation Pilot*
19 *Plant Site, Southeast New Mexico.* U.S. Geological Survey Water-Resources Investigations 79-98.
20 Albuquerque, NM: U.S. Geological Survey.
- 21 Mercer, J.W., R.L. Beauheim, R.P. Snyder, and G.M. Fairer. 1987. *Basic Data Report for Drilling and*
22 *Hydrologic Testing of Drillhole DOE-2 at the Waste Isolation Pilot Plant (WIPP) Site.* SAND86-0611.
23 Albuquerque, NM: Sandia National Laboratories.
- 24 Milankovitch, M. 1941. *Canon of Insolation and the Ice-age Problem.* Koniglich Serbische Akademie, Beograd.
25 (English translation by the Israel Program for Scientific Translations; published by the U.S. Department of
26 Commerce and the National Science Foundation, Washington, D.C.).
- 27 Mills, P.G. 1984. *Blowout Prevention Theory and Applications.* Boston, MA: International Human Resources
28 Development Corporation. 27-28.
- 29 Mitchell, J.F.B. 1989. "The 'Greenhouse Effect' and Climate Change," *Reviews of Geophysics.* Vol. 27, no. 1,
30 115-139.

References

- 1 Munson, D.E., A.F. Fossum, and P.E. Senseny. 1989a. *Advances in Resolution of Discrepancies Between*
2 *Predicted and Measured In Situ WIPP Room Closures*. SAND88-2948. Albuquerque, NM: Sandia
3 National Laboratories.
- 4 Munson, D.E., A.F. Fossum, and P.E. Senseny. 1989b. *Approach to First Principles Model Prediction of*
5 *Measured WIPP In Situ Room Closure in Salt*. SAND88-2535. Albuquerque, NM: Sandia National
6 Laboratories.
- 7 NEA (Nuclear Energy Agency). 1992. *Safety Assessment of Radioactive Waste Repositories: Systematic*
8 *Approaches to Scenario Development*. Paris: Nuclear Energy Agency, Organisation for Economic Co-
9 Operation and Development.
- 10 Neuman, S.P. 1990. "Universal Scaling of Hydraulic Conductivities and Dispersivities in Geologic Media,"
11 *Water Resources Research*. Vol. 26, no. 8, 1749-1758.
- 12 Nowak, E.J. 1980. *Radionuclide Sorption and Migration Studies of Getters for Backfill Barriers*. SAND79-
13 1110. Albuquerque, NM: Sandia National Laboratories.
- 14 Nowak, E.J., and J.C. Stormont. 1987. *Scoping Model Calculations of the Reconsolidation of Crushed Salt in*
15 *WIPP Shafts*. SAND87-0879. Albuquerque, NM: Sandia National Laboratories.
- 16 Nowak, E.J., D.F. McTigue, and R. Beraun. 1988. *Brine Inflow to WIPP Disposal Rooms: Data, Modeling,*
17 *and Assessment*. SAND88-0112. Albuquerque, NM: Sandia National Laboratories.
- 18 Nowak, E.J., J.R. Tillerson, and T.M. Torres. 1990. *Initial Reference Seal System Design: Waste Isolation Pilot*
19 *Plant*. SAND90-0355. Albuquerque, NM: Sandia National Laboratories.
- 20 NuPac (Nuclear Packaging, Inc.). 1989. *Safety Analysis Report for the TRUPACT-II Shipping Package*. NuPac
21 TRUPACT-II SAR Rev. 4. Washington, DC: Nuclear Packaging, Inc.
- 22 Oldroyd, J.G. 1958. "Non-Newtonian Effects in Steady Motion of Some Idealized Elastico-Viscous Liquids,"
23 *Proceedings of the Royal Society of London*. Series A, Vol. 245, no. 1241, 278-297.
- 24 Pace, B.O. 1990. Appendix A, "Letter 1b: Changes to Bar graphs," *Data Used in Preliminary Performance*
25 *Assessment of the Waste Isolation Pilot Plant (1990)*. R.P. Rechar, H. Iuzzolino, and J.S. Sandha
26 (Report Authors). SAND89-2408. Albuquerque, NM: Sandia National Laboratories. A-165 through A-
27 170.
- 28 Parry, G.W. 1988. "On the Meaning of Probability in Probabilistic Safety Assessment," *Reliability*
29 *Engineering and System Safety*. Vol. 23, no. 4, 309-314.
- 30 Paté-Cornell, M.E. 1986. "Probability and Uncertainty in Nuclear Safety Decisions," *Nuclear Engineering and*
31 *Design*. Vol. 93, no. 3, 319-327.

- 1 Peterson, E.W., P.L. Lagus, and K. Lic. 1987. *Fluid Flow Measurements of Test Series A and B for the Small*
2 *Scale Seal Performance Tests*. SAND87-7041. Albuquerque, NM: Sandia National Laboratories.
- 3 Pfeifle, T.W., and N. S. Brodsky. 1991. *Swelling Pressure, Water Uptake, and Permeability of 70/30 Crushed*
4 *Salt Bentonite*. SAND91-7070. Albuquerque, NM: Sandia National Laboratories.
- 5 Popielak, R.S., R.L. Beauheim, S.R. Black, W.E. Coons, C.T. Ellingson, and R.L. Olsen. 1983. *Brine*
6 *Reservoirs in the Castile Fm., Waste Isolation Pilot Plant (WIPP) Project, Southeastern New Mexico*.
7 TME-3153. Carlsbad, NM: U.S. Department of Energy.
- 8 Powers, D.W., and R.M. Holt. 1990. "Sedimentology of the Rustler Formation near the Waste Isolation Pilot
9 Plant (WIPP) Site," *Geological and Hydrological Studies of Evaporites in the Northern Delaware Basin*
10 *for the Waste Isolation Pilot Plant (WIPP), New Mexico, Geological Society of America 1990 Annual*
11 *Meeting, Dallas, TX, October 29-November 1, 1990*. Geological Society of America 1990 Annual
12 Meeting, Field Trip #14 Guidebook. Dallas, TX: Dallas Geological Society. 79-106.
- 13 Powers, D.W., S.J. Lambert, S-E. Shaffer, L.R. Hill, and W.D. Weart, eds. 1978a. *Geological Characterization*
14 *Report, Waste Isolation Pilot Plant (WIPP) Site, Southeastern New Mexico*. SAND78-1596.
15 Albuquerque, NM: Sandia National Laboratories. Vol. I.
- 16 Powers, D.W., S.J. Lambert, S-E. Shaffer, L.R. Hill, and W.D. Weart, eds. 1978b. *Geological Characterization*
17 *Report, Waste Isolation Pilot Plant (WIPP) Site, Southeastern New Mexico*. SAND78-1596.
18 Albuquerque, NM: Sandia National Laboratories. Vol. II.
- 19 Public Law 102-579. 1992. *Waste Isolation Pilot Plant Land Withdrawal Act*.
- 20 RamaRao, B.S., and M. Reeves. 1990. *Theory and Verification for the GRASP II Code for Adjoint-Sensitivity*
21 *Analysis of Steady-State and Transient Ground-Water Flow*. SAND89-7143. Albuquerque, NM: Sandia
22 National Laboratories.
- 23 Rechar, R.P. 1989. *Review and Discussion of Code Linkage and Data Flow in Nuclear Waste Compliance*
24 *Assessments*. SAND87-2833. Albuquerque, NM: Sandia National Laboratories.
- 25 Rechar, R.P., ed. 1992. *User's Reference Manual for CAMCON: Compliance Assessment Methodology*
26 *Controller Version 3.0*. SAND90-1983. Albuquerque, NM: Sandia National Laboratories.
- 27 Rechar, R.P., H.J. Iuzzolino, J.S. Rath, A.P. Gilkey, R.D. McCurley, and D.K. Rudeen. 1989. *User's Manual*
28 *for CAMCON: Compliance Assessment Methodology Controller*. SAND88-1496. Albuquerque, NM:
29 Sandia National Laboratories.
- 30 Rechar, R.P., H. Iuzzolino, and J.S. Sandha. 1990a. *Data Used in Preliminary Performance Assessment of*
31 *the Waste Isolation Pilot Plant (1990)*. SAND89-2408. Albuquerque, NM: Sandia National Laboratories.

References

- 1 Rechard, R.P., W. Beyeler, R.D., McCurley, D.K. Rudeen, J.E. Bean, and J.D. Schreiber. 1990b. *Parameter*
2 *Sensitivity Studies of Selected Components of the Waste Isolation Pilot Plant Repository/Shaft System.*
3 SAND89-2030. Albuquerque, NM: Sandia National Laboratories.
- 4 Robinson, T.W., and W.B. Lang. 1938. *Geology and Ground-Water Conditions of the Pecos River Valley in the*
5 *Vicinity of Laguna Grande de la Sal, New Mexico, With Special Reference to the Salt Content of the*
6 *River Water.* New Mexico State Engineer 12th-13th Biennial Reports 1934-1938. Santa Fe, NM: State
7 Engineer. 77-100.
- 8 Saulnier, G.J., Jr. 1987. *Analysis of Pumping Tests of the Culebra Dolomite Conducted at the H-11 Hydropad at*
9 *the Waste Isolation Pilot Plant (WIPP) Site.* SAND87-7124. Albuquerque, NM: Sandia National
10 Laboratories.
- 11 Saulnier, G.J., Jr., and J.D. Avis. 1988. *Interpretation of Hydraulic Tests Conducted in the Waste-Handling*
12 *Shaft at the Waste Isolation Pilot Plant (WIPP) Site.* SAND88-7001. Albuquerque, NM: Sandia National
13 Laboratories.
- 14 Savins, J.G., and G.C. Wallick. 1966. "Viscosity Profiles, Discharge Rates, Pressures, and Torques for a
15 Rheologically Complex Fluid in a Helical Flow," *A.I.Ch.E. Journal.* Vol. 12, no. 2, 357-363.
- 16 Scheidegger, A.E. 1960. *The Physics of Flow Through Porous Media.* Rev. ed. Toronto, Canada: University of
17 Toronto Press.
- 18 Serne, R.J., D. Rai, M.J. Mason, and M.A. Molecke. 1977. *Batch Kd Measurements of Nuclides to Estimate*
19 *Migration Potential at the Proposed Waste Isolation Pilot Plant in New Mexico.* PNL-2448. Richland,
20 WA: Battelle Pacific Northwest Laboratories.
- 21 Sewards, T. 1991. *Characterization of Fracture Surfaces in Dolomite Rock, Culebra Dolomite Member,*
22 *Rustler Formation.* SAND90-7019. Albuquerque, NM: Sandia National Laboratories.
- 23 Sewards, T., M.L. Williams, and K. Keil. 1991a. *Mineralogy of the Culebra Dolomite Member of the Rustler*
24 *Formation.* SAND90-7008. Albuquerque, NM: Sandia National Laboratories.
- 25 Sewards, T., R. Glenn, and K. Keil. 1991b. *Mineralogy of the Rustler Formation in the WIPP-19 Core.*
26 SAND87-7036. Albuquerque, NM: Sandia National Laboratories.
- 27 Sewards, T., A. Brearley, R. Glenn, I.D.R. MacKinnon, and M.D. Siegel. 1992. *Nature and Genesis of Clay*
28 *Minerals of the Rustler Formation in the Vicinity of the Waste Isolation Pilot Plant in Southeastern New*
29 *Mexico.* SAND90-2569. Albuquerque, NM: Sandia National Laboratories.
- 30 Shinozuka, M., and C-M. Jan. 1972. "Digital Simulation of Random Processes and Its Applications," *Journal*
31 *of Sound and Vibration.* Vol. 25, no. 1, 111-128.

- 1 Short, J.A. 1982. *Drilling and Casing Operations*. Tulsa, OK: PennWell Books. 183-184.
- 2 Siegel, M.D. 1990. Appendix A, "Memo 3a: Representation of Radionuclide Retardation in the Culebra
3 Dolomite in Performance Assessment Calculations," *Data Used in Preliminary Performance Assessment*
4 *of the Waste Isolation Pilot Plant* (1990). R.P. Rechar, H. Iuzzolino, and J.S. Sandha (Report Authors).
5 SAND89-2408. Albuquerque, NM: Sandia National Laboratories. A-43 through A-62.
- 6 Siegel, M.D., J.O. Leckie, S.W. Park, S.L. Phillips, and T. Sowards. 1990. *Studies of Radionuclide Sorption*
7 *by Clays in the Culebra Dolomite at the Waste Isolation Pilot Plant Site, Southeastern New Mexico*.
8 SAND89-2387. Albuquerque, NM: Sandia National Laboratories.
- 9 Siegel, M.D., and S.J. Lambert. 1991. Chapter 1: "Summary of Hydrogeochemical Constraints on Groundwater
10 Flow and Evolution in the Rustler Formation," *Hydrogeochemical Studies of the Rustler Formation and*
11 *Related Rocks in the Waste Isolation Pilot Plant Area, Southeastern New Mexico*. Eds. M.D. Siegel, S.J.
12 Lambert, and K.L. Robinson. SAND88-0196. Albuquerque, NM: Sandia National Laboratories. 1-1
13 through 1-109.
- 14 Siegel, M.D., K.L. Robinson, and J. Myers. 1991. Chapter 2: "Solute Relationships in Groundwaters from the
15 Culebra Dolomite and Related Rocks in the Waste Isolation Pilot Plant Area, Southeastern New Mexico,"
16 *Hydrogeochemical Studies of the Rustler Formation and Related Rocks in the Waste Isolation Pilot Plant*
17 *Area, Southeastern New Mexico*. Eds. M. D. Siegel, S.J. Lambert, and K.L. Robinson. SAND88-0196.
18 Albuquerque, NM: Sandia National Laboratories. 2-1 through 2-164.
- 19 Skokan, C., J. Starrett, and H.T. Anderson. 1988. *Final Report: Feasibility Study of Seismic Tomography to*
20 *Monitor Underground Pillar Integrity at the WIPP Site*. SAND88-7096. Albuquerque, NM: Sandia
21 National Laboratories.
- 22 Smith, L., and R.A. Freeze. 1979. "Stochastic Analysis of Steady State Groundwater Flow in a Bounded
23 Domain, 2. Two-Dimensional Simulations," *Water Resources Research*. Vol. 15, no. 6, 1543-1559.
- 24 Smith, L., and F.W. Schwartz. 1981. "Mass Transport, 2. Analysis of Uncertainty in Prediction," *Water*
25 *Resources Research*. Vol. 17, no. 2, 351-369.
- 26 Snyder, R.P. 1985. *Dissolution of Halite and Gypsum, and Hydration of Anhydrite to Gypsum, Rustler*
27 *Formation, in the Vicinity of the Waste Isolation Pilot Plant, Southeastern New Mexico*. Open-File
28 Report 85-229. Denver, CO: U.S. Geological Survey.
- 29 Stone, C.M., R.D. Krieg, and Z.E. Beisinger. 1985. *SANCHO: A Finite Element Computer Program for the*
30 *Quasistatic, Large Deformation, Inelastic Response of Two-Dimensional Solids*. SAND84-2618.
31 Albuquerque, NM: Sandia National Laboratories.
- 32 Stormont, J.C. 1988. *Preliminary Seal Design Evaluation for the Waste Isolation Pilot Plant*. SAND87-3083.
33 Albuquerque, NM: Sandia National Laboratories.

References

- 1 Stormont, J.C., E.W. Peterson, and P.L. Lagus. 1987. *Summary of and Observations About WIPP Facility*
2 *Horizon Flow Measurements Through 1986*. SAND87-0176. Albuquerque, NM: Sandia National
3 Laboratories.
- 4 Swift, P.N. 1991. "Appendix A: Climate and recharge variability parameters for the 1991 WIPP PA
5 calculations," *Preliminary Comparison with 40 CFR Part 191, Subpart B for the Waste Isolation Pilot*
6 *Plant, December 1991 — Volume 3: Reference Data*. WIPP Performance Assessment Division (Report
7 Author). SAND91-0893/3. Albuquerque, NM: Sandia National Laboratories. A-107 through A-122.
- 8 Swift, P.N. 1992. *Long-Term Climate Variability at the Waste Isolation Pilot Plant, Southeastern New*
9 *Mexico, USA*. SAND91-7055. Albuquerque, NM: Sandia National Laboratories.
- 10 Taylor, L.M., D.P. Flanagan, and W.C. Mills-Curran. 1987. *The GENESIS Finite Element Mesh File Format*.
11 SAND86-0910. Albuquerque, NM: Sandia National Laboratories.
- 12 Tien, P-L., F.B. Nimick, A.B. Muller, P.A. Davis, R.V. Guzowski, L.E. Duda, and R.L. Hunter. 1983.
13 *Repository Site Data and Information in Bedded Salt: Palo Duro Basin, Texas*. SAND82-2223,
14 NUREG/CR-3129. Albuquerque, NM: Sandia National Laboratories.
- 15 Tierney, M.S. 1990. *Constructing Probability Distributions of Uncertain Variables in Models of the*
16 *Performance of the Waste Isolation Pilot Plant: The 1990 Performance Simulations*. SAND90-2510.
17 Albuquerque, NM: Sandia National Laboratories.
- 18 Trauth, K.M., S.C. Hora, R.P. Rechar, and D.R. Anderson. 1992. *The Use of Expert Judgment to Quantify*
19 *Uncertainty in Solubility and Sorption Parameters for Waste Isolation Pilot Plant Performance*
20 *Assessment*. SAND92-0479. Albuquerque, NM: Sandia National Laboratories.
- 21 Tyler, L.D., R.V. Matalucci, M.A. Molecke, D.E. Munson, E.J. Nowak, and J.C. Stormont. 1988. *Summary*
22 *Report for the WIPP Technology Development Program for Isolation of Radioactive Waste*. SAND88-
23 0844. Albuquerque, NM: Sandia National Laboratories.
- 24 U.S. DOE (Department of Energy). 1980. *Final Environmental Impact Statement: Waste Isolation Pilot Plant*.
25 DOE/EIS-0026. Washington, DC: U.S. Department of Energy. Vols. 1-2.
- 26 U.S. DOE (Department of Energy). 1990a. *WIPP Test Phase Plan: Performance Assessment*. DOE/WIPP 89-
27 011, Rev. 0. Carlsbad, NM: U.S. Department of Energy, Waste Isolation Pilot Plant.
- 28 U.S. DOE (Department of Energy). 1990b. *Recommended Initial Waste Forms for the WIPP Experimental Test*
29 *Program, May 1990, Engineered Alternatives Task Force*. DOE/WIPP 90-009. Carlsbad, NM:
30 Westinghouse Electric Corporation.
- 31 U.S. DOE (Department of Energy). 1991a. *Waste Acceptance Criteria for the Waste Isolation Pilot Plant*.
32 WIPP-DOE-069, Rev. 4.0. Carlsbad, NM: Westinghouse Electric Corporation.

- 1 U.S. DOE (Department of Energy). 1991b. *Integrated Data Base for 1991: U.S. Spent Fuel and Radioactive*
2 *Waste Inventories, Projections, and Characteristics*. DOE/RW-0006, Rev. 7. Oak Ridge, TN: Oak
3 Ridge National Laboratory.
- 4 U.S. DOE (Department of Energy). 1991c. *Draft Report: Evaluation of the Effectiveness and Feasibility of the*
5 *Waste Isolation Pilot Plant Engineered Alternatives: Final Report of the Engineered Alternatives Task*
6 *Force*. DOE/WIPP 91-007, Revision 0. Carlsbad, NM: Westinghouse Electric Corporation.
- 7 U.S. DOE (Department of Energy). 1992. *WIPP Test Phase Activities in Support of Critical Performance*
8 *Assessment Information Needs (40 CFR 191, Subpart B)*. Attachment I. Washington, DC: U.S.
9 Department of Energy.
- 10 U.S. DOE (Department of Energy) and State of New Mexico. 1981, as modified. "Agreement for Consultation
11 and Cooperation" on WIPP by the State of New Mexico and U.S. Department of Energy, modified
12 11/30/84, 8/4/87, and 4/18/88.
- 13 U.S. EPA (Environmental Protection Agency). 1985. "40 CFR Part 191: Environmental Standards for the
14 Management and Disposal of Spent Nuclear Fuel, High-Level and Transuranic Radioactive Wastes Final
15 Rule," *Federal Register*. Vol. 50, no. 182, 38066-38089.
- 16 U.S. EPA (Environmental Protection Agency). 1986. "40 CFR Part 268 Land Disposal Restrictions," as
17 amended and published in the most recent *Code of Federal Regulations*. Washington, DC: Office of the
18 Federal Register, National Archives and Records Administration.
- 19 University of New Mexico. 1989. *New Mexico Statistical Abstract 1989*. Albuquerque, NM: Bureau of Business
20 and Economic Research, University of New Mexico.
- 21 Vesely, W.E., and D.M. Rasmuson. 1984. "Uncertainties in Nuclear Probabilistic Risk Analyses," *Risk*
22 *Analysis*. Vol. 4, no. 4, 313-322.
- 23 Vine, J.D. 1963. *Surface Geology of the Nash Draw Quadrangle, Eddy County, New Mexico*. U.S. Geological
24 Survey Bulletin 1141-B. Washington, DC: U.S. Government Printing Office.
- 25 Walker, R.E. 1976. "Hydraulic Limits are Set by Flow Restrictions," *Oil and Gas Journal*. Vol. 74, no. 40,
26 86-90.
- 27 Walker, R.E., and W.E. Holman. 1971. "Computer Program Predicting Drilling-Fluid Performance," *Oil and*
28 *Gas Journal*. Vol. 69, no. 13, 80-90.
- 29 Ward, R.F., C.G. St. C. Kendall, and P.M. Harris. 1986. "Upper Permian (Guadalupian) Facies and Their
30 Association with Hydrocarbons - Permian Basin, West Texas and New Mexico," *American Association of*
31 *Petroleum Geologists Bulletin*. Vol. 70, no. 3, 239-262.

References

- 1 Wehr, R.M., J.A. Richards, Jr., and T.W. Adair III. 1984. *Physics of the Atom*. 4th ed. Reading, MA. Addison-
2 Wesley Publishing Company.
- 3 Whittaker, A., ed. 1985. *Theory and Application of Drilling Fluid Hydraulics*. Boston, MA: International
4 Human Resources Development Corporation.
- 5 Williamson, C.R. 1978. "Depositional Processes, Diagenesis and Reservoir Properties of Permian Deep-Sea
6 Sandstone Bell Canyon Formation." Ph.D. dissertation. Austin, TX: University of Texas.
- 7 WIPP PA (Performance Assessment) Division. 1991a. *Preliminary Comparison with 40 CFR Part 191, Subpart
8 B for the Waste Isolation Pilot Plant, December 1991 — Volume 1: Methodology and Results*. SAND91-
9 0893/1. Albuquerque, NM: Sandia National Laboratories.
- 10 WIPP PA (Performance Assessment) Division. 1991b. *Preliminary Comparison with 40 CFR Part 191, Subpart
11 B for the Waste Isolation Pilot Plant, December 1991— Volume 2: Probability and Consequence
12 Modeling*. SAND91-0893/2. Albuquerque, NM: Sandia National Laboratories.
- 13 WIPP Performance Assessment Division (WIPP PA Division). 1991c. *Preliminary Comparison with 40 CFR
14 Part 191, Subpart B for the Waste Isolation Pilot Plant, December 1991 — Volume 3: Reference Data*.
15 SAND91-0893/3. Albuquerque, NM: Sandia National Laboratories.
- 16 Zimmerman, A., and J.L. Wilson. 1990. *Description of and User's Manual for TUBA: A Computer Code for
17 Generating Two-Dimensional Random Fields via the Turning Bands Method*. Albuquerque, NM: Gram,
18 Inc.

**APPENDIX A:
BRAGFLO AND PANEL**

APPENDIX A: BRAGFLO AND PANEL

A.1 Background

The WIPP PA Department has developed a computational model called BRAGFLO (BRine And Gas FLOW) to simulate two-phase flow through porous, heterogeneous reservoirs. BRAGFLO numerically solves the coupled nonlinear partial differential equations (PDEs) describing the mass conservation of the gas and brine components distributed between the gas and liquid phases. Finite difference methods are used to develop analogs of the mass conservation PDEs in two spatial dimensions. These analogs are integrated over time using a modified Newton-Raphson method and variable time spacing.

BRAGFLO output is used to provide input for an equilibrium-mixing cell mathematical model called PANEL to evaluate radionuclide concentrations resulting from the mixing of brine with waste. PANEL has no geometry; it can be thought of as a point. The brine flow up the borehole that is calculated by BRAGFLO is input to PANEL so that appropriate amounts of radionuclides determined by their respective solubilities can be added to the brine flow.

A.1.1 BRAGFLO Features and Limitations

BRAGFLO is a modeling tool that can accommodate conceptual model changes and is therefore well suited to test various alternative conceptual models. This flexibility results, in part, from the highly structured and modular coding style used. BRAGFLO is also designed to be robust and numerically stable when simulating multiphase flow over a wide range of conditions and input property values.

Current limitations of BRAGFLO include:

- Only isothermal two-phase flow is modeled.
- Only two components or chemical species are modeled, and only one of the components can be distributed between both phases, such as a gas component existing in the gas phase and a water or oil phase as dissolved gas. In the case of the WIPP performance assessment, the waste-generated gas exists in both the gas phase and the brine phase, but the brine exists only in the brine phase (the brine has zero vapor pressure).
- The porous medium within each numerical grid block is treated as a single continuum; discrete fracturing or dual porosity is not considered.
- Grid block connectivity is not arbitrary and is fixed by spatial constraints. The solution domain cannot be modeled by mixed dimensionality.

- 1 • If two phases or components exist anywhere in the repository, both component mass balances must be
2 solved everywhere in the repository even though isolated areas may be governed solely by single-phase
3 flow.

- 4 • Non-Darcy flow, where flow is proportional to a potential gradient (for example, molecular diffusion) is not
5 modeled.

- 6 • Fluids are assumed to exhibit Newtonian behavior (fluid viscosity does not vary with rate or time of shear).

7 **A.1.2 Performance Assessment Role of BRAGFLO and PANEL**

8 The WIPP PA Department is using BRAGFLO to study the effects of gas on the flow of brine through the
9 repository and up an intrusion borehole. Specifically, BRAGFLO models the effects of the interaction of the
10 following phenomena:

- 11 • gas generation from corrosion and microbiological degradation of the waste,

- 12 • brine movement from the surrounding rock through the waste over time,

- 13 • possible saturation of the waste by mixing with brine from an underlying pressurized reservoir that reaches
14 the waste through a borehole created by an exploratory drill bit, and

- 15 • creep closure of the surrounding host rock.

16 BRAGFLO uses wells to model gas generation from corrosion and microbiological degradation of the waste,
17 the brine flow from a breached underlying pressurized brine pocket, and brine influx from the surrounding host
18 rock. In BRAGFLO, wells may be accommodated by using simple well models or by directly including well
19 geometry and properties in the numerical mesh. This process is described in detail in the 1991 performance
20 assessment documentation (see Section 5.2.2.5 of WIPP PA Division, 1991).

21 PANEL uses the results of BRAGFLO to predict mixing of radionuclides with brine (see Section A.3).

22 Creep closure of the host rock surrounding the repository will result in pressurization or rock deformation,
23 changing material porosities and permeabilities. Presently, BRAGFLO is capable of using as input varying room
24 porosity, which changes with closure as predicted by SANCHO (Appendix B). Porosities and absolute
25 permeabilities of all other materials in the modeled waste room are currently treated as imprecisely known
26 constants.

A.2 Flow (BRAGFLO)

A.2.1 Fundamental Equations

The BRAGFLO flow model simultaneously solves five equations:

- a partial differential equation that describes the mass conservation of gas in the repository and surrounding formation,
- a partial differential equation that describes the mass conservation of the brine in the repository and surrounding formation,
- a saturation constraint equation,
- a mass fraction constraint equation on the components making up the brine phase, and
- a capillary pressure constraint equation.

The above equations, along with appropriate boundary and initial conditions and material property relationships, form the basis of the model's fundamental equations. These equations are described in detail in Volume 3 of this report (Section 1.4.1) and the 1991 performance assessment documentation (see Section 5.2 of WIPP PA Division, 1991).

A.2.2 General Conceptualization

BRAGFLO can simulate the simultaneous flow of two immiscible phases through a porous anisotropic reservoir. The reservoir may consist of many materials with widely differing characteristics. Reservoir properties may also vary spatially within a particular material type.

A description of multiphase porous media flow is necessary to understand the assumptions involved in modeling multiphase flow through porous media. Details of the equations of motion for multiphase flow describing assumptions, derivations, and implementation are wide-spread throughout the petroleum literature (Bear et al., 1968; Bear, 1975, 1979; Dake, 1978; Crichlow, 1977; Collins, 1961; Aziz and Settari, 1979; Peaceman, 1977; Crookston et al., 1979; Coats, 1980; Vaughn, 1986; Rubin and Vinsome, 1979; Scheidegger, 1960). The nomenclature, assumptions, and conceptualization used here are typical of those found in much of the multiphase reservoir modeling literature referenced above.

BRAGFLO is based on a description of porous media presented by Bear (1975), Bear et al. (1968), and Bear and Bachmat (1967). The porous media is characterized as a portion of space occupied by heterogeneous matter made up of a solid phase and at least one fluid phase. The space that is occupied by the fluid phases is called the

1 pore or void space. Some of the pores are interconnected (effective porosity) and others are not. This void space
 2 forms a tortuous network of randomly sized and located channels. The porous medium forms a continuum with
 3 the solid matrix present in each representative volume.

4 The conceptualization of fluid flow through such a porous media is consistent with assumptions and
 5 descriptions presented in Bear (1975). The fluids are assumed to be Newtonian and may be compressible. The
 6 flow in the void space is laminar and confined to well-defined channels with fluid particles moving parallel to the
 7 channel walls. The forces acting on the fluid particles result only from pressure, gravity, capillary action, and
 8 shear. Flow in the network of channels contained in a given volume gives rise to average gradients that are
 9 independent of the geometry of individual channels.

10 BRAGFLO simulates multiphase flow through porous media. Two types of multiphase flow are possible,
 11 miscible and immiscible. BRAGFLO considers immiscible displacement only. In this case, both fluids flow
 12 simultaneously through the porous network. The two fluid phases are separated by an interface whose curvature
 13 and surface tension give rise to a capillary pressure difference across the interface (Brooks and Corey, 1964; Corey,
 14 1986; Peaceman, 1977; Dake, 1978; Crichlow, 1977; Collins, 1961). The interface is assumed to be abrupt and
 15 any transitions from one phase to another occur over a distance of negligible length compared to the channel
 16 diameter (Bear, 1975).

17 The concept of saturation is introduced to describe the occupation of void space by more than one fluid.
 18 Saturation is defined as the volume fraction of void space occupied by a particular fluid. Interfacial tension exists
 19 where the two immiscible fluids contact each other. The shape of the resulting meniscus defines the wettability of
 20 the system (Brooks and Corey, 1964; Bear, 1975). For example, the convex side of the meniscus faces toward the
 21 wetting phase, while the concave side faces toward the non-wetting phase. Interfacial tension and wettability may
 22 depend on the direction the interface is moving. This phenomenon is called hysteresis. Hysteresis is a secondary
 23 effect and is not currently modeled (Brooks and Corey, 1964).

24 Three saturation regions are differentiated in the two-phase system, brine and gas, for example. Assuming a
 25 brine-wet reservoir, at low brine saturations, brine forms in isolated rings or exists as a thin film. As brine
 26 saturation increases, a condition is reached where the brine forms a continuous phase that is capable of
 27 transmitting pressure. Above this critical saturation or "irreducible saturation," brine flow is possible. Potential
 28 flow of brine below the irreducible brine saturation will not occur. At high brine saturations, brine isolates the
 29 gas and the gas no longer forms a continuous phase. This occurs at the irreducible gas saturation.

30 Bear's continuum approach is assumed for multiphase flow (Bear, 1975). Each fluid is a continuum and the
 31 various continua occupy the void space simultaneously. The equations of motion for multiphase flow used here
 32 are based on heuristic extensions of Darcy's law (Hubbert, 1956; Bear, 1975, 1979; Dake, 1978; Crichlow, 1977;
 33 Collins, 1961; Dullien, 1979; Hiatt, 1968; de Marsily, 1986; De Wiest, 1965; Aziz and Settari, 1979).

34 The following is a statement of Darcy's law in differential form:

$$35 \quad q_v = -\frac{k}{\mu} [\nabla P - \rho g] \quad (\text{A-1})$$

1 where q_v is the volumetric flow rate per unit cross-sectional area, k is the absolute or intrinsic permeability of the
2 porous media, μ is the fluid viscosity, ρ is the fluid density, g is the gravitational constant, and P is the fluid
3 pressure.

4 Darcy's original observations were made on the one-dimensional vertical flow of water through a fully
5 saturated porous medium (Hubbert, 1956). Darcy postulated the law, which states that the flow of water under
6 these conditions is proportional to the change in potential. Many generalizations of Darcy's law can be found in
7 the literature (Bear, 1975, 1979; Bear et al., 1968; Bear and Bachmat, 1967; Dake, 1978; Crichlow, 1977;
8 Collins, 1961; Dullien, 1979; Hiatt, 1968; de Marsily, 1986; De Wiest, 1965; Aziz and Settari, 1979). These
9 generalizations extend Darcy's observation to other fluids, to the simultaneous flow of immiscible fluids, to
10 multiple dimensions, and to compressible fluids. These generalizations are used in obtaining the equations of
11 motion governing the two-phase flow assumed in BRAGFLO.

12 The first extension is a generalization from an isotropic to an anisotropic medium. This extension is
13 developed heuristically as well as theoretically in Bear (1975). Implicit in this generalization is the extension to
14 two and three dimensions.

15 The second extension is that of accounting for fluid compressibility effects. Hubbert (1940) shows that
16 extensions of Darcy's law to compressible fluids, such as gas, are valid provided the density of the fluid is a
17 function of pressure only and the flow is irrotational.

18 The third extension of Darcy's law accounts for the presence and flow of multiple immiscible phases. Once
19 steady-state flow is achieved, Darcy's law may be extended to describe the separate flow of each phase (Bear, 1975).
20 This extension introduces the concept of effective permeabilities, relative permeabilities, and capillary pressure.

21 For each phase, the absolute permeability of Equation A-1 is replaced by the effective phase permeability, and
22 the pressure of Equation A-1 is replaced by the phase pressure. These effective permeabilities are empirically
23 determined by pressure drop and flow measurements. Numerous experiments verify the validity of this extension
24 and suggest that the effective permeability depends on characteristics of the rock, the wettability characteristics,
25 surface tension, the shape of the interface separating the phases, and phase saturation. The effective permeabilities
26 do not appear to depend on fluid viscosities or their specific discharges (Bear, 1975; Scheidegger, 1960). Instead of
27 using effective permeabilities, it is more convenient to refer to relative permeabilities, which are defined for each
28 phase as the ratio of the effective phase permeability to the absolute or intrinsic permeability of the medium
29 (measured when the medium is saturated with a single fluid).

30 **A.2.3. Geometry**

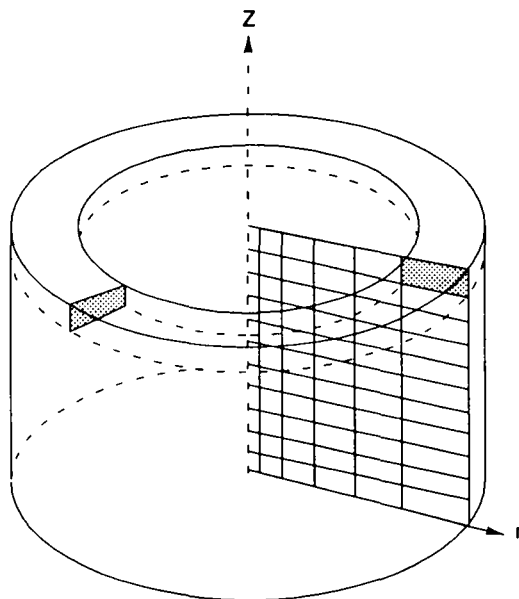
31 BRAGFLO is developed in terms of a one-, two- or three-dimensional block-centered grid system. In general,
32 the three-dimensional numerical methods are normally based on Cartesian xyz coordinates. The finite difference
33 formulations in BRAGFLO are sufficiently general to handle grid block "stretching" (variable grid spacing) in the
34 directions of flow, as well as variable grid thickness or cross-sectional area in directions normal to flow. In

1 addition, the coordinate system may be rotated in three-dimensional space, with respect to the direction of gravity
2 resulting in the generalized case of gravity components in each of the coordinate directions.

3 Because of these generalities, many geometries may be considered. Some of these include the following:

- 4 • Cartesian geometry (one-dimensional linear vertical, horizontal, or inclined flow; two-dimensional planar
5 areal sweep, vertical or inclined flow; three-dimensional flow),
- 6 • Cylindrical geometry (two-dimensional axisymmetric cylindrical geometry with axis of symmetry oriented
7 parallel, normal, or inclined to the direction of gravity),
- 8 • Spherical symmetry, and
- 9 • Non-Cartesian geometry (variable grid thickness and cross-sectional areas normal to flow).

10 To model in axisymmetric cylindrical geometry or spherical symmetry requires only an external
11 transformation to obtain the equivalent Cartesian grid block sizes required for BRAGFLO. For example, consider
12 the two-dimensional convergent flow toward a well in radial coordinates r and z (Figure A-1) (symmetry is
13 assumed in the angular direction, θ).



TPI-6342-1476-1

14

15

Figure A-1. Schematic representation of an axisymmetric cylindrical model.

1 If the coordinate transformations of $x(x, z) = r$, $y(x, z) = 2\pi r$ and $z(x, z) = z$, then an equivalent Cartesian
 2 system of the cylindrical geometry is defined. In the Cartesian system, flow is in the x and z directions. The
 3 length in the non-flow or symmetric direction, y , varies with x and accounts for the increase in cross-sectional area
 4 (normal to radial flow) with radial distance from the well. The transformation are justified by the equivalence of
 5 the volume integration in the two coordinate systems. An arbitrary function of r and z , $f(r, z)$ is integrated over
 6 the cylindrical element volume as

$$7 \quad F = \int_{z_k}^{z_{k+1}} \int_{r_i}^{x_{i+1}} \int_0^{2\pi} f(r, z) r \, d\Theta \, dr \, dz \quad (\text{A-2})$$

8 When the above transformations are defined, Equation A-2 is identical to the integration in Cartesian coordinates
 9 carried out below:

$$10 \quad G = \int_{z_k}^{z_{k+1}} \int_{x_i}^{x_{i+1}} \int_0^{2\pi} g(x, z) \, dx \, dy \, dz \quad (\text{A-3})$$

11 Therefore, the conversion from radial geometry to the BRAGFLO Cartesian formulation requires only setting the
 12 mesh width (y) of each grid block equal to the circumference of a circle passing through the center of that grid
 13 block.

14 The way in which grid block sizes may vary is not arbitrary and depends on restrictions concerning grid block
 15 connectivity and interface cross-sectional areas. In BRAGFLO, two criteria determine valid grid block stretchings.
 16 First, grid-block stretchings are confined to certain directions dependent on the dimensionality of the flow. For
 17 example, in one-dimensional flow, the length of all grid blocks (Δx , Δy , and Δz) may vary in the direction of
 18 flow. In two-dimensional flow (x and y directions), the length Δx can vary only in the x -direction while the length
 19 Δy can vary only in the y -direction. For three-dimensional flow, the length of the grid blocks can only vary in
 20 the direction of flow coincident to their respective orientations. That is, Δx varies only in x , Δy varies only in y ,
 21 and $\Delta z =$ varies only in z . The reasons for these restrictions arise when determining appropriate averages for flows
 22 across block interfaces, given values evaluated at the centers of adjacent blocks. Secondly, grid block sizes may
 23 vary only in a way that results in a one-to-one connectivity between grid blocks in each direction starting from
 24 the origin. Grid block stretchings that violate only the first criterion may or may not be physically valid and are
 25 acceptable by BRAGFLO, although a warning message alerts the user to possible problems. Stretchings that
 26 violate criterion two above will not run. The grid patterns of Figure A-2 (a, b, and c) depict grid stretchings in
 27 one, two, and three dimensions, respectively, which are consistent with both criteria above.

28 The reason that some violations of the first criterion above present problems is that they may require
 29 restrictive assumptions concerning the average cross-sectional area between adjacent grid blocks for calculating
 30 interblock transmissibilities, flow rates, and velocities. The reason violations of the second criterion are not
 31 acceptable is because they are inconsistent with the bookkeeping assumed in BRAGFLO for mapping the
 32 coordinates of the grid block centers from their spatial positions to their locations in the numerical space.

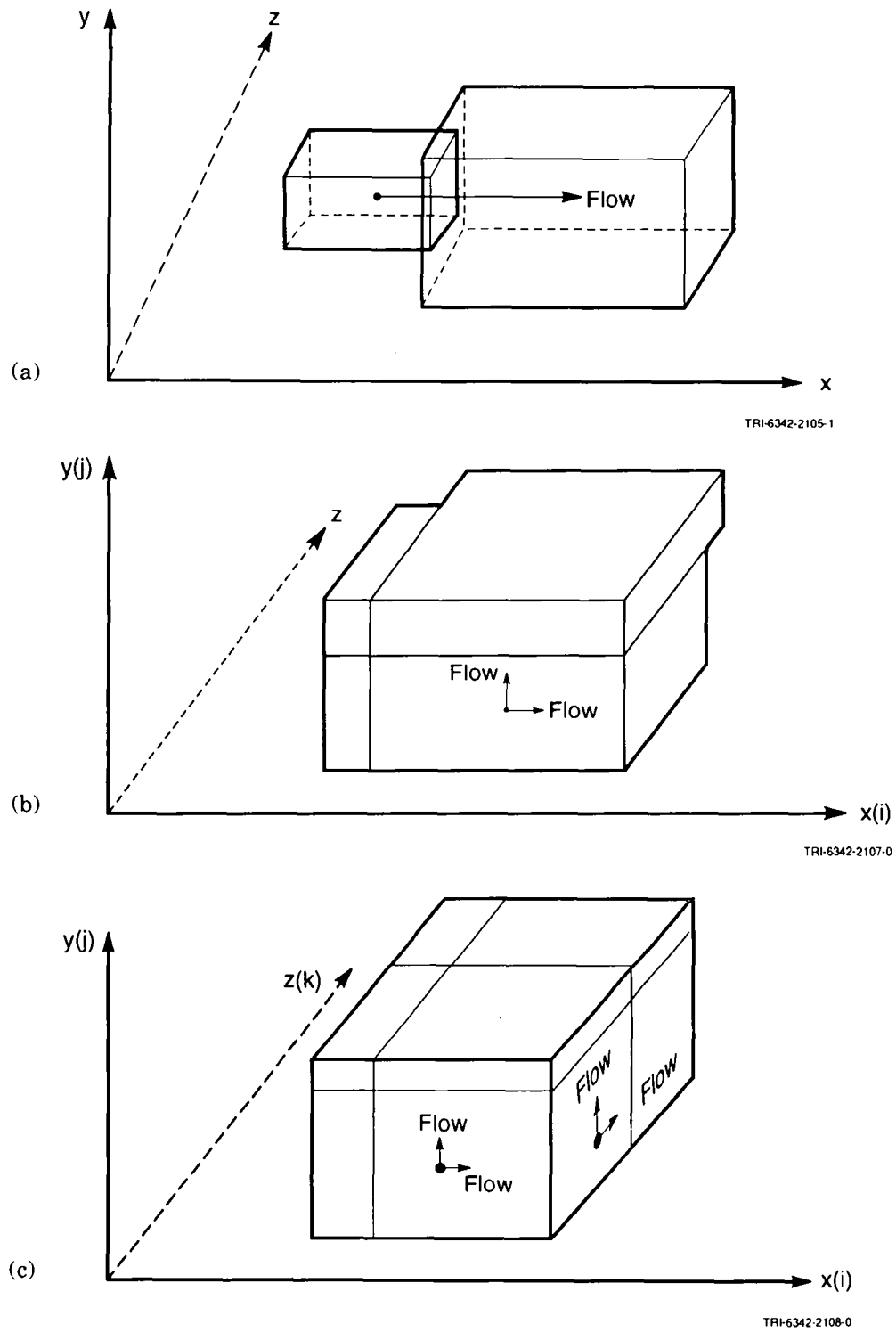
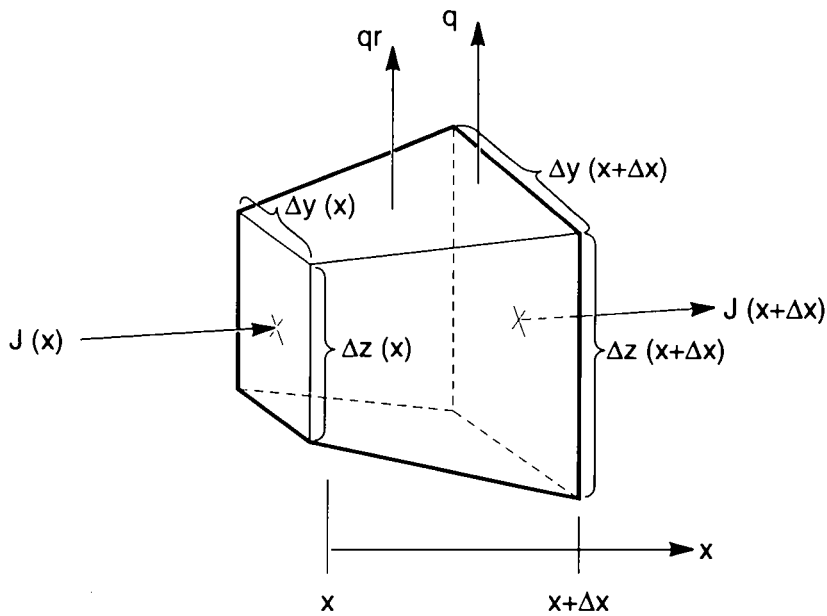


Figure A-2. Grid-block stretching for flow in (a) one, (b) two, or (c) three dimensions.

1 **A.2.4 Derivation of Flow Equations**

2 The derivation of the flow equations begins by consideration of mass conservation in a differential volume
 3 element. The derivation will initially be presented for one-dimensional compressible flow and then generalized to
 4 other dimensionalities. The derivation is generalized to allow for the cross-sectional area normal to flow to vary
 5 in the direction of flow.

6 Consider the mass conservation of a single component in a two-phase system about the control volume
 7 depicted in Figure A-3.



TRI-6342-2101-0

8

9 Figure A-3. Control volume for derivation of flow equations.

10 Flow is in the x direction across a length Δx . The cross-sectional area normal to flow varies with x
 11 as $A(x) = \Delta y(x) \cdot \Delta z(x)$. Therefore, the cross-section areas at the left boundary and right boundary are
 12 $\Delta y(x) \cdot \Delta z(x)$ and $\Delta y(x + \Delta x) \cdot \Delta z(x + \Delta x)$ respectively. The mass flux entering the element at the left face is
 13 $J(x)$, while the mass flux leaving at the right face is $J(x + \Delta x)$. Included in the mass balance are terms for mass
 14 rate of injection (per unit volume of reservoir) due to wells, q , and chemical reaction, q_r . We also acknowledge
 15 that the density and saturation of the component, as well as the porosity of the reservoir, may change with time.

16 The mass conservation equation simply states that

17
$$[\text{rate in}] - [\text{rate out}] + [\text{rate injected}] + [\text{rate reacted}] = [\text{rate accumulated}] \quad (\text{A-4})$$

Appendix A: BRAGFLO and PANEL

1 The rate at which mass enters the element from the left boundary is

$$2 \quad J(x) \cdot \Delta y(x) \cdot \Delta z(x)$$

3 The rate at which mass exits the element at the right boundary is

$$4 \quad J(x + \Delta x) \cdot \Delta y(x + \Delta x) \cdot \Delta z(x + \Delta x)$$

5 The rate at which mass is injected or produced by or from a well into the element is

$$6 \quad q \cdot \overline{\Delta y \cdot \Delta z} \cdot \Delta x = q \cdot \bar{A} \cdot \Delta x,$$

7 where \bar{A} is an average value of the product of Δy and Δz across the block length Δx , the volume of the block
8 being $\overline{\Delta y \cdot \Delta z} \cdot \Delta x$.

9 Similarly, the rate at which mass is reacted in the element is

$$10 \quad q_r \cdot \overline{\Delta y \cdot \Delta z} \cdot \Delta x = q_r \cdot \bar{A} \cdot \Delta x$$

11 The rate at which mass is accumulated in the element volume is

$$12 \quad \frac{\partial}{\partial t} (\bar{\phi} \bar{\rho} \bar{S}) \cdot \bar{A} \Delta x,$$

13 because $\bar{\phi} \cdot \bar{\rho} \cdot \bar{S} \cdot \bar{A} \Delta x$ is the mass contained in the element. The bars signify an average of the value in the
14 element. We have assumed that the size of the element does not change with time.

15 The statement of component mass conservation (Equation A-4) is written as

$$16 \quad [J_x \Delta y \Delta z]_x - [J_x \Delta y \Delta z]_{x+\Delta x} + [q \overline{\Delta y \Delta z} \Delta x] + [q_r \overline{\Delta y \Delta z} \Delta x] = \overline{\Delta y \Delta z} \Delta x \frac{\partial (\bar{\phi} \bar{\rho} \bar{S})}{\partial t} \quad (\text{A-5})$$

17

18 Dividing Equation A-5 by Δx gives

19

$$20 \quad \frac{-[J_x \Delta y \Delta z]_{x+\Delta x} + [J_x \Delta y \Delta z]_x}{\Delta x} + [q \overline{\Delta y \Delta z}] + [q_r \overline{\Delta y \Delta z}] = \overline{\Delta y \Delta z} \frac{\partial (\bar{\phi} \bar{\rho} \bar{S})}{\partial t} \quad (\text{A-6})$$

21

22 If we define a derivative to be

$$23 \quad \frac{\partial f(x)}{\partial x} = \lim_{\Delta x \rightarrow 0} \frac{f(x + \Delta x) - f(x)}{\Delta x},$$

1 then in this limit, the differential form of the component mass conservation equation is

$$2 \quad -\frac{\partial(J_x \Delta y \Delta z)}{\partial x} + q \Delta y \Delta z + q_r \Delta y \Delta z = \Delta y \Delta z \frac{\partial(\phi \rho S)}{\partial t} \quad (\text{A-7})$$

3 where we have noted in the limit as $\Delta x \rightarrow 0$ that $\overline{\Delta y \Delta z} \rightarrow \Delta y(x) \Delta z(x)$, $\bar{\rho} \rightarrow \rho(x)$, $\bar{\phi} \rightarrow \phi(x)$, and $\bar{S} \rightarrow S(x)$.

5 Following a similar procedure in considering two-dimensional and three-dimensional flow results in the
6 following differential forms of the component mass conservation equations:

7 Two-dimensional form:

$$8 \quad -\frac{\partial(J_x \Delta z)}{\partial x} - \frac{\partial(J_y \Delta z)}{\partial y} + q \Delta z + q_r \Delta z = \Delta z \frac{\partial(\phi \rho S)}{\partial t} \quad (\text{A-8})$$

9 Three-dimensional form:

$$10 \quad -\frac{\partial(J_x)}{\partial x} - \frac{\partial(J_y)}{\partial y} - \frac{\partial(J_z)}{\partial z} + q + q_r = \frac{\partial(\phi \rho S)}{\partial t} \quad (\text{A-9})$$

12 We have generalized to allow flux in the y and z directions, J_y and J_z respectively.

13 If Equations A-7, A-8, and A-9 are compared, the differential component mass conservation equations may be
14 generalized for arbitrary dimensionality as follows:

$$15 \quad -\nabla \cdot \alpha \bar{J} + \alpha(q + q_r) = \alpha \frac{\partial(\phi \rho S)}{\partial t} \quad (\text{A-10})$$

16 where α is a geometric factor and depends on dimensionality as follows:

18 one dimension: $\alpha(x, y, z) = \Delta y(x) \Delta z(x)$,

19 two dimensions: $\alpha(x, y, z) = \Delta z(x, y)$,

20 three dimensions: $\alpha(x, y, z) = 1$,

21 and $\nabla \cdot \alpha \bar{J}$ is shorthand for $\frac{\partial(\alpha J_x)}{\partial x} + \frac{\partial(\alpha J_y)}{\partial y} + \frac{\partial(\alpha J_z)}{\partial z}$.

22 It is important to note that, in general, α varies spatially and, therefore, remains inside the above derivative terms.

23 In two-dimensional flow, J_z is zero, and in one-dimensional flow, both J_y and J_z are zero.

1 Equation (A-11) is written for one component. In multicomponent systems, the mass of each component
 2 must be conserved. This results in multiple conservation equations (one for each component) similar to Equation
 3 A-11.

4 The development leading up to Equation A-11 assumed that the component exists in one phase because its
 5 mass is assumed equal to the product $\phi\rho S$. We now relax this assumption and write the two mass conservation
 6 equations for a two-phase, two-component system in which each component may be distributed between each of
 7 the phases. Such conditions arise when gas dissolves in liquid or liquid vaporizes into gas.

8 For convenience and generality, the two phases will consist of a wetting and a non-wetting phase denoted by
 9 lowercase w and n , respectively. The two components will be distinguished according to wetting and non-wetting
 10 and denoted by uppercase W and N . We recognize that wettability is a characteristic of the phase and not a
 11 component property. The nomenclature "wetting component" is used to indicate that this component in general
 12 dominates the wetting phase and similarly for the non-wetting component.

13 Component concentrations are required when a phase may consist of more than one component. Define C_{ij}
 14 as the mass fraction of the i th component in the j th phase. Using the above nomenclature, four concentration
 15 terms can be defined for the general two-component, two-phase system: C_{Nw} , C_{Ww} , C_{Nn} , and C_{Wn} . Because all
 16 the mass in a phase must come from the two components, then the component concentrations in each phase are
 17 related as

$$18 \quad C_{Nw} + C_{Ww} = 1.0 \text{ and } C_{Nn} + C_{Wn} = 1.0 \quad (\text{A-11})$$

19 With the above concepts and nomenclature defined, Equation A-10 is applied to both the wetting and non-
 20 wetting components as follows:

21 Non-wetting component mass balance:

$$22 \quad -\nabla \cdot \alpha \bar{J}_N + \alpha(q_N + q_{rN}) = \alpha \frac{\partial}{\partial t} (\phi \rho_n S_n C_{Nn} + \phi \rho_w S_w C_{Nw}) \quad (\text{A-12})$$

23 Wetting component mass balance:

$$24 \quad -\nabla \cdot \alpha \bar{J}_W + \alpha(q_W + q_{rW}) = \alpha \frac{\partial}{\partial t} (\phi \rho_n S_n C_{Wn} + \phi \rho_w S_w C_{Ww}) \quad (\text{A-13})$$

25 Comparison of Equations A-12 and A-13 with A-10 shows that aside from the addition of some subscripts, the
 26 major differences come from allowing for the possibility of component mass in the element volume to be
 27 distributed between the two phases. For example, in the wetting component mass balance (Equation A-13), the
 28 first term in the time derivative, $\phi \rho_n S_n C_{Wn}$ is the mass of the wetting component distributed to the non-wetting
 29 phase in the element volume. The second term in the time derivative, $\phi \rho_w S_w C_{Ww}$ is the mass of the wetting
 30 component distributed to the wetting phase in the element volume.

1 The component mass flux vectors \vec{J}_N and \vec{J}_W consist of contributions from both phases. The flux can be
2 expanded and written to account for these contributions as follows:

$$3 \quad \vec{J}_N = C_{Nn}\rho_n\vec{V}_n + C_{Nw}\rho_w\vec{V}_w \quad (\text{A-14})$$

$$4 \quad \vec{J}_W = C_{Wn}\rho_n\vec{V}_n + C_{Ww}\rho_w\vec{V}_w. \quad (\text{A-15})$$

5 \vec{V}_n and \vec{V}_w are the superficial velocities for the non-wetting and wetting phases, respectively.

6 So far in this development, no assumptions have been made concerning the velocities or their relationships to
7 pressure or potential. In BRAGFLO, Darcy's original law, extended to multiphase and multidimensional flow and
8 accounting for gravity and capillary forces, relates superficial velocities to potential.

9 As mentioned in Section A.2.2, when two immiscible fluids occupy the pore space, they become separated by
10 an interface. The curvature and surface tension of this interface produces a pressure difference called the capillary
11 pressure. This capillary pressure has been experimentally observed to vary with saturation. In BRAGFLO, the
12 capillary pressure is defined by Equation A-16 as the difference between non-wetting phase pressure and wetting
13 phase pressure.

$$14 \quad P_c(S_w) = P_n - P_w \quad (\text{A-16})$$

15 Assuming each phase pressure is partially responsible for the flow of only that phase, Darcy's law in
16 differential form becomes

$$17 \quad \vec{V}_n = -\frac{K_n}{\mu_n}(\nabla P_n - \rho_n g \nabla D) \quad (\text{A-17})$$

$$18 \quad \vec{V}_w = -\frac{K_w}{\mu_w}(\nabla P_w - \rho_w g \nabla D), \quad (\text{A-18})$$

19 where g is the gravitational constant of acceleration and D is the depth, which may vary spatially with all three
20 coordinates.

21 In Equation A-17 and A-18, K_n and K_w are the effective permeabilities to flow for each phase. Unlike the
22 absolute permeability of a porous medium in Darcy's original law that is independent of the flowing fluid (except
23 for gas at low pressures), the effective permeability depends on the characteristics of the rock and fluid and has
24 been experimentally observed to vary with the type and amount of fluid present (i.e., to vary with saturation).
25 Instead of effective permeability, it is more common to encounter relative permeabilities in the reservoir literature.
26 The relative permeabilities are defined as the ratio of the effective permeability of a phase to the absolute
27 permeability (or single fluid permeability) of the porous medium.

$$28 \quad k_{rn} = \frac{K_n}{K} \quad (\text{A-19})$$

$$k_{rw} = \frac{K_w}{K} \quad (\text{A-20})$$

The dependence of capillary pressure and relative permeability on fluid saturation is described in more detail in Volume 3, Section 2.3.1 of this report.

Substitution of Equations A-14, A-15, A-17, A-18, A-19, and A-20 into A-12 and A-13 results in the two-component mass conservation equations, A-21 and A-22.

$$-\nabla \cdot \left[\frac{\alpha C_{Nn} \rho_n k_m K}{\mu_n} (\nabla P_n - \rho_n g \nabla D) + \frac{\alpha C_{Nw} \rho_w k_{rw} K}{\mu_w} (\nabla P_w - \rho_w g \nabla D) \right] + \alpha (q_N + q_{rN})$$

$$= \alpha \frac{\partial}{\partial t} [\phi \rho_n S_n C_{Nn} + \phi \rho_w S_w C_{Nw}] \quad (\text{A-21})$$

$$-\nabla \cdot \left[\frac{\alpha C_{Wn} \rho_n k_m K}{\mu_n} (\nabla P_n - \rho_n g \nabla D) + \frac{\alpha C_{Ww} \rho_w k_{rw} K}{\mu_w} (\nabla P_w - \rho_w g \nabla D) \right] + \alpha (q_N + q_{rN})$$

$$= \alpha \frac{\partial}{\partial t} [\phi \rho_n S_n C_{Wn} + \phi \rho_w S_w C_{Ww}] \quad (\text{A-22})$$

Equations A-21 and A-22, along with A-11, A-16, and the phase saturation constraint, Equation A-23, form the system of equations solved simultaneously in BRAGFLO.

$$S_n + S_w = 1.0 \quad (\text{A-23})$$

The constraint on saturation simply states that all of the pore space volume is occupied by the fluid phases.

The absolute permeability that appears in Equations A-21 and A-23 is directional and may be in general viewed as a second-order tensor. When the permeability of a porous medium depends on direction, the medium is characterized as being anisotropic. In BRAGFLO, the anisotropic porous medium is assumed to be orthotropic with the three orthogonal axes of the medium being aligned with the three coordinate axes. The off-diagonal elements of the permeability tensor are zero for an orthotropic porous medium. The diagonal permeabilities are K_x , K_y , and K_z . Some pre-processing of permeability data may be required if the data is taken in directions not aligned with the model's coordinate axes.

Assuming the concentrations and all of the physical properties of the fluids and the porous media are defined, the system of equations defines the spatial and temporal variation in the four dependent variables S_n , S_w , P_n , and P_w . The saturation constraint (Equation A-23) and the definition of capillary pressure (Equation A-16) are used to eliminate two of the dependent variables.

1 Theoretically, any two of the variables may be eliminated from the system, leaving two primary dependent
2 variables. Some combinations may be numerically more advantageous than others. Selecting both phase
3 pressures as primary dependent variables is not appropriate because saturation would then be obtained from the
4 capillary pressure dependence on saturation, which may not be defined below residual saturations or capillary
5 pressure may not uniquely specify a saturation.

6 In BRAGFLO, the primary dependent variables are selected as S_n and P_w . S_n is aligned with the non-wetting
7 mass conservation partial differential equation (Equation A-21), while P_w is aligned with Equation A-22.
8 Equation A-23 determines S_w from S_n , and Equation A-16 is used to obtain P_n once S_w and P_w are known. No
9 fundamental difference was observed when the primary dependent variables of P_n and S_w were used during simple
10 test problems. Nevertheless, the current BRAGFLO formulation assumes S_n and P_w as primary dependent
11 variables.

12 A.2.5 Initial and Boundary Conditions

13 S_n , S_w , P_n , and P_w

14
15 Specification of boundary and initial conditions is required to complete the formulation. Upon examination
16 of Equations A-21 and A-22, it is evident that they are second-order with respect to non-wetting phase pressure
17 (P_n) and wetting phase pressure (P_w). Thus, two boundary conditions are required for each phase pressure in each
18 dimension (two for P_n and P_w in x , two for P_n and P_w in y , and two for P_n and P_w in z). BRAGFLO handles
19 boundary conditions in a way that typifies reservoir models; that is, the reservoir of interest is enclosed by a
20 boundary across which there is no flow in the direction normal to it. Mathematically, these types of conditions
21 are Neumann boundary conditions in which the normal derivative of pressure to the boundary is zero. In
22 BRAGFLO, this is accomplished by assigning a zero value to the normal transmissibilities along each of the
23 boundaries for both the gas and brine phases.

24 Through the use of wells, BRAGFLO has the capability to override the no-flow conditions. By locating
25 pressure-constrained or flow-constrained fictitious wells along the boundaries, fixed pressures along the boundary
26 or non-zero flow into or out of the reservoir across the boundary can be approximated.

27 No-flow boundary conditions may occur on two types of boundaries: one is the physical boundary of the
28 reservoir being modeled; the other is along a line of symmetry. An implicit assumption in the use of no-flow
29 boundaries is that the boundaries are located far enough away from the wells or other regions of interest that the
30 boundaries exert negligible influence on the flow behavior in the reservoir over the duration of simulation time.

31 A number of variables and properties must be specified at time $t = 0$. These initial conditions consist of: (1)
32 the two dependent variables aligned with Equation A-21 and Equation A-22 (S_n and P_w), (2) the reservoir
33 properties of porosity and the directional permeabilities, and (3) the concentrations of metal and cellulose. These
34 variables must be specified throughout the simulation volume and along the boundaries. All other material
35 properties (fluid and reservoir properties) must also be specified; however, properties such as relative

1 permeabilities, capillary pressures, densities, viscosities, dissolved gas, etc., are functions of the previously
2 specified dependent variables and are calculated in BRAGFLO.

3 **A.2.6 Numerical Solution Techniques**

4 The numerical techniques in the BRAGFLO flow model are based on a fully implicit finite difference
5 representation of the nonlinear conservation equations. In implicit methods, the dependent variable at a particular
6 location is evaluated as a function of the current values of its neighbors and the current value of any coefficients.
7 In explicit methods, current values of the dependent variables are evaluated as a function of previously determined
8 (or past-dated) values of dependent variables and coefficients. Implicit methods are inherently more numerically
9 stable compared to their explicit or hybrid (IMPES) counterparts (Fanchi et al., 1982; Carnahan et al., 1969;
10 Smith, 1965). The penalty for this increased stability is the increased computational effort associated with the
11 simultaneous solution of the resulting finite difference analogs of the conservation equations at each grid block
12 center. A complete discussion of numerical solution techniques is provided in the 1991 performance assessment
13 documentation (see Section 5.2 of WIPP PA Division, 1991).

14 **A.2.7 Benchmark Results**

15 BRAGFLO has been benchmarked against two other multiphase reservoir codes (BOAST II and TOUGH).
16 The results of four one-dimensional, radial benchmarks (with/without dissolved gas and with/without gas
17 generation) showed excellent agreement among the three codes. Benchmark results are provided in the 1991
18 performance assessment documentation (see Section 5.2.2.3 of WIPP PA Division, 1991).

19 **A.2.8 Postprocessing**

20 BRAGFLO output has in the past consisted solely of various distributions—pressures, saturations,
21 interblock, flows, etc. However, detailed analyses of the results, such as those discussed in the RCRA report
22 (WIPP PA Department, 1992) and the 1991 sensitivity analysis report (Helton et al., 1992), require more detailed
23 output. Examples include extents of gas flow in particular regions (such as the anhydrite layers) and especially
24 numerous integrated quantities, such as integrated flows up intrusion boreholes or flows through drift or shaft
25 seals.

26 Last year, these integrations and summary types of calculations were done externally to BRAGFLO using
27 CAMCON postprocessing tools, in particular, ALGEBRA. However, the postprocessors can deal only with data
28 in the BRAGFLO output files. Because the quantity of output from BRAGFLO can be vast, results are generally
29 printed out only every 15 or 20 time steps. For most purposes, this provides an adequate amount of detail.
30 However, some of the integrations are done on quantities that can vary extremely rapidly. For example, the rate of
31 brine flow up an intrusion borehole can sometimes be very high immediately following the intrusion, but last for
32 only a few time steps. Assuming that the high rate lasts for 15 or 20 steps, rather than just two steps, can
33 seriously overestimate the quantity of brine that flowed up the borehole in that time period.

1 This shortcoming was corrected in 1992 by performing these integrations internally to BRAGFLO. All
2 integrations and summary statistics used in detailed analysis of BRAGFLO output are now calculated at each step
3 of a performance calculation. Thus, these results are as accurate as the fundamental solution quantities calculated
4 in BRAGFLO (brine pressures and gas saturations). No additional errors are introduced by postprocessing partial
5 results.

6 A drawback to performing these integrations internally to BRAGFLO is that portions of the code become
7 mesh specific. In order to integrate flows up an intrusion borehole, for example, the location of the borehole
8 must be "hardwired" into the code. In addition, quantities that are of interest in one mesh do not even exist in
9 another mesh because the conceptual model differs. To program the integration and summary calculations to be
10 completely general to enable it to perform on any mesh is not feasible under the PA time constraints. Thus,
11 multiple versions of BRAGFLO currently are used, each one differing only in the number and type of output
12 summary calculations that are done for the particular mesh and conceptual model being used. All other internal
13 workings of the different versions are identical.

14 **A.3 Waste Mobilization (PANEL)**

15 PANEL's waste mobilization model mathematically computes the radionuclide concentrations in the brine
16 that result from the waste mixing with the brine. This model assumes that the concentrations of all species are
17 uniform through the waste room, that the concentrations of all species are always in equilibrium, and that
18 solubility limits for a given element are allocated among its isotopes on the basis of relative abundance.
19 Radioactive decay based on the Bateman equations (Section 7.1 of this volume; WIPP PA Division 1991, Section
20 7.2.3) is also taken into consideration. A complete description of the waste mobilization model is provided in the
21 PANEL discussions found in Volume 3 of this report (Section 1.4.4) and in the 1991 performance assessment
22 documentation (see Section 5.3.2 of WIPP PA Division, 1991).

Appendix A References

- 1
- 2 Aziz, K., and A. Settari. 1979. *Petroleum Reservoir Simulation*. London: Applied Science Publishers.
- 3 Bear, J. 1975. *Dynamics of Fluids in Porous Media*. New York, NY: Elsevier Publishing Company.
- 4 Bear, J. 1979. *Hydraulics of Groundwater*. New York, NY: McGraw-Hill, Inc.
- 5 Bear, J., and Y. Bachmat. 1967. "A Generalized Theory on Hydrodynamic Dispersion in Porous Media,"
6 *I.A.S.H. Symp. Artificial Recharge and Management of Aquifers*. IASH, P.N. 72. Haifa, Israel. 7-16.
- 7 Bear, J., D. I. H. Zaslavskii, and S. Irmay. 1968. *Physical Principles of Water Percolation and Seepage*.
8 Paris: UNESCO.
- 9 Brooks, R.H., and A.T. Corey. 1964. *Hydraulic Properties of Porous Media*. Hydrology Paper No. 3. Fort
10 Collins, CO: Civil Engineering Department, Colorado State University.
- 11 Carnahan, B., H.A. Luther, and J.O. Wilkes. 1969. *Applied Numerical Methods*. New York, NY: John Wiley
12 & Sons, Inc.
- 13 Coats, K.H. 1980. "In-Situ Combustion Model," *Society of Petroleum Engineers Journal*. Vol. 26, no. 6,
14 533-554.
- 15 Collins, R.E. 1961. *Flow of Fluids Through Porous Materials*. New York, NY: Reinhold Publishing
16 Corporation.
- 17 Corey, A.T. 1986. *Mechanics of Immiscible Fluids in Porous Media*. Littleton, CO: Water Resources
18 Publications.
- 19 Crichlow, H.B. 1977. *Modern Reservoir Engineering - A Simulation Approach*. Englewood Cliffs, NJ:
20 Prentice-Hall, Inc.
- 21 Crookston, R.B., W.E. Culham, and W.H. Chen. 1979. "Numerical Simulation Model for Thermal Recovery
22 Processes," *Society of Petroleum Engineers Journal*. Vol. 19, no. 1, 37-58.
- 23 Dake, L.P. 1978. *Fundamentals of Reservoir Engineering*. New York, NY: Elsevier Scientific Publishing
24 Company.
- 25 de Marsily, G. 1986. *Quantitative Hydrogeology: Groundwater Hydrology for Engineers*. Orlando, FL:
26 Academic Press, Inc.
- 27 De Wiest, R.J.M. 1965. *Geohydrology*. New York, NY: John Wiley and Sons.
- 28 Dullien, F.A.L. 1979. *Porous Media Fluid Transport and Pore Structure*. New York, NY: Academic Press,
29 Inc.
- 30 Fanchi, J.R., K.J. Harpole, and S.W. Bujnowsky. 1982. *BOAST: A Three-Dimensional Three-Phase Black Oil
31 Applied Simulation Tool (Version 1)*. DOE/BC/10033-3. Tulsa, OK: Keplinger and Associates, Inc.

- 1 Helton, J.C., J.W. Garner, R.P. Rechar, D.K. Rudeen, and P.N. Swift. 1992. *Preliminary Comparison with*
2 *40 CFR Part 191, Subpart B for the Waste Isolation Pilot Plant, December 1991—Volume 4: Uncertainty*
3 *and Sensitivity Analysis Results*. SAND91-0893/4. Albuquerque, NM: Sandia National Laboratories.
- 4 Hiatt, W.N. 1968. "Mathematical Basis of Two-Phase, Incompressible, Vertical Flow Through Porous Media
5 and Its Implications in the Study of Gravity-Drainage-Type Petroleum Reservoirs," *Society of Petroleum*
6 *Engineers Journal*. Vol. 8, no. 3, 225-230.
- 7 Hubbert, M.K. 1940. "The Theory of Ground-Water Motion," *The Journal of Geology*. Vol. 48, no. 8, pt. 1,
8 785-944.
- 9 Hubbert, M.K. 1956. "Darcy's Law and the Field Equations of the Flow of Underground Fluids," *Journal of*
10 *Petroleum Technology*. Vol. 8, 222-239.
- 11 Peaceman, D.W. 1977. *Fundamentals of Numerical Reservoir Simulation*. New York: Elsevier Scientific
12 Publishing Company.
- 13 Rubin, B., and P.K.W. Vinsome. 1979. "Simulation of the In-Situ Combustion Process in One Dimension
14 Using a Highly Implicit Finite Difference Scheme," *Preprint, 30th Annual Meeting of the Canadian*
15 *Institute of Mining and Metallurgy, Banff, Canada, May 8-11, 1979*. Paper 79-30-14. Montreal, Quebec:
16 Canadian Institute of Mining and Metallurgy, Petroleum Society.
- 17 Scheidegger, A. E. 1960. *The Physics of Flow Through Porous Media*. Rev. ed. Toronto, Canada: University
18 of Toronto Press.
- 19 Smith, G.D. 1965. *Numerical Solution of Partial Differential Equations, with Exercises and Worked*
20 *Solutions*. New York, NY: Oxford University Press.
- 21 Vaughn, P. 1986. *A Numerical Model for Thermal Recovery Processes in Tar Sand: Description and*
22 *Application*. DOE/FE/60177-2219. (Available from National Technical Information Service, Springfield,
23 VA.)
- 24 WIPP Performance Assessment (PA) Department. 1992. *Long-Term Gas and Brine Migration at the Waste*
25 *Isolation Pilot Plant: Preliminary Sensitivity Analyses for Post-Closure 40 CFR 268 (RCRA), May 1992*.
26 SAND92-1933. Albuquerque, NM: Sandia National Laboratories.
- 27 WIPP Performance Assessment (PA) Division. 1991. *Preliminary Comparison with 40 CFR Part 191, Subpart*
28 *B for the Waste Isolation Pilot Plant, December 1991 - Volume 2: Probability and Consequence*
29 *Modeling*. SAND91-0893/2. Albuquerque, NM: Sandia National Laboratories.

**APPENDIX B:
SANCHO**

APPENDIX B: SANCHO

B.1 Overview

SANCHO is a special purpose, finite-element computer program developed at Sandia National Laboratories to solve problems of the quasistatic, large-deformation, inelastic response of two-dimensional (i.e., planar or axisymmetric) solids (Stone et al., 1985). This program numerically solves the general, nonlinear partial differential equations that govern relaxation to equilibrium between stresses and applied loads in a solid body. Because the general equations are an underdetermined system, they must be supplemented with constitutive equations for up to three optional material models: a finite strain, elastic-plastic strain-hardening model; a volumetric plasticity model; and a metallic creep model. The material models actually used in the 1992 series of PA calculations are described in Section 1.4.7 of Volume 3.

SANCHO uses a finite-element method to obtain a numerical solution; the elements are bilinear, isoparametric quadrilaterals with constant bulk strain. The solution strategy for obtaining equilibrium includes the use of an iterative scheme designed around a self-adaptive, dynamic relaxation algorithm; the iterative scheme is an explicit, central-difference, pseudo-time integration with artificial damping. Because the scheme is explicit, no stiffness matrix is formed or factored — a feature that can reduce computer storage requirements.

B.2 Summary of Theory and Fundamental Equations

The theory underlying SANCHO is that of the motion of point-like particles that are imbedded within a solid body V , which occupies a region of three-dimensional space and is subject to deformation under the influence of prescribed body and surface forces. These particles usually occupy the corners or centers of elements of a mesh that is placed over the volume V at the time ($t = 0$) that deformation begins; the configuration at this time is called the *reference configuration* and the position of a particle is specified by its vector of material coordinates, \mathbf{X} . In the reference configuration, the solid body is assumed to be strain free, though not necessarily stress free. As time increases and the body deforms, the particles move with the material along trajectories denoted by

$$x = \xi(\mathbf{X}, t). \quad (\text{B-1})$$

The vector function ξ describes the motion of a particle that starts at \mathbf{X} at $t = 0$; clearly

$$\xi(\mathbf{X}, 0) = \mathbf{X}.$$

It is the vector function ξ that is the basic dependent variable in problems of this kind because knowledge of it permits graphic visualization of the change in shape of the deforming body. For purposes of computing the dynamics of deformation, however, it is more convenient to view the flow of the particles through three-dimensional space as though they were imbedded in a continuous fluid moving with a velocity field,

$$1 \quad \mathbf{v} = \frac{\partial}{\partial t} \xi(\mathbf{X}, t) = \eta(\mathbf{x}, t), \quad (\text{B-2})$$

2 defined for $t \geq 0$ and any point $\mathbf{x} \in \mathbb{R}^3$ (note that \mathbf{x} is now an arbitrary point in space); this is called the *Eulerian*
 3 *point of view*.

4 The Eulerian point of view permits the calculation of the true acceleration of an element of mass that is
 5 instantaneously located at \mathbf{x} : from (B-1) and (B-2) and the chain rule of calculus, it is seen that the true
 6 acceleration is just the material derivative of V ,

$$7 \quad \frac{d\mathbf{v}}{dt} = \frac{\partial \mathbf{v}}{\partial t} + \mathbf{v} \cdot \nabla \mathbf{v} \quad (\text{B-3})$$

8 The fundamental equation governing the deformation of the solid body V follows by application of Newton's Laws
 9 of Motion to an arbitrary element of mass in volume V (see Malvern, 1969 Section 5.3):

$$10 \quad \rho \frac{d\mathbf{v}}{dt} = \nabla \cdot \mathbf{T} + \rho \mathbf{b} \quad (\text{B-4})$$

11 where

12 $\rho =$ mass density (kg/m^3)

13 $\mathbf{T} =$ the Cauchy stress tensor ($\text{kg/m} \cdot \text{s}^2$)

14 $\mathbf{b} =$ sum of specific body forces (i.e., forces per unit mass: usually, gravity; m/s^2).

15 The mass density must also satisfy the continuity equation:

$$16 \quad \frac{d\rho}{dt} = -\rho \nabla \cdot \mathbf{v} \quad (\text{B-5})$$

17 SANCHO was actually designed to solve the equilibrium equations associated with (B-4) and (B-5), i.e., the
 18 dynamical equations that apply when $|\mathbf{v}|$ and the time rate-of-change of density are small or zero [but in numerical
 19 practice a "quasistatic" approximation is employed that requires the re-introduction of artificial time derivatives
 20 having much the same form as the left-hand sides of (B-4) and (B-5)]. The quasistatic approximation to the
 21 equations of motion takes the form (Stone et al., 1985)

$$22 \quad \nabla \cdot \mathbf{T} + \rho \mathbf{b} = 0, \quad (\text{B-6})$$

23 and allows for three kinds of boundary conditions:

24 1. Jump condition at a contact discontinuity defined by some *internal* surface S_0 ; this condition requires that

$$25 \quad (\mathbf{T}^+ - \mathbf{T}^-) \cdot \mathbf{n}_0 = 0 \quad \text{on } S_0 \quad (\text{B-7})$$

1 where \mathbf{n}_0 is the outward unit normal on S_0 , and the (+) and (-) signs on the stress tensors signify respectively
 2 values taken on the outer and inner sides of S_0 .

3 2. Traction boundary conditions on some *external* surface S_1 , of the form

$$4 \quad \mathbf{T} \cdot \mathbf{n}_1 = \mathbf{S}(t) \quad \text{on } S_1 \quad (\text{B-8})$$

5 where \mathbf{n}_1 is the outward unit normal on S_1 , and $S(t)$ is a prescribed vector function of time.

6 3. Displacement boundary conditions on some *external* surface S_2 ;

$$7 \quad \xi(\mathbf{X}, t) = \mathbf{k}(t) \quad \text{on } S_2 \quad (\text{B-9})$$

8 where $\mathbf{k}(t)$ is a prescribed vector function of time.

9 Taken alone, equations (B-6) and the boundary conditions (B-7) through (B-9) obviously do not determine
 10 stress distributions. In the two-dimensional geometries of the SANCHO code, the stress tensor has three
 11 independent components; in matrix notation,

$$12 \quad \mathbf{T} = \begin{pmatrix} t_{11} & t_{12} \\ t_{21} & t_{22} \end{pmatrix}, \text{ with } t_{12} = t_{21},$$

13 and so one more relation is needed in order to make a determinate system of equations. The *constitutive*
 14 *equations* or the stress-strain relations defining the nature of the material under consideration are usually chosen in
 15 a way that supplies the required, addition relationships (note, however, that the form of the constitutive equations
 16 may vary in space because different kinds of materials may occupy different parts of the solid body V).

17 The constitutive equations in SANCHO are usually expressed as ordinary differential equations (ODEs) for the
 18 components of the stress tensor or the components of the deviatoric stress tensor,

$$19 \quad \mathbf{T}' = \mathbf{T} - \sigma \mathbf{I} = \mathbf{T} + p \mathbf{I} \quad (\text{B-10})$$

20 where σ denotes the mean normal stress and p is the mean normal pressure. For examples of the ODEs
 21 governing material models used in the 1992 PA calculations, see Section 1.4.7 of Volume 3.

1

Appendix B References

2

Malvern, L.E. 1969. *Introduction to the Mechanics of a Continuous Medium*. Englewood Cliffs, NJ: Prentice-Hall, Inc.

3

4

Stone, C.M., R.D. Krieg, and Z.E. Besinger. 1985. *SANCHO — A Finite Element Computer Program for the Quasistatic, Large Deformation, Inelastic Response of Two-Dimensional Solids*. SAND84-2618. Albuquerque, NM: Sandia National Laboratories.

5

6

**APPENDIX C:
SECO FLOW AND TRANSPORT MODEL**

APPENDIX C: SECO FLOW AND TRANSPORT MODEL

C.1 Flow

SECO_2DH calculates single-phase Darcy flow for groundwater flow problems in two dimensions. The formulation is based on a single partial differential equation for a hydraulic head using fully implicit time differencing. Both confined and unconfined aquifer conditions are simulated. The flow is solved in both a regional and a local grid, each of which is defined independently of the grid that defines the aquifer properties. A semi-coarsening multigrid solvers is used to increase solution efficiency for large array dimensions. High-order accuracy particle tracking is available for both grids. The codes are written in DEC VMS FORTRAN. The codes are designed specifically for execution on VAX computers operating under the VMS operating system. The guiding philosophy for the SECO codes is to make the problem definition convenient and to facilitate as much as possible the running of grid-convergence tests and local-area simulations within the larger regional-area simulation. The codes are particularly well suited for testing alternative conceptual models for flow and transport.

C.1.1 Governing Equation

SECO_2DH simulates groundwater flow at regional and local scales within the Culebra Dolomite by solving the following partial differential equation in two dimensions (x, y) in time (t) for potentiometric head, h :

$$S_s \frac{\partial h}{\partial t} = \nabla \cdot (K \nabla h) - W \quad (\text{C-1})$$

where K is the (tensor) hydraulic conductivity, S_s is the specific storage of the porous material (the Culebra), t is time, and W is a volumetric flux (out of the Culebra) per unit volume of formation (used to simulate wells or recharge). The principal axes of K must be aligned along the coordinate directions x and y . S_s , K , and W may be functions of (x, y, t) . For a derivation of this equation from Darcy's flow and the equation of mass conservation, see McDonald and Harbaugh (1988).

C.1.2 Discretization and Solvers

Equation C-1 (or the steady-state version with $\partial h / \partial t = 0$) is discretized using standard second-order differences in space and first-order backward (fully implicit) differences in time (McDonald and Harbaugh, 1988; Roache, 1976). The fully implicit time differencing produces unconditional stability for this linear equation, but requires solution of an elliptic equation at each time step. In MODFLOW and other common groundwater hydrology codes, this linear, elliptic equation is solved by either the two-line successive over-relaxation (SOR) iterative method or by a direct solver. The direct solver is not considered to be practical for realistic grids (sufficiently fine resolution), being excessively sensitive to computer round-off error (especially on VAX-class computers) and very slow. In SECO_2DH, the solver options are point SOR, (single) line SOR (e.g., see Roache, 1976), and the

1 semi-coarsening multigrid solver MGSS2, which was developed at Ecodynamics (personal communication with P.
2 Knapp, Ecodynamics Research Associates, Albuquerque, NM).

3 The semi-coarsening multigrid solver (MGSS2) is the default option. For very coarse resolution (e.g., a 6×6
4 grid that might be used for development of code enhancements), the point SOR solver is fastest. However,
5 MGSS2 results in significantly increased efficiency for problems with fine resolution and strongly varying
6 conductance (due to either hydraulic conductivity variations or highly stretched grids). Further, the MGSS2 solver
7 does not require that the user estimate an optimum relaxation factor, as SOR solvers do.

8 **C.1.3 Block-Centered Discretization**

9 SECO_2DH has been written with an option flag called MAC to select either the most common block-
10 centered discretization (MAC=1), with the cell edge coincident with the aquifer edge, or node-centered discretization
11 (MAC=0), with the cell center (or node) on the aquifer edge. Unless required by a specific study, the default cell
12 configuration is MAC=1. This configuration clearly more accurately locates the aquifer edge for both Dirichlet
13 (fixed-head) and Neumann (fixed-gradient) boundary conditions. For QA purposes, MAC=0 is unsupported in
14 SECO_2DH.

15 **C.1.4 Problem Decoupling**

16 To make the problem definition convenient and to facilitate the running of grid convergence tests and local-
17 area simulations within the larger regional-area simulation, the problem definition is decoupled from the
18 computational grid. The aquifer properties are defined on a discrete data base that can be independent of the
19 computational grids. A sequence of grid solutions does not require the user to define aquifer properties point by
20 point in each computational grid; likewise, the regional computational grid is decoupled from the local
21 computational grid, both in space and time. A number of parameters, including the boundaries of the
22 computational regions, the spatial increments (cell sizes), the simulation times, and the time steps, are all
23 decoupled in both space and time. The only requirement is that the local grid-problem domain of definition must
24 lie within the regional grid-problem domain of definition. Likewise, definition of boundary conditions (types and
25 values) and wells (locations and pumping schedules) are decoupled from the computational grid and are defined in
26 the continuum.

27 **C.2 Transport**

28 SECO_TP uses a total variational diminishing (TVD) scheme to solve the two-dimensional radionuclide
29 transport equation in a fractured porous medium (Salari et al., 1992). The TVD scheme employed by SECO_TP
30 uses three-level time differencing and directional splitting to improve accuracy and execution time.

31 An overview theoretical development of SECO_TP that follows has been extracted from Salari et al. (1992).
32 A more detailed explanation is available from Salari et al. (1992) and the work cited below.

1 C.2.1 Governing Equation

2 The relevant partial differential equation contains advection, dispersion, absorption, source, and decay terms.
3 The radionuclide transport problem consists of N species equations, $k = 1, \dots, N$:

$$4 \quad \nabla \cdot [D \nabla C_k - V C_k] = \phi R_k \frac{\partial C_k}{\partial t} + \phi R_k \lambda_k C_k - \phi R_{k-1} \lambda_{k-1} C_{k-1} - Q \hat{C}_k - \Gamma_k, \quad (C-2)$$

5
6 where the dependent variables are C_k , the concentration of the k th radionuclide. Physical parameters include
7 $D(x, t)$, a 2×2 hydrodynamic dispersion tensor (velocity-dependent); $V(\mathbf{x})$, the Darcy velocity; $\phi(\mathbf{x})$, the fracture
8 porosity; R_k , the retardation coefficient; λ_k , the species decay constant; and \hat{C}_k , the concentration of the k th
9 injected radionuclide. The well injection rate is Q . Detailed physical descriptions of these terms can be found in
10 Huyakorn and Pinder (1983) and Bear and Bachmat (1990). A dual-continuum model requires the additional source
11 term Γ_k to represent the flux due to the exchange of contaminant between the fracture and matrix domain.
12 Fracture flow (single-porosity) and fracture/matrix-flow (dual-porosity) versions of Equation C-2 are presented and
13 discussed in detail in Volume 3 of this report (Section 1.4.6). The N equations are linear and sequentially coupled.

14 A general Robin boundary condition is assumed:

$$15 \quad \alpha C_k + \beta \frac{\partial C_k}{\partial n} = \gamma \quad (C-3)$$

16 on a planar rectangular domain Ω . For various choices of $\alpha(\mathbf{x})$, $\beta(\mathbf{x})$, and $\gamma(\mathbf{x})$, one may obtain Dirichlet,
17 Neumann, or Cauchy boundary conditions on different portions of the boundary. The flow field is obtained from
18 SECO_2DH.

19 The two-dimensional governing equation is solved using an approximate factorization (Fletcher, 1988) with
20 an implicit treatment of boundary conditions. The convective terms are modeled by TVD (Yee, 1987) and the
21 remaining terms by central differencing. Solution of the governing equation is explained in detail in Salari et al.
22 (1992).

23 C.2.2 Code Verification

24 The SECO_TP code has been applied to test problems and is shown to be accurate for both high and low
25 mesh Peclet numbers. SECO_TP has been verified for temporal and spatial accuracy using the following unsteady
26 equation and its solution, with $V = ui$:

$$27 \quad C_t + u C_x = \alpha_L u C_{xx} + \alpha_T u C_{yy} - g(x, y, t), \quad (C-4)$$

1 where

$$2 \quad g(x, y, t) = (x - ut)^2 + y^2,$$

3 and $0 < x < 1$, $0 < y < 1$. The initial condition is given by

$$4 \quad C(x, y, 0) = \frac{1}{12u} \left[\frac{x^4}{\alpha_L} + \frac{y^4}{\alpha_T} \right] \quad (C-5)$$

5 The exact solution to Equation C-4 is

$$6 \quad C(x, y, t) = \frac{1}{12u} \left[\frac{(x - ut)^4}{\alpha_L} + \frac{y^4}{\alpha_T} \right]. \quad (C-6)$$

7 Because the computational domain is finite, the Dirichlet boundary conditions are time dependent and may be
8 obtained from the exact solution.

9 Table C-1 presents the computed solution to Equation C-4 at time = 25 for four different grid sizes and time
10 steps. The magnitude of the coefficients are $u = 0.1$, $\alpha_L = 0.1$, and $\alpha_T = 0.1$. Examination of the ratio of root
11 mean square (RMS) of errors shows that the overall solution is second-order accurate in time and space.

12 The SECO_TP code has also been benchmarked against exact transport solutions in Javandel et al. (1984),
13 Tang et al. (1981), and Knupp and Salari (1992).

14 Table C-1. Convergence Results, Uniform Grid

Size	Δx	Δy	RMS	RMS Ratio
20×20	0.05	0.25	7.697E-3	
40×40	0.025	0.125	1.954E-3	3.94
80×80	0.0125	0.0625	4.921E-4	3.97
160×160	0.00625	0.03125	1.234E-4	3.99

15

Appendix C References

- 1
- 2 Bear, J., and Y. Bachmat. 1990. *Introduction to Modeling of Transport Phenomena in Porous Media*.
3 Dordrecht, Netherlands: Kluwer Academic Publishers.
- 4 Fletcher, C.A.J. 1988. *Computational Techniques for Fluid Dynamics*. New York, NY: Springer-Verlag.
5 Vols. 1-2.
- 6 Huyakorn, P.S., and G.F. Pinder. 1983. *Computational Methods in Subsurface Flow*. New York, NY:
7 Academic Press.
- 8 Javandel, I., C. Doughty, and C-F. Tsang. 1984. *Groundwater Transport: Handbook of Mathematical*
9 *Models*. Water Resources Monograph No. 10. Washington, DC: American Geophysical Union.
- 10 Knupp, P.M., and K. Salari. 1992. *Contributions of an Analytical Solution to a 2D Radionuclide Transport*
11 *Problem for Site Performance Assessment*. Albuquerque, NM: Ecodynamics Research Associates
12 Technical Report. (Copy on file in Waste Management and Transportation Library, Sandia National
13 Laboratories, Albuquerque, NM.)
- 14 McDonald, M.G., and A.W. Harbaugh. 1988. *A Modular Three-Dimensional Finite-Difference Ground-Water*
15 *Flow Model*. Techniques of Water-Resources Investigations of the United States Geological Survey, Book
16 6, Modeling Techniques. Reston, VA: U.S. Geological Survey.
- 17 Roache, P.J. 1976. *Computational Fluid Dynamics*. Rev. printing. Albuquerque, NM: Hermosa Publishers.
- 18 Salari, K., P. Knupp, P. Roache, and S. Steinberg. 1992. "TVD Applied to Radionuclide Transport in Fractured
19 Porous Media," *Proceedings of IX International Conference on Computational Methods in Water*
20 *Resources, Denver, Colorado*. 141-148. (Copy on file in Waste Management and Transportation
21 Library, Sandia National Laboratories, Albuquerque, NM.)
- 22 Tang, D.H., E.O. Frind, and E.A. Sudicky. 1981. "Contaminant Transport in Fractured Porous Media:
23 Analytical Solution for a Single Fracture," *Water Resources Research*. Vol. 17, no. 3, 555-564.
- 24 Yee, H.C. 1987. "Construction of Explicit and Implicit Symmetric TVD Schemes and Their Applications,"
25 *Journal of Computational Physics*. Vol. 68, no. 1, 151-179.

**APPENDIX D:
CULEBRA TRANSMISSIVITY FIELD SIMULATIONS**

APPENDIX D: CULEBRA TRANSMISSIVITY FIELD SIMULATIONS

The information presented in this appendix is extracted from LaVenue and RamaRao (1992).

D.1 Background

Efforts to incorporate uncertainty in the Culebra transmissivity field into PA calculations have been somewhat evolutionary. In the 1990 PA calculations, the Culebra was divided into seven zones or regions. A mean transmissivity value and an associated standard deviation was assigned to each zone. By sampling from the distributions associated with each zone, multiple realizations of zonal transmissivity values were subsequently used as input to the flow and transport calculations. Although computationally elegant, the specification of zones significantly reduces the spatial variability within a given realization because each zone has a constant value. In addition, large differences in the values assigned to each zone in a given realization may occur generating severe step changes in the permeability field.

In an effort to improve the transmissivity field used in the 1991 PA calculations, conditional simulations (CS) of Culebra transmissivity fields were produced by conditioning upon the observed transmissivity values and the pilot points which were added in the LaVenue et al. (1990) model. The CS transmissivity fields were then used in a groundwater flow model (WIPP PA Division, 1991). The boundary conditions necessary to reduce the differences between the observed and calculated steady-state heads were then determined. Those realizations that did not meet a minimum error criteria were not considered adequate and were discarded. This work resulted in over 60 conditional simulations that had acceptable fits to the observed steady-state freshwater heads. These 60 fields were subsequently used in the calculations by sampling on a uniformly distributed variable assigned to each CS field (WIPP PA Division, 1991). The differences between each realization is depicted by a groundwater travel-time cumulative-distribution function, where travel times range from approximately 10,000 years to 30,000 years. These travel times are used as an internal diagnostic measure in the generation of CS transmissivity fields. Travel times used in the calculation of Environmental Protection Agency (EPA) normalized releases of radionuclides to the accessible environment are calculated using the CS transmissivity fields and the SECO flow and transport codes.

In March of 1991, a geostatistics/stochastic-hydrology expert panel (GXG) was convened to provide guidance for adequately incorporating the uncertainty of the Culebra transmissivity field into the PA calculations. After reviewing the previous work, the GXG had several concerns regarding the approach taken in LaVenue et al. (1990). One of the principal concerns raised by the GXG panel members related to the subjectivity inherent in the manual calibration approach. For example, the model was calibrated in a piecewise fashion by sequentially selecting regions to be calibrated, instead of calibrating the whole model area at the same time. The model was sequentially calibrated in the northwest (upgradient) region, southwest region, southern region, and central region or WIPP-site boundary area. As mentioned in the 1990 study, the regions upgradient and downgradient from the WIPP-site area were calibrated prior to making any changes within the WIPP-site boundary. This approach was employed in order to reproduce the regional hydraulic gradients across the northern and southern WIPP-site boundaries; it is analogous to producing a regional flow model to provide boundary conditions for a local scale

1 model. The GXG panel wondered whether there would be any major differences in the calibrated transmissivity
2 field had the entire model area been calibrated at the same time.

3 Several recommendations were proposed by the GXG panel members and are described in detail in Gallegos
4 (1992). One of their recommendations included repeating the modeling performed by LaVenue et al. (1990),
5 which included steady-state and transient model calibration, numerous times. However, instead of simply kriging
6 the transmissivities, conditional simulations would be generated and subsequently calibrated. The conditional
7 simulations would allow for different transmissivity fields to be used as the initial fields for the model. These
8 fields would initially be conditioned on the observed transmissivity data only. Subsequent model calibration
9 would then condition each of the conditionally simulated fields to the observed steady-state and transient heads.
10 Because the GXG panel also expressed concerns regarding the manual assignment of transmissivities to the pilot
11 points, the approach used in LaVenue et al. (1990) was also enhanced to include optimization routines that were
12 needed to assign transmissivity values to the pilot points once their location was selected.

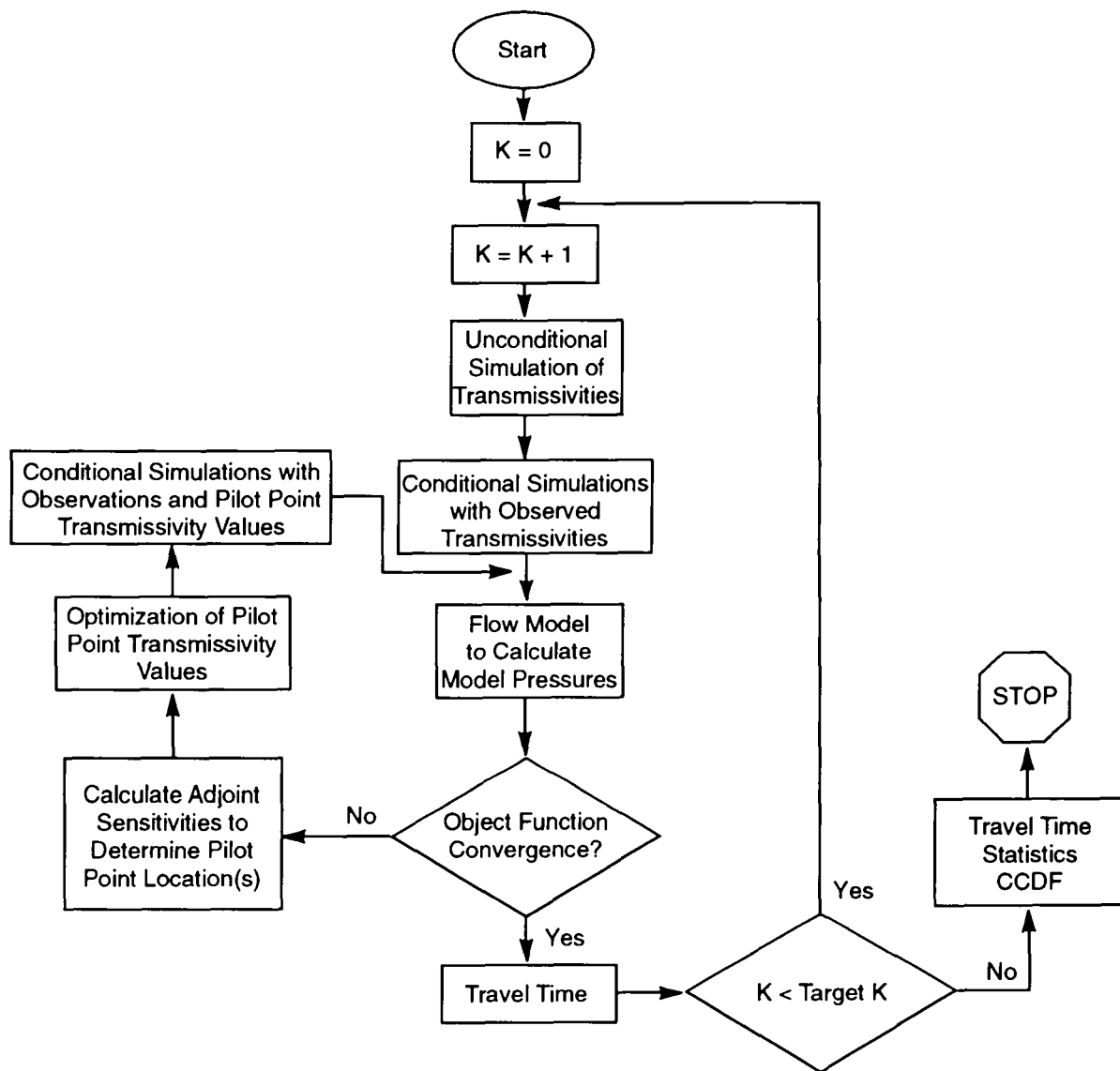
13 The present study addresses the uncertainty in the travel time by embedding the problem in a probabilistic
14 framework. The true transmissivity distribution at the WIPP site is conceptualized to be one realization of a
15 stochastic process. Accordingly, a large number of realizations of this stochastic process, which are very plausible
16 versions of the true transmissivity at the WIPP site, are generated. This ensemble of realizations is thus used
17 with the groundwater flow model to generate an ensemble of the corresponding travel times. The distribution of
18 the travel times provides an understanding of the uncertainty. While several statistical measures can be used to
19 quantify the uncertainty, a complimentary cumulative distribution function (CCDF) is commonly used for a
20 graphical display of the uncertainty in travel time.

21 This appendix describes the methodology of this new approach as it is used in the Culebra system. (A more
22 complete explanation of this new approach and its application is provided in LaVenue and RamaRao [1992].)
23 Seventy calibrated conditionally simulated (CCS) transmissivity fields were produced using this approach; these
24 fields are discussed in Section 2.6.3 of Volume 3 of this report and are presented in Appendix C of Volume 3 of
25 this report.

26 **D.2 Overview of Methodology**

27 The solution methodology involves the generation of a large number of random transmissivity fields, each of
28 which is in close agreement with all the measured data at the WIPP site. The collected data at the WIPP site is
29 comprised of (1) transmissivity measurements, and (2) pressure measurements (both steady state and transient
30 state). Conformity between a random transmissivity field and the measured data is achieved in stages, as described
31 below. Figure D-1 presents an overview of the different steps in this study.

32 First, unconditional simulations of the WIPP transmissivity fields are generated. These are random fields,
33 having the same statistical moments (the mean and the variance) and the same spatial correlation structure, as
34 indicated by the transmissivity measurements. (These fields need not, however, match the measured
35 transmissivities at the location of their measurements.)



TRI-6342-3301-0

Figure D-1. Calibration of conditionally simulated transmissivity fields: flow chart.

1 These transmissivity fields are then conditioned, so that they honor exactly the measured transmissivities at
2 the locations of their measurements. The resulting fields are called conditional simulations of the transmissivity
3 fields.

4 The conditional simulations of transmissivity field are then further conditioned, such that the pressures
5 computed by the groundwater flow model (both steady and transient state) agree closely with the measured
6 pressures, in a least-square sense. This phase is known as calibration or the solution of inverse problem, and
7 accounts for a large part of the time and effort in this study. When the calibration is completed, one obtains a
8 random transmissivity field that is in conformity with all the data at the WIPP site, and may therefore be regarded
9 as a plausible version of the true distribution of transmissivity at the WIPP site.

10 In this study model calibration is done by an indirect approach. An objective function is defined as the
11 weighted sum of the squared deviations between the model computed pressures and the observed pressures, with the
12 summation being extended in the spatial and temporal domain where pressure measurements are taken. The
13 classical formulation of the calibration then requires the minimization of the objective function, subject to the
14 constraints of the groundwater flow equations in the steady and transient state. This approach is implemented by
15 iteratively adjusting the transmissivity distribution until the objective function is reduced to a prescribed
16 minimum value.

17 A common approach to calibration consists in dividing the model domain into a few zones, in each of which
18 the transmissivity is treated as constant. The transmissivities in the different zones constitute the parameters to be
19 adjusted in the optimization process. Clearly, the delineation of zones is a subjective process and does affect the
20 results of the calibration. Thus, it may become necessary to consider several alternative zonation patterns for
21 calibration. Also, in this approach, uniform transmissivities are assigned to each zone. This representation may
22 be considered as inadequate, particularly while addressing the issues of spatial variability (within a zone).

23 To avoid the above difficulties of the zonation approach, an approach using pilot points as parameters is
24 adopted here. A pilot point is a synthetic transmissivity data point, that is added to an existing measured
25 transmissivity data set during the course of calibration. A pilot-point is defined by its spatial location and by the
26 transmissivity value assigned to it. After a pilot point is added to the transmissivity data set, the augmented data
27 set is used to obtain kriged or conditionally simulated transmissivity fields, for a subsequent iteration in
28 calibration. With the addition of a pilot point, the transmissivity distribution in the neighborhood of the pilot
29 point gets modified with dominant modifications being closer to the pilot-point location. The modifications in
30 the different grid blocks are determined by kriging weights and are not uniform (as in the zonation approach).
31 Conceptually, a pilot point may be viewed as a simple model to effect realistic modifications of transmissivity in
32 a large region of the model.

33 A coupled kriging-and-adjoint sensitivity analysis is used for the location of the pilot point; optimization
34 algorithms are used for assigning the transmissivity of a pilot point. Thus, the pilot-point approach to calibration
35 has been rendered objective, a feature considered very desirable for the WIPP site. Further, a multistage approach
36 has been used in implementing this methodology. This aspect bears similarity to the dynamic programming
37 method of optimization.

D.3 Code Development: An Overview

A comprehensive code package has been assembled using many of the codes already developed and frequently used in groundwater flow simulations. They are listed below. For details of the theory and application of these codes, the following references cited may be consulted:

- TUBA, unconditional simulation of transmissivity field (Zimmerman and Wilson, 1990),
- AKRIP, generalized kriging (Kafritsas and Bras, 1981),
- SWIFT II, modeling pressures (steady and transient state) (Reeves et al., 1986a,b,c)
- GRASP II, adjoint sensitivity analysis (steady and transient state) (Wilson et al., 1986; RamaRao and Reeves, 1990), and
- STLINE, groundwater travel time and travel paths (Intera, Inc., 1989).

In addition to using the above codes, the following new codes have been developed in the present task. The details of the new codes are provided in LaVenue and RamaRao (1992).

- MAIN—drives the different modules
- CONSIM—generates conditional simulations of transmissivity from the unconditional simulations of transmissivity
- PILOTL—locates the pilot points based on sensitivity analysis
- PAREST—assigns the pilot point transmissivities by minimization of a least square objective function

D.4 Simulated Transmissivities

In the earlier modeling efforts for WIPP (LaVenue et al., 1990), kriging has been employed to address the issue of spatial variability in transmissivity. In an effort where only one calibrated field is to be produced, kriging becomes an obvious choice. Kriging provides optimal estimate of the transmissivity at a point, thereby necessarily smoothing out the true variability between measurement points. On the contrary, simulated values reproduce the fluctuation patterns in transmissivity, which may lead to extreme values in travel times. Thus, simulated fields are useful to resolve the residual uncertainty not addressed by kriging.

1 D.4.1 Unconditional Simulation

2 An unconditional simulation of transmissivity field is a random field having the same statistical moments
 3 (mean and variance) and the same spatial correlation structure as indicated by the measured transmissivities in the
 4 field. An unconditionally simulated transmissivity field is said to be isomorphic with the true field, and is
 5 independent of the true field. The following methods have been used earlier in groundwater hydrology for
 6 generating unconditional simulations:

- 7 • nearest neighbor method (Smith and Schwartz, 1981; Smith and Freeze, 1979),
- 8 • matrix decomposition,
- 9 • multidimensional spectral analysis (Shinozuka and Jan, 1972; Mejía and Rodríguez-Iturbe, 1974), and
- 10 • turning bands method (Matheron, 1971, 1973; Mantoglou and Wilson, 1982; Zimmerman and Wilson,
 11 1990).

12 In this study, the turning bands method has been used. It is an extremely fast and efficient algorithm and the code
 13 TUBA to implement this, is available in public domain.

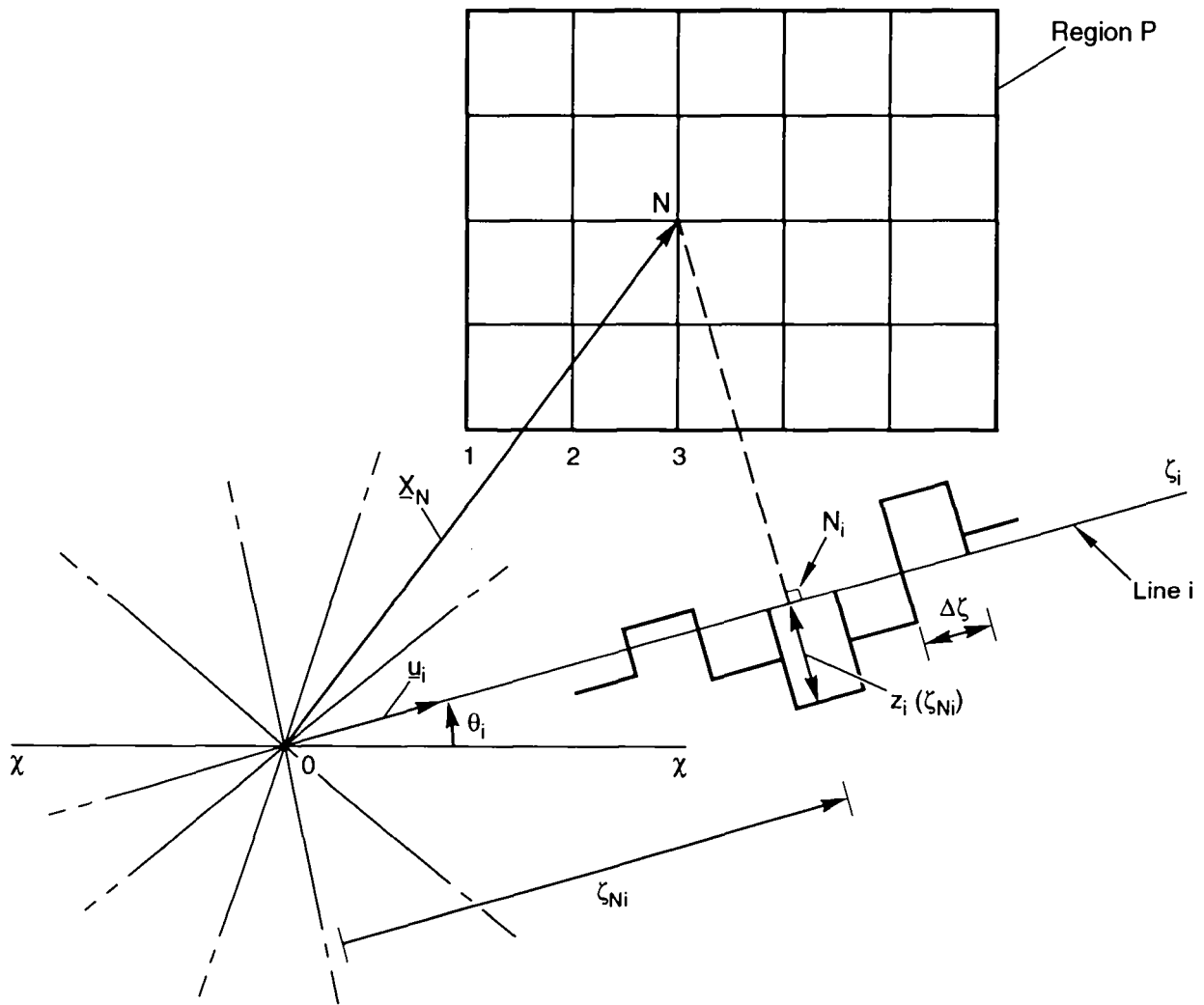
14 A two-dimensional (or a three-dimensional) stochastic process is generated in this method by the summation
 15 of a series of equivalent one-dimensional processes. Figure D-2 shows a definition sketch taken from Mantoglou
 16 and Wilson (1982). The region P shows a grid of points at each of which the two-dimensional field is to be
 17 generated. In particular, consider a point N in the grid where the two-dimensional field $[Z_s(N)]$ is to be simulated.

18 Consider a particular line i , the length along which, from the origin O , is measured by ζ_i . This line is
 19 divided into a number of intervals (bands), of length $\Delta\zeta_i$, in each of which the one-dimensional process Z_i is
 20 computed. Let N_i be the projection of the point N onto the line i . Let $Z_i(\zeta_i)$ be the one-dimensional process in
 21 the band containing N_i . Then the two-dimensional process $[Z_s(N)]$ is obtained by summing the contributions
 22 from the different lines, by the relation

$$23 \quad Z_s(N) = \frac{\sum_{i=1}^L Z_i(\zeta_{N_i})}{\sqrt{L}}, \quad (D-1)$$

24 where L is the number of lines selected. Usually L is between 16 and 20.

25 LaVenue et al. (1990) analyzed the WIPP transmissivity data and identified the spatial structure of the two-
 26 dimensional transmissivity field. They modeled it as an isotropic process and as an intrinsic random function of
 27 order zero (IRF-0), with the generalized covariance function (GCF) given by



TRI-6342-3303-0

Figure D-2. Schematic representation of the field and turning bands lines (Mantoglou and Wilson, 1982).

$$\begin{aligned}
 & k_2(r) = -a_0 r \quad (\text{GCF}) \\
 & r = \text{a radial distance} \\
 & a_0 = \text{a constant}
 \end{aligned} \tag{D-2}$$

The subscript 2 denotes a two-dimensional process.

If $k_1(r)$ is the GCF for an equivalent one-dimensional process,

$$k_1(r) = -\left(\frac{\pi}{2}\right)a_0 r. \tag{D-3}$$

The Weiner-Levy process is known to be an IRF-0 process and is accordingly used to generate the line process. The relevant equations are given below.

$$Z_i(\zeta) = W(\zeta), \tag{D-4}$$

where $W(\zeta)$ is the Weiner-Levy Process.

$$W(0) = 0, \tag{D-5}$$

$$W(\zeta + \Delta\zeta) = W(\zeta) + gU(\zeta), \tag{D-6}$$

$$U(\zeta) = U\left[-\frac{1}{2}, \frac{1}{2}\right], \tag{D-7}$$

and

$$g = \sqrt{12\pi a_0 \Delta\zeta}, \tag{D-8}$$

where $U(\zeta)$ is a uniformly distributed random variable.

D.4.2 Conditional Simulation

An unconditionally simulated transmissivity field, which is made to honor exactly the measured transmissivity at the locations of the measurements, is called a conditionally simulated transmissivity field. The procedure of conditioning is described below.

Let $Z(x)$ be the true value (not known) of the field at a point x . One may decompose $Z(x)$ as below:

$$Z(x) = Z_{ok}(x) + [Z(x) - Z_{ok}(x)], \tag{D-9}$$

1 where $Z_{ok}(x)$ is the kriged estimate of Z , at x , based on the observed values of Z at the locations of the
2 observations.

3 Here, $[Z(x) - Z_{ok}(x)]$ is a true kriging error and is unknown, since the true value of $Z(x)$ is unknown. It is
4 possible to simulate this error.

5 Using the unconditionally simulated values (Z_{uc}) at the locations of the observations (not the actual
6 observations), a kriged field (Z_{uk}) is generated. One may write, using a similar decomposition as above,

$$7 \quad Z_{uc}(x) = Z_{uk}(x) + [Z_{uc}(x) - Z_{uk}(x)] \quad (D-10)$$

8 where $[Z_{uc}(x) - Z_{uk}(x)]$ is also a kriging error, and is known and may be called a simulated kriging error. This
9 error is isomorphic with the true kriging error. More importantly, this error is independent of the kriged values:

$$10 \quad E[Z_{ok}(x), \{Z_{uc}(y) - Z_{uk}(y)\}] = 0 \text{ for all } x, y \quad (D-11)$$

11 Substituting the known simulated kriging error for the true but unknown kriging error, in Equation D-9, one
12 obtains:

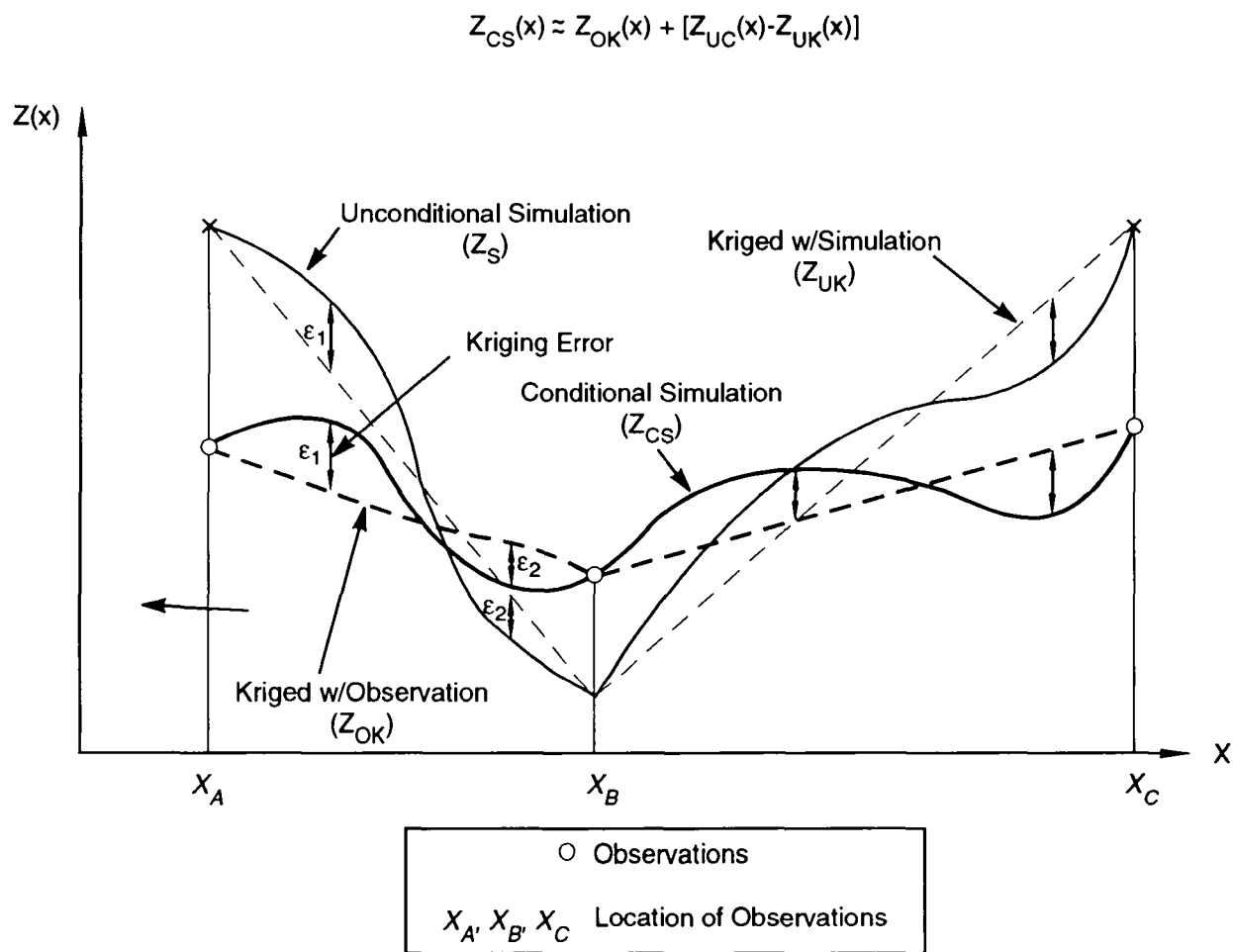
$$13 \quad Z(x) \approx Z_{ok}(x) + [Z_{uc}(x) - Z_{uk}(x)] \quad (D-12)$$

14 Equation D-12 clarifies the conditioning step as one of adding of simulated kriging error on a kriged field
15 using the measured data. This step involves kriging twice, once with the measured transmissivities and another
16 time with the unconditionally simulated transmissivities, both at the location of the observations. The
17 superposition of the three different transmissivity fields is graphically illustrated in Figure D-3.

18 The (average) transmissivity of each grid block is obtained here, using Gaussian quadrature. A 2×2 Gauss
19 point scheme is used for quadrature in each grid block.

20 The conditional simulations constitute the most important input to the groundwater flow model. It is useful
21 to appreciate the following properties of a conditional simulation (CS):

- 22 1. **The CS field honors the measured values exactly at the measurement locations.** This
23 follows from the fact the kriging is an exact interpolator, so that the simulated kriging error is zero at
24 measurement locations and, further, the kriged value from observations (Z_{ok}) reduces to the measured
25 value, for the same reason.



TRI-6342-3304-0

Figure D-3. Conditional and unconditional simulation: relationships.

- 1 2. **The CS field has the same spatial correlation structure as indicated by the measured**
2 **data.** This follows from an orthogonality property of the kriging errors (Equation D-11), which states
3 that the kriging errors (both true and simulated) are uncorrelated with any kriged values for stationary field
4 and with generalized increments for the intrinsic fields (Delfiner, 1976; Delhomme, 1979). Accordingly,
5 the addition of simulated kriging error field to a kriged field does not alter the spatial correlation structure
6 of the kriged field. It may be recalled that the kriged field itself has the same correlation structure as
7 implied by the data.

- 8 3. **The average of many CS fields at a location x , is merely the kriged estimate at x**
9 **$[Z_{ok}(x)]$.**

- 10 4. **The variance of many CS fields at a location x is given by the kriging variance.**

- 11 5. **The CS fields reproduce the true variability of the field, in contrast to a smoothed**
12 **field given by kriging.**

- 13 6. **The conditioning step introduces a robustness with respect to the features of the**
14 **reality that are not specifically known or imposed on the (unconditionally)**
15 **simulated field.** This robustness increases with the amount of the conditioning data.

16 D.4.3 Computational Options for Simulated Fields

17 The simulated kriging error is rendered zero at all observation points (see Figure D-4). When a pilot point is
18 added to the observed transmissivity data set, two options exist:

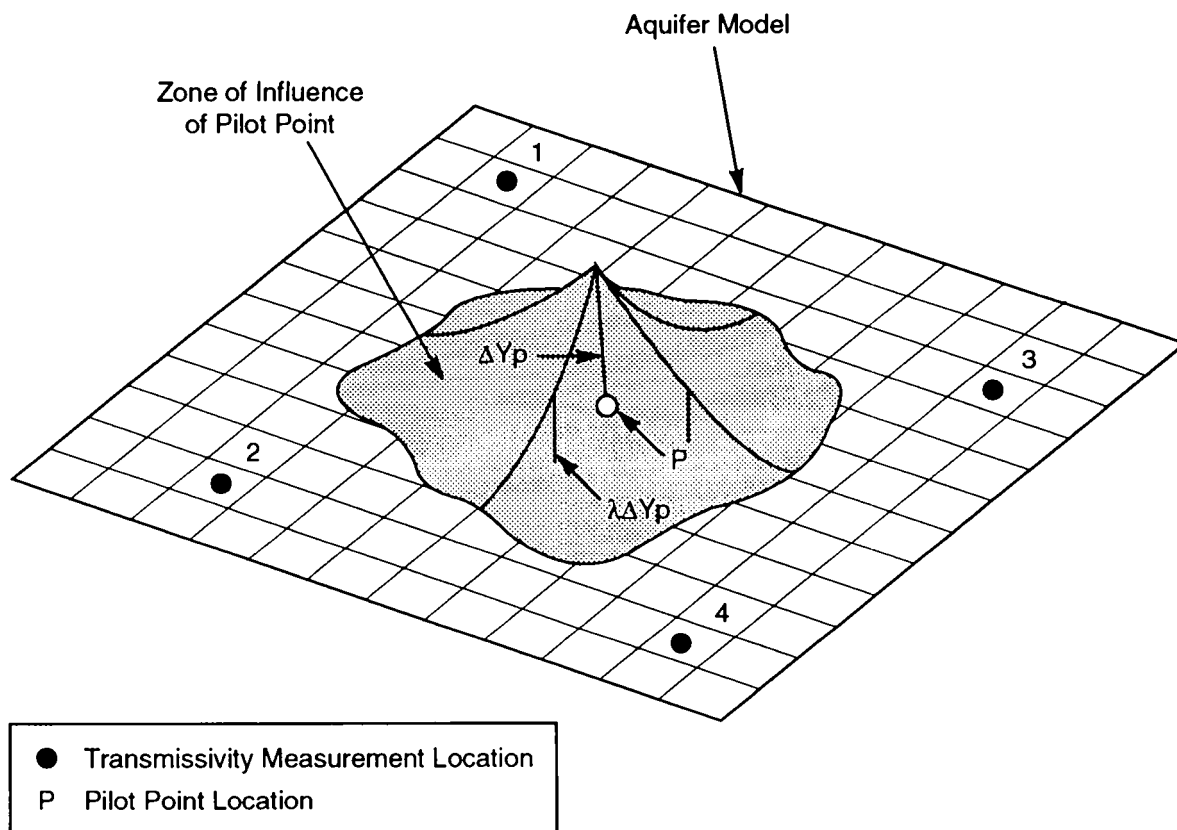
- 19 • The pilot point may be given the full status of an observed data point. Then the simulated kriging error at
20 the pilot point is also rendered zero. In this case, the simulated kriged error field varies from one iteration
21 to the other, and needs to be computed at every iteration.

- 22 • The simulated kriging error is rendered zero only at the observed data point and not at the pilot points.
23 Thus, the pilot points are used to obtain the kriged field using the 'augmented' data. But the simulated
24 kriged error field remains the same as the initial field through all the iterations. It does not need to be
25 recomputed during the various iterations.

26 While obtaining the kriged field using the simulated data at the measurement locations, two options exist:

- 27 • Assume that the simulated value (Z_{uc}) has the same errors as the actual measurements.

- 28 • Assume that the simulated value (Z_{uc}) has no errors.



Pilot Point - Schematic

		X	Y	T	y	σ_y
Measured Transmissivity	1	150	1050	$10^{-3.1}$	-3.1	0.5
	2					
	⋮					
	4					
Pilot Points added in Calibration	P_1	650	620	$10^{-4.81}$	-4.81	0.84
	P_2					
	⋮					
	P_n					

TRI-6342-3305-0

Figure D-4. Pilot point: schematic.

1 D.4.4 Validation of Simulations

2 For every CS field, the mean and variance of the transmissivity are computed and compared with that of the
3 WIPP data. Also, using the code AKRIP, the generalized covariance function (GCF) of the field is obtained and is
4 compared with that obtained from measured data at the WIPP. A close agreement between the two provides
5 verification that the generated CS field is a plausible version of the reality at the WIPP site. The procedure is
6 repeated for all the CS fields.

7 A collection of all the CS fields generated constitutes an ensemble. For any one location in the field,
8 transmissivity values across all the fields in the ensemble are studied and their mean and variance computed. A
9 spatial distribution of the ensemble mean and variance should closely agree with the spatial distribution of kriged
10 values and kriging variance obtained from the kriging exercise itself.

11 D.5 Automated Calibration

12 In an automatic algorithm, it becomes necessary to restrict the number of parameters (to be identified) to a
13 small number; this step is called parameterization. The zonation approach and the pilot-point methodology can
14 both be viewed as two alternative paths for parameterization. As shown above, the pilot-point approach
15 eliminates an inherent subjectivity in the zonation approach and provides for the most objective inverse algorithm.

16 D.5.1 Objective Function

17 The objective function that is to be minimized in the calibration is a weighted least-square-error criterion
18 function. It comprises of two components, a model-fit criterion and a plausibility criterion. The model-fit
19 criterion is a weighted sum of the squared deviations between the computed and measured pressures taken over all
20 points in spatial and temporal domains, where pressure measurements have been made. The plausibility criterion
21 demands that the calibrated transmissivities be not too far from their prior estimates. A relative weight η between
22 the plausibility criterion and the model-fit criterion has been used. In the present study, due to the nature of the
23 pilot point methodology (de Marsily et al., 1984), the plausibility criterion is disregarded by setting $\eta = 0$; the
24 code, however, has the capability to use it.

25 Equation D-13 defines the objective function in general terms:

$$26 \quad J(\underline{u}) = \sum_{k=1}^L \underline{e}_p^T(k) \underline{R}^{-1}(k) \underline{e}_p(k) \quad (\text{model fit})$$

$$27 \quad + \eta \cdot \underline{e}_u^T \cdot \underline{U}^{-1} \cdot \underline{e}_u \quad (\text{plausibility}), \quad (\text{D-13})$$

28 where:

- 1 $J(\underline{u})$ = weighted least square (WLS) error criterion function
 2 $\underline{e}_p = \{p(k) - p_{ob}(k)\}$
 3 $\underline{e}_u = \{u - u_{est}\}$
 4 \underline{R} = covariance matrix of errors in p_{ob}
 5 \underline{U} = covariance matrix of errors in \underline{u}
 6 \underline{u} = vector of parameters ($Y_p = \log_{10} T_p$)
 7 η = relative weight of the plausibility criterion to model fit criterion
 8 k = time step number
 9 $\underline{p}(k)$ = pressures computed
 10 $p_{ob}(k)$ = pressures observed
 11 T = transpose
 12 T_p = pilot point transmissivity
 13 L = number of time steps.

14 After optimal estimates of \underline{u} are obtained, the posterior covariance matrix of the parameters is given by

$$15 \quad \underline{P}_{uu} = \left\{ \sum_{k=1}^L \underline{S}^T(k) \underline{R}^{-1}(k) \underline{S}(k) + \underline{U}^{-1} \right\}^{-1} \quad (D-14)$$

$$16 \quad \underline{S}^T(k) = \text{Jacobian Matrix} = \left[\frac{dp(k)}{du'} \right],$$

17

18 where \underline{P}_{uu} is the posterior covariance matrix of the parameters.

19 D.5.2 Parameters of Calibration

20 The pilot-point transmissivities are the parameters that are adjusted for calibration. However, in the
 21 mathematical implementation, the logarithms (to base 10) of the transmissivities (and not the transmissivity) are
 22 treated as parameters. The calibration parameters are given by

$$23 \quad Y_p = \log_{10} T_p$$

24 where T_p is the transmissivity at a pilot point (suffix p denotes pilot point). Figure D-4 illustrates the concepts
 25 of pilot points presented above.

1 D.5.3 Pilot-Point Location

2 Pilot points are placed at locations where their potential for reducing the objective function is the highest.
 3 This potential is quantified by the sensitivity coefficients (dJ/dY) of the objective function J , with respect to Y ,
 4 the logarithm (to base 10) of pilot-point transmissivity. A large number of candidate pilot points are considered,
 5 usually the centroids of all the grid blocks in the flow-model grid. The selected candidate pilot points are ranked in
 6 the descending order of the magnitude of their absolute sensitivity coefficients, i.e., $|dJ/dY|$. The required number
 7 of pilot points is chosen from the top of the ranked list of points.

8 Coupled adjoint sensitivity analysis and kriging is used to compute the required derivatives, and the procedure
 9 is documented in RamaRao and Reeves (1990). It is described briefly here.

10 Let P be a pilot point added to a set of N observation points. Let T_p be the transmissivity assigned to pilot
 11 point P . Kriging is done using Y_p , where

$$12 \quad Y_p = \log_{10} T_p \quad (D-15)$$

13 The kriged estimate (Y^*) at the centroid of a gridblock m , is given by

$$14 \quad Y_m^* = \sum_{k=1}^N Y_k \cdot \gamma_{m,k} + Y_p \cdot \gamma_{m,p}, \quad (D-16)$$

15 where k is the subscript for observation point, p is the subscript for pilot point, and $\gamma_{m,k}$ and $\gamma_{m,p}$ are the
 16 kriging weights for the interpolation point m and data point k and interpolation point m and data point p ,
 17 respectively.

18

19 When a pilot point transmissivity is perturbed, the kriged transmissivities and, hence, the permeabilities in
 20 all gridblocks are altered, causing the objective function J to change. Accordingly, using the chain rule,

$$21 \quad \frac{dJ}{dY_p} = \sum_{m=1}^M \frac{dJ}{dY_m^*} \frac{dY_m^*}{dY_p} \quad (D-17)$$

22 where M is the total number of grid blocks in the flow model.

$$23 \quad \frac{dY_m^*}{dY_p} = \gamma_{m,p} \quad (\text{from Equation D-16})$$

$$\frac{dJ}{dY_p} = \sum_{m=1}^M \frac{dJ}{dY_m^*} \gamma_{m,p} \quad (D-18)$$

$$Y_m^* = \log_{10}(T_m^*)$$

$$T_m^* = K_m \frac{\rho_m}{\mu_m} g b_m$$

$$\frac{dJ}{dY_m^*} = \ln(10) K_m \frac{dJ}{dK_m} \quad (D-19)$$

where T^* is the estimated transmissivity, K^* is the estimated permeability, ρ is fluid density, μ is fluid viscosity, g is acceleration due to gravity, b is gridblock thickness, and m is the subscript denoting gridblock.

Combining Equations D-18 and D-19

$$\frac{dJ}{dY_p} = \ln(10) \sum_{m=1}^M \gamma_{m,p} K_m \frac{dJ}{dK_m} \quad (D-20)$$

The sensitivity coefficient, dJ/dK_m of the objective function with respect to the permeability in a gridblock m is obtained by adjoint sensitivity analysis.

Adjoint sensitivity analysis provides an extremely fast algorithm, particularly when, for a given objective function J , the sensitivity coefficients are to be computed for a large number of parameters (permeabilities in thousands of grid blocks, as is the case here).

Let the groundwater flow model be represented by the following matrix equation:

$$\underline{\underline{A}} p^n = \underline{\underline{B}} p^{n-1} + \underline{\underline{f}}^n \quad (D-21)$$

where for a fully implicit scheme of time integration adopted here,

$\underline{\underline{p}}$ = vector of gridblock pressures

$\underline{\underline{A}} = \underline{\underline{C}} + \underline{\underline{B}}$

$\underline{\underline{B}} = \underline{\underline{S}}/\Delta t$

$\underline{\underline{C}}$ = conductance matrix

$\underline{\underline{S}}$ = storativity matrix

$\underline{\underline{f}}^n$ = vector of source terms

$\Delta t = t^n - t^{n-1}$

t = time

n = time level (1,2,3 L)

1 $L =$ maximum time level of the simulation.

2 First, an adjoint state vector $\{\lambda\}$ is obtained by the solution of the following equation:

$$3 \quad \underline{A}\underline{\lambda}^{n-1} = \underline{B}\underline{\lambda}^n + \left[\frac{\partial J}{\partial \underline{p}^n} \right]^T \quad (D-22)$$

4 where T denotes the transpose of the matrix.

5 Equation D-22 is solved backwards in time, from $n = L$ to $n = 1$ with

$$6 \quad \underline{\lambda}^L = 0 \quad (D-23)$$

7 If α_i is a generic sensitivity parameter in the gridblock i , the sensitivity coefficient $dJ/d\alpha_i$ is evaluated by
8 the expression:

$$9 \quad \frac{dJ}{d\alpha_i} = \frac{\partial J}{\partial \alpha_i} + \sum_{n=1}^L \underline{\lambda}^{nT} \cdot \left[\frac{\partial \underline{A}}{\partial \alpha_i} \underline{p}^n - \frac{\partial \underline{B}}{\partial \alpha_i} \underline{p}^{n-1} - \frac{\partial \underline{f}^n}{\partial \alpha_i} \right] \quad (D-24)$$

10

11 Here, the Equation D-24 is evaluated with $\alpha_i = K_i$, the permeability in the i^{th} gridblock.

12 **D.5.4 Pilot Points: Transmissivities**

13 The transmissivities at pilot points are assigned by an unconstrained optimization algorithm and a subsequent
14 imposition of constraints.

15 The optimization algorithm chosen here belongs to a class of iterative search algorithms. It involves a
16 repeated application of the following equation until convergence is achieved:

$$17 \quad \underline{Y}_{i+1} = \underline{Y}_i + \beta_i \bullet \underline{d}_i, \quad (D-25)$$

18 where i is the iteration index, \underline{d}_i is the direction vector, β_i is the step length (a scalar), and \underline{Y}_i is the vector of
19 parameters to be optimized (i.e., logarithms of pilot-point transmissivities to base 10).

20 The steps in the implementation of this algorithm are as follows:

- 21 1. For the selected number of pilot points, choose the initial estimates of the parameters ($Y_p = \log_{10} T_p$).
- 22 These are taken to be the kriged or the conditionally simulated values in the gridblocks, where pilot
- 23 points are located depending upon the option chosen.

1 the transmissivity field. One of the objectives in calibration can then be to limit the maximum change to a
2 specified value, so that the geostatistical structure is not altered significantly.

3 Consider the k th parameter, whose value is Y_k (k th element in the vector of parameters, \underline{Y}). Then,

$$\begin{aligned} \Delta Y_{k,i} &= (Y_{k,i+1} - Y_{k,i}) \\ &= \beta_i \cdot d_{k,i} \end{aligned} \quad , \quad (D-26)$$

5 where i is an iteration index.

6 Constraint 1: The parameter value should lie within the confidence band.

$$Y_{k,o} - m\sigma_{y_o} \leq Y_{k,i} \leq Y_{k,o} + m\sigma_{y_o}, \quad (D-27)$$

8 where the subscript o indicates initially kriged value, based on the measured data only. Thus $Y_{k,o}$ gives the
9 initially kriged value at the location of the k^{th} pilot point, and $\sigma_{y_o}^2$ gives the initially computed kriging variance
10 at the same location, m is the multiplier of the standard deviation, which gives the semi width of the confidence
11 band. If normal distribution is assumed for kriging errors, and if 95% confidence levels are desired; $m = 2$.

12 Constraint 2: The change in any parameters must be limited to ΔY_{\max} .

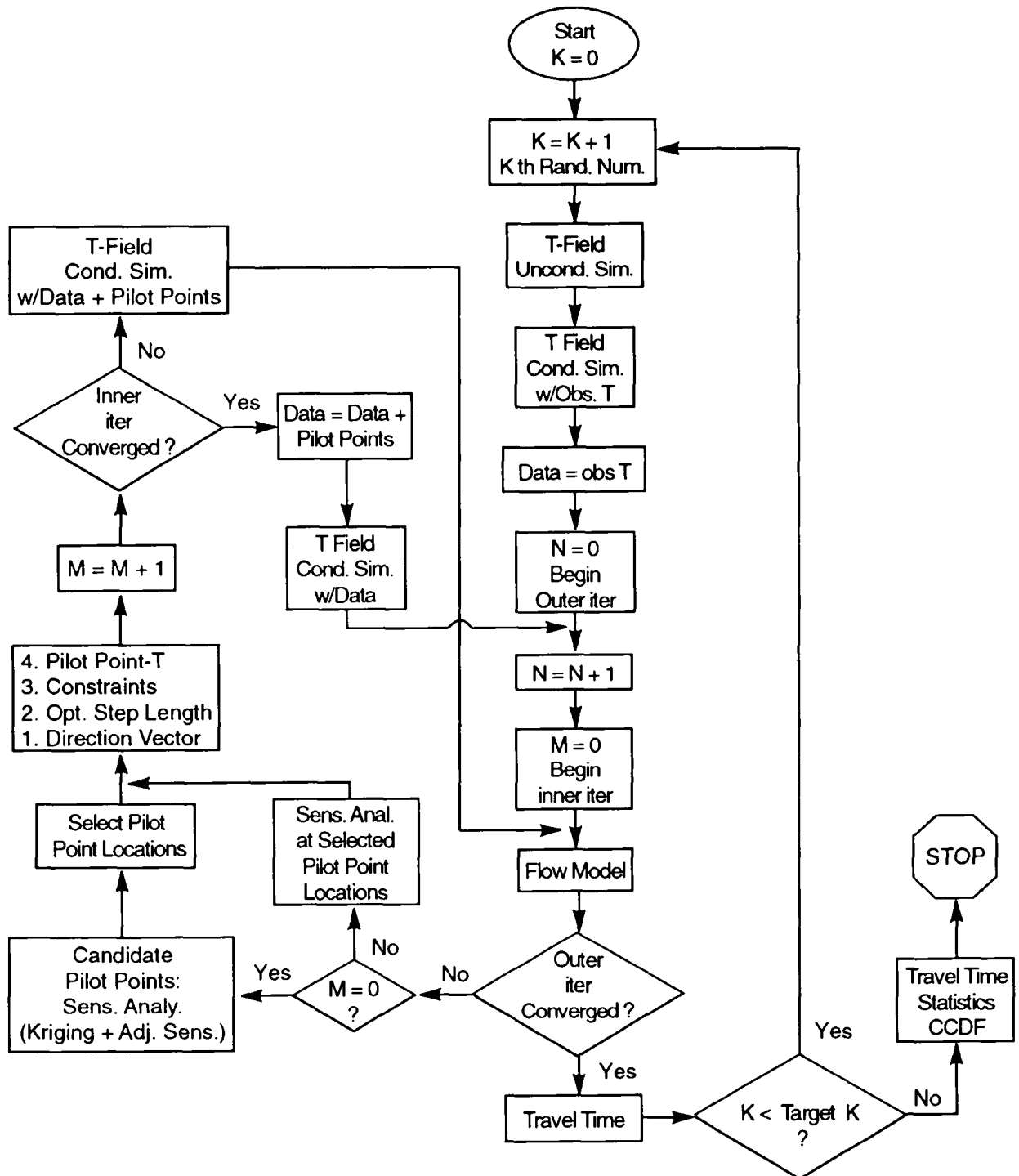
$$\Delta Y_{k,i} \leq \Delta Y_{\max} \quad (D-28)$$

14 After the optimization, these constraints are implemented for each parameter. In reality, only one constraint
15 is active for a pilot-point. Also, in implementation, the optimal step length computed is reduced if the constraint
16 became active, still preserving the direction.

17 D.5.6 Convergence Criteria

18 It may be noted that there are two levels of iteration, designated as inner and outer iterations. An inner
19 iteration relates to the iterations needed to optimize the transmissivities of the pilot points. Thus, when an inner
20 iteration is repeated, the pilot-point locations are fixed as at the beginning of the sequence of inner iterations.
21 When the convergence of an inner iteration is achieved, the pilot points are added to the transmissivity data set.
22 This then sets the stage for an outer iteration. During the course of outer iteration, optimal location of the next
23 set of pilot points is done using coupled kriging and adjoint sensitivity analysis. Subsequently, their
24 transmissivities are optimized by a sequence of inner iterations. Figure D-5 clarifies these points.

25 It may be noted that both inner and outer iterations go through all phases of the algorithm, except that inner
26 iterations skip the phase of selecting pilot points from a grid of candidate pilot points.



TRI-6342-3306-0

Figure D-5. Inner and outer iterations of calibration.

1 D.5.6.1 CONVERGENCE CRITERIA: INNER ITERATIONS.

- 2 1. The performance measure J drops below a prescribed minimum value (JMIN):

3
$$J \leq \text{JMIN} \tag{D-29}$$

- 4 2. The number of iterations (NITER) equals a prescribed maximum number of iterations, for the inner
5 iterations (ITERMX1):

6
$$\text{NITER} \geq \text{ITERMX1} \tag{D-30}$$

- 7 3. The ratio of the norm of the gradient, to the initial-gradient norm reduces below a prescribed value
8 (GRNR):

9
$$\frac{\|g\|}{\|g_0\|} \leq \text{GRNR} \tag{D-31}$$

(gradient norm ratio)

- 10 4. The gradient norm $\|g\|$ is less than a prescribed minimum (GRMIN):

11
$$\|g\| \leq \text{GRMIN} \tag{D-32}$$

- 12 5. The relative change in objective function is defined, as $\Delta J/J$, where ΔJ is the change in the objective
13 function during one iteration. Iterations are terminated if this relative change falls below a prescribed
14 value (RELCJ):

15
$$\frac{\Delta J}{J} \leq \text{RELCJ} \tag{D-33}$$

16 D.5.6.2 CONVERGENCE CRITERIA: OUTER ITERATIONS.

17 Outer iterations are terminated essentially on criteria (1) and (2) of inner iterations. They are not repeated.

18

Appendix D References

- 1
- 2 Carrera, J., and S.P. Neuman. 1986. "Estimation of Aquifer Parameters Under Transient and Steady State
3 Conditions 2, Uniqueness, Stability, and Solution Algorithms," *Water Resources Research*. Vol. 22,
4 no. 2, 211-227.
- 5 Delfiner, P. 1976. "Linear Estimation of Non Stationary Spatial Phenomena," *Advanced Geostatistics in the
6 Mining Industry, Proceedings of the NATO Advanced Study Institute, University of Rome, October 13-
7 25, 1975*. Eds. M. Guarescio, M. David, and C. Huijbregts. Hingham, MA: D. Reidel, 49-68.
- 8 Delhomme, J.P. 1979. "Spatial Variability and Uncertainty in Groundwater Flow Parameters: A Geostatistical
9 Approach," *Water Resources Research*. Vol. 15, no. 2, 269-280.
- 10 de Marsily, G, G. Lavedan, M. Boucher, and G. Fasanino. 1984. "Interpretation of Interference Tests in a Well
11 Feild Using Geostatistical Techniques to Fit the Permeability Distribution in a Reservoir Model,"
12 *Geostatistics for Natural Resources Characterization, South Lake Tahoe, CA, Sept. 6-17, 1983*. Eds. G.
13 Verly, M. David, A.G. Journel, and A. Marechai. Hingham, MA: D. Reidel, Pt. 2, 831-849.
- 14 Gallegos, D.P., P.I. Pohl , and C.D. Updegraff. 1992. *An Investigation of the Impact of Conceptual Model
15 Uncertainty on the Estimated Performance of a Hypothetical High-Level Nuclear Waste Repository Site
16 in Unsaturated, Fractured Tuff*. SAND90-2882. Albuquerque, NM: Sandia National Laboratories.
- 17 Gill, P.E., W. Murray, and M.H. Wright. 1981. *Practical Optimization*. New York, NY: Academic Press,
18 Inc.
- 19 Intera, Inc. 1989. *Users Manual for STLINE*. 097B-12C-001B.
- 20 Kafritsas, J., and R.L. Bras. 1981. *The Practice of Kriging*. Technical Report 263. Cambridge, MA: Ralph M.
21 Parsons Laboratory, Massachusetts Institute of Technology.
- 22 LaVenue, A.M., T.L. Cauffman, and J.F. Pickens. 1990. *Ground-Water Flow Modeling of the Culebra
23 Dolomite. Volume I: Model Calibration*. SAND89-7068/1. Albuquerque, NM: Sandia National
24 Laboratories.
- 25 LaVenue, A.M., and B.S. RamaRao. 1992. *A Modeling Attempt to Address Spatial Variability within the
26 Culebra Dolomite Transmissivity Field*. SAND92-7306. Albuquerque, NM: Sandia National
27 Laboratories.
- 28 Luenberger, D.G. 1973. *Introduction to Linear and Nonlinear Programming*. Reading, MA: Addison-Wesley
29 Publishing Co.

- 1 Mantoglou, A., and J.L. Wilson. 1982. "Turning Bands Method for Simulation of Random Fields Using Line
2 Generation by a Spectral Method," *Water Resources Research*. Vol. 18, no. 5, 1379-1394.
- 3 Matheron, G. 1971. *The Theory of Regionalized Variables and its Applications*. Paris, France: École National
4 Supérieure des Mines.
- 5 Matheron, G. 1973. "The Intrinsic Random Functions and Their Applications," *Advances in Applied*
6 *Probability*. Vol. 5, no. 3, 439-468.
- 7 Mejía, J. M., and I. Rodríguez-Iturbe. 1974. "On the Synthesis of Random Fields Sampling From the
8 Spectrum: An Application to the Generation of Hydrologic Spatial Processes," *Water Resources*
9 *Research*. Vol. 10, no. 4, 705-711.
- 10 RamaRao, B.S., and M. Reeves. 1990. *Theory and Verification for the GRASP II Code for Adjoint-Sensitivity*
11 *Analysis of Steady-State and Transient Ground-Water Flow*. SAND89-7143. Albuquerque, NM: Sandia
12 National Laboratories.
- 13 Reeves, M., D.S. Ward, N.D. Johns, and R.M. Cranwell. 1986a. *Theory and Implementation for SWIFT II, the*
14 *Sandia Waste-Isolation Flow and Transport Model for Fractured Media, Release 4.84*.
15 NUREG/CR-3328. SAND83-1159. Albuquerque, NM: Sandia National Laboratories.
- 16 Reeves, M., D.S. Ward, N.D. Johns, and R.M. Cranwell. 1986b. *Data Input Guide for SWIFT II, The Sandia*
17 *Waste-Isolation Flow and Transport Model for Fractured Media, Release 4.84*. NUREG/CR-3162.
18 SAND83-0242. Albuquerque, NM: Sandia National Laboratories.
- 19 Reeves, M., D.S. Ward, P.A. Davis, and E.J. Bonano. 1986c. *Swift II Self-Teaching Curriculum: Illustrative*
20 *Problems for the Sandia Waste Isolation Flow and Transport Model for Fractured Media*.
21 NUREG/CR-3925. SAND84-1586. Albuquerque, NM: Sandia National Laboratories.
- 22 Shinozuka, M., and C-M. Jan. 1972. "Digital Simulation of Random Processes and Its Applications," *Journal*
23 *of Sound and Vibration*. Vol. 25, no. 1, 111-128.
- 24 Smith, L., and R.A. Freeze. 1979. "Stochastic Analysis of Steady State Groundwater Flow in a Bounded
25 Domain. 2. Two-dimensional Simulations," *Water Resources Research*. Vol. 15, no. 6, 1543-1559.
- 26 Smith, L., and F.W. Schwartz. 1981. "Mass Transport. 2. Analysis of Uncertainty in Prediction," *Water*
27 *Resources Research*. Vol. 17, no. 2, 351-369.
- 28 Wilson, J.L., B.S. RamaRao, and J.A. McNeish. 1986. *GRASP: A Computer Code to Perform Post-SWENT*
29 *Adjoint Sensitivity Analysis of Stead-State Ground-Water Flow*. BMI/ONWI-625. Columbus, OH:
30 Office of Nuclear Waste Isolation, Battelle Memorial Institute.

- 1 WIPP Performance Assessment (PA) Division. 1991. *Preliminary Comparison with 40 CFR Part 191, Subpart*
2 *B for the Waste Isolation Pilot Plant, December 1991 — Volume 2: Probability and Consequence*
3 *Modeling*. SAND91-0893/2. Albuquerque, NM: Sandia National Laboratories.

- 4 Zimmerman, D.A., and J.L. Wilson. 1990. *Description of and User's Manual for TUBA: A Computer Code*
5 *for Generating Two-Dimensional Random Fields via the Turning Bands Method*. Albuquerque, NM:
6 Gram, Inc.

DISTRIBUTION

(Send Distribution list changes to M.M. Gruebel, Dept. 6342, Sandia
National Laboratories, PO Box 5800, Albuquerque, NM 87185-5800)

Federal Agencies

US Department of Energy (2)
Office of Environmental Restoration
and Waste Management
Attn: L.P. Duffy, EM-1
C. Frank, EM-50
Washington, DC 20585

US Department of Energy (3)
Office of Environmental Restoration
and Waste Management
Attn: M. Frei, EM-34 (Trevion II)
Director, Waste Management Projects
Washington, DC 20585-0002

US Department of Energy
Office of Environmental Restoration
and Waste Management
Attn: J. Lytle, EM-30 (Trevion II)
Washington, DC 20585-0002

US Department of Energy
Office of Environmental Restoration
and Waste Management
Attn: S. Schneider, EM-342
(Trevion II)
Washington, DC 20585-0002

US Department of Energy (3)
WIPP Task Force
Attn: G.H. Daly
S. Fucigna
B. Bower
12800 Middlebrook Rd.
Suite 400
Germantown, MD 20874

US Department of Energy (4)
Office of Environment, Safety and
Health
Attn: R.P. Berube, EH-20
C. Borgstrum, EH-25
R. Pelletier, EH-231
K. Taimi, EH-232
Washington, DC 20585

US Department of Energy (5)
WIPP Project Integration Office
Attn: W.J. Arthur III
R. Becker
P. Dickman
L.W. Gage
P.J. Higgins
D.A. Olona
PO Box 5400
Albuquerque, NM 87115-5400

US Department of Energy (10)
WIPP Project Site Office (Carlsbad)
Attn: A. Hunt (4)
V. Daub (4)
J. Lippis
K. Hunter
PO Box 3090
Carlsbad, NM 88221-3090

US Department of Energy, (5)
Office of Civilian Radioactive Waste
Management
Attn: Deputy Director, RW-2
Associate Director, RW-10
Office of Program
Administration and
Resources Management
Associate Director, RW-20
Office of Facilities
Siting and Development
Associate Director, RW-30
Office of Systems
Integration and
Regulations
Associate Director, RW-40
Office of External
Relations and Policy
Office of Geologic Repositories
Forrestal Building
Washington, DC 20585

US Department of Energy
Attn: National Atomic Museum Library
Albuquerque Operations Office
PO Box 5400
Albuquerque, NM 87185

US Department of Energy
Research & Waste Management Division
Attn: Director
PO Box E
Oak Ridge, TN 37831

US Department of Energy (2)
Idaho Operations Office
Fuel Processing and Waste
Management Division
785 DOE Place
Idaho Falls, ID 83402

US Department of Energy
Savannah River Operations Office
Defense Waste Processing
Facility Project Office
Attn: W.D. Pearson
PO Box A
Aiken, SC 29802

US Department of Energy (2)
Richland Operations Office
Nuclear Fuel Cycle & Production
Division
Attn: R.E. Gerton
825 Jadwin Ave.
PO Box 500
Richland, WA 99352

US Department of Energy (3)
Nevada Operations Office
Attn: J.R. Boland
D. Livingston
P.K. Fitzsimmons
2753 S. Highland Drive
Las Vegas, NV 89183-8518

US Department of Energy (2)
Technical Information Center
PO Box 62
Oak Ridge, TN 37831

US Department of Energy (2)
Chicago Operations Office
Attn: J.C. Haugen
9800 South Cass Avenue
Argonne, IL 60439

US Department of Energy
Los Alamos Area Office
528 35th Street
Los Alamos, NM 87544

US Department of Energy (3)
Rocky Flats Area Office
Attn: W.C. Rask
G. Huffman
T. Lukow
PO Box 928
Golden, CO 80402-0928

US Department of Energy
Dayton Area Office
Attn: R. Grandfield
PO Box 66
Miamisburg, OH 45343-0066

US Department of Energy
Attn: E. Young
Room E-178
GAO/RCED/GTN
Washington, DC 20545

US Bureau of Land Management
101 E. Mermod
Carlsbad, NM 88220

US Bureau of Land Management
New Mexico State Office
PO Box 1449
Santa Fe, NM 87507

US Environmental Protection
Agency (2)
Office of Radiation Protection Programs
(ANR-460)
Washington, DC 20460

US Nuclear Regulatory Commission
Division of Waste Management
Attn: H. Marson
Mail Stop 4-H-3
Washington, DC 20555

US Nuclear Regulatory Commission (4)
Advisory Committee on Nuclear Waste
Attn: D. Moeller
M.J. Steindler
P.W. Pomeroy
W.J. Hinze
7920 Norfolk Avenue
Bethesda, MD 20814

Defense Nuclear Facilities Safety Board
Attn: D. Winters
625 Indiana Avenue, NW
Suite 700
Washington, DC 20004

Nuclear Waste Technical Review
Board (2)
Attn: Library
Suite 910
1100 Wilson Blvd.
Arlington, VA 22209-2297

Energy and Science Division
Office of Management and Budget
Attn: K. Yuracko
725 17th Street NW
Washington, DC 20503

US Geological Survey (2)
Water Resources Division
Attn: C. Peters
Suite 200
4501 Indian School NE
Albuquerque, NM 87110

New Mexico Congressional Delegation

Jeff Bingaman
U.S. Senate
110 Hart SOB
Washington, DC 20510-3102

Pete V. Domenici
U.S. Senate
427 Dirksen Bldg.
Washington, DC 20510-3101

Bill Richardson
House of Representatives
2349 Rayburn HOB
Washington, DC 20515

Steven H. Schiff
House of Representatives
1009 Longworth HOB
Washington, DC 20515

Joe Skeen
House of Representatives
2367 Rayburn HOB
Washington, DC 20515

State Agencies

New Mexico Bureau of Mines
and Mineral Resources
Socorro, NM 87801

New Mexico Energy, Minerals and Natural
Resources Department
Attn: Librarian
2040 South Pacheco
Santa Fe, NM 87505

New Mexico Energy, Minerals and Natural
Resources Department
New Mexico Radioactive Task Force (2)
(Governor's WIPP Task Force)
Attn: A. Lockwood, Chairman
C. Wentz, Coordinator/Policy Analyst
2040 South Pacheco
Santa Fe, NM 87505

Bob Forrest
Mayor, City of Carlsbad
PO Box 1569
Carlsbad, NM 88221

Executive Director
Carlsbad Department of Development
Attn: C. Bernard
PO Box 1090
Carlsbad, NM 88221

New Mexico Environment Department
Secretary of the Environment (3)
Attn: J. Espinosa
PO Box 968
1190 St. Francis Drive
Santa Fe, NM 87503-0968

New Mexico Environment Department
Attn: P. McCasland
WIPP Project Site Office
PO Box 3090
Carlsbad, NM 88221-3090

New Mexico State Engineer's Office
Attn: M. Chudnoff
PO Box 25102
Santa Fe, NM 87504-5102

Environmental Evaluation Group (5)
Attn: R. Neill
Suite F-2
7007 Wyoming Blvd. NE
Albuquerque, NM 87109

Advisory Committee on Nuclear Facility Safety

John F. Ahearne
Executive Director, Sigma Xi
99 Alexander Drive
Research Triangle Park, NC 27709

James E. Martin
109 Observatory Road
Ann Arbor, MI 48109

**WIPP Panel of National Research Council's
Board on Radioactive Waste Management**

Charles Fairhurst, Chairman
Department of Civil and
Mineral Engineering
University of Minnesota
500 Pillsbury Dr., SE
Minneapolis, MN 55455-0220

John O. Blomeke
3833 Sandy Shore Drive
Lenoir City, TN 37771-9803

John D. Bredehoeft
Western Region Hydrologist
Water Resources Division
US Geological Survey (M/S 439)
345 Middlefield Road
Menlo Park, CA 94025

Fred M. Ernsberger
1325 NW 10th Avenue
Gainesville, FL 32601

Rodney C. Ewing
Department of Geology
University of New Mexico
200 Yale, NE
Albuquerque, NM 87131

B. John Garrick
PLG, Inc.
Suite 400
4590 MacArthur Blvd.
Newport Beach, CA 92660-2027

Leonard F. Konikow
US Geological Survey
431 National Center
Reston, VA 22092

Jeremiah O'Driscoll
505 Valley Hill Drive
Atlanta, GA 30350

Christopher Whipple
Clement International Corp.
160 Spear St.
Suite 1380
San Francisco, CA 94105-1535

National Research Council (3)
Board on Radioactive
Waste Management
RM HA456
Attn: P.B. Myers,
Staff Director (2)
G.J. Grube
2101 Constitution Avenue
Washington, DC 20418

Performance Assessment Peer Review Panel

G. Ross Heath
College of Ocean and
Fishery Sciences HN-15
583 Henderson Hall
University of Washington
Seattle, WA 98195

Thomas H. Pigford
Department of Nuclear Engineering
4159 Etcheverry Hall
University of California
Berkeley, CA 94720

Thomas A. Cotton
JK Research Associates, Inc.
4429 Butterworth Place, NW
Washington, DC 20016

Robert J. Budnitz
President, Future Resources
Associates, Inc.
2000 Center Street
Suite 418
Berkeley, CA 94704

C. John Mann
Department of Geology
245 Natural History Bldg.
1301 West Green Street
University of Illinois
Urbana, IL 61801

Frank W. Schwartz
Department of Geology and Mineralogy
The Ohio State University
Scott Hall
1090 Carmack Rd.
Columbus, OH 43210

National Laboratories

Argonne National Laboratory (2)

Attn: A. Smith
D. Tomasko
9700 South Cass, Bldg. 201
Argonne, IL 60439

Battelle Pacific Northwest Laboratory (3)

Attn: R.E. Westerman
S. Bates
H.C. Burkholder
Battelle Boulevard
Richland, WA 99352

Idaho National Engineering Laboratory (2)

Attn: H. Loo
R. Klinger
Mail Stop 5108
Idaho Falls, ID 83403-4000

Los Alamos National Laboratory

Attn: B. Erdal, CNC-11
PO Box 1663
Los Alamos, NM 87545

Los Alamos National Laboratory

Attn: A. Meijer
PO Box 1663, Mail Stop J514
Los Alamos, NM 87545

Los Alamos National Laboratory (3)

HSE-8
Attn: M. Enoris
L. Soholt
J. Wenzel
PO Box 1663
Los Alamos, NM 87545

Los Alamos National Laboratory

EM-7
Attn: S. Kosiewicz
PO Box 1663, Mail Stop J595
Los Alamos, NM 87545

Oak Ridge National Laboratory

Transuranic Waste Manager
Attn: D.W. Turner
PO Box 2008, Bldg. 3047
Oak Ridge, TN 37831-6060

Pacific Northwest Laboratory

Attn: B. Kennedy
PO Box 999
Richland, WA 99352

Savannah River Laboratory (3)

Attn: N. Bibler
M.J. Plodinec
G.G. Wicks
Aiken, SC 29801

Savannah River Plant (2)

Attn: R.G. Baxter
Bldg. 704-S
K.W. Wierzbicki
Bldg. 703-H
Aiken, SC 29808-0001

Corporations/Members of the Public

Benchmark Environmental Corp.

Attn: C. Frederickson
4501 Indian School NE
Suite 105
Albuquerque, NM 87110

City of Albuquerque
Public Works Department
Utility Planning Division
Attn: W.K. Summers
PO Box 1293
Albuquerque, NM 87103

Deuel and Associates, Inc.

Attn: R.W. Prindle
7208 Jefferson NE
Albuquerque, NM 87109

Disposal Safety, Inc.

Attn: B. Ross
1660 L Street NW
Suite 314
Washington, DC 20036

Ecodynamics (2)

Attn: P. Roache
R. Blaine
PO Box 9229
Albuquerque, NM 87119-9229

EG & G Idaho (3)

1955 Fremont Street
Attn: C. Atwood
C. Hertzler
T.I. Clements
Idaho Falls, ID 83415

Geomatrix

Attn: K. Coppersmith
100 Pine Street, Suite 1000
San Francisco, CA 94111

Golder Associates, Inc. (3)
Attn: M. Cunnane
R. Kossik
I. Miller
4104 148th Avenue NE
Redmond, WA 98052

INTERA, Inc. (2)
Attn: J.F. Pickens
A.M. LaVenve
6850 Austin Center Blvd.
Suite 300
Austin, TX 78731

INTERA, Inc.
Attn: W. Stensrud
PO Box 2123
Carlsbad, NM 88221

INTERA, Inc.
Attn: W. Nelson
101 Convention Center Drive
Suite 540
Las Vegas, NV 89109

IT Corporation (2)
Attn: R.F. McKinney
J. Myers
Regional Office, Suite 700
5301 Central Avenue NE
Albuquerque, NM 87108

John Hart and Associates, P.A.
Attn: J.S. Hart
2815 Candelaria Road NW
Albuquerque, NM 87107

John Hart and Associates, P.A.
Attn: K. Lickliter
1009 North Washington
Tacoma, WA 98406

MACTEC (2)
Attn: J.A. Thies
D.K. Duncan
8418 Zuni Road SE, Suite 200
Albuquerque, NM 87108

Newman and Holtzinger
Attn: C. Mallon
1615 L Street NW, Suite 1000
Washington, DC 20036

RE/SPEC, Inc. (2)
Attn: W. Coons
4775 Indian School NE, Suite 300
Albuquerque, NM 87110

RE/SPEC, Inc.
Attn: J.L. Ratigan
PO Box 725
Rapid City, SD 57709

Reynolds Elect/Engr. Co., Inc.
Attn: E.W. Kendall
Building 790, Warehouse Row
PO Box 98521
Las Vegas, NV 89193-8521

Roy F. Weston, Inc.
CRWM Tech. Supp. Team
Attn: C.J. Noronha
955 L'Enfant Plaza SW
North Building, Eighth Floor
Washington, DC 20024

Science Applications International Corporation
(SAIC)
Attn: H.R. Pratt
10260 Campus Point Drive
San Diego, CA 92121

Science Applications International Corporation
(2)
Attn: D.C. Royer
C.G. Pflum
101 Convention Center Dr.
Las Vegas, NV 89109

Science Applications International Corporation
(2)
Attn: M. Davis
J. Tollison
2109 Air Park Road SE
Albuquerque, NM 87106

Science Applications International Corporation
(2)
Attn: J. Young
D. Lester
18706 North Creek Parkway, Suite 110
Bothell, WA 98011

Southwest Research Institute
Center for Nuclear Waste Regulatory Analysis
(2)
Attn: P.K. Nair
6220 Culebra Road
San Antonio, TX 78228-0510

Systems, Science, and Software (2)
Attn: E. Peterson
P. Lagus
Box 1620
La Jolla, CA 92038

TASC
Attn: S.G. Oston
55 Walkers Brook Drive
Reading, MA 01867

Tech Reps, Inc. (6)
Attn: J. Chapman
C. Crawford
D. Marchand
J. Stikar
P. Oliver
D. Scott
5000 Marble NE, Suite 222
Albuquerque, NM 87110

Tolan, Beeson & Associates
Attn: T.L. Tolan
2320 W. 15th Avenue
Kennewick, WA 99337

TRW Environmental Safety Systems
Attn: I. Sacks
2650 Park Tower Drive, Suite 800
Vienna, VA 22180

Westinghouse Electric Corporation (5)
Attn: Library
L. Trego
C. Cox
L. Fitch
R.F. Kehrman
PO Box 2078
Carlsbad, NM 88221

Westinghouse Hanford Company
Attn: D. E. Wood
MSIN HO-32
PO Box 1970
Richland, WA 99352

Western Water Consultants
Attn: D. Fritz
1949 Sugarland Drive #134
Sheridan, WY 82801-5720

Western Water Consultants
Attn: P.A. Rechard
PO Box 4128
Laramie, WY 82071

P. Drez
8816 Cherry Hills Road, NE
Albuquerque, NM 87111

D.W. Powers
Star Route Box 87
Anthony, TX 79821

Shirley Thieda
PO Box 2109, RR1
Bernalillo, NM 87004

Jack Urich
c/o CARD
144 Harvard SE
Albuquerque, NM 87106

Universities

University of California
Mechanical, Aerospace, and
Nuclear Engineering Department (2)
Attn: W. Kastenberg
D. Browne
5532 Boelter Hall
Los Angeles, CA 90024

University of California
Mine Engineering Dept.
Attn: Neville Cook
Rock Mechanics Engineering
Berkeley, CA 94720

University of Hawaii at Hilo
Attn: S. Hora
Business Administration
Hilo, HI 96720-4091

University of New Mexico
Geology Department
Attn: Library
Albuquerque, NM 87131

University of New Mexico
Research Administration
Attn: H. Schreyer
102 Scholes Hall
Albuquerque, NM 87131

University of Wyoming
Department of Civil Engineering
Attn: V.R. Hasfurther
Laramie, WY 82071

University of Wyoming
Department of Geology
Attn: J.I. Drever
Laramie, WY 82071

University of Wyoming
Department of Mathematics
Attn: R.E. Ewing
Laramie, WY 82071

Libraries

Thomas Brannigan Library
Attn: D. Dresp
106 W. Hadley St.
Las Cruces, NM 88001

Hobbs Public Library
Attn: M. Lewis
509 N. Ship Street
Hobbs, NM 88248

New Mexico State Library
Attn: N. McCallan
325 Don Gaspar
Santa Fe, NM 87503

New Mexico Tech
Martin Speere Memorial Library
Campus Street
Socorro, NM 87810

New Mexico Junior College
Pannell Library
Attn: R. Hill
Lovington Highway
Hobbs, NM 88240

Carlsbad Municipal Library
WIPP Public Reading Room
Attn: L. Hubbard
101 S. Halagueno St.
Carlsbad, NM 88220

University of New Mexico
General Library
Government Publications Department
Albuquerque, NM 87131

NEA/Performance Assessment Advisory Group (PAAG)

P. Duerden
ANSTO
Lucas Heights Research Laboratories
Private Mail Bag No. 1
Menai, NSW 2234, AUSTRALIA

Gordon S. Linsley
Division of Nuclear Fuel Cycle and Waste
Management
International Atomic Energy Agency
PO Box 100
A-1400 Vienna, AUSTRIA

Nicolo Cadelli
Commission of the European Communities
200, Rue de la Loi
B-1049 Brussels, BELGIUM

R. Heremans
Organisme Nationale des Déchets Radioactifs
et des Matières Fissiles
ONDRAF
Place Madou 1, Boitec 24/25
B-1030 Brussels, BELGIUM

J. Marivoet
Centre d'Etudes de l'Energie Nucléaire
CEN/SCK
Boeretang 200
B-2400 Mol, BELGIUM

P. Conlon
Waste Management Division
Atomic Energy Control Board (AECB)
PO Box 1046
Ottawa, Canada K1P 5S9, CANADA

A.G. Wikjord
Manager, Environmental and Safety
Assessment Branch
Atomic Energy of Canada Limited
Whiteshell Nuclear Research Establishment
Pinewa, Manitoba R0E 1L0, CANADA

Jukka-Pekka Salo
Teollisuuden Voima Oy (TVO)
Fredrikinkatu 51-53 B
SF-00100 Helsinki, FINLAND

Timo Vieno
Technical Research Centre of Finland (VTT)
Nuclear Energy Laboratory
PO Box 208
SF-02151 Espoo, FINLAND

Timo Äikäs
Teollisuuden Voima Oy (TVO)
Fredrikinkatu 51-53 B
SF-00100 Helsinki, FINLAND

M. Claude Ringard
Division de la Sécurité et de la Protection de
l'Environnement (DSPE)
Commissariat à l'Energie Atomique
Agence Nationale pour la Gestion des Déchets
Radioactifs (ANDRA)
Route du Panorama Robert Schuman
B. P. No. 38
F-92266 Fontenay-aux-Roses Cedex
FRANCE

Gérald Ouzounian
Agence Nationale pour la Gestion des Déchets
Radioactifs (ANDRA)
Route du Panorama Robert Schuman
B. P. No. 38
F-92266 Fontenay-aux-Roses Cedex
FRANCE

Claudio Pescatore
Division of Radiation Protection and Waste
Management
OECD Nuclear Energy Agency
38, Boulevard Suchet
F-75016 Paris, FRANCE

M. Dominique Greneche
Commissariat à l'Energie Atomique
IPSN/DAS/SASICC/SAED
B. P. No. 6
F-92265 Fontenay-aux-Roses Cedex,
FRANCE

Robert Fabriol
Bureau de Recherches Géologiques et Minières
(BRGM)
B. P. 6009
45060 Orléans Cedex 2, FRANCE

P. Bogorinski
Gesellschaft für Reaktorsicherheit (GRS) mbH
Schwertnergasse 1
D-5000 Köln 1, GERMANY

R. Storck
GSF - Institut für Tieflagerung
Theodor-Heuss-Strabe 4
D-3300 Braunschweig, GERMANY

Ferruccio Gera
ISMES S.p.A
Via del Crociferi 44
I-00187 Rome, ITALY

Hiroyuki Umeki
Isolation System Research Program
Radioactive Waste Management Project
Power Reactor and Nuclear Fuel Development
Corporation (PNC)
1-9-13, Akasaka
Minato-ku
Tokyo 107, JAPAN

P. Carboneras Martinez
ENRESA
Calle Emilio Vargas 7
R-28043 Madrid, SPAIN

Tönis Papp
Swedish Nuclear Fuel and Waste Management
Co.
Box 5864
S 102 48 Stockholm, SWEDEN

Conny Hägg
Swedish Radiation Protection Institute (SSI)
Box 60204
S-104 01 Stockholm, SWEDEN

J. Hadermann
Paul Scherrer Institute
Waste Management Programme
CH-5232 Villigen PSI, SWITZERLAND

J. Vigfusson
USK- Swiss Nuclear Safety Inspectorate
Federal Office of Energy
CH-5303 Würenlingen, SWITZERLAND

D.E. Billington
Departmental Manager - Assessment Studies
Radwaste Disposal R&D Division
AEA Decommissioning & Radwaste
Harwell Laboratory, B60
Didcot Oxfordshire OX11 ORA
UNITED KINGDOM

P. Grimwood
Waste Management Unit
BNFL
Sellafield
Seascale, Cumbria CA20 1PG
UNITED KINGDOM

Alan J. Hooper
UK Nirex Ltd
Curie Avenue
Harwell, Didcot
Oxfordshire, OX11 ORH
UNITED KINGDOM

Jerry M. Boak
Yucca Mountain Project Office
US Department of Energy
PO Box 98608
Las Vegas, NV 89193

Seth M. Coplan (Chairman)
US Nuclear Regulatory Commission
Division of High-Level Waste Management
Mail Stop 4-H-3
Washington, DC 20555

A.E. Van Luik
INTERA/M&O
The Valley Bank Center
101 Convention Center Dr.
Las Vegas, NV 89109

NEA/PSAG User's Group

Shaheed Hossain
Division of Nuclear Fuel Cycle and Waste
Management
International Atomic Energy Agency
Wagramerstrasse 5
PO Box 100
A-1400 Vienna, AUSTRIA

Alexander Nies (PSAC Chairman)
Gesellschaft für Strahlen- und
Institut für Tief Lagerung
Abteilung für Endlagersicherheit
Theodor-Heuss-Strasse 4
D-3300 Braunschweig, GERMANY

Eduard Hofer
Gesellschaft für Reaktorsicherheit (GRS) MBH
Forschungsgelände
D-8046 Garching, GERMANY

Andrea Saltelli
Commission of the European Communities
Joint Research Centre of Ispra
I-21020 Ispra (Varese), ITALY

Alejandro Alonso
Cátedra de Tecnología Nuclear
E.T.S. de Ingenieros Industriales
José Gutiérrez Abascal, 2
E-28006 Madrid, SPAIN

Pedro Prado
CIEMAT
Instituto de Tecnología Nuclear
Avenida Complutense, 22
E-28040 Madrid, SPAIN

Miguel Angel Cuñado
ENRESA
Emilio Vargas, 7
E-28043 Madrid, SPAIN

Francisco Javier Elorza
ENRESA
Emilio Vargas, 7
E-28043 Madrid, SPAIN

Nils A. Kjellbert
Swedish Nuclear Fuel and Waste Management
Company (SKB)
Box 5864
S-102 48 Stockholm, SWEDEN

Björn Cronhjort
Swedish National Board for Spent Nuclear
Fuel (SKN)
Sehlsedtskatan 9
S-115 28 Stockholm, SWEDEN

Richard A. Klos
Paul-Scherrer Institute (PSI)
CH-5232 Villigen PSI
SWITZERLAND

NAGRA (2)
Attn: C. McCombie
F. Van Dorp
Parkstrasse 23
CH-5401 Baden, SWITZERLAND

N. A. Chapman
Intera Information Technologies
Park View House, 14B Burton Street
Melton Mowbray
Leicestershire, LE13 1AE
UNITED KINGDOM

Daniel A. Galson
Galson Sciences Ltd.
35, Market Place
Oakham
Leicestershire LE15 6DT
UNITED KINGDOM

David P. Hodgkinson
Intera Information Technologies
Chiltern House
45 Station Road
Henley-on-Thames
Oxfordshire RG9 1AT, UNITED KINGDOM

Brian G.J. Thompson
Department of the Environment: Her
Majesty's Inspectorate of Pollution
Room A5.33, Romney House
43 Marsham Street
London SW1P 2PY, UNITED KINGDOM

Intera Information Technologies
Attn: M.J.Apted
3609 South Wadsworth Blvd.
Denver, CO 80235

US Nuclear Regulatory Commission (2)
Attn: R. Codell
N. Eisenberg
Mail Stop 4-H-3
Washington, DC 20555

Battelle Pacific Northwest Laboratories
Attn: P.W. Eslinger
PO Box 999, MS K2-32
Richland, WA 99352

Center for Nuclear Waste Regulatory Analysis
(CNWRA)
Southwest Research Institute
Attn: B. Sagar
PO Drawer 28510
6220 Culebra Road
San Antonio, TX 78284

Geostatistics Expert Working Group (GXG)

Rafael L. Bras
R.L. Bras Consulting Engineers
44 Percy Road
Lexington, MA 02173

Jesus Carrera
Universidad Politècnica de Catalunya
E.T.S.I. Caminos
Jordi, Girona 31
E-08034 Barcelona, SPAIN

Gedeon Dagan
Department of Fluid Mechanics and Heat
Transfer
Tel Aviv University
PO Box 39040
Ramat Aviv, Tel Aviv 69978, ISRAEL

Ghislain de Marsily (GXG Chairman)
University Pierre et Marie Curie
Laboratoire de Geologie Applique
4, Place Jussieu - T.26 - 5^e etage
75252 Paris Cedex 05, FRANCE

Alain Galli
Centre de Geostatistique
Ecole des Mines de Paris
35 Rue St. Honore
77035 Fontainebleau, FRANCE

Steve Gorelick
Department of Applied Earth Sciences
Stanford University
Stanford, CA 94305-2225

Peter Grindrod
INTERA Information Technologies Ltd.
Chiltern House, 45 Station Road
Henley-on-Thames
Oxfordshire, RG9 1AT
UNITED KINGDOM

Alan Gutjahr
Department of Mathematics
New Mexico Institute of Mining and
Technology
Socorro, NM 87801

C. Peter Jackson
Harwell Laboratory
Theoretical Studies Department
Radwaste Disposal Division
Bldg. 424.4
Oxfordshire Didcot Oxon OX11 0RA
UNITED KINGDOM

Peter Kitanidis
60 Peter Coutts Circle
Stanford, CA 94305

Rae Mackay
Department of Civil Engineering
University of Newcastle Upon Tyne
Newcastle Upon Tyne NE1 7RU
UNITED KINGDOM

Dennis McLaughlin
Parsons Laboratory
Room 48-209
Department of Civil Engineering
Massachusetts Institute of Technology
Cambridge, MA 02139

Shlomo P. Neuman
College of Engineering and Mines
Department of Hydrology and Water Resources
University of Arizona
Tucson, AZ 85721

Christian Ravenne
Geology and Geochemistry Division
Institut Francais du Pétrole
1 & 4, av. de Bois-Préau BP311
92506 Rueil Malmaison Cedex
FRANCE

Yoram Rubin
Department of Civil Engineering
University of California
Berkeley, CA 94720

Foreign Addresses

Studiecentrum Voor Kernenergie
Centre D'Energie Nucleaire
Attn: A. Bonne
SCK/CEN
Boeretang 200
B-2400 Mol, BELGIUM

Atomic Energy of Canada, Ltd. (3)
Whiteshell Research Estab.
Attn: M.E. Stevens
B.W. Goodwin
D. Wushke
Pinewa, Manitoba
ROE 1L0, CANADA

Esko Peltonen
Industrial Power Company Ltd.
TVO
Fredrikinkatu 51-53
SF-00100 Helsinki 10, FINLAND

Jean-Pierre Olivier
OECD Nuclear Energy Agency (2)
38, Boulevard Suchet
F-75016 Paris, FRANCE

D. Alexandre, Deputy Director
ANDRA
31 Rue de la Federation
75015 Paris, FRANCE

Claude Sombret
Centre D'Etudes Nucleaires
De La Vallee Rhone
CEN/VALRHO
S.D.H.A. BP 171
30205 Bagnols-Sur-Ceze, FRANCE

Bundesministerium fur Forschung und
Technologie
Postfach 200 706
5300 Bonn 2, GERMANY

Bundesanstalt fur Geowissenschaften
und Rohstoffe
Attn: M. Langer
Postfach 510 153
3000 Hanover 51, GERMANY

Gesellschaft fur Reaktorsicherheit (GRS) (2)
Attn: B. Baltes
W. Muller
Schwertnergasse 1
D-5000 Cologne, GERMANY

Institut fur Tieflagerung (2)
Attn: K. Kuhn
Theodor-Heuss-Strasse 4
D-3300 Braunschweig, GERMANY

Physikalisch-Technische
Bundesanstalt
Attn: P. Brenneke
Postfach 33 45
D-3300 Braunschweig, GERMANY

Shingo Tashiro
Japan Atomic Energy Research Institute
Tokai-Mura, Ibaraki-Ken
319-11, JAPAN

Netherlands Energy Research
Foundation (ECN)
Attn: L.H. Vons
3 Westerduinweg
PO Box 1
1755 ZG Petten, THE NETHERLANDS

Johan Andersson
Swedish Nuclear Power Inspectorate
Statens Kärnkraftinspektion (SKI)
Box 27106
S-102 52 Stockholm, SWEDEN

Fred Karlsson
Svensk Karnbransleforsorjning
AB SKB
Box 5864
S-102 48 Stockholm, SWEDEN

Nationale Genossenschaft fur die Lagerung
Radioaktiver Abfalle (NAGRA) (2)
Attn: S. Vomvoris
P. Zuidema
Hardstrasse 73
CH-5430 Wettingen, SWITZERLAND

AEA Technology
Attn: J.H. Rees
D5W/29 Culham Laboratory
Abington
Oxfordshire OX14 3DB, UNITED KINGDOM

AEA Technology
Attn: W.R. Rodwell
O44/A31 Winfrith Technical Centre
Dorchester
Dorset DT2 8DH, UNITED KINGDOM

AEA Technology
Attn: J.E. Tinson
B4244 Harwell Laboratory
Didcot, Oxfordshire OX11 0RA
UNITED KINGDOM

9300 J.E. Powell
9310 J.D. Plimpton
9330 J.D. Kennedy

D.R. Knowles
British Nuclear Fuels, plc
Risley, Warrington
Cheshire WA3 6AS, 1002607
UNITED KINGDOM

Internal

1 A. Narath
20 O.E. Jones
1502 J.C. Cummings
1511 D.K. Gartling
6000 D.L. Hartley
6115 P.B. Davies
6119 E.D. Gorham
6119 Staff (14)
6121 J.R. Tillerson
6121 Staff (7)
6233 J.C. Eichelberger
6300 D.E. Ellis
6302 L.E. Shephard
6303 S.Y. Pickering
6303 W.D. Weart
6305 S.A. Goldstein
6306 A.L. Stevens
6312 F.W. Bingham
6313 L.S. Costin
6331 P.A. Davis
6341 Sandia WIPP Central Files (300)
6342 D.R. Anderson
6342 Staff (30)
6343 S.A. Orrell, Acting
6343 Staff (3)
6345 R.C. Lincoln
6345 Staff (9)
6347 D.R. Schafer
6348 J.T. Holmes
6351 R.E. Thompson
6352 D.P. Garber
6352 S.E. Sharpton
6400 N.R. Ortiz
6613 R.M. Cranwell
6613 R.L. Iman
6613 C. Leigh
6622 M.S.Y. Chu
6641 R.E. Luna, Acting
7141 Technical Library (5)
7151 Technical Publications
7613-2 Document Processing for DOE/OSTI
(10)
8523-2 Central Technical Files

Dist-13

THIS PAGE INTENTIONALLY LEFT BLANK